Fundamentals of Laser Modeling, Simulation, and Design

An Introduction to Laser Physics

R. G. Beausoleil

Hewlett Packard Labs

820 N. McCarthy Blvd., Milpitas, CA 95035

January 17, 2026

Preface

This text is adapted from a set of lecture notes hand-written during 1989–1995 for graduate classes taught at the University of Washington. I am updating these notes as I type them into LaTeX, because they were quite uneven, and didn't incorporate many of the details that I used to build *Melody*, a library of Fortran codes that I once used to model a variety of laser components, devices, and systems. Over the next few years, I'll add as many of those details as I can remember (and cull from old notebooks) to these notes, and I'll try to update the concepts so that there's a higher likelihood that they'll remain relevant in a era that includes extraordinary advances in new areas such as photonic crystals, negative index materials, and plasmonics. My goal is to rebuild *Melody* as an object-oriented library in MATLAB (any day now), enabling applications in fields ranging from microphotonic lasers to gravitational-wave interferometers.

Contents

Chapter 1

Introduction and Overview
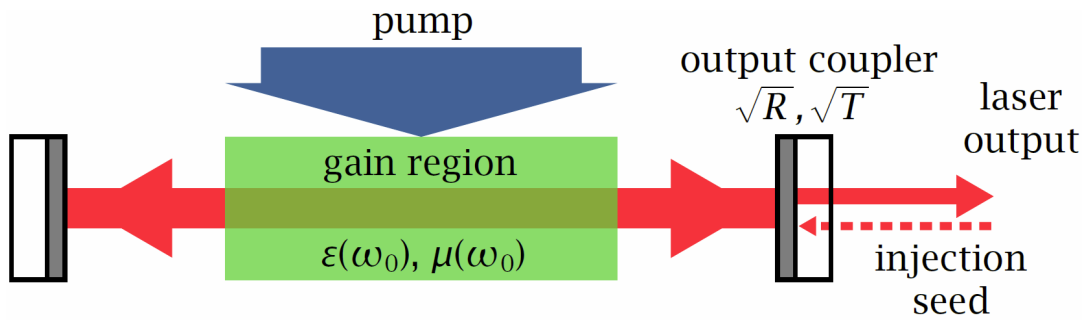
(a) Standing-wave laser resonator
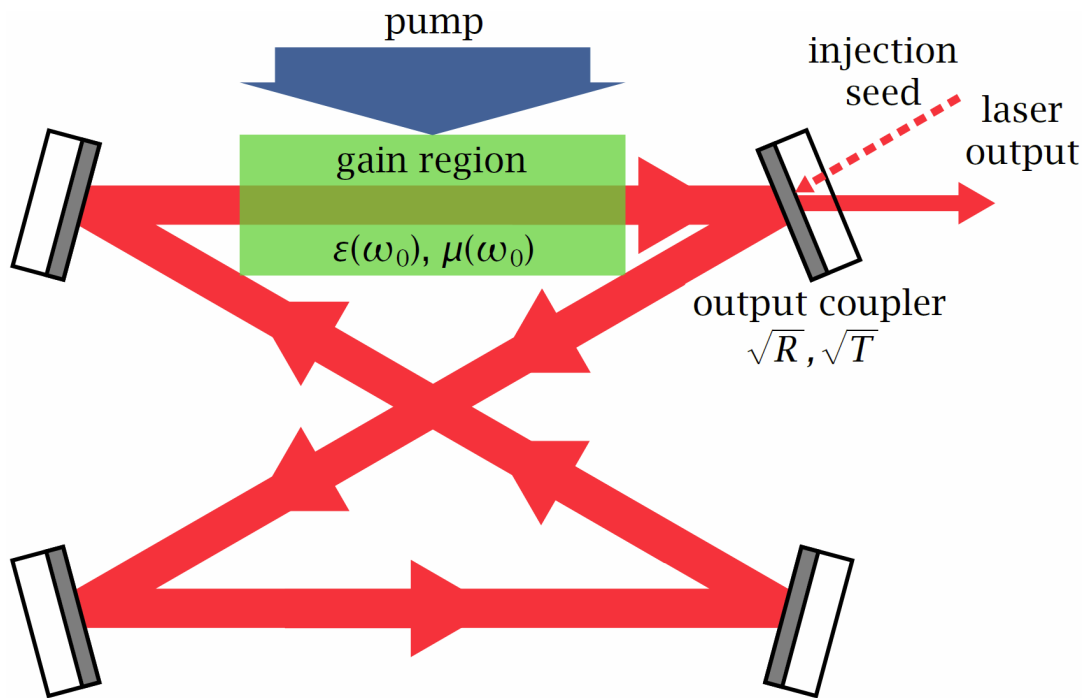
(b) Ring laser resonator

Figure 1.1:   The two most common paraxial laser resonators.

Chapter 2

Electromagnetic Wave Propagation

2.1 Electrodynamics in Vacuum

2.1.1 The Microscopic Maxwell-Lorentz Equations

Let's begin by considering a region of space containing a collection of N point-particles with mass m_n and charge q_n, $n \in \{1, \dots, N\}$, located at position $\mathbf{r}_n(t)$ with velocity $\mathbf{v}_n(t) = d\mathbf{r}_n(t)/dt$. The charge and current densities of this system can be written as

$$\rho(\mathbf{r}, t) = \sum_n q_n \, \delta\left[\mathbf{r} - \mathbf{r}_n(t)\right], \tag{2.1a}$$

$$\mathbf{j}(\mathbf{r}, t) = \sum_n q_n \, \mathbf{v}_n(t) \, \delta\left[\mathbf{r} - \mathbf{r}_n(t)\right], \tag{2.1b}$$

where $\delta(\mathbf{r}) \equiv \delta(x)\delta(y)\delta(z)$ is the three-dimensional Dirac delta function [1]. These expressions satisfy the microscopic continuity equation

$$\boldsymbol{\nabla} \cdot \mathbf{j}(\mathbf{r}, t) + \frac{\partial}{\partial t} \rho(\mathbf{r}, t) = 0. \tag{2.2}$$

We can demonstrate this claim explicitly by relying on the vector identity Eq. (A.44) and proving that[2.1]

$$\mathbf{v}_n(t) \cdot \boldsymbol{\nabla} \delta\left[\mathbf{r} - \mathbf{r}_n(t)\right] + \frac{\partial}{\partial t} \delta\left[\mathbf{r} - \mathbf{r}_n(t)\right] = 0,$$

or by representing the delta function using its Fourier transform as given by Eq. (A.36) and then showing that

$$\mathbf{v}_n(t) \cdot \boldsymbol{\nabla} \exp\left\{i\mathbf{k} \cdot \left[\mathbf{r} - \mathbf{r}_n(t)\right]\right\} + \frac{\partial}{\partial t} \exp\left\{i\mathbf{k} \cdot \left[\mathbf{r} - \mathbf{r}_n(t)\right]\right\} = 0.$$

Equation (2.2) is a local (differential) expression of the conservation of the global electric charge

$$Q = \int_{\mathcal{V}} d^3r \, \rho(\mathbf{r}, t) \tag{2.3}$$

as the surface of the bounding volume $\mathcal{V}$ becomes infinitely large.

[2.1]This sort of blithe treatment of $\delta(x)$ as just another function — or the movement of differentiation operators into and out of integrals, or changes in the order of integration over different variables — is a staple in physics and can frustrate students who prefer that more attention be paid to formal mathematical details. Given the appropriate understanding of $\delta(x)$ as the limit (in the sense of distributions) of sequences of well-behaved sharply-peaked functions with unit area, all is well here. However, we will rarely specify the validity conditions needed to justify a particular instance of mathematical horseplay, because a physicist's love of mathematical rigor is almost always unrequited: our models of the underlying physical systems will break down long before our mathematical assumptions become untenable.

The dynamics of the motion of each particle under the influence of electric and magnetic forces are described by the Newton-Lorentz equation as

$$\mathbf{F}_n(t) \equiv m_n \frac{d^2}{dt^2} \mathbf{r}_n = q_n \left\{ \boldsymbol{\mathcal{E}} \left[\mathbf{r}_n(t), t \right] + \mathbf{v}_n(t) \times \boldsymbol{\mathcal{B}} \left[\mathbf{r}_n(t), t \right] \right\}, \tag{2.4}$$

where $\boldsymbol{\mathcal{E}}(\mathbf{r}, t)$ is the external electric field and $\boldsymbol{\mathcal{B}}(\mathbf{r}, t)$ is the external magnetic induction (or magnetic flux density).[2.2] At the same time, these external fields evolve under the influence of both the local charge and current densities according to the microscopic Maxwell equations, given in MKS units by [2]

$$\nabla \cdot \boldsymbol{\mathcal{E}}(\mathbf{r}, t) = \frac{1}{\varepsilon_0} \rho(\mathbf{r}, t) \qquad \text{Gauss's Law} \tag{2.5a}$$

$$\nabla \cdot \boldsymbol{\mathcal{B}}(\mathbf{r}, t) = 0 \qquad \text{Gauss's Law for Magnetism} \tag{2.5b}$$

$$\nabla \times \boldsymbol{\mathcal{E}}(\mathbf{r}, t) + \frac{\partial}{\partial t} \boldsymbol{\mathcal{B}}(\mathbf{r}, t) = 0 \qquad \text{Faraday's Law} \tag{2.5c}$$

$$\nabla \times \boldsymbol{\mathcal{B}}(\mathbf{r}, t) - \varepsilon_0 \mu_0 \frac{\partial}{\partial t} \boldsymbol{\mathcal{E}}(\mathbf{r}, t) = \mu_0 \boldsymbol{j}(\mathbf{r}, t) \qquad \text{Ampere's Law} \tag{2.5d}$$

When Maxwell's displacement current ($\varepsilon_0 \mu_0 \, \partial \boldsymbol{\mathcal{E}} / \partial t$) is included in Ampere's Law, charge conservation is implicit in Eq. (2.5): the continuity equation (2.2) can be derived by taking the divergence of Eq. (2.5d) and applying Gauss's Law (2.5a). Also, note that Faraday's Law Eq. (2.5c) is consistent with Eq. (2.5b). The constants ε_0 and μ_0 are known as the permittivity of the vacuum and the permeability of the vacuum, respectively, and satisfy $\varepsilon_0 \mu_0 c^2 = 1$, where the speed of light in vacuum is defined to have the value $c \equiv 299\,792\,458$ m/s [3]. Since the constant $\mu_0 \equiv 4\pi \times 10^{-7}$ N/A is defined exactly, the value of $\varepsilon_0 \equiv (\mu_0 c^2)^{-1} \approx 8.85418782 \times 10^{-12}$ F/m is also exact.

2.1.2   Poynting's Theorem in Vacuum

The rate at which work is done by the external fields on particle n is given by Eq. (2.4) as

$$\begin{aligned}
\mathbf{F}_n(t) \cdot \mathbf{v}_n(t) &= q_n \mathbf{v}_n(t) \cdot \boldsymbol{\mathcal{E}} \left[\mathbf{r}_n(t), t \right] \\
&= \int_{\mathcal{V}} d^3 r \, \delta \left[\mathbf{r} - \mathbf{r}_n(t) \right] q_n \mathbf{v}_n(t) \cdot \boldsymbol{\mathcal{E}}(\mathbf{r}, t),
\end{aligned} \tag{2.6}$$

since $\mathbf{v}_n(t) \cdot \left\{ \mathbf{v}_n(t) \times \boldsymbol{\mathcal{B}} \left[\mathbf{r}_n(t), t \right] \right\} = 0$. Therefore, the total work W done by the fields on *all* of the particles changes with time according to

$$\begin{aligned}
\frac{dW}{dt} &= \sum_n \mathbf{F}_n(t) \cdot \mathbf{v}_n(t) = \int_{\mathcal{V}} d^3 r \sum_n \delta \left[\mathbf{r} - \mathbf{r}_n(t) \right] q_n \mathbf{v}_n(t) \cdot \boldsymbol{\mathcal{E}}(\mathbf{r}, t) \\
&= \int_{\mathcal{V}} d^3 r \, \boldsymbol{j}(\mathbf{r}, t) \cdot \boldsymbol{\mathcal{E}}(\mathbf{r}, t).
\end{aligned} \tag{2.7}$$

Using Eq. (2.5c), Eq. (2.5d), and the vector identity given by Eq. (A.48), we can rewrite the integrand on the right-hand side of Eq. (2.7) as

$$\begin{aligned}
\boldsymbol{j}(\mathbf{r}, t) \cdot \boldsymbol{\mathcal{E}}(\mathbf{r}, t) &= \left[\frac{1}{\mu_0} \nabla \times \boldsymbol{\mathcal{B}}(\mathbf{r}, t) - \varepsilon_0 \frac{\partial}{\partial t} \boldsymbol{\mathcal{E}}(\mathbf{r}, t) \right] \cdot \boldsymbol{\mathcal{E}}(\mathbf{r}, t) \\
&= \frac{1}{\mu_0} \boldsymbol{\mathcal{B}}(\mathbf{r}, t) \cdot \nabla \times \boldsymbol{\mathcal{E}}(\mathbf{r}, t) - \frac{1}{\mu_0} \nabla \cdot \left[\boldsymbol{\mathcal{E}}(\mathbf{r}, t) \times \boldsymbol{\mathcal{B}}(\mathbf{r}, t) \right] - \varepsilon_0 \boldsymbol{\mathcal{E}}(\mathbf{r}, t) \cdot \frac{\partial}{\partial t} \boldsymbol{\mathcal{E}}(\mathbf{r}, t) \\
&= - \left\{ \frac{1}{\mu_0} \nabla \cdot \left[\boldsymbol{\mathcal{E}}(\mathbf{r}, t) \times \boldsymbol{\mathcal{B}}(\mathbf{r}, t) \right] + \varepsilon_0 \boldsymbol{\mathcal{E}}(\mathbf{r}, t) \cdot \frac{\partial}{\partial t} \boldsymbol{\mathcal{E}}(\mathbf{r}, t) + \frac{1}{\mu_0} \boldsymbol{\mathcal{B}}(\mathbf{r}, t) \cdot \frac{\partial}{\partial t} \boldsymbol{\mathcal{B}}(\mathbf{r}, t) \right\}.
\end{aligned} \tag{2.8}$$

[2.2]We will (usually) use bold calligraphic characters to denote *real* rapidly-varying vector field quantities.

Equation (2.8) is correct as it stands, since it relies only on the validity of Maxwell's equations. However, we will be studying characteristics of optical fields — such as intensity, peak power, and average power — that can be measured by conventional square-law photodetectors. Generally, these instruments are sensitive over a frequency range that has a maximum well below typical optical frequencies, which suggests that we should try to factor out high-frequency behavior that will be averaged out of the detector's photocurrent. Therefore, we consider *nearly harmonic* fields at some optical "carrier" frequency ω_0, so that (for example) we can write the real field $\boldsymbol{\mathcal{E}}(\mathbf{r}, t)$ as

$$
\begin{aligned}
\boldsymbol{\mathcal{E}}(\mathbf{r}, t) &\equiv \mathrm{Re}\left[e^{-i\omega_0 t} \mathbf{E}(\mathbf{r}, t) \right] \\
&= \frac{e^{-i\omega_0 t}}{2} \mathbf{E}(\mathbf{r}, t) + \frac{e^{+i\omega_0 t}}{2} \mathbf{E}^*(\mathbf{r}, t) \\
&\equiv \frac{e^{-i\omega_0 t}}{2} \mathbf{E}(\mathbf{r}, t) + \text{c.c.},
\end{aligned}
\tag{2.9}
$$

where "c.c." indicates the complex conjugate, and $\mathbf{E}(\mathbf{r}, t)$ is a complex envelope function that varies slowly relative to $e^{-i\omega_0 t}$. In other words, we assume that

$$
\frac{d}{dt} \mathbf{E}(\mathbf{r}, t) \ll -i\omega_0 \mathbf{E}(\mathbf{r}, t),
\tag{2.10}
$$

where the inequality is separately true for both the real and imaginary parts of the relation. This assumption is known as the "slowly-varying envelope approximation" (SVEA), and we will use it often in both the temporal and spatial domains to simplify Maxwell's equations in physically appropriate situations. In Section A.1 of Appendix A, we show that the time average of the product of two nearly harmonic variables $\mathcal{A}(t)$ and $\mathcal{B}(t)$ — defined by Eq. (A.2) — is given by Eq. (A.6) as

$$
\overline{\mathcal{A}(t)\mathcal{B}(t)} \cong \frac{1}{4} A(t) B^*(t) + c.c. = \frac{1}{2} \mathrm{Re}\left[A(t) B^*(t) \right],
\tag{2.11}
$$

where we have assumed that both $\mathcal{A}(t)$ and $\mathcal{B}(t)$ oscillate near frequency ω_0 (i.e., that $\omega_a = \omega_b$). In Section A.1, we note that the corresponding averaging time is greater than $2\pi/\omega_0$, but much smaller than the characteristic time of the complex envelope functions $A(t)$ and $B(t)$. Therefore, with the goal of understanding detectable lower-frequency electrodynamic behavior, we ignore terms oscillating rapidly at optical frequencies and take the time average of Eq. (2.8). For example, given $\boldsymbol{\mathcal{B}}(\mathbf{r}, t) \equiv \mathrm{Re}[e^{-i\omega_0 t} \mathbf{B}(\mathbf{r}, t)]$ and $\boldsymbol{j}(\mathbf{r}, t) \equiv \mathrm{Re}[e^{-i\omega_0 t} \mathbf{j}(\mathbf{r}, t)]$, we note that

$$
\overline{\boldsymbol{j}(\mathbf{r}, t) \cdot \boldsymbol{\mathcal{E}}(\mathbf{r}, t)} = \frac{1}{2} \mathrm{Re}\left[\mathbf{j}(\mathbf{r}, t) \cdot \mathbf{E}^*(\mathbf{r}, t) \right],
\tag{2.12}
$$

and

$$
\begin{aligned}
\overline{\boldsymbol{\mathcal{B}}(\mathbf{r}, t) \cdot \frac{\partial}{\partial t} \boldsymbol{\mathcal{B}}(\mathbf{r}, t)} &= \frac{1}{2} \mathrm{Re}\left[\mathbf{B}(\mathbf{r}, t) \cdot \frac{\partial}{\partial t} \mathbf{B}^*(\mathbf{r}, t) \right] \\
&= \frac{1}{4}\left[\mathbf{B}(\mathbf{r}, t) \cdot \frac{\partial}{\partial t} \mathbf{B}^*(\mathbf{r}, t) + \mathbf{B}^*(\mathbf{r}, t) \cdot \frac{\partial}{\partial t} \mathbf{B}(\mathbf{r}, t) \right] \\
&= \frac{1}{4} \frac{\partial}{\partial t}\left[\mathbf{B}(\mathbf{r}, t) \cdot \mathbf{B}^*(\mathbf{r}, t) \right] \\
&= \frac{1}{4} \frac{\partial}{\partial t} |\mathbf{B}(\mathbf{r}, t)|^2 .
\end{aligned}
\tag{2.13}
$$

Thus, if we define the time-averaged Poynting vector

$$
\mathbf{S}(\mathbf{r}, t) \equiv \frac{1}{2} \varepsilon_0 c^2 \, \mathrm{Re}\left[\mathbf{E}(\mathbf{r}, t) \times \mathbf{B}^*(\mathbf{r}, t) \right]
\tag{2.14}
$$

and the time-averaged energy density

$$u(\mathbf{r}, t) \equiv \frac{\varepsilon_0}{4} \left| \mathbf{E}(\mathbf{r}, t) \right|^2 + \frac{1}{4\mu_0} \left| \mathbf{B}(\mathbf{r}, t) \right|^2 = \frac{\varepsilon_0}{4} \left[\left| \mathbf{E}(\mathbf{r}, t) \right|^2 + c^2 \left| \mathbf{B}(\mathbf{r}, t) \right|^2 \right], \tag{2.15}$$

where we have used $\varepsilon_0 \mu_0 c^2 = 1$, then we can take the time average of both sides of Eq. (2.8) and write *Poynting's Theorem* as

$$\frac{\partial}{\partial t} u(\mathbf{r}, t) + \boldsymbol{\nabla} \cdot \mathbf{S}(\mathbf{r}, t) = -\frac{1}{2\mu_0} \mathrm{Re} \left[\mathbf{j}(\mathbf{r}, t) \cdot \mathbf{E}^*(\mathbf{r}, t) \right]. \tag{2.16}$$

Perhaps it is easiest to interpret this result by taking the volume integral of both sides, as in Eq. (2.7). We consider an integration volume $\mathcal{V}$ with a bounding surface S large enough to contain all of the charges in the system. The term on the right-hand side of Eq. (2.16) is the time-averaged rate at which energy is being transferred from the charged particles to the fields, while the first term on the left-hand side of Eq. (2.16), $(\partial/\partial t) \int_{\mathcal{V}} d^3r \, u(\mathbf{r}, t)$, is the time-averaged rate at which the energy stored in the fields is changing. Using the Divergence Theorem given by Eq. (A.55), the second term on the left-hand side can be written

$$\int_{\mathcal{V}} d^3r \, \boldsymbol{\nabla} \cdot \mathbf{S}(\mathbf{r}, t) = \int_{S} d\mathbf{a} \, \hat{\mathbf{n}} \cdot \mathbf{S}(\mathbf{r}, t), \tag{2.17}$$

representing the time-averaged rate at which energy stored in the fields is flowing out of $\mathcal{V}$ through S. The magnitude of the Poynting vector is usually referred to as either "energy flux" in electromagnetics or "intensity" in laser physics and engineering, and it has units of power (energy per unit time) per unit area.

2.1.3 Electromagnetic Wave Propagation in Vacuum

Let us now study the behavior of optical-frequency electromagnetic fields in a volume within which there are no charges, or $\rho(\mathbf{r}, t) = 0$ and $\mathbf{j}(\mathbf{r}, t) = 0$. Taking the curl of Eq. (2.5c) and then employing Eq. (2.5d), we find

$$\boldsymbol{\nabla} \times \boldsymbol{\nabla} \times \boldsymbol{\mathcal{E}}(\mathbf{r}, t) = -\frac{\partial}{\partial t} \boldsymbol{\nabla} \times \boldsymbol{\mathcal{B}}(\mathbf{r}, t) = -\frac{1}{c^2} \frac{\partial^2}{\partial t^2} \boldsymbol{\mathcal{E}}(\mathbf{r}, t). \tag{2.18}$$

We can find an identical relationship for $\boldsymbol{\mathcal{B}}(\mathbf{r}, t)$ by taking the curl of Eq. (2.5d), and then applying Eq. (2.5c). Using Eq. (A.43), and noting that $\boldsymbol{\nabla} \cdot \boldsymbol{\mathcal{E}}(\mathbf{r}, t) = 0$ and $\boldsymbol{\nabla} \cdot \boldsymbol{\mathcal{B}}(\mathbf{r}, t) = 0$, we derive the second-order decoupled wave equations

$$\nabla^2 \boldsymbol{\mathcal{E}}(\mathbf{r}, t) - \frac{1}{c^2} \frac{\partial^2}{\partial t^2} \boldsymbol{\mathcal{E}}(\mathbf{r}, t) = 0, \text{ and} \tag{2.19a}$$

$$\nabla^2 \boldsymbol{\mathcal{B}}(\mathbf{r}, t) - \frac{1}{c^2} \frac{\partial^2}{\partial t^2} \boldsymbol{\mathcal{B}}(\mathbf{r}, t) = 0. \tag{2.19b}$$

These wave equations are solved by any function $\boldsymbol{\mathcal{F}}(\hat{\mathbf{n}} \cdot \mathbf{r} - ct)$, where $\hat{\mathbf{n}} \equiv \{n_x, n_y, n_z\}$ is an arbitrary unit vector, since $\nabla^2 \boldsymbol{\mathcal{F}} = 2(n_x^2 + n_y^2 + n_z^2) \boldsymbol{\mathcal{F}}'' = 2 \boldsymbol{\mathcal{F}}''$, and $\partial^2 \boldsymbol{\mathcal{F}}/\partial t^2 = 2c^2 \boldsymbol{\mathcal{F}}''$. Physically, $\boldsymbol{\mathcal{E}}$ and $\boldsymbol{\mathcal{B}}$ represent *vector* waves of constant shape traveling in the $\hat{\mathbf{n}}$ direction at speed c. For example, let $\hat{\mathbf{n}} = \hat{\mathbf{z}}$. Then, in Fig. 2.1, the amplitude of the field point A corresponds to a fixed value of the argument $z - ct = \text{constant}$, which implies $\partial z/\partial t = 0$.

Rather than examine in detail other properties of general solutions to Eq. (2.19), we will analyze the case where the fields are nearly harmonic and propagate nearly unidirectionally, or $\boldsymbol{\mathcal{E}}(\mathbf{r}, t) = \mathrm{Re}\{\exp[i(\mathbf{k} \cdot \mathbf{r} - \omega_0 t)] \mathbf{E}(\mathbf{r}, t)\}$ and $\boldsymbol{\mathcal{B}}(\mathbf{r}, t) = \mathrm{Re}\{\exp[i(\mathbf{k} \cdot \mathbf{r} - \omega_0 t)] \mathbf{B}(\mathbf{r}, t)\}$ for a choice of $\mathbf{k}$ that will capture rapidly-varying spatial behavior. Since

$$\frac{\partial^n}{\partial t^n} \left[e^{-i\omega_0 t} f(t) \right] = e^{-i\omega_0 t} (-i)^n \left(\omega_0 + i \frac{\partial}{\partial t} \right)^n f(t), \tag{2.20}$$
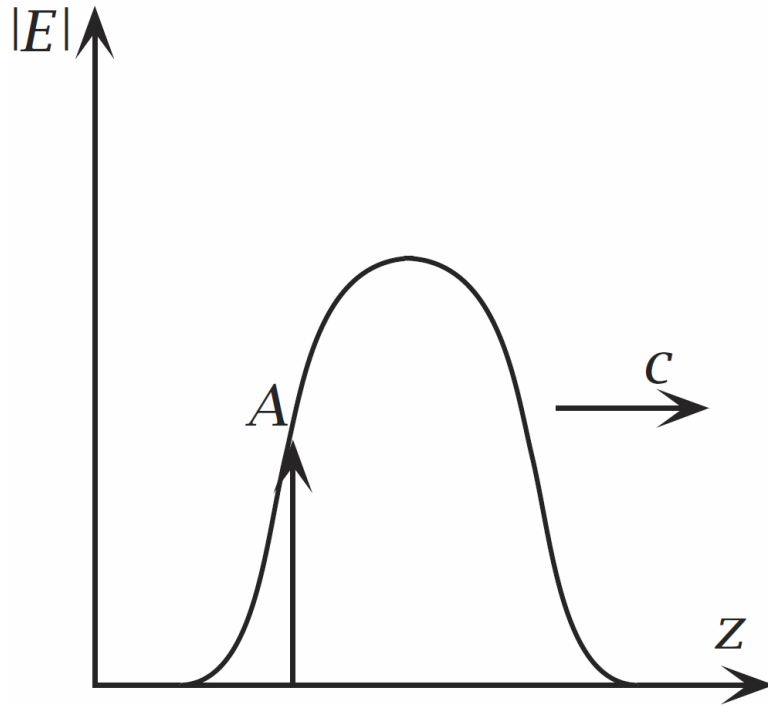
Figure 2.1: Propagation of a constant field with amplitude $|\mathbf{E}(z,t)|$.

where $(\omega_0 + i\partial/\partial t)^n$ represents the operator $\omega_0 + i\partial/\partial t$ applied n consecutive times, by judicious use of Eq. (A.44) and Eq. (A.45) we find that the complex amplitude functions $\mathbf{E}(\mathbf{r},t)$ and $\mathbf{B}(\mathbf{r},t)$ obey the complex Maxwell equations

$$\nabla \cdot \mathbf{E}(\mathbf{r},t) + i\mathbf{k} \cdot \mathbf{E}(\mathbf{r},t) = 0 \tag{2.21a}$$

$$\nabla \cdot \mathbf{B}(\mathbf{r},t) + i\mathbf{k} \cdot \mathbf{B}(\mathbf{r},t) = 0 \tag{2.21b}$$

$$\nabla \times \mathbf{E}(\mathbf{r},t) + i\mathbf{k} \times \mathbf{E}(\mathbf{r},t) - i\left(\omega_0 + i\frac{\partial}{\partial t}\right)\mathbf{B}(\mathbf{r},t) = 0 \tag{2.21c}$$

$$\nabla \times \mathbf{B}(\mathbf{r},t) + i\mathbf{k} \times \mathbf{B}(\mathbf{r},t) + \frac{i}{c^2}\left(\omega_0 + i\frac{\partial}{\partial t}\right)\mathbf{E}(\mathbf{r},t) = 0 \tag{2.21d}$$

In the case of nearly unidirectional propagation, we can adopt the slowly-varying envelope approximation

$$\nabla \cdot \mathbf{E}(\mathbf{r},t) \ll i\mathbf{k} \cdot \mathbf{E}(\mathbf{r},t), \text{ and} \tag{2.22a}$$

$$\nabla \times \mathbf{E}(\mathbf{r},t) \ll i\mathbf{k} \times \mathbf{E}(\mathbf{r},t), \tag{2.22b}$$

with similar expressions for $\mathbf{B}(\mathbf{r},t)$. As in the case of Eq. (2.10), these inequalities hold for both the real and imaginary parts of the corresponding relations. Applying the SVEA to Eq. (2.21), we see immediately that

$$\mathbf{k} \cdot \mathbf{E}(\mathbf{r},t) \approx 0 \qquad\qquad \mathbf{k} \times \mathbf{E}(\mathbf{r},t) \approx \omega_0 \mathbf{B}(\mathbf{r},t)$$

$$\mathbf{k} \cdot \mathbf{B}(\mathbf{r},t) \approx 0 \qquad\qquad \mathbf{k} \times \mathbf{B}(\mathbf{r},t) \approx -\frac{\omega_0}{c^2}\mathbf{E}(\mathbf{r},t)$$

In other words, both $\mathbf{E}(\mathbf{r},t)$ and $\mathbf{B}(\mathbf{r},t) \approx \mathbf{k} \times \mathbf{E}(\mathbf{r},t)/\omega_0$ are approximately perpendicular to $\mathbf{k}$, and the orientations of the three vectors $\mathbf{k}$, $\mathbf{E}(\mathbf{r},t)$, and $\mathbf{B}(\mathbf{r},t)$ follow the right-hand rule if they are purely real. Since, by Eq. (A.39), $\mathbf{k} \times [\mathbf{k} \times \mathbf{E}(\mathbf{r},t)] = -(\mathbf{k} \cdot \mathbf{k})\mathbf{E}(\mathbf{r},t)$, the two equations on the right-hand side are

consistent if $\mathbf{k}$ is real and $|\mathbf{k}| = \omega_0/c$. In this case, we can use Eq. (2.14) and Eq. (2.15) to calculate the time-averaged Poynting vector and energy density for a nearly unidirectional wave to be

$$S(\mathbf{r}, t) = \frac{1}{2}\varepsilon_0 c \, |\mathbf{E}(\mathbf{r}, t)|^2 \, \hat{k}, \text{ and} \tag{2.23}$$

$$u(\mathbf{r}, t) = \frac{1}{2}\varepsilon_0 \, |\mathbf{E}(\mathbf{r}, t)|^2, \tag{2.24}$$

where $\hat{k} \equiv \mathbf{k}/|\mathbf{k}|$ is a unit vector oriented in the primary direction of propagation. Note that $|S(\mathbf{r}, t)| = c\,u(\mathbf{r}, t)$, consistent with our interpretation of the left-hand side of Eq. (2.16).

If we apply Eq. (A.46) and Eq. (2.20) to Eq. (2.19a), then we find the modified wave equation for the complex electric field amplitude function $\mathbf{E}(\mathbf{r}, t)$ to be

$$\left(\nabla^2 - \frac{1}{c^2}\frac{\partial^2}{\partial t^2}\right)\mathbf{E}(\mathbf{r}, t) + i\,2\,(\mathbf{k}\cdot\nabla)\,\mathbf{E}(\mathbf{r}, t) + i\frac{2\omega_0}{c^2}\frac{\partial}{\partial t}\mathbf{E}(\mathbf{r}, t) - \left[|\mathbf{k}|^2 - \left(\frac{\omega_0}{c}\right)^2\right]\mathbf{E}(\mathbf{r}, t) = 0, \tag{2.25}$$

or, in the time-independent case where $\partial \mathbf{E}(\mathbf{r}, t)/\partial t = 0$,

$$\nabla^2 \mathbf{E}(\mathbf{r}) + i\,2\,k_z\frac{\partial}{\partial z}\mathbf{E}(\mathbf{r}) - \left[k_z^2 - \left(\frac{\omega_0}{c}\right)^2\right]\mathbf{E}(\mathbf{r}) = 0, \tag{2.26}$$

where we have taken $\mathbf{k}$ to be parallel to the $+z$-axis. Depending on the relevant boundary conditions and assumptions made about the functional form of $\mathbf{E}(\mathbf{r}, t)$, there are a number of well-known analytic solutions to Eq. (2.26) found in textbooks and the literature, including:

Plane Waves. If we choose $\mathbf{E}(\mathbf{r}, t)$ to be completely independent of space and time, then the resulting electric and magnetic fields are given by

$$\boldsymbol{\mathcal{E}}(z, t) = \frac{1}{2}e^{i(kz - \omega_0 t)}\mathbf{E} + \text{c.c.}, \text{ and} \tag{2.27a}$$

$$\boldsymbol{\mathcal{B}}(z, t) = \frac{1}{2}e^{i(kz - \omega_0 t)}\mathbf{B} + \text{c.c.}, \tag{2.27b}$$

where $k = \omega_0/c$ exactly. Both $\boldsymbol{\mathcal{E}}(z, t)$ and $\boldsymbol{\mathcal{B}}(z, t)$ are infinite in extent transverse to the z-axis, and for any particular value of z the spatial contribution to the phase of each field is constant over the xy-plane. These *plane waves* are often useful for building an intuitive picture of the physics of some matter-field system, particularly in the context of the Fourier expansion given by Eq. (A.12a), which may be thought of as a sum over coherent contributions from a collection of plane waves $e^{+i(\mathbf{k}\cdot\mathbf{r} - \omega_0 t)}$ that have different propagation directions in space. By inspection of Eq. (2.21a), given $\mathbf{k} = \hat{z}\,\omega_0/c$ the constant complex vector amplitude for the electric field can be written as

$$\mathbf{E} = E\,\hat{\epsilon} \equiv E\left(\epsilon_x\hat{x} + \epsilon_y\hat{y}\right), \tag{2.28}$$

where E is a real number and ϵ_x and ϵ_y are complex numbers satisfying $|\epsilon_x|^2 + |\epsilon_y|^2 = 1$. Then Eq. (2.21c) yields

$$\mathbf{B} = \frac{E}{c}\,\hat{z}\times\hat{\epsilon} = \frac{E}{c}\left(-\epsilon_y\hat{x} + \epsilon_x\hat{y}\right). \tag{2.29}$$

We see immediately that $\mathbf{E}\cdot\mathbf{B} = 0$, and a little algebra shows that $\boldsymbol{\mathcal{E}}(z, t)\cdot\boldsymbol{\mathcal{B}}(z, t) = 0$ exactly even though $\mathbf{E}\cdot\mathbf{B}^* \neq 0$. From Eq. (2.23) and Eq. (2.24), we note the energy density is constant everywhere in space, so that the total energy $U = \int d^3r\,u(\mathbf{r}, t)$ diverges. In other words, we'd need infinite energy to generate a true plane wave, so we usually pretend that a model plane wave under consideration has a finite transverse extent.

Nondiffracting Beams. If we consider only azimuthally symmetric scalar fields that are independent of z, then $\mathbf{E}(\mathbf{r}) \equiv E(\rho)$, where $\boldsymbol{\rho} \equiv \rho \hat{\boldsymbol{\rho}} \equiv \hat{\boldsymbol{x}}\, x + \hat{\boldsymbol{y}}\, y$. Applying Eq. (A.68) to Eq. (2.26) yields

$$\frac{\partial^2}{\partial \rho^2} E + \frac{1}{\rho}\frac{\partial}{\partial \rho} E + k_\rho^2 E = 0, \tag{2.30}$$

where $k_\rho^2 = (\omega_0/c)^2 - k_z^2$. This is simply Bessel's equation of order 0 [4], which has the solution

$$E(\rho) = J_0(k_\rho \rho). \tag{2.31}$$

Note that (by assumption) the transverse profile of this field is invariant as it propagates along the z-axis, leading to its designation as a "nondiffracting" beam [5]. As in the case of the plane wave, the total energy of the field diverges [6], but there are a number of laboratory techniques that can be used to create quasi-Bessel beams with a large depth of field [7]. Practical applications of the quasi-Bessel beams include micromanipulation and guiding of particles [8] and long-range optical coherence tomography [9].

Gaussian Beams. Suppose now that we allow $\mathbf{E}(\mathbf{r})$ to vary with z, but we make the *paraxial approximation* and assume that $\mathbf{E}$ transversely expands (or contracts) and longitudinally attenuates (or grows) very slowly compared to $e^{\pm ikz}$. Then, in Eq. (2.26), we have (1) $k_x^2 + k_y^2 = k_\rho^2 + k_\phi^2 \ll k_z^2 \approx (\omega_0/c)^2$, and (2) $\partial^2 \mathbf{E}/\partial z^2 \ll ik_z \partial \mathbf{E}/\partial z$, giving [10, 11]

$$\nabla_\perp^2 \mathbf{E}(\mathbf{r}) + i\, 2\, k_z \frac{\partial}{\partial z}\mathbf{E}(\mathbf{r}) = 0, \tag{2.32}$$

where, by Eq. (A.64) and Eq. (A.68),

$$\nabla_\perp^2 \equiv \frac{\partial^2}{\partial x^2} + \frac{\partial^2}{\partial y^2} = \frac{1}{\rho}\frac{\partial}{\partial \rho}\left(\rho \frac{\partial}{\partial \rho}\right) + \frac{1}{\rho^2}\frac{\partial^2}{\partial \phi^2}. \tag{2.33}$$

Well-known analytic solutions to Eq. (2.32) — denoted collectively as "Gaussian beams" for reasons that will become clear in Chapter 8 — exist for both forms of $\nabla_\perp^2$. These fields are eigenmodes of stable spherical-mirror laser resonators, and in each of these cases the integral of the energy density over the transverse plane converges. In laser modeling problems where mirror substrates are circular and cylindrical symmetry is likely to hold, families of analytic solutions to Eq. (2.32) known as "circular beams" [12] have been studied extensively, but this symmetry is less relevant in practice than one might think. First, many laser resonators (such as the ring cavity shown in Fig. 1.1b) do not necessarily have cylindrical symmetry, because of astigmatism in the xy-plane due to off-axis reflection from curved mirrors or asymmetric gain or thermal loading in the laser amplifier. Even in the case of a standing-wave resonator with circular mirrors (such as the cavity shown in Fig. 1.1a), the mirror mounts generally have cartesian adjustments, and we will often see high-order cartesian beams in the laboratory as a result. Nevertheless, unless we need to make highly accurate predictions of cavity stability under conditions of large-angle alignment errors [13], we will usually take advantage of cylindrical symmetry when we model optimum laser system performance.

2.2 Inhomogeneous Dispersive Media

We will eventually model laser amplifiers as ensembles of quantum dipoles (e.g., nearly resonant interactions with two-level systems such as atoms, molecules, or electron-hole pairs) embedded in a background material that can be modeled mesoscopically as a classical electromagnetic material. With

this approach in mind, we introduce the macroscopic Maxwell equations, given by [2]

$$\nabla \cdot \boldsymbol{D}(\mathbf{r}, t) = \rho_f(\mathbf{r}, t) \tag{2.34a}$$

$$\nabla \cdot \boldsymbol{B}(\mathbf{r}, t) = 0 \tag{2.34b}$$

$$\nabla \times \boldsymbol{E}(\mathbf{r}, t) + \frac{\partial}{\partial t} \boldsymbol{B}(\mathbf{r}, t) = 0 \tag{2.34c}$$

$$\nabla \times \boldsymbol{H}(\mathbf{r}, t) - \frac{\partial}{\partial t} \boldsymbol{D}(\mathbf{r}, t) = \boldsymbol{j}_f(\mathbf{r}, t) \tag{2.34d}$$

$$\nabla \cdot \boldsymbol{j}_f(\mathbf{r}, t) + \frac{\partial}{\partial t} \rho_f(\mathbf{r}, t) = 0 \tag{2.34e}$$

where "f" denotes "free," and the electric displacement $\boldsymbol{D}$ and the magnetic field $\boldsymbol{H}$ are defined in terms of the electric polarization $\boldsymbol{P}$ and the magnetization $\boldsymbol{M}$ as

$$\boldsymbol{D}(\mathbf{r}, t) \equiv \varepsilon_0 \boldsymbol{E}(\mathbf{r}, t) + \boldsymbol{P}(\mathbf{r}, t) \tag{2.35a}$$

$$\boldsymbol{B}(\mathbf{r}, t) \equiv \mu_0 \boldsymbol{H}(\mathbf{r}, t) + \mu_0 \boldsymbol{M}(\mathbf{r}, t) \tag{2.35b}$$

The electric polarization should not be confused with the polarization of an electromagnetic wave, and should be thought of as a macroscopic sum of microscopic electric dipole moments (per unit volume). Similarly, the magnetization is the magnetic dipole moment per unit volume.

Equation (2.34) are not the "true" Maxwell equations in the sense that they are not more general than their microscopic counterparts. They simply reflect a convenient separation of charge and current into free and bound contributions. They can be derived from Eq. (2.5) in a phenomenological fashion [2] by averaging the fields over volumes and times that are large compared to spatial and temporal variations in the underlying bound charge structure. The free charge and current therefore arise from material variations that have characteristic length scales and times that are large compared to those of the averaging procedure.

2.2.1 Constitutive Relations for Isotropic Dielectrics

Let's consider the relationship between microscopic and macroscopic fields in a way that is consistent with the models that we'll build of laser amplifiers and oscillators. We will generally assume that the laser gain region can be decomposed into a host (or background material) that is characterized by a macroscopic *linear* polarization $\boldsymbol{P}_L(\mathbf{r}, t)$ and a *nonlinear* polarization $\boldsymbol{P}(\mathbf{r}, t)$ that describes the gain elements (such as atoms, ions, or electron-hole pairs) embedded in the host. Furthermore, we will describe the linear contribution to the total macroscopic polarization by a relative permittivity ε, such that $\varepsilon_0 E + P_L \sim \varepsilon_0 \varepsilon E$, and we will assume that the host material has a purely linear permanent magnetization that can be characterized by a relative permeability μ, or $\mu_0 H + M \sim \mu_0 \mu H$. We will initially concentrate on the development of expressions for $\boldsymbol{D}(\mathbf{r}, t)$ as functions of frequency components of $\boldsymbol{E}(\mathbf{r}, t)$; the parallel discussion of $\boldsymbol{B}(\mathbf{r}, t)$ will be obvious, and we'll state the corresponding results near the end of this section.

There are a number of laser materials that are anisotropic, such as Nd:YVO$_4$ (positive uniaxial) and Ti:Sapphire (negative uniaxial). However, in these cases the crystals are cut so that the laser field's propagation vector and electric field vector are aligned with two of the available crystallographic axes. Therefore, we will assume that the host is *isotropic*, in the sense that the dependence of the relative permittivity on the host's orientation can be ignored.[2.3] However, we will allow the background material to be both spatially inhomogeneous (but local) and temporally dispersive. Following Section A.3, this means that we can write $\boldsymbol{D}$ in terms of a complex relative dielectric function $\varepsilon(\mathbf{r}, \omega)$ as

$$\boldsymbol{D}(\mathbf{r}, t) = \varepsilon_0 \int_{-\infty}^{\infty} \frac{d\omega'}{2\pi} e^{-i\omega' t} \varepsilon(\mathbf{r}, \omega') \boldsymbol{E}(\mathbf{r}, \omega') + \boldsymbol{P}(\mathbf{r}, t), \tag{2.36}$$

[2.3]It is a bit tedious (but not conceptually difficult) to treat anisotropic hosts with full generality. We simply describe the relative permittivity as a tensor, and then honor the order of matrix multiplications as we continue our analysis.

where $\pmb{\mathcal{E}}(\mathbf{r}, \omega')$ is the temporal Fourier transform of $\pmb{\mathcal{E}}(\mathbf{r}, t)$.[2.4] If we assume that $\pmb{\mathcal{E}}(\mathbf{r}, t)$ is nearly harmonic, as given by Eq. (2.9), then the corresponding Fourier transform can be written

$$
\begin{aligned}
\pmb{\mathcal{E}}(\mathbf{r}, \omega') = {}& \frac{1}{2} \int_{-\infty}^{\infty} dt\, e^{+i(\omega' - \omega_0)t}\, \mathbf{E}(\mathbf{r}, t) \\
& + \frac{1}{2} \int_{-\infty}^{\infty} dt\, e^{+i(\omega' + \omega_0)t}\, \mathbf{E}^*(\mathbf{r}, t).
\end{aligned}
\tag{2.37}
$$

The first term on the right-hand side of this expression is clearly just $\frac{1}{2}\mathbf{E}(\mathbf{r}, \omega' - \omega_0)$. However, the second term requires a little thought, because the Fourier transform of a complex conjugate is not the same thing as the complex conjugate of a Fourier transform, and we'd like to rely on the latter so that we can continue to allow the "c.c." terms to get along with little or no supervision from us. To make the problem clearer, we write the Fourier transform of $\mathbf{E}(\mathbf{r}, t)$ as

$$
\mathbf{E}(\mathbf{r}, \omega) = \int_{-\infty}^{\infty} dt\, e^{+i\omega t}\, \mathbf{E}(\mathbf{r}, t).
\tag{2.38}
$$

If we take the complex conjugate of both sides of this expression, it is evident that we will *not* obtain $\int dt\, \exp(+i\omega t)\mathbf{E}^*(\mathbf{r}, t)$ because the argument of the exponential factor has the wrong sign. The simplest way to calculate $\int dt\, \exp[+i(\omega' + \omega_0)t]\mathbf{E}^*(\mathbf{r}, t)$ is to take its complex conjugate, obtain $\mathbf{E}(\mathbf{r}, -\omega' - \omega_0)$, and then take the complex conjugate again, giving

$$
\pmb{\mathcal{E}}(\mathbf{r}, \omega') = \frac{1}{2}\mathbf{E}(\mathbf{r}, \omega' - \omega_0) + \frac{1}{2}\mathbf{E}^*(\mathbf{r}, -\omega' - \omega_0).
\tag{2.39}
$$

Since $\pmb{\mathcal{E}}(\mathbf{r}, t)$ is real, we could have derived the second term of Eq. (2.39) from Eq. (A.14) and the relation $\pmb{\mathcal{E}}(\mathbf{r}, -\omega') = \pmb{\mathcal{E}}^*(\mathbf{r}, \omega')$.

   If we substitute Eq. (2.39) into Eq. (2.36), then we obtain

$$
\begin{aligned}
\pmb{\mathcal{D}}(\mathbf{r}, t) - \pmb{\mathcal{P}}(\mathbf{r}, t) = {}& \frac{\varepsilon_0}{2} \int_{-\infty}^{\infty} \frac{d\omega'}{2\pi}\, e^{-i\omega' t} \varepsilon(\mathbf{r}, \omega')\, \mathbf{E}(\mathbf{r}, \omega' - \omega_0) \\
& + \frac{\varepsilon_0}{2} \int_{-\infty}^{\infty} \frac{d\omega'}{2\pi}\, e^{-i\omega' t} \varepsilon(\mathbf{r}, \omega')\, \mathbf{E}^*(\mathbf{r}, -\omega' - \omega_0) \\
= {}& \frac{\varepsilon_0}{2} e^{-i\omega_0 t} \int_{-\infty}^{\infty} \frac{d\omega}{2\pi}\, e^{-i\omega t} \varepsilon(\mathbf{r}, \omega_0 + \omega)\, \mathbf{E}(\mathbf{r}, \omega) \\
& + \frac{\varepsilon_0}{2} e^{+i\omega_0 t} \int_{-\infty}^{\infty} \frac{d\omega}{2\pi}\, e^{+i\omega t} \varepsilon^*(\mathbf{r}, \omega_0 + \omega)\, \mathbf{E}^*(\mathbf{r}, \omega) \\
\equiv {}& \frac{e^{-i\omega_0 t}}{2} \mathbf{D}(\mathbf{r}, t) + \text{c.c.},
\end{aligned}
\tag{2.40}
$$

where we have again used Eq. (A.14) to set $\varepsilon(\mathbf{r}, -\omega_0 - \omega) = \varepsilon^*(\mathbf{r}, \omega_0 + \omega)$, and we have defined the linear contribution of the host material to the total electric displacement in terms of

$$
\mathbf{D}(\mathbf{r}, \omega) = \varepsilon_0\, \varepsilon(\mathbf{r}, \omega_0 + \omega)\, \mathbf{E}(\mathbf{r}, \omega), \text{ and}
\tag{2.41}
$$

$$
\mathbf{D}(\mathbf{r}, t) = \int_{-\infty}^{\infty} \frac{d\omega}{2\pi}\, e^{-i\omega t}\, \mathbf{D}(\mathbf{r}, \omega).
\tag{2.42}
$$

Given the constraint Eq. (2.10), we anticipate that $\mathbf{E}(\mathbf{r}, \omega)$ will take on significant values only when $\omega \ll \omega_0$, so we can follow Section A.3.6 and formally expand $\varepsilon(\mathbf{r}, \omega_0 + \omega)$ in a Taylor series about ω_0

[2.4]We will usually avoid festooning Fourier transforms of vectors with other symbols if we can use the argument (e.g., ω) as an unambiguous label.

to obtain

$$
\mathbf{D}(\mathbf{r}, t) \equiv \varepsilon_0 \int_{-\infty}^{\infty} \frac{d\omega}{2\pi} e^{-i\omega t} \sum_{m=0}^{\infty} \frac{\omega^m}{m!} \frac{\partial^m \varepsilon(\mathbf{r}, \omega_0)}{\partial \omega_0^m} \mathbf{E}(\mathbf{r}, \omega)
$$

$$
= \varepsilon_0 \sum_{m=0}^{\infty} \frac{1}{m!} \frac{\partial^m \varepsilon(\mathbf{r}, \omega_0)}{\partial \omega_0^m} \int_{-\infty}^{\infty} \frac{d\omega}{2\pi} e^{-i\omega t} \omega^m \mathbf{E}(\mathbf{r}, \omega) \tag{2.43}
$$

$$
= \varepsilon_0 \sum_{m=0}^{\infty} \frac{1}{m!} \frac{\partial^m \varepsilon(\mathbf{r}, \omega_0)}{\partial \omega_0^m} \left(i \frac{\partial}{\partial t} \right)^m \mathbf{E}(\mathbf{r}, t),
$$

where $\partial^m f(\omega_0)/\partial \omega_0^m \equiv \partial^m f(\omega)/\partial \omega^m |_{\omega=\omega_0}$, and in the last step we have applied the Fourier Differentiation Theorem given by Eq. (A.17). If we follow the notation convention of Eq. (A.25) and write

$$
\varepsilon \left(\mathbf{r}, \omega_0 + i \frac{\partial}{\partial t} \right) \equiv \sum_{m=0}^{\infty} \frac{1}{m!} \frac{\partial^m \varepsilon(\mathbf{r}, \omega_0)}{\partial \omega_0^m} \left(i \frac{\partial}{\partial t} \right)^m, \tag{2.44}
$$

then we finally have the expression

$$
\mathbf{D}(\mathbf{r}, t) = \varepsilon_0 \, \varepsilon \left(\mathbf{r}, \omega_0 + i \frac{\partial}{\partial t} \right) \mathbf{E}(\mathbf{r}, t), \tag{2.45}
$$

correct to all orders in the dispersion. Depending on the temporal behavior of $\mathbf{E}(\mathbf{r}, t)$, we choose how many orders of $\partial \mathbf{E}(\mathbf{r}, t)/dt$ to keep in Maxwell's equations.

In later sections, we will need to compute partial time derivatives of $\boldsymbol{\mathcal{D}}(\mathbf{r}, t)$ to solve a variety of problems in power flow and wave propagation. We define $\boldsymbol{\mathcal{P}}(\mathbf{r}, t) \equiv \mathrm{Re}[e^{-i\omega_0 t} \mathbf{P}(\mathbf{r}, t)]$; therefore, using Eq. (2.20), we have

$$
\frac{\partial^n}{\partial t^n} \boldsymbol{\mathcal{D}}(\mathbf{r}, t) = \frac{e^{-i\omega_0 t}}{2} (-i)^n \left(\omega_0 + i \frac{\partial}{\partial t} \right)^n [\mathbf{D}(\mathbf{r}, t) + \mathbf{P}(\mathbf{r}, t)] + \mathrm{c.c.}
$$

$$
= \frac{e^{-i\omega_0 t}}{2} (-i)^n \left(\omega_0 + i \frac{\partial}{\partial t} \right)^n \left[\varepsilon_0 \, \varepsilon \left(\mathbf{r}, \omega_0 + i \frac{\partial}{\partial t} \right) \mathbf{E}(\mathbf{r}, t) + \mathbf{P}(\mathbf{r}, t) \right] + \mathrm{c.c.}. \tag{2.46}
$$

Our notation is a fairly compact representation that can be used to quickly generate a series of time derivatives of the complex field amplitude functions $\mathbf{E}(\mathbf{r}, t)$ and $\mathbf{P}(\mathbf{r}, t)$. If we generalize Eq. (2.44) to any function of frequency $f(\mathbf{r}, \omega)$, and then define $f(\mathbf{r}, \omega_0) \equiv \omega_0^n \varepsilon(\mathbf{r}, \omega_0)$, we can quickly expand the right-hand side of Eq. (2.46) using

$$
(-i)^n \left(\omega_0 + i \frac{\partial}{\partial t} \right)^n \mathbf{D}(\mathbf{r}, t) = (-i)^n \varepsilon_0 f \left(\mathbf{r}, \omega_0 + i \frac{\partial}{\partial t} \right) \mathbf{E}(\mathbf{r}, t)
$$

$$
= (-i)^n \varepsilon_0 \sum_{m=0}^{\infty} \frac{1}{m!} \frac{\partial^m}{\partial \omega_0^m} [\omega_0^n \varepsilon(\mathbf{r}, \omega_0)] \left(i \frac{\partial}{\partial t} \right)^m \mathbf{E}(\mathbf{r}, t). \tag{2.47}
$$

Expressions analogous to Eq. (2.36) appear frequently in linear systems theory, and our treatment is general enough to cover a wide variety of problems of interest.

The corresponding results for the magnetic induction in the host material are straightforward extensions of those for the electric displacement, without the complication of a nonlinear magnetization. Following Eq. (2.36), we can write $\boldsymbol{\mathcal{B}}$ in terms of a complex relative magnetic permeability function $\mu(\mathbf{r}, \omega)$ as

$$
\boldsymbol{\mathcal{B}}(\mathbf{r}, t) = \mu_0 \int_{-\infty}^{\infty} \frac{d\omega}{2\pi} e^{-i\omega t} \mu(\mathbf{r}, \omega) \, \boldsymbol{\mathcal{H}}(\mathbf{r}, \omega), \tag{2.48}
$$

where $\boldsymbol{\mathcal{H}}(\mathbf{r}, \omega)$ is the Fourier transform of $\boldsymbol{\mathcal{H}}(\mathbf{r}, t)$. When $\boldsymbol{\mathcal{H}}(\mathbf{r}, t)$ is nearly harmonic, we define $\boldsymbol{\mathcal{H}}(\mathbf{r}, t) \equiv \mathrm{Re}[e^{-i\omega_0 t} \mathbf{H}(\mathbf{r}, t)]$ and

$$
\mathbf{B}(\mathbf{r}, \omega) = \mu_0 \, \mu \, (\mathbf{r}, \omega_0 + \omega) \, \mathbf{H}(\mathbf{r}, \omega) \tag{2.49}
$$

to obtain

$$\mathbf{B}(\mathbf{r}, t) \equiv \mu_0 \int_{-\infty}^{\infty} \frac{d\omega}{2\pi} e^{-i\omega t} \mu(\mathbf{r}, \omega_0 + \omega) \mathbf{H}(\mathbf{r}, \omega)$$
$$= \mu_0 \mu \left(\mathbf{r}, \omega_0 + i\frac{\partial}{\partial t}\right) \mathbf{H}(\mathbf{r}, t). \tag{2.50}$$

Then, following Eq. (2.46) and Eq. (2.47), we can calculate partial time derivatives of $\mathcal{B}(\mathbf{r}, t)$ using

$$\frac{\partial^n}{\partial t^n} \mathcal{B}(\mathbf{r}, t) = \frac{e^{-i\omega_0 t}}{2} (-i)^n \left(\omega_0 + i\frac{\partial}{\partial t}\right)^n \mathbf{B}(\mathbf{r}, t) + \text{c.c.}$$
$$= \frac{e^{-i\omega_0 t}}{2} (-i)^n \left(\omega_0 + i\frac{\partial}{\partial t}\right)^n \mu_0 \mu \left(\mathbf{r}, \omega_0 + i\frac{\partial}{\partial t}\right) \mathbf{H}(\mathbf{r}, t) + \text{c.c.} \tag{2.51}$$
$$= \frac{e^{-i\omega_0 t}}{2} (-i)^n \mu_0 \sum_{m=0}^{\infty} \frac{1}{m!} \frac{\partial^m}{\partial \omega_0^m} [\omega_0^n \mu(\mathbf{r}, \omega_0)] \left(i\frac{\partial}{\partial t}\right)^m \mathbf{H}(\mathbf{r}, t) + \text{c.c..}$$

2.2.2 Poynting's Theorem in a Dispersive Medium

In writing Eq. (2.34), we have chosen some method to separate the charge and current into free and bound components, and subsequently in Eq. (2.36) we have further divided the macroscopic polarization into a linear (in $\mathbf{E}(\mathbf{r}, t)$) contribution from the background or host material, and a generally nonlinear contribution. Here we wish to extend Poynting's Theorem, derived in Eq. (2.16) for charges in vacuum, to describe power flow between electromagnetic fields, free charges and currents, and bound charges. We follow the approach we used in Section 2.1, and compute the rate at which work is done by the fields on the free charges to be

$$\frac{dW_f}{dt} = \int_{\mathcal{V}} d^3r \, \mathbf{j}_f(\mathbf{r}, t) \cdot \boldsymbol{\mathcal{E}}(\mathbf{r}, t). \tag{2.52}$$

Using Eq. (2.34c), Eq. (2.34d), and the vector identity given by Eq. (A.48), we can rewrite the integrand on the right-hand side of Eq. (2.52) as

$$\mathbf{j}_f(\mathbf{r}, t) \cdot \boldsymbol{\mathcal{E}}(\mathbf{r}, t) = \left[\boldsymbol{\nabla} \times \boldsymbol{\mathcal{H}}(\mathbf{r}, t) - \frac{\partial}{\partial t} \boldsymbol{\mathcal{D}}(\mathbf{r}, t)\right] \cdot \boldsymbol{\mathcal{E}}(\mathbf{r}, t)$$
$$= \boldsymbol{\mathcal{H}}(\mathbf{r}, t) \cdot \boldsymbol{\nabla} \times \boldsymbol{\mathcal{E}}(\mathbf{r}, t) - \boldsymbol{\nabla} \cdot [\boldsymbol{\mathcal{E}}(\mathbf{r}, t) \times \boldsymbol{\mathcal{H}}(\mathbf{r}, t)] - \boldsymbol{\mathcal{E}}(\mathbf{r}, t) \cdot \frac{\partial}{\partial t} \boldsymbol{\mathcal{D}}(\mathbf{r}, t) \tag{2.53}$$
$$= -\left\{\boldsymbol{\nabla} \cdot [\boldsymbol{\mathcal{E}}(\mathbf{r}, t) \times \boldsymbol{\mathcal{H}}(\mathbf{r}, t)] + \boldsymbol{\mathcal{E}}(\mathbf{r}, t) \cdot \frac{\partial}{\partial t} \boldsymbol{\mathcal{D}}(\mathbf{r}, t) + \boldsymbol{\mathcal{H}}(\mathbf{r}, t) \cdot \frac{\partial}{\partial t} \boldsymbol{\mathcal{B}}(\mathbf{r}, t)\right\}.$$

Using Eq. (2.46), Eq. (2.47) and Eq. (2.51), we can calculate the time derivatives in Eq. (2.53) to first order in $\partial/\partial t$, giving

$$\frac{\partial}{\partial t} \boldsymbol{\mathcal{D}}(\mathbf{r}, t) \cong \frac{e^{-i\omega_0 t}}{2} \varepsilon_0 \left\{-i\omega_0 \varepsilon(\mathbf{r}, \omega_0) \mathbf{E}(\mathbf{r}, t) + \frac{\partial}{\partial \omega_0} [\omega_0 \varepsilon(\mathbf{r}, \omega_0)] \frac{\partial}{\partial t} \mathbf{E}(\mathbf{r}, t)\right\}$$
$$- \frac{e^{-i\omega_0 t}}{2} i\left(\omega_0 + i\frac{\partial}{\partial t}\right) \mathbf{P}(\mathbf{r}, t) + \text{c.c.}, \tag{2.54a}$$
$$\frac{\partial}{\partial t} \boldsymbol{\mathcal{B}}(\mathbf{r}, t) \cong \frac{e^{-i\omega_0 t}}{2} \mu_0 \left\{-i\omega_0 \mu(\mathbf{r}, \omega_0) \mathbf{H}(\mathbf{r}, t) + \frac{\partial}{\partial \omega_0} [\omega_0 \mu(\mathbf{r}, \omega_0)] \frac{\partial}{\partial t} \mathbf{H}(\mathbf{r}, t)\right\} + \text{c.c..} \tag{2.54b}$$

If we substitute Eq. (2.54) into Eq. (2.53) and take the time average of $\mathbf{j}_f(\mathbf{r}, t) \cdot \boldsymbol{\mathcal{E}}(\mathbf{r}, t)$ following Sec-

tion A.1, then we obtain

$$
\nabla \cdot \left\{ \frac{1}{2} \operatorname{Re} \left[\mathbf{E}(\mathbf{r}, t) \times \mathbf{H}^*(\mathbf{r}, t) \right] \right\}
$$

$$
+ \frac{1}{2} \operatorname{Re} \left\{ \varepsilon_0 \frac{\partial}{\partial \omega_0} \left[\omega_0 \, \varepsilon(\mathbf{r}, \omega_0) \right] \mathbf{E}^*(\mathbf{r}, t) \frac{\partial}{\partial t} \mathbf{E}(\mathbf{r}, t) + \mu_0 \frac{\partial}{\partial \omega_0} \left[\omega_0 \, \mu(\mathbf{r}, \omega_0) \right] \mathbf{H}^*(\mathbf{r}, t) \frac{\partial}{\partial t} \mathbf{H}(\mathbf{r}, t) \right\}
$$

$$
\cong -\frac{1}{2} \operatorname{Re} \left[\mathbf{j}_f(\mathbf{r}, t) \cdot \mathbf{E}^*(\mathbf{r}, t) \right] + \frac{\omega_0}{2} \operatorname{Re} \left[i \, \mathbf{P}(\mathbf{r}, t) \cdot \mathbf{E}^*(\mathbf{r}, t) \right]
$$

$$
+ \frac{\omega_0}{2} \operatorname{Re} \left[i \, \varepsilon_0 \varepsilon(\mathbf{r}, \omega_0) \, |\mathbf{E}(\mathbf{r}, t)|^2 + i \, \mu_0 \mu(\mathbf{r}, \omega_0) \, |\mathbf{H}(\mathbf{r}, t)|^2 \right], \quad (2.55)
$$

where we have assumed that $\mathbf{P}(\mathbf{r}, t)$ is sufficiently slowly varying that we can neglect $\partial \mathbf{P}/\partial t$ in Eq. (2.54a). The second and third terms on the right-hand side of this equation can be simplified using the identity $\operatorname{Re}(i z) = -\operatorname{Im}(z)$ for a complex number z. We assume that the laser host material is nearly transparent at frequency ω_0, so that $\operatorname{Re}[\epsilon] \gg \operatorname{Im}[\epsilon]$ and $\operatorname{Re}[\mu] \gg \operatorname{Im}[\mu]$. Therefore, the last term on the right-hand side represents the lowest-order contributions of the imaginary parts of $\varepsilon(\mathbf{r}, \omega_0)$ and $\mu(\mathbf{r}, \omega_0)$ (proportional to ω_0), and we will apply the slowly-varying envelope approximation and neglect terms proportional to $\operatorname{Im}[\epsilon]$ and $\operatorname{Im}[\mu]$ in the second term on the left-hand side of Eq. (2.55). With these simplifications, we define the macroscopic time-averaged Poynting vector

$$
\mathbf{S}(\mathbf{r}, t) \equiv \frac{1}{2} \operatorname{Re} \left[\mathbf{E}(\mathbf{r}, t) \times \mathbf{H}^*(\mathbf{r}, t) \right], \tag{2.56}
$$

and, using Eq. (2.13) as a guide, the macroscopic time-averaged energy density

$$
u(\mathbf{r}, t) \equiv \frac{1}{4} \left\{ \varepsilon_0 \frac{\partial}{\partial \omega_0} \operatorname{Re} \left[\omega_0 \, \varepsilon(\mathbf{r}, \omega_0) \right] |\mathbf{E}(\mathbf{r}, t)|^2 + \mu_0 \frac{\partial}{\partial \omega_0} \operatorname{Re} \left[\omega_0 \, \mu(\mathbf{r}, \omega_0) \right] |\mathbf{H}(\mathbf{r}, t)|^2 \right\}. \tag{2.57}
$$

Equation (2.55) therefore becomes

$$
\nabla \cdot \mathbf{S}(\mathbf{r}, t) + \frac{\partial}{\partial t} u(\mathbf{r}, t) \cong -\frac{1}{2} \operatorname{Re} \left[\mathbf{j}_f(\mathbf{r}, t) \cdot \mathbf{E}^*(\mathbf{r}, t) \right] - \frac{\omega_0}{2} \operatorname{Im} \left[\mathbf{P}(\mathbf{r}, t) \cdot \mathbf{E}^*(\mathbf{r}, t) \right]
$$
$$
- \frac{\omega_0}{2} \left[\varepsilon_0 \operatorname{Im} \left[\varepsilon(\mathbf{r}, \omega_0) \right] |\mathbf{E}(\mathbf{r}, t)|^2 + \mu_0 \operatorname{Im} \left[\mu(\mathbf{r}, \omega_0) \right] |\mathbf{H}(\mathbf{r}, t)|^2 \right]. \tag{2.58}
$$

This result is the generalization of Poynting's Theorem in vacuum, given by Eq. (2.16), to macroscopic media. From our derivation of Eq. (2.16), we recall that the first term on the right-hand side of Eq. (2.58) represents the time-averaged rate at which energy is being transferred from the free charged particles to the fields. Similarly, the second term describes the rate at which gain elements embedded in the host transfer energy to the fields, and will appear again later in our treatment of the Maxwell-Bloch laser evolution equations. The final term on the right-hand side is the rate at which energy is absorbed from the fields by the bound charges in the background host material and converted to heat. If some of the absorbed energy is converted by the host into (scattered) light, then the analysis becomes more complicated, since this radiation would have to be included in both $\mathbf{S}$ and u.

For many years, there has been some dispute over the precise expression for electromagnetic *momentum* density in the presence of bound charges [2], with the Minkowski form $\mathbf{D} \times \mathbf{B}$ [14] and the Abraham form $\mathbf{E} \times \mathbf{H}/c^2$ [15] remaining the most popular. Recently, this dilemma appears to have been resolved by Barnett [16], who has shown that both forms are correct, with the Abraham density representing the kinetic momentum and the Minkowski density describing the canonical momentum. The version of the Poynting Theorem given by Eq. (2.58) does not depend on considerations of electromagnetic field momentum, and should remain a useful guide when we build our density matrix evolution equations in later chapters.

2.2.3 Electromagnetic Wave Propagation in a Dispersive Medium

We now begin to model the behavior of optical-frequency electromagnetic fields in a volume containing a (generally) inhomogeneous dispersive medium. As we shall soon discover, considerations of the physics of the most common laser amplifier host materials will allow us to make simplifying assumptions that in turn cause the laser evolution equations to become analytically and numerically tractable. Again focusing on the characteristics of nearly-harmonic fields, we begin by taking the Fourier transform of macroscopic Maxwell equations given by Eq. (2.34) and then applying Eq. (A.17) to obtain equations describing the frequency-domain slowly-varying complex field amplitude functions:

$$\nabla \cdot \mathbf{D}(\mathbf{r}, \omega) = \rho_{\omega_0}(\mathbf{r}, \omega) \tag{2.59a}$$

$$\nabla \cdot \mathbf{B}(\mathbf{r}, \omega) = 0 \tag{2.59b}$$

$$\nabla \times \mathbf{E}(\mathbf{r}, \omega) - i\,(\omega_0 + \omega)\,\mathbf{B}(\mathbf{r}, \omega) = 0 \tag{2.59c}$$

$$\nabla \times \mathbf{H}(\mathbf{r}, \omega) + i\,(\omega_0 + \omega)\,\mathbf{D}(\mathbf{r}, \omega) = \mathbf{j}_f(\mathbf{r}, \omega) - i\,(\omega_0 + \omega)\,\mathbf{P}(\mathbf{r}, \omega) \tag{2.59d}$$

where $\mathbf{D}(\mathbf{r}, \omega)$ is given by Eq. (2.41), $\mathbf{B}(\mathbf{r}, \omega)$ is given by Eq. (2.49), and $\rho_{\omega_0}(\mathbf{r}, \omega)$ is the Fourier transform of a slowly-varying complex amplitude function defined such that $\rho_f(\mathbf{r}, t) \equiv \mathrm{Re}[e^{-i\omega_0 t}\rho_{\omega_0}(\mathbf{r}, t)]$.

So that we may focus on modeling *efficient* laser designs, we will continue to assume that the laser host material is nearly transparent, so that $\mathrm{Re}[\varepsilon(\mathbf{r}, \omega_0)] \gg \mathrm{Im}[\varepsilon(\mathbf{r}, \omega_0)]$ and $\mathrm{Re}[\mu(\mathbf{r}, \omega_0)] \gg \mathrm{Im}[\mu(\mathbf{r}, \omega_0)]$. In addition, we wish to minimize the power dissipated by interactions between the laser electric field and any free charges, so we assume that the laser resonator has been designed so that the free charge $\rho_{\omega_0}(\mathbf{r}, \omega)$ can be ignored in Eq. (2.59a) and — by charge conservation as established using Eq. (2.34e) — the free current $\mathbf{j}_f(\mathbf{r}, \omega)$ can be ignored in Eq. (2.59d). If these assumptions hold, then we can rewrite Eq. (2.59) as

$$\nabla \cdot [\varepsilon(\mathbf{r}, \omega_0 + \omega)\,\mathbf{E}(\mathbf{r}, \omega)] = 0 \tag{2.60a}$$

$$\nabla \cdot [\mu(\mathbf{r}, \omega_0 + \omega)\,\mathbf{H}(\mathbf{r}, \omega)] = 0 \tag{2.60b}$$

$$\nabla \times \mathbf{E}(\mathbf{r}, \omega) - i\,\mu_0\,\mu(\mathbf{r}, \omega_0 + \omega)\,(\omega_0 + \omega)\mathbf{H}(\mathbf{r}, \omega) = 0 \tag{2.60c}$$

$$\nabla \times \mathbf{H}(\mathbf{r}, \omega) + i\,\varepsilon_0\,\varepsilon(\mathbf{r}, \omega_0 + \omega)\,(\omega_0 + \omega)\mathbf{E}(\mathbf{r}, \omega) = -i(\omega_0 + \omega)\mathbf{P}(\mathbf{r}, \omega) \tag{2.60d}$$

In this source-free case, the transversality constraints of the electric and magnetic field amplitudes are given by Eq. (2.60a), Eq. (2.60b), and Eq. (A.44) as

$$\nabla \cdot \mathbf{E}(\mathbf{r}, \omega) = \mathbf{E}(\mathbf{r}, \omega) \cdot \nabla \ln \varepsilon^{-1}(\mathbf{r}, \omega_0 + \omega), \text{ and} \tag{2.61a}$$

$$\nabla \cdot \mathbf{H}(\mathbf{r}, \omega) = \mathbf{H}(\mathbf{r}, \omega) \cdot \nabla \ln \mu^{-1}(\mathbf{r}, \omega_0 + \omega), \tag{2.61b}$$

$$\tag{2.61c}$$

since, for example, $-\varepsilon^{-1}\nabla\varepsilon = \nabla(\ln\varepsilon^{-1})$. We note in passing that taking the divergence of Eq. (2.60d) gives

$$\nabla \cdot \mathbf{P}(\mathbf{r}, \omega) \approx 0 \tag{2.62}$$

under the same assumptions that led to Eq. (2.60).

If we solve Eq. (2.60c) for $\mathbf{H}(\mathbf{r}, \omega)$, substitute the result into Eq. (2.60d), and then multiply through by $\mu(\mathbf{r}, \omega_0 + \omega)$, we obtain

$$\mu(\mathbf{r}, \omega_0 + \omega)\,\nabla \times \left[\mu^{-1}(\mathbf{r}, \omega_0 + \omega)\,\nabla \times \mathbf{E}(\mathbf{r}, \omega)\right]$$
$$- \left(\frac{\omega_0 + \omega}{c}\right)^2 \varepsilon(\mathbf{r}, \omega_0 + \omega)\,\mu(\mathbf{r}, \omega_0 + \omega)\,\mathbf{E}(\mathbf{r}, \omega)$$
$$= \mu_0\,(\omega_0 + \omega)^2\,\mu(\mathbf{r}, \omega_0 + \omega)\,\mathbf{P}(\mathbf{r}, \omega). \tag{2.63}$$

For the sake of analytic progress, we will now make several simplifying assumptions:

- In virtually all cases of practical interest, the relative permeability is unity, but we can safely assume that it does not depend on position, so that $\mu(\mathbf{r}, \omega) \equiv \mu(\omega)$.

- We will assume that the variation in the relative permittivity parallel to $\mathbf{E}(\mathbf{r}, \omega)$ is small enough that $\nabla \cdot \mathbf{E}(\mathbf{r}, \omega) \approx 0$ by Eq. (2.61a).

- We will ignore the small imaginary part of μ on the right-hand side of Eq. (2.63), as well as apply the temporal slowly-varying approximation , neglecting the first and second derivatives of $\mathbf{P}(\mathbf{r}, t)$. Therefore, $(\omega_0 + \omega)^2 \mu(\mathbf{r}, \omega_0 + \omega) \approx \omega_0^2 \mu(\omega_0)$.

Under these conditions, using Eq. (A.43), Eq. (2.63) becomes

$$\nabla^2 \mathbf{E}(\mathbf{r}, \omega) + \left(\frac{\omega_0 + \omega}{c}\right)^2 \varepsilon(\mathbf{r}, \omega_0 + \omega) \, \mu(\omega_0 + \omega) \, \mathbf{E}(\mathbf{r}, \omega) = -\mu_0 \, \omega_0^2 \, \mathrm{Re}\left[\mu(\omega_0)\right] \mathbf{P}(\mathbf{r}, \omega). \qquad (2.64)$$

Either Eq. (2.63) or Eq. (2.64) can be used to numerically analyze the spatiotemporal structure of the electric field given some macroscopic polarization $\mathbf{P}(\mathbf{r}, t)$. But we'll need to apply a few more simplifying assumptions to make the wave equation analytically tractable. Consider a region of space where the predominant direction of electromagnetic power flow is along the z-axis. We seek a separation of the electric field into a set of mode functions that allow us to distinguish the rapidly-varying behavior of the field due to propagation through the background material from the slowly-varying amplification by the quantum dipoles embedded in that material. To this end, we assume that *in the absence of laser gain* we can find a complex spatial mode function $\mathbf{U}(\mathbf{r})$, normalized so that $\mathbf{U}(\mathbf{0}) = 1$, to represent the spatial profile of the electric field $\mathbf{E}(\mathbf{r}, \omega)$ at any reference plane z as

$$\mathbf{E}(\mathbf{r}, \omega) \equiv e^{i\,\mathbf{k}(\omega_0)\cdot\mathbf{r}}\,\mathbf{U}(\mathbf{r})\,E(z, \omega), \qquad (2.65)$$

where $\mathbf{k}(\omega_0) \equiv \pm k(\omega_0)\hat{z}$ is a wavevector (with a magnitude k to be chosen later for convenience) that allows us to consider both forward and backward propagating fields. The idea here is to capture the rapidly varying behavior in the $\hat{z}$ direction, so that we can apply the slowly-varying approximations $|\partial \mathbf{U}(\mathbf{r})/\partial z| \ll k(\omega_0)|\mathbf{U}(\mathbf{r})|$, and $|\partial E(z, \omega)/\partial z| \ll k(\omega_0)|E(z, \omega)|$. Given this form of $\mathbf{E}(\mathbf{r}, \omega)$, we momentarily drop the space and frequency arguments and use Eq. (A.53) to obtain

$$\begin{aligned}
\nabla^2 \left(e^{i\mathbf{k}\cdot\mathbf{r}}\mathbf{U}E\right) &= e^{i\mathbf{k}\cdot\mathbf{r}}\left(\nabla^2 + i\,2\,\mathbf{k}\cdot\nabla - k^2\right)\mathbf{U}E \\
&\approx e^{i\mathbf{k}\cdot\mathbf{r}}\left[E\left(\nabla_\perp^2 + i\,2\,\mathbf{k}\cdot\nabla - k^2\right)\mathbf{U} + i\,2\,\mathbf{U}\mathbf{k}\cdot\nabla E\right],
\end{aligned} \qquad (2.66)$$

where in cartesian coordinates $\nabla_\perp = \hat{x}\,\partial/\partial x + \hat{y}\,\partial/\partial y$. Taken together, the form of Eq. (2.65) and the SVEA are known as the "paraxial approximation," as discussed in Section 2.1.3. The paraxial approximation is surprisingly effective in a wide variety of both free-space and guided applications where some degree of analytic understanding helps elucidate fundamental aspects of laser behavior. However, in laser resonator geometries with dielectric functions that vary so significantly in space that we cannot assume that the divergence of $\mathbf{E}(\mathbf{r}, \omega)$ is zero, or that the longitudinal variation of $\mathbf{E}(\mathbf{r}, \omega)$ is small compared to a physical wavelength, a numerical solution using either Eq. (2.64) or an even more general approach to Maxwell's equations is required [17].

Substitution of Eq. (2.65) and Eq. (2.66) into Eq. (2.64) yields

$$\begin{aligned}
\sum e^{i\mathbf{k}(\omega_0)\cdot\mathbf{r}} &\left\{ i\,2\,\mathbf{U}(\mathbf{r})\left[\mathbf{k}(\omega_0)\cdot\nabla\right]E(z, \omega) - k^2(\omega_0)\mathbf{U}(\mathbf{r})E(z, \omega) \right. \\
&+ \left[\mathbf{U}(\mathbf{r}) + i\,2\left[\mathbf{k}(\omega_0)\cdot\nabla\right]\mathbf{U}(\mathbf{r}) + \left(\frac{\omega_0 + \omega}{c}\right)^2 \varepsilon(\mathbf{r}, \omega_0 + \omega)\,\mu(\mathbf{r}, \omega_0 + \omega)\,\mathbf{U}(\mathbf{r})\right]E(z, \omega) \right\} \\
&= -\mu_0\,\omega_0^2\,\mu(\omega_0)\,\mathbf{P}(\mathbf{r}, \omega). \qquad (2.67)
\end{aligned}$$

In Chapter 8, we will show that — given particular spatial boundary conditions for the electric and magnetic fields — we can find both $\mathbf{U}(\mathbf{r})$ and a constant β that satisfy the eigenvalue equation

$$
\nabla_\perp^2 \mathbf{U}(\mathbf{r}) + i\,2\,[\mathbf{k}(\omega_0) \cdot \nabla]\,\mathbf{U}(\mathbf{r})
$$
$$
+ \left(\frac{\omega_0 + \omega}{c}\right)^2 \varepsilon(\mathbf{r}, \omega_0 + \omega)\,\mu(\omega_0 + \omega)\,\mathbf{U}(\mathbf{r}) = \beta^2(\omega_0 + \omega)\,\mathbf{U}(\mathbf{r}), \quad (2.68)
$$

so that Eq. (2.67) becomes

$$
e^{i\,\mathbf{k}(\omega_0)\cdot\mathbf{r}}\,\mathbf{U}(\mathbf{r})\left\{i\,2\,[\mathbf{k}(\omega_0)\cdot\nabla]\,E(z,\omega) + \left[\beta^2(\omega_0+\omega) - k^2(\omega_0)\right]E(z,\omega)\right\}
$$
$$
= -\mu_0\,\omega_0^2\,\mathrm{Re}\,[\mu(\omega_0)]\,\mathbf{P}(\mathbf{r},\omega). \quad (2.69)
$$

We now choose the magnitude of the *real* propagation vector to be

$$
k(\omega_0) \equiv \mathrm{Re}\,[\beta(\omega_0)]. \tag{2.70}
$$

If we assume that $\mathrm{Im}\,[\beta(\omega_0)] \ll \mathrm{Re}\,[\beta(\omega_0)]$, and we neglect dispersion in the small imaginary part of $\beta(\omega_0)$, then

$$
\beta^2(\omega_0+\omega) - \mathrm{Re}\,[\beta(\omega_0)]^2 \cong 2\,\mathrm{Re}\,[\beta(\omega_0)]\,\{\mathrm{Re}\,[\beta(\omega_0+\omega)] - \mathrm{Re}\,[\beta(\omega_0)] + i\,\mathrm{Im}\,[\beta(\omega_0)]\}
$$
$$
= 2\,\mathrm{Re}\,[\beta(\omega_0)]\left\{\sum_{j=1}^{\infty} \frac{\omega^j}{j!}\frac{d^j}{d\omega_0^j}\,\mathrm{Re}\,[\beta(\omega_0)] + i\,\mathrm{Im}\,[\beta(\omega_0)]\right\}
$$
$$
\equiv 2\,\frac{\omega\,\omega_0}{c^2}\,n(\omega_0)\,n'(\omega_0) + 2\,\frac{\omega_0}{c}\,n(\omega_0)\,\mathcal{D}(\omega_0,\omega)
$$
$$
+ i\,\frac{\omega_0}{c}\,n(\omega_0)\,\alpha(\omega_0), \tag{2.71}
$$

where we have defined the effective refractive index, the effective group index, the effective linear absorption coefficient, and the effective dispersion, respectively, as

$$
n(\omega_0) \equiv \frac{c}{\omega_0}\,\mathrm{Re}\,[\beta(\omega_0)], \tag{2.72}
$$
$$
n'(\omega_0) \equiv c\,\frac{\partial}{\partial\omega_0}\,\mathrm{Re}\,[\beta(\omega_0)], \tag{2.73}
$$
$$
\alpha(\omega_0) \equiv 2\,\mathrm{Im}\,[\beta(\omega_0)], \text{ and} \tag{2.74}
$$
$$
\mathcal{D}(\omega_0,\omega) \equiv \sum_{j=2}^{\infty}\frac{\omega^j}{j!}\frac{d^j}{d\omega_0^j}\,\mathrm{Re}\,[\beta(\omega_0)]. \tag{2.75}
$$

Our forward/backward wave equation is now

$$
e^{\pm i\,(\omega_0/c)\,n(\omega_0)\,z}\,\mathbf{U}(\mathbf{r})\left[\pm\frac{\partial}{\partial z}E(z,\omega) - i\,\frac{\omega}{c}\,n'(\omega_0)\,E(z,\omega) - i\,\mathcal{D}(\omega_0,\omega)\,E(z,\omega) + \frac{1}{2}\alpha(\omega_0)\,E(z,\omega)\right]
$$
$$
= i\,\frac{\omega_0}{2\,\epsilon_0\,c}\,\frac{\mathrm{Re}\,[\mu(\omega_0)]}{n(\omega_0)}\,\mathbf{P}(\mathbf{r},\omega). \quad (2.76)
$$

In practice, Eq. (2.68) will be satisfied by a set of eigenfunctions $\mathbf{U}_m(\mathbf{r})$ and eigenvalues $\beta_m(\omega_0+\omega)$. In the general case, we cannot guarantee that the eigenfunctions are mutually orthogonal, but we can often find a corresponding set of functions $\mathbf{U}_m^\dagger(\mathbf{r})$ that that satisfy the biorthogonality relationship

$$
\int_S d^2r\,\mathbf{U}_m^\dagger(\mathbf{r})\cdot\mathbf{U}_{m'}(\mathbf{r}) = \delta_{m,m'} \tag{2.77}
$$

over the reference plane S located at each values of z. In this case, we can attempt to expand $\mathbf{E}(\mathbf{r}, \omega)$ in the paraxial approximation as

$$\mathbf{E}(\mathbf{r}, \omega) = \sum_m \mathbf{E}_m(\mathbf{r}, \omega) \equiv \sum_m e^{i\,\mathbf{k}_m(\omega_0)\cdot\mathbf{r}}\,\mathbf{U}_m(\mathbf{r})\,E_m(z, \omega), \tag{2.78}$$

where, from Eq. (2.70) and Eq. (2.72), $|\mathbf{k}_m(\omega_0)| \equiv k_m(\omega_0) = (\omega_0/c)n_m(\omega_0)$. Adding the subscript m' to the left-hand side of Eq. (2.76), and then applying Eq. (2.77), we obtain

$$\pm \frac{\partial}{\partial z} E_m(z, \omega) - i\,\frac{\omega}{c}\,n'_m(\omega_0)\,E_m(z, \omega) - i\,\mathcal{D}(\omega_0, \omega)\,E_m(z, \omega) + \frac{1}{2}\alpha_m(\omega_0)\,E_m(z, \omega)$$

$$= i\,\frac{\omega_0}{2\,\epsilon_0\,c}\,\eta_m(\omega_0)\,e^{\mp i\,k_m(\omega_0)\,z} \int_S d^2 r\,\mathbf{U}_m^\dagger(\mathbf{r}) \cdot \mathbf{P}(\mathbf{r}, \omega), \tag{2.79}$$

where $\eta_m(\omega_0) \equiv \mathrm{Re}\,[\mu(\omega_0)]\,/n_m(\omega_0)$ is the effective characteristic dielectric impedance of transverse mode m.

In the unidirectional propagation case, we generally assume that we can expand $\mathbf{P}(\mathbf{r}, \omega)$ in a fashion similar to Eq. (2.78), and the leading factor of $e^{\mp i\,k_m(\omega_0)z}$ on the right-hand side of Eq. (2.79) can be absorbed by $\mathbf{P}(\mathbf{r}, \omega)$. But we cannot do so when the electromagnetic field is a coherent superposition of components propagating in both the positive and negative z directions, such as

$$E_m(z, \omega) = E_m^+(z, \omega)\,e^{+i\,k_m(\omega_0)\,z} + E_m^-(z, \omega)\,e^{-i\,k_m(\omega_0)\,z}. \tag{2.80}$$

As we shall see in Section 5.4, interference between these counterpropagating fields creates a rapidly-varying modulation of the gain in the laser medium, which results in a corresponding spatial fine structure in the macroscopic polarization. Since $E_m^\pm(z, \omega)$ remain slowly-varying, we can separate the wave equation into two equations — one for each direction — by taking the spatial average of Eq. (2.79) over a single physical wavelength $2\pi/k_m(\omega_0)$, and defining the polarization components

$$P_m^\pm(z, \omega) \equiv \frac{k_m(\omega_0)}{2\pi} \int_{z-\pi/k_m(\omega_0)}^{z+\pi/k_m(\omega_0)} dz'\,e^{\mp i\,k_m(\omega_0)\,z'} \int_S d^2 r\,\mathbf{U}_m^\dagger(\mathbf{r}') \cdot \mathbf{P}(\mathbf{r}', \omega), \tag{2.81}$$

where $\mathbf{r}' \equiv \{x, y, z'\}$. With this definition, Eq. (2.79) becomes

$$\pm \frac{\partial}{\partial z} E_m^\pm(z, \omega) - i\,\frac{\omega}{c}\,n'_m(\omega_0)\,E_m^\pm(z, \omega) - i\,\mathcal{D}(\omega_0, \omega)\,E_m^\pm(z, \omega) + \frac{1}{2}\alpha_m(\omega_0)\,E_m^\pm(z, \omega)$$

$$= i\,\frac{\omega_0}{2\,\epsilon_0\,c}\,\eta_m(\omega_0)\,P_m^\pm(z, \omega). \tag{2.82}$$

Finally, using Eq. (A.17), we can write our wave equation in the time domain as

$$\frac{\partial}{\partial t} E_m^\pm(z, t) \pm \frac{c}{n'_m(\omega_0)}\,\frac{\partial}{\partial z} E_m^\pm(z, t) - i\,\sum_{j=2}^\infty \frac{\mathcal{D}_j(\omega_0)}{j!}\left(i\,\frac{\partial}{\partial t}\right)^j E_m^\pm(z, t)$$

$$+ \frac{c}{2\,n'_m(\omega_0)}\,\alpha_m(\omega_0)\,E_m^\pm(z, t) = i\,\frac{\omega_0}{2\,\varepsilon_0}\,\frac{\eta_m(\omega_0)}{n'_m(\omega_0)}\,P_m^\pm(z, t), \tag{2.83}$$

where

$$\mathcal{D}_j(\omega_0) \equiv \frac{c}{n'_m(\omega_0)}\,\frac{d^j}{d\omega_0^j}\,\mathrm{Re}\,[\beta(\omega_0)]\,. \tag{2.84}$$

We will often drop the subscript m from this expression, and assume that the transverse spatial extent of $\mathbf{U}(\mathbf{r})$ is so large that we can approximate it by $\mathbf{U}(\mathbf{r}) \approx \hat{\epsilon}$, where $\hat{\epsilon}$ is the complex unit vector defined by Eq. (2.28). In the case of unidirectional propagation, this allows us to write the complex electric field and macroscopic polarization envelope functions as

$$\mathbf{E}(\mathbf{r}, \omega) \equiv \hat{\epsilon}\,e^{i\,k(\omega_0)z}\,E(z, \omega), \text{ and} \tag{2.85a}$$

$$\mathbf{P}(\mathbf{r}, \omega) \equiv \hat{\epsilon}\,e^{i\,k(\omega_0)z}\,P(z, \omega), \tag{2.85b}$$

This one-dimensional treatment is particularly effective when exploring fundamental phenomena in laser dynamics.

Given the approximations we've made to develop Eq. (2.82) and Eq. (2.83), let's transform Eq. (2.60c) to the time domain,

$$\nabla \times \mathbf{E}(\mathbf{r}, t) - i\mu_0 \mu \left(\omega_0 + i\frac{\partial}{\partial t}\right) \left(\omega_0 + i\frac{\partial}{\partial t}\right) \mathbf{H}(\mathbf{r}, t) = 0, \tag{2.86}$$

and calculate $\mathbf{H}(\mathbf{r}, t)$ to determine the Poynting vector $\mathbf{S}(\mathbf{r}, t)$ and energy density $u(\mathbf{r}, t)$ for our one-dimensional electromagnetic field in a region of space where $\varepsilon(z, \omega_0) \equiv \varepsilon(\omega_0)$. Assuming that the slowly-varying envelope approximation is valid in both the space and time domains, we neglect the term proportional to $\partial \mathbf{H}(\mathbf{r}, t)/\partial t$ and (consistent with the development of Poynting's Theorem in Section 2.2.2) the contribution of $\text{Im}[\varepsilon(\omega_0)]$ and $\text{Im}[\mu(\omega_0)]$, and using Eq. (A.45) we obtain for a forward-propagating field

$$\mathbf{H}(\mathbf{r}, t) = -\frac{i}{\mu_0 \, \text{Re}[\mu(\omega_0)]\omega_0} \nabla \times \mathbf{E}(\mathbf{r}, t) = \hat{z} \times \hat{\epsilon} \, e^{i k(\omega_0)z} H(z, t), \tag{2.87}$$

where

$$H(z, t) \equiv \frac{n(\omega_0)]}{\mu_0 c \, \text{Re}[\mu(\omega_0)]} E(z, t) = \frac{\varepsilon_0 c}{\eta(\omega_0)} E(z, t). \tag{2.88}$$

Therefore, substituting the right-hand side of Eq. (2.87) into Eq. (2.56), we find the one-dimensional Poynting vector

$$\mathbf{S}(z, t) = \frac{1}{2} \frac{\varepsilon_0 c}{\eta(\omega_0)} |E(z, t)|^2 \, \hat{z}. \tag{2.89}$$

Similarly, in a region of space where the general energy density defined by Eq. (2.57) leads to the one-dimensional quantity

$$u(z, t) = \frac{1}{2}\varepsilon_0 \frac{n'(\omega_0)}{\eta(\omega_0)} |E(z, t)|^2, \tag{2.90}$$

where in one dimension we note that $\beta(\omega_0) \approx \sqrt{\varepsilon(\omega_0)\mu(\omega_0)}$, and therefore

$$n'(\omega_0) = \frac{\partial}{\partial \omega_0} (\omega_0 \sqrt{\varepsilon\mu}) = \frac{1}{2}\sqrt{\frac{\mu}{\varepsilon}} \frac{\partial}{\partial \omega_0} (\omega_0\varepsilon) + \frac{1}{2}\sqrt{\frac{\varepsilon}{\mu}} \frac{\partial}{\partial \omega_0} (\omega_0\mu).$$

In this case, we have found that $|\mathbf{S}(z, t)| = v_g(z, \omega_0)u(z, t)$, where the velocity of energy flow

$$v_g(\omega_0) \equiv \frac{c}{n'(\omega_0)}$$

is the group velocity in the medium, consistent with our interpretation of the Poynting vector as a directed energy flux in Section 2.1.2.

As a simple application of Eq. (2.83), let's analyze the experiment shown in Fig. 2.2a, where a weak laser pulse with with an electric field $\mathcal{E}(\mathbf{r}, t)$ enters a block of dielectric material of length L that has no nonlinear macroscopic polarization $\mathbf{P}(\mathbf{r}, t)$. We assume that the crystal has effective refractive indices $n(\omega_0)$ and $n'(\omega_0)$, and linear absorption coefficient $\alpha(\omega_0)$, at the laser carrier frequency ω_0, as well as an intensity transmission T_0 at each interface. (In other words, if $\alpha = 0$, an input pulse entering the block at $z = 0$ with vacuum intensity $I \equiv |\mathbf{S}| = \varepsilon_0 c E^2/2$ would emerge from the block at $z = L$ with vacuum intensity $T_0^2 I$.) Inside the block, the wave equation is

$$\frac{\partial}{\partial z}E(z, \omega) - i\frac{\omega}{c} n'(\omega_0) E(z, \omega) + \frac{1}{2}\alpha(\omega_0) E(z, \omega) = 0, \tag{2.91}$$

which has the solution (including the intensity transmission coefficients of the block interfaces)

$$E(L, \omega) = T_0 \exp\left[i\frac{\omega}{c}n'(\omega_0)z - \frac{1}{2}\alpha(\omega_0)z\right] E(0, \omega). \tag{2.92}$$

(a) Schematic of the experiment

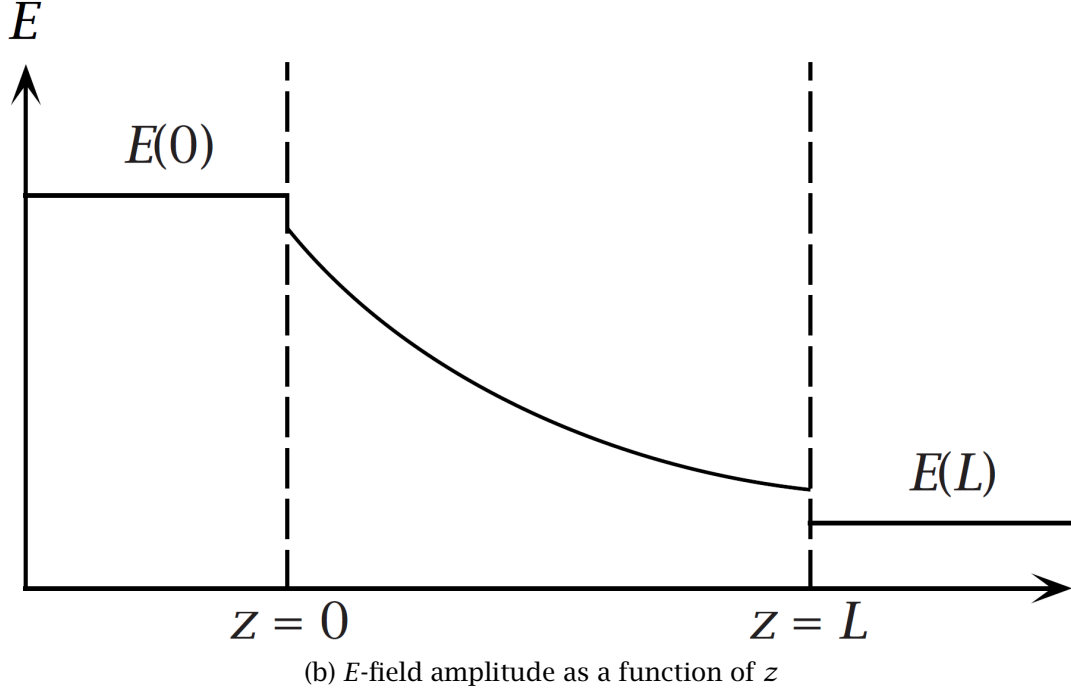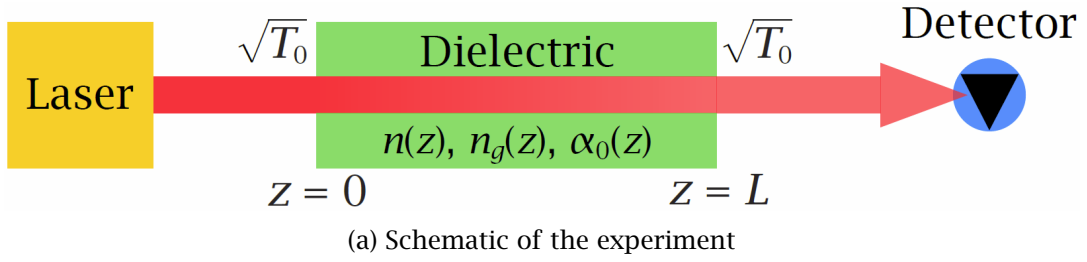(b) E-field amplitude as a function of z

Figure 2.2: (a) Schematic of a linear absorption experiment using a weak laser, an almost-transparent dielectric block, and a photodiode. The input face of the block is located at $z = 0$, the output face at $z = L$, and there is a small intensity loss $1 - T_0$ due to scattering and/or absorption at each interface. (b) Plot of the (real and positive) continuous-wave laser field amplitude $E(z)$ as a function of position.

If we define the group propagation time $\tau_g \equiv n'(\omega_0)/c$, and use the Fourier Shift Theorem Eq. (A.15), in the time domain we have

$$E\left(L, t\right) = T_0 \, \exp\left[-\frac{1}{2}\alpha(\omega_0)z\right] E\left(0, t - \tau_g\right). \tag{2.93}$$

Equation Eq. (2.93) is known as *Beer's Law*, and — when substituted into Eq. (2.85a) — describes the attenuation of an arbitrary input field due to linear absorption, and the delay due to propagation through the dielectric block at the group velocity $v_g(\omega_0) = c/n'(\omega_0)$. In Fig. 2.2b, we have plotted the field envelope function as a function of z for the case where α is real, positive, and constant, and the laser is "continuous-wave" (or steady state) so that $E(z,t) \equiv E(z)$.

2.2.4   Time Reversal in a Dispersive Medium

Our development of the scattering matrix representation of mirrors and other general two-port optical components in Section 4.1.2 relies on the behavior of the solutions to the macroscopic Maxwell equations under time-reversal symmetry [2]. Suppose that the source charge density $\rho_f(\mathbf{r}, t)$ and current

$j_f(\mathbf{r}, t)$ are specified in a particular volume of space over some time interval $\{-\tau/2, \tau/2\}$[2.5], and that we have solved the macroscopic Maxwell equations for the fields $\boldsymbol{\mathcal{E}}(\mathbf{r}, t)$, $\boldsymbol{\mathcal{H}}(\mathbf{r}, t)$, $\boldsymbol{\mathcal{D}}(\mathbf{r}, t)$, and $\boldsymbol{\mathcal{B}}(\mathbf{r}, t)$ given appropriate boundary and initial conditions. Applying the time-reversal transformation corresponds to "running the movie backwards:" we *reverse* the directions of all currents, take the values of the *forward* fields at the time $\tau/2$ as their initial values at the reversed initial time $-\tau/2$, and then evolve the *backward* fields over a time interval of duration τ. How do we express the values of the time-reversed electromagnetic fields in terms of the original forward solutions? Naively, if we treat both time arguments simply as labels, we might expect the reversed electric field $\boldsymbol{\mathcal{E}}_T(\mathbf{r}, t)$ to have the values $\boldsymbol{\mathcal{E}}_T(\mathbf{r}, -\tau/2) = \boldsymbol{\mathcal{E}}(\mathbf{r}, \tau/2)$ and $\boldsymbol{\mathcal{E}}_T(\mathbf{r}, \tau/2) = \boldsymbol{\mathcal{E}}(\mathbf{r}, -\tau/2)$, implying that

$$\boldsymbol{\mathcal{E}}_T(\mathbf{r}, t) = \boldsymbol{\mathcal{E}}(\mathbf{r}, -t). \tag{2.94}$$

This approach is in fact correct for the electric field, but in general we must be guided by the invariance of Maxwell's equations under time reversal: Eq. (2.34) must retain the same mathematical form, regardless of the direction of the flow of time. For example, we expect charge — and, therefore, the free charge density $\rho_f(\mathbf{r}, t)$ — to be a scalar under the time reversal operation $t \longrightarrow -t$, and since the directions of the particle velocities $\mathbf{v}_n(t)$ in Eq. (2.1b) will change sign under the same operation, we anticipate that all currents will reverse direction. This intuition is consistent with the transformation properties of the macroscopic continuity equation given by Eq. (2.34e), since $\partial/\partial t \longrightarrow -\partial/\partial t$; hence

$$\rho_T(\mathbf{r}, t) = \rho_f(\mathbf{r}, -t), \text{ and} \tag{2.95a}$$

$$\boldsymbol{j}_T(\mathbf{r}, t) = -\boldsymbol{j}_f(\mathbf{r}, -t). \tag{2.95b}$$

Therefore, from Eq. (2.34a), we deduce that $\boldsymbol{\mathcal{D}}_T(\mathbf{r}, t) = \boldsymbol{\mathcal{D}}(\mathbf{r}, -t)$, and, from Eq. (2.34d), that $\boldsymbol{\mathcal{H}}_T(\mathbf{r}, t) = -\boldsymbol{\mathcal{H}}(\mathbf{r}, -t)$. Applying the same reasoning to Eq. (2.5), we find that $\boldsymbol{\mathcal{B}}_T(\mathbf{r}, t) = -\boldsymbol{\mathcal{B}}(\mathbf{r}, -t)$, and from Eq. (2.35) we conclude that $\boldsymbol{\mathcal{P}}_T(\mathbf{r}, t) = \boldsymbol{\mathcal{P}}(\mathbf{r}, -t)$ and $\boldsymbol{\mathcal{M}}_T(\mathbf{r}, t) = -\boldsymbol{\mathcal{M}}(\mathbf{r}, -t)$. However, time-reversal considerations of background materials with dissipative losses are quite subtle, particularly in the formalism described by Eq. (2.36) where we have separated the polarization into linear background and nonlinear gain contributions. Therefore, in Section 4.1.2 we will limit our discussion of the symmetries of the scattering matrix to the case where $\text{Im}[\epsilon((\omega_0))\mu((\omega_0))] = 0$.

We now examine the implications of the time-reversal transformation for the envelope functions $\mathbf{E}(\mathbf{r}, t)$ and $\mathbf{H}(\mathbf{r}, t)$, as well as their Fourier transforms. Given the expansion of the nearly harmonic real electric field described by Eq. (2.9), and the symmetry condition established by Eq. (2.94), we write $\boldsymbol{\mathcal{E}}_T(\mathbf{r}, t)$ as

$$\begin{aligned}
\boldsymbol{\mathcal{E}}_T(\mathbf{r}, t) &\equiv \frac{e^{-i\omega_0 t}}{2} \mathbf{E}_T(\mathbf{r}, t) + \frac{e^{+i\omega_0 t}}{2} \mathbf{E}_T^*(\mathbf{r}, t) \\
&= \boldsymbol{\mathcal{E}}(\mathbf{r}, -t) \\
&= \frac{e^{-i\omega_0 t}}{2} \mathbf{E}^*(\mathbf{r}, -t) + \frac{e^{+i\omega_0 t}}{2} \mathbf{E}(\mathbf{r}, -t),
\end{aligned} \tag{2.96}$$

so that a direct comparison of the coefficients of terms with similarly signed optical carrier frequencies allows us to make the identification

$$\mathbf{E}_T(\mathbf{r}, t) = \mathbf{E}^*(\mathbf{r}, -t). \tag{2.97}$$

Note that this result is completely consistent with the simple one-dimensional envelope function given

---

[2.5]Here we take the time interval to be symmetric about the origin of the time axis for the sake of algebraic simplicity, but the main results that we present in this section do not depend on the way that we label the time axis.

by Eq. (2.85a) in the time domain, since

$$
\begin{aligned}
\boldsymbol{\mathcal{E}}_T(\mathbf{r}, t) &\equiv \frac{e^{-i\omega_0 t}}{2} \mathbf{E}_T(\mathbf{r}, t) + \text{c.c.} \\
&= \frac{e^{-i\omega_0 t}}{2} \mathbf{E}^*(\mathbf{r}, -t) + \text{c.c.} \\
&= \frac{1}{2}\hat{\epsilon} \exp\left\{-i\frac{\omega_0}{c}\left[n(\omega_0)z + ct\right]\right\} E^*(z, -t) + \text{c.c.}
\end{aligned}
\tag{2.98}
$$

corresponds to a real electric field with carrier frequency ω_0 propagating parallel to $-\hat{z}$. Next, following the same line of reasoning that led to Eq. (2.39), the Fourier transform of $\mathbf{E}_T(\mathbf{r}, t)$ is

$$
\mathbf{E}_T(\mathbf{r}, \omega) = \int_{-\infty}^{\infty} dt\, e^{+i\omega t} \mathbf{E}_T(\mathbf{r}, t) = \int_{-\infty}^{\infty} dt\, e^{+i\omega t} \mathbf{E}^*(\mathbf{r}, -t) = \mathbf{E}^*(\mathbf{r}, \omega).
\tag{2.99}
$$

Given that $\boldsymbol{\mathcal{H}}_T(\mathbf{r}, t) = -\boldsymbol{\mathcal{H}}(\mathbf{r}, -t)$, the same approach to the time-reversed magnetic field amplitude function $\mathbf{H}_T(\mathbf{r}, t)$ yields

$$
\mathbf{H}_T(\mathbf{r}, t) = -\mathbf{H}^*(\mathbf{r}, -t), \text{ and} \tag{2.100a}
$$
$$
\mathbf{H}_T(\mathbf{r}, \omega) = -\mathbf{H}^*(\mathbf{r}, \omega). \tag{2.100b}
$$

The time-reversed Poynting vector is related to that of the forward-propagation solution by

$$
\begin{aligned}
\mathbf{S}_T(\mathbf{r}, t) &\equiv \frac{1}{2}\,\text{Re}\left[\mathbf{E}_T(\mathbf{r}, t) \times \mathbf{H}_T^*(\mathbf{r}, t)\right] \\
&= -\frac{1}{2}\,\text{Re}\left[\mathbf{E}^*(\mathbf{r}, -t) \times \mathbf{H}(\mathbf{r}, -t)\right] \\
&= -\frac{1}{2}\,\text{Re}\left[\mathbf{E}(\mathbf{r}, -t) \times \mathbf{H}^*(\mathbf{r}, -t)\right] \\
&= -\mathbf{S}(\mathbf{r}, -t),
\end{aligned}
\tag{2.101}
$$

since $\text{Re}(z) = \text{Re}(z^*)$ for any complex number z. Therefore, as a result of the behavior of the magnetic field under the time-reversal operation, the energy flux reverses direction (as expected).

Chapter 3

Laser Gain Media

3.1 The Density Matrix Equations of Motion

3.1.1 The von Neumann Evolution Equations

We use a specified semiclassical Hamiltonian operator $\hat{H}(t)$ and an appropriate set of initial conditions to solve the von Neumann density operator equation of motion [1]

$$\frac{d}{dt}\hat{\rho}(t) = -\Gamma[\hat{\rho}(t)] - \frac{i}{\hbar}\left[\hat{H}(t), \hat{\rho}(t)\right],\tag{3.1}$$

where we have incorporated damping in an open quantum system through the decoherence operator $\Gamma[\hat{\rho}(t)]$. We adopt the Lindblad form [18, 19] of $\Gamma[\hat{\rho}]$, given by

$$\Gamma[\hat{\rho}] = \sum_m \gamma_m \left[\frac{1}{2}\left(\hat{\rho}\,\hat{L}_m^\dagger\,\hat{L}_m + \hat{L}_m^\dagger\,\hat{L}_m\,\hat{\rho}\right) - \hat{L}_m\,\hat{\rho}\,\hat{L}_m^\dagger\right],\tag{3.2}$$

to preserve both positive probabilities and a positive semidefinite density operator. The Lindblad operator $\hat{L}_m$ represents a general dissipative process occurring at the rate γ_m. For example, we can describe the decay of the state $|a\rangle$ to the state $|b\rangle$ due to spontaneous emission at the rate γ_{ab} using the lowering operator

$$\hat{L}'_{ab} = \hat{\sigma}_{ab} \equiv |a\rangle\langle b|\tag{3.3}$$

and pure dephasing of the state $|a\rangle$ at the rate γ_a (e.g., due to atomic collisions or phonon scattering) using the operator

$$\hat{L}_a \equiv \frac{1}{\sqrt{2}}\left(\hat{1} - 2\hat{\sigma}_{aa}\right),\tag{3.4}$$

where $\hat{1} \equiv \sum_j \hat{\sigma}_{jj}$ is the identity operator.

3.1.2 The Liouville Evolution Equations

Although abstract calculations involving the temporal evolution of the density operator are often performed using Eq. (3.1), the $n \times n$ square matrix representation of $\hat{\rho}(t)$ is inconvenient when we use mathematical software packages to solve the von Neumann equation. For example, functions that numerically solve temporal coupled ordinary differential equations often specify that the initial values (and, therefore, the solutions at a particular time) be supplied as elements of a column vector. Referring to Eq. (3.1) and Eq. (3.2), we see that there are three different operator orderings involving $\hat{\rho}$ that we would like to recast into a form where the density matrix elements are rewritten as a column

vector ρ that has n^2 elements:

$$\left(\hat{A}\,\hat{\rho}\right)_{jk} = \sum_{\ell} \hat{A}_{j\ell}\,\hat{\rho}_{\ell k} = \sum_{\ell m} \hat{A}_{j\ell}\,\delta_{mk}\,\hat{\rho}_{\ell m}, \tag{3.5a}$$

$$\left(\hat{\rho}\,\hat{B}\right)_{jk} = \sum_{m} \hat{\rho}_{jm}\,\hat{B}_{mk} = \sum_{\ell m} \delta_{j\ell}\,\hat{B}_{mk}\,\hat{\rho}_{\ell m}, \text{ and} \tag{3.5b}$$

$$\left(\hat{A}\,\hat{\rho}\,\hat{B}\right)_{jk} = \sum_{\ell m} \hat{A}_{j\ell}\,\hat{B}_{mk}\hat{\rho}_{\ell m}. \tag{3.5c}$$

Note that the pair of integers ℓ and m—which take the values 1 through n—will enumerate all of the elements of the density matrix in the order in which the terms of the sum are taken. If we choose m as the "rapidly" varying index, then we can make the associations

$$\hat{A}\,\hat{\rho} \longrightarrow \left(\hat{A} \otimes \hat{1}_n\right)\rho, \tag{3.6a}$$

$$\hat{\rho}\,\hat{B} \longrightarrow \left(\hat{1}_n \otimes \hat{B}^{\mathrm{T}}\right)\rho, \text{ and} \tag{3.6b}$$

$$\hat{A}\,\hat{\rho}\,\hat{B} \longrightarrow \left(\hat{A} \otimes \hat{B}^{\mathrm{T}}\right)\rho, \tag{3.6c}$$

where $\hat{1}_n$ is the $n \times n$ matrix representation of the identity operator and the symbol "$\otimes$" represents the Kronecker product. In Mathematica, the $n^2 \times n^2$ product of the two $n \times n$ matrices A and B^{T} is implemented as KroneckerProduct[A, Transpose[B]], while the same operation in MATLAB is kron(A,B.').

In this vector representation of ρ, we rewrite Eq. (3.1) as a Liouville equation of motion in the form

$$\frac{d}{dt}\rho(t) = -\left[\mathcal{L}_\Gamma + \frac{i}{\hbar}\,\mathcal{L}_H(t)\right]\rho(t), \tag{3.7}$$

where

$$\mathcal{L}_\Gamma = \sum_m \gamma_m \left\{ \frac{1}{2}\left[\left(\hat{L}_m^\dagger\,\hat{L}_m\right) \otimes \hat{1}_n + \hat{1}_n \otimes \left(\hat{L}_m^\dagger\,\hat{L}_m\right)^{\mathrm{T}}\right] + \hat{L}_m \otimes \hat{L}_m^*\right\}, \text{ and} \tag{3.8a}$$

$$\mathcal{L}_H(t) = \hat{H}(t) \otimes \hat{1}_n - \hat{1}_n \otimes \hat{H}^{\mathrm{T}}(t). \tag{3.8b}$$

3.2 Rate Equation Representations of Multi-Level Systems

3.2.1 Two-Level Systems

For example, in the case $j = 2$, we have depopulation of level a to level b at the rate γ'_{ab} with the corresponding Lindblad operator

$$L'_{ab} \equiv |a\rangle\langle b| = \hat{\sigma}_{ab} = \begin{bmatrix} 0 & 0 \\ 0 & 1 \end{bmatrix} \tag{3.9}$$

and dephasing of levels a and b[3.1] at the rates γ''_{aa} and γ''_{bb}, respectively, with the operators

$$L''_{aa} \equiv \frac{1}{\sqrt{2}}\left(\hat{1} - 2\hat{\sigma}_{aa}\right) = \frac{1}{\sqrt{2}}\left(-\sigma_{aa} + \sigma_{bb}\right) = \frac{1}{\sqrt{2}}\begin{bmatrix} -1 & 0 \\ 0 & 1 \end{bmatrix}, \text{ and} \tag{3.10a}$$

$$L''_{bb} \equiv \frac{1}{\sqrt{2}}\left(\hat{1} - 2\hat{\sigma}_{bb}\right) = \frac{1}{\sqrt{2}}\left(\sigma_{aa} - \sigma_{bb}\right) = \frac{1}{\sqrt{2}}\begin{bmatrix} 1 & 0 \\ 0 & -1 \end{bmatrix}. \tag{3.10b}$$

[3.1]In the case of the strictly two-level atom, we do not need to model dephasing of the lower — or "ground" — state, since we can use the phase of level b as a reference. However, in our description of the ideal four-level laser gain medium below, we'll rely on the general dephasing model of the laser levels used in the discussion here.

Using Eq. (3.2) to compute the von Neumann form of the damping operator, we obtain

$$\Gamma[\rho] = \begin{bmatrix} \gamma_{ab}\rho_{aa} & \gamma_{\perp}\rho_{ab} \\ \gamma_{\perp}\rho_{ba} & -\gamma_{ab}\rho_{aa} \end{bmatrix}, \tag{3.11}$$

where

$$\gamma_{ab} \equiv \gamma''_{aa}, \text{ and} \tag{3.12a}$$

$$\gamma_{\perp} \equiv \frac{1}{2}\gamma'_{ab} + \gamma''_{aa} + \gamma''_{bb}. \tag{3.12b}$$

The corresponding Liouville superoperator is derived from Eq. (3.8a) as

$$\mathcal{L}_{\Gamma} = \begin{bmatrix} \gamma_{ab} & 0 & 0 & 0 \\ 0 & \gamma_{\perp} & 0 & 0 \\ 0 & 0 & \gamma_{\perp} & 0 \\ -\gamma_{ab} & 0 & 0 & 0 \end{bmatrix}. \tag{3.13}$$

$$\hat{H}(t) = \begin{bmatrix} \hbar\omega_a & V_{ab}(t) \\ V_{ba}(t) & \hbar\omega_b \end{bmatrix}. \tag{3.14}$$

$$\mathcal{L}_H(t) = \begin{bmatrix} 0 & -V_{ab}^*(t) & V_{ab}(t) & 0 \\ -V_{ab}(t) & \hbar\omega_{ab} & 0 & V_{ab}(t) \\ V_{ab}^*(t) & 0 & -\hbar\omega_{ab} & -V_{ab}^*(t) \\ 0 & V_{ab}^*(t) & -V_{ab}(t) & 0 \end{bmatrix}. \tag{3.15}$$

$$-\left[\mathcal{L}_{\Gamma} + \frac{i}{\hbar}\mathcal{L}_H(t)\right] = \begin{bmatrix} -\gamma_{ab} & \frac{i}{\hbar}V_{ab}^*(t) & -\frac{i}{\hbar}V_{ab}(t) & 0 \\ \frac{i}{\hbar}V_{ab}(t) & -\gamma_{\perp} - i\omega_{ab} & 0 & -\frac{i}{\hbar}V_{ab}(t) \\ -\frac{i}{\hbar}V_{ab}^*(t) & 0 & -\gamma_{\perp} + i\omega_{ab} & \frac{i}{\hbar}V_{ab}^*(t) \\ \gamma_{ab} & -\frac{i}{\hbar}V_{ab}^*(t) & \frac{i}{\hbar}V_{ab}(t) & 0 \end{bmatrix}. \tag{3.16}$$

$$\frac{d}{dt}\rho_{aa}(t) = -\gamma_{ab}\rho_{aa}(t) + \frac{i}{\hbar}\left[V_{ab}^*(t)\rho_{ab}(t) - \text{c.c.}\right], \tag{3.17a}$$

$$\frac{d}{dt}\rho_{bb}(t) = +\gamma_{ab}\rho_{aa}(t) - \frac{i}{\hbar}\left[V_{ab}^*(t)\rho_{ab}(t) - \text{c.c.}\right], \text{ and} \tag{3.17b}$$

$$\frac{d}{dt}\rho_{ab}(t) = -i(\omega_{ab} - i\gamma_{\perp})\rho_{ab}(t) + \frac{i}{\hbar}V_{ab}(t)\left[\rho_{aa}(t) - \rho_{bb}(t)\right]. \tag{3.17c}$$

If we multiply both sides of Eq. (3.17c) by $e^{i(\omega_{ab} - i\gamma_{\perp})t}$, we can formally integrate the equation of motion for $\rho_{ab}(t)$ to obtain

$$\rho_{ab}(t) = \frac{i}{\hbar}e^{-i(\omega_{ab} - i\gamma_{\perp})t}\int_{-\infty}^{t}dt'\, e^{i(\omega_{ab} - i\gamma_{\perp})t'}\,V_{ab}(t')\left[\rho_{aa}(t') - \rho_{bb}(t')\right]. \tag{3.18}$$

Suppose that we can write the matrix element of the interaction potential energy as

$$V_{ab}(t) \equiv V_{ab}^+(t)e^{-i\omega_0 t} + V_{ab}^-(t)e^{i\omega_0 t}, \tag{3.19}$$

where both $V_{ab}^+(t)$ and $V_{ab}^-(t)$ vary slowly compared to $e^{\mp i\omega_0 t}$, and $\omega_0 \approx \omega_{ab}$. If we substitute Eq. (3.19) into Eq. (3.18), then we see that we have two integrands contributing to $\rho_{ab}(t)$, with time dependencies $e^{i(\omega_{ab} \pm \omega_0 - i\gamma_{\perp})t}$. To understand their relative impact on the final result, let's consider the case where $V_{ab}^{\pm}$, ρ_{aa}, and ρ_{bb} do not depend on time (or, at least, are slowly varying compared to $e^{\pm\gamma_{\perp}t}$). Then Eq. (3.18) immediately gives

$$\rho_{ab}(t) = \frac{1}{\hbar}\left[\frac{V_{ab}^+}{\omega_0 - \omega_{ab} + i\gamma_{\perp}}e^{-i\omega_0 t} - \frac{V_{ab}^-}{\omega_0 + \omega_{ab} - i\gamma_{\perp}}e^{i\omega_0 t}\right](\rho_{aa} - \rho_{bb}). \tag{3.20}$$

When studying laser physics, ω_0 and ω_{ab} are typically optical frequencies with values of 10^{14}–10^{15} Hertz, while the dephasing rate $\gamma_\perp$ is at least several orders of magnitude smaller. Therefore, the first term in Eq. (3.20) is generally far larger than the second, and in practice we can usually neglect the term proportional to $e^{i\omega_0 t}$ altogether. This approach is known as the *rotating-wave approximation*, and is equivalent to writing the interaction potential energy as

$$V_{ab}(t) \equiv V_{ab}^+(t)e^{-i\omega_0 t}. \tag{3.21}$$

We make one more simplification to the two-level density matrix equations of motion to capture the remaining $e^{-i\omega_0 t}$ time dependence in Eq. (3.20). We move into a co-rotating frame by defining

$$\rho_{ab}(t) \equiv \tilde{\rho}_{ab}(t)e^{-i\omega_0 t}. \tag{3.22}$$

When we substitute this expression into Eq. (3.17), we obtain

$$\frac{d}{dt}\rho_{aa}(t) = -\gamma_{ab}\,\rho_{aa}(t) + \frac{i}{\hbar}\left[V_{ab}^{+*}(t)\tilde{\rho}_{ab}(t) - \text{c.c.}\right], \tag{3.23a}$$

$$\frac{d}{dt}\rho_{bb}(t) = +\gamma_{ab}\,\rho_{aa}(t) - \frac{i}{\hbar}\left[V_{ab}^{+*}(t)\tilde{\rho}_{ab}(t) - \text{c.c.}\right], \text{ and} \tag{3.23b}$$

$$\frac{d}{dt}\tilde{\rho}_{ab}(t) = i\,(\omega_0 - \omega_{ab} + i\gamma_\perp)\,\tilde{\rho}_{ab}(t) + \frac{i}{\hbar}V_{ab}^+(t)\left[\rho_{aa}(t) - \rho_{bb}(t)\right]. \tag{3.23c}$$

or

$$\frac{d}{dt}\rho_{aa}(t) = -\gamma_{ab}\,\rho_{aa}(t) - \frac{2}{\hbar}\,\text{Im}\left[V_{ab}^{+*}(t)\tilde{\rho}_{ab}(t)\right], \tag{3.24a}$$

$$\frac{d}{dt}\rho_{bb}(t) = +\gamma_{ab}\,\rho_{aa}(t) + \frac{2}{\hbar}\,\text{Im}\left[V_{ab}^{+*}(t)\tilde{\rho}_{ab}(t)\right], \text{ and} \tag{3.24b}$$

$$\frac{d}{dt}\tilde{\rho}_{ab}(t) = i\,(\omega_0 - \omega_{ab} + i\gamma_\perp)\,\tilde{\rho}_{ab}(t) + \frac{i}{\hbar}V_{ab}^+(t)\left[\rho_{aa}(t) - \rho_{bb}(t)\right]. \tag{3.24c}$$

We define the semiclassical radiative electric dipole interaction Hamiltonian as

$$\hat{V}(\mathbf{r}, t) = -\hat{\mathbf{d}} \cdot \boldsymbol{\mathcal{E}}(\mathbf{r}, t) \tag{3.25}$$

where the dipole moment operator $\hat{\mathbf{d}} = e\,\hat{\mathbf{r}}$, and $e = -|e|$ is the charge of the electron. Following Eq. (2.9), we define $\boldsymbol{\mathcal{E}}(\mathbf{r}, t)$ as

$$\boldsymbol{\mathcal{E}}(\mathbf{r}, t) \equiv \frac{e^{-i\omega_0 t}}{2}\,\hat{\epsilon}\tilde{E}(\mathbf{r}, t) + \text{c.c.}, \tag{3.26}$$

where $\tilde{E}(\mathbf{r}, t)$ is a complex scalar electric field amplitude that varies rapidly in space but slowly in time. We assume that the electric dipole approximation is valid, so that $\tilde{E}(\mathbf{r}, t)$ is essentially constant over the extent of the electronic wave function, and therefore $\langle a|\hat{\mathbf{d}}\,\tilde{E}(\mathbf{r}, t)|b\rangle = \mathbf{d}_{ab}\tilde{E}(\mathbf{r}, t)$, where $\mathbf{d}_{ab} \equiv \langle a|\hat{\mathbf{d}}|b\rangle$.

$$V_{ab}^+(\mathbf{r}, t) == -\frac{1}{2}\,\hat{\epsilon}\cdot\langle a|\hat{\mathbf{d}}|b\rangle\tilde{E}(\mathbf{r}, t) \equiv -\frac{d_{ab}}{2}\,\tilde{E}(\mathbf{r}, t), \tag{3.27}$$

where $d_{ab} = d_{ba}^* \equiv \hat{\epsilon}\cdot\langle a|\hat{\mathbf{d}}|b\rangle$.

3.2.1.1   Level Populations and the Macroscopic Polarization

Let $\mathcal{N}$ represent the density of gain dipoles per unit volume[3.2] in the laser amplifier. Then we define the population densities of the two energy levels a and b as

$$N_a(\mathbf{r}, t) \equiv \mathcal{N}\rho_{aa}(\mathbf{r}, t) \qquad \text{and} \qquad N_b(\mathbf{r}, t) \equiv \mathcal{N}\rho_{bb}(\mathbf{r}, t). \tag{3.28}$$

[3.2]Here we presume that the distribution of dipoles is uniform throughout the gain volume, but it is straightforward to relax this assumption and allow $\mathcal{N}$ to vary with $\mathbf{r}$.

If we multiply Eq. (3.24a) and Eq. (3.24b) by $\mathcal{N}$ and apply Eq. (3.27), we obtain

$$\frac{\partial}{\partial t} N_a(\mathbf{r}, t) = -\gamma_{ab} N_a(\mathbf{r}, t) + \frac{2}{\hbar} \operatorname{Im}\left[\mathcal{N} d_{ba} \tilde{\rho}_{ab}(\mathbf{r}, t) \tilde{E}^*(\mathbf{r}, t) \right], \text{ and} \qquad (3.29a)$$

$$\frac{\partial}{\partial t} N_b(\mathbf{r}, t) = +\gamma_{ab} N_a(\mathbf{r}, t) - \frac{2}{\hbar} \operatorname{Im}\left[\mathcal{N} d_{ba} \tilde{\rho}_{ab}(\mathbf{r}, t) \tilde{E}^*(\mathbf{r}, t) \right], \qquad (3.29b)$$

where we have used $d_{ab}^* = d_{ba}$.

We define the macroscopic polarization in terms of the expectation value of the microscopic electric dipole moment operator as

$$
\begin{aligned}
\boldsymbol{\mathcal{P}}(\mathbf{r}, t) &\equiv \frac{e^{-i\omega_0 t}}{2} \mathbf{P}(\mathbf{r}, t) + \text{c.c.} \\
&= \mathcal{N} \operatorname{Tr}\left[\hat{\rho}(\mathbf{r}, t) \hat{\mathbf{d}} \right] \\
&= \mathcal{N} \left[\mathbf{d}_{ba} \rho_{ab}(\mathbf{r}, t) + \mathbf{d}_{ab} \rho_{ba}(\mathbf{r}, t) \right] \\
&= \mathcal{N} \mathbf{d}_{ba} \tilde{\rho}_{ab}(\mathbf{r}, t) e^{-i\omega_0 t} + \text{c.c.},
\end{aligned}
\qquad (3.30)
$$

Hence, we see that we can associate a complex scalar macroscopic polarization amplitude function (slowly varying in time, but rapidly varying in space) with the microscopic density matrix as

$$\tilde{P}(\mathbf{r}, t) \equiv \hat{\epsilon}^* \cdot \mathbf{P}(\mathbf{r}, t) = 2\mathcal{N} d_{ba} \tilde{\rho}_{ab}(\mathbf{r}, t). \qquad (3.31)$$

$$\frac{\partial}{\partial t} \tilde{P}(\mathbf{r}, t) = -\gamma_\perp (1 - i\Omega_0) \tilde{P}(\mathbf{r}, t) - i \frac{|d_{ab}|^2}{\hbar} D(\mathbf{r}, t) \tilde{E}(\mathbf{r}, t), \qquad (3.32a)$$

$$\frac{\partial}{\partial t} N_a(\mathbf{r}, t) = -\gamma_{ab} N_a(\mathbf{r}, t) + \frac{1}{2\hbar} \operatorname{Im}\left[\tilde{E}^*(\mathbf{r}, t) \tilde{P}(\mathbf{r}, t) \right], \text{ and} \qquad (3.32b)$$

$$\frac{\partial}{\partial t} N_b(\mathbf{r}, t) = +\gamma_{ab} N_a(\mathbf{r}, t) - \frac{1}{2\hbar} \operatorname{Im}\left[\tilde{E}^*(\mathbf{r}, t) \tilde{P}(\mathbf{r}, t) \right], \qquad (3.32c)$$

where we have defined the population difference

$$D(\mathbf{r}, t) \equiv N_a(\mathbf{r}, t) - N_b(\mathbf{r}, t), \qquad (3.33)$$

and the relative detuning angular frequency

$$\Omega_0 \equiv \frac{\omega_0 - \omega_{ab}}{\gamma_\perp}, \qquad (3.34)$$

3.2.2 Three-Level Systems

3.2.3 Four-Level Systems

$$\frac{\partial}{\partial t} \tilde{P}(\mathbf{r}, t) = -\gamma_\perp (1 - i\Omega_0) \tilde{P}(\mathbf{r}, t) - i \frac{|d_{ab}|^2}{\hbar} D(\mathbf{r}, t) \tilde{E}(\mathbf{r}, t), \qquad (3.35a)$$

$$\frac{\partial}{\partial t} N_a(\mathbf{r}, t) = \Lambda_a(\mathbf{r}, t) - \gamma_{ag} N_a(\mathbf{r}, t) - \gamma_{ab} N_a(\mathbf{r}, t) + \frac{1}{2\hbar} \operatorname{Im}\left[\tilde{E}^*(\mathbf{r}, t) \tilde{P}(\mathbf{r}, t) \right], \text{ and} \qquad (3.35b)$$

$$\frac{\partial}{\partial t} N_b(\mathbf{r}, t) = \Lambda_b(\mathbf{r}, t) - \gamma_{bg} N_b(\mathbf{r}, t) + \gamma_{ab} N_a(\mathbf{r}, t) - \frac{1}{2\hbar} \operatorname{Im}\left[\tilde{E}^*(\mathbf{r}, t) \tilde{P}(\mathbf{r}, t) \right]. \qquad (3.35c)$$

In an *ideal* four-level laser, $\gamma_{bg} \gg \gamma_{ag} \gg \gamma_{ab}$, so henceforth we neglect γ_{ab}. In addition, if we assume that γ_{bg} is large enough that $N_b(\mathbf{r}, t)$ adiabatically follows $\text{Im}\left[\tilde{E}^*\tilde{P}\right]$, then $\partial N_b(\mathbf{r}, t)/\partial t \approx 0$, and

$$\frac{\partial}{\partial t}\left[N_a(\mathbf{r}, t) - N_b(\mathbf{r}, t)\right] \approx \frac{\partial}{\partial t}N_a(\mathbf{r}, t), \text{ and}$$

$$\frac{\partial}{\partial t}\left[N_a(\mathbf{r}, t) - \frac{\gamma_{ag}}{\gamma_{bg}}N_b(\mathbf{r}, t)\right] \approx \frac{\partial}{\partial t}N_a(\mathbf{r}, t).$$

Therefore

$$\frac{\partial}{\partial t}D(\mathbf{r}, t) \approx \gamma_{ag}\left[\frac{\Lambda_a(\mathbf{r}, t)}{\gamma_{ag}} - \frac{\Lambda_b(\mathbf{r}, t)}{\gamma_{bg}}\right] - \gamma_{ag}D(\mathbf{r}, t) + \frac{\gamma_{ag}}{2\hbar}\left(\frac{1}{\gamma_{ag}} + \frac{1}{\gamma_{bg}}\right)\text{Im}\left[\tilde{E}^*(\mathbf{r}, t)\tilde{P}(\mathbf{r}, t)\right].$$

If we define

$$\overline{D}(\mathbf{r}, t) \equiv \frac{\Lambda_a(\mathbf{r}, t)}{\gamma_{ag}} - \frac{\Lambda_b(\mathbf{r}, t)}{\gamma_{bg}}, \text{ and} \tag{3.36}$$

$$\frac{1}{\gamma_\parallel} \equiv \frac{1}{\gamma_{ag}} + \frac{1}{\gamma_{bg}}, \tag{3.37}$$

then in the ideal case where $1/\gamma_{ag} \gg 1/\gamma_{bg}$ we have

$$\frac{\partial}{\partial t}D(\mathbf{r}, t) = -\gamma_\parallel\left[D(\mathbf{r}, t) - \overline{D}(\mathbf{r}, t)\right] + \frac{1}{2\hbar}\text{Im}\left[\tilde{E}^*(\mathbf{r}, t)\tilde{P}(\mathbf{r}, t)\right]. \tag{3.38}$$

Together, Eq. (3.35a) and Eq. (3.38) will allow us to analyze a wide variety of laser phenomena.

We can check by direct differentiation that Eq. (3.35a) has the formal solution

$$\tilde{P}(\mathbf{r}, t) = -i\frac{|d_{ab}|^2}{\hbar}e^{-\gamma_\perp(1-i\Omega_0)t}\int_{-\infty}^{t}dt'\, e^{\gamma_\perp(1-i\Omega_0)t'}D(\mathbf{r}, t')\,\tilde{E}(\mathbf{r}, t'). \tag{3.39}$$

In many cases of practical interest, the dephasing rate $\gamma_\perp$ is so large that we can assume that $\tilde{P}(\mathbf{r}, t)$ adiabatically follows the driving term $D(\mathbf{r}, t)\tilde{E}(\mathbf{r}, t)$. We must be careful, though, if $\tilde{E}(\mathbf{r}, t)$ has a rapidly-varying time dependence on the scale of $1/\gamma_\perp$. For example, suppose that $\tilde{E}(\mathbf{r}, t) \equiv E'(\mathbf{r}, t)e^{-i\omega t}$, where $\omega \sim \gamma_\perp$, and $\partial E'(\mathbf{r}, t)/\partial t \ll \gamma_\perp E'(\mathbf{r}, t)$. Then we can move $D(\mathbf{r}, t)E'(\mathbf{r}, t)$ outside the time integral, and we obtain $\tilde{P}(\mathbf{r}, t)$ in the *rate equation approximation* (REA) and solve Eq. (3.35a) as

$$\tilde{P}(\mathbf{r}, t) \cong -i\frac{|d_{ab}|^2}{\hbar\,\gamma_\perp}\frac{1 + i\Omega}{1 + \Omega^2}D(\mathbf{r}, t)\tilde{E}(\mathbf{r}, t), \tag{3.40}$$

where

$$\Omega \equiv \frac{\omega_0 + \omega - \omega_{ab}}{\gamma_\perp}. \tag{3.41}$$

If the REA is valid, then Eq. (3.38) becomes

$$\frac{\partial}{\partial t}D(\mathbf{r}, t) = -\gamma_\parallel\left[D(\mathbf{r}, t) - \overline{D}(\mathbf{r}, t)\right] - \frac{|d_{ab}|^2}{2\hbar^2\gamma_\perp}\frac{\left|\tilde{E}(\mathbf{r}, t)\right|^2}{1 + \Omega^2}. \tag{3.42}$$

If, in addition, both $\overline{D}(\mathbf{r}, t)$ and $|\tilde{E}(\mathbf{r}, t)|$ are constant in time, then the steady-state population difference is

$$D(\mathbf{r}) = \frac{1 + \Omega^2}{1 + \Omega^2 + \frac{|d_{ab}|^2}{2\hbar^2\gamma_\perp\gamma_\parallel}\left|\tilde{E}(\mathbf{r})\right|^2}\overline{D}(\mathbf{r}), \tag{3.43}$$

explicitly showing that the population density is *saturated* as the electric field intensity increases.

3.3 Single-Mode One-Dimensional Laser Amplifier Evolution Equations

In the coming chapters, we will often take the opportunity to understand the fundamental physics and engineering design principles of laser amplifiers and oscillators by reducing the model to a single transverse mode in only one dimension. In this case, we can express the position, field, polarization, and population variables in Eq. (2.83), Eq. (3.35a), and Eq. (3.38) as dimensionless quantities to simplify them considerably for both analytical and numerical use. We begin by introducing the *effective laser cross-section* (sometimes referred to as the "differential gain" in the case of a semiconductor laser), given by

$$\sigma(\omega_0) \equiv \frac{\eta(\omega_0)\,\omega_0\,|d_{ab}|^2}{\varepsilon_0\,c\,\hbar\,\gamma_\perp}, \tag{3.44}$$

and the *saturation intensity*

$$I_s(\omega_0) \equiv \frac{\gamma_\parallel\,\hbar\,\omega_0}{\sigma(\omega_0)} = \frac{\varepsilon_0\,c\,\hbar^2\,\gamma_\parallel\,\gamma_\perp}{\eta(\omega_0)\,|d_{ab}|^2}. \tag{3.45}$$

We then scale $E^\pm(z)$, $P^\pm(z)$, $D(z)$, and the position z and time t as follows:

- rescale the position z by a convenient physical length L (such as the length of the amplifier, or the round-trip length of the laser cavity), and the time by the corresponding group travel time $\tau_g \equiv n'(\omega_0)L/c$:

$$z \longrightarrow L\,z \qquad \text{and} \qquad t \longrightarrow \tau_g\,t\,;$$

- express $E^\pm(z,t)$ in units of I_s, so that the propagating intensity carried by the field is given by $I_s|E^\pm(z,t)|^2$:

$$E^\pm(z,t) \longrightarrow \sqrt{\frac{2\,\eta(\omega_0)}{\varepsilon_0\,c}}\,I_s\,e^{-i\delta\omega_0 t}\,E^\pm(z,t)\,,$$

where $\delta\omega_0 \ll \omega_0$ represents a small frequency shift away from the carrier frequency ω_0;

- rewrite $P^\pm(z,t)$ in terms of a new variable $F^\pm(z,t)$ as

$$P^\pm(z,t) \longrightarrow -i\,2\,\frac{\varepsilon_0\,c}{\eta(\omega_0)\,\omega_0\,L}\sqrt{\frac{2\,\eta(\omega_0)}{\varepsilon_0\,c}}\,I_s\,e^{-i\delta\omega_0 t}\,F^\pm(z,t)\,;\text{ and}$$

- define the dimensionless gain $G(z,t) \equiv \sigma(\omega_0)\,L\,D(z,t)$, with $\overline{G}(z,t) \equiv \sigma(\omega_0)\,\overline{D}(z,t)$.

With these modifications, Eq. (2.83), Eq. (3.35a), and Eq. (3.38) become

$$\frac{\partial}{\partial t}E^\pm(z,t) \pm \frac{\partial}{\partial z}E^\pm(z,t) = \left[i\,\delta\omega_0 + i\,\widehat{\mathcal{D}}(\omega_0) - \frac{1}{2}\alpha(\omega_0)\right]E^\pm(z,t) + F^\pm(z,t)\,, \tag{3.46a}$$

$$\frac{\partial}{\partial t}\tilde{F}(z,t) = -\frac{1}{\tau_\perp}\left[(1 - i\,\Omega)\,\tilde{F}(z,t) - \frac{1}{2}\tilde{G}(z,t)\tilde{E}(z,t)\right]\,,\text{ and} \tag{3.46b}$$

$$\frac{\partial}{\partial t}\tilde{G}(z,t) = -\frac{1}{\tau_\parallel}\left\{\tilde{G}(z,t) - \overline{G}(z,t) + 2\,\mathrm{Re}\left[\tilde{E}^*(z,t)\tilde{F}(z,t)\right]\right\}\,, \tag{3.46c}$$

where $\tau_\perp \equiv 1/\gamma_\perp$, $\tau_\parallel \equiv 1/\gamma_\parallel$, $\Omega \equiv (\omega_0 + \delta\omega_0 - \omega_{ab})\tau_\perp$,

$$\widehat{\mathcal{D}}(\omega_0) \equiv \sum_{l=2}^{\infty}\frac{D_l(\omega_0)}{l!}\left(i\,\frac{\partial}{\partial t}\right)^l\,,\text{ and} \tag{3.47a}$$

$$D_l(\omega_0) = \frac{L}{\tau_g^l}\frac{d^l}{d\omega_0^l}\,\mathrm{Re}\left[\beta(\omega_0)\right]\,. \tag{3.47b}$$

Note that we are using $\tilde{G}(z,t)$ to represent the dimensionless gain, since we will find that the gain can be spatially rapidly-varying in the case of a standing-wave laser amplifier. We have scaled $\delta\omega_0$ by τ_g^{-1}

and $\alpha(\omega_0)$ by L^{-1}; by default, our unit of time is τ_g, and our unit of length is L. Also, the form of Eq. (3.47b) is consistent with the published tables of values of $d^l \operatorname{Re}[\beta(\omega_0)]/d\omega_0^l$, which are usually given in units of second^l/meter. For example, suppose that we have a material with a *group velocity dispersion* $d^2 \operatorname{Re}[\beta(\omega_0)]/d\omega_0^2 = 1000$ fs^2/mm in a laser cavity with $L = 4$ mm and $\tau_g = 60$ ps. Then $D_2(\omega_0) \cong 10^{-6}$, and is dimensionless. When we discuss dynamical laser oscillators in Chapter 6, we will make slightly different scaling choices for the polarization and gain variables, but the form of the evolution equations will be the same.

We can describe a broader class of (spectrally homogeneous but asymmetric) gain media by introducing two coefficients $\mathcal{A}$ and $\mathcal{B}$ and rewriting the evolution equation for the macroscopic polarization given by Eq. (3.46b) as

$$
\begin{aligned}
\frac{\partial}{\partial t}\tilde{F}(z,t) &= -\frac{1}{\tau_\perp}\left[(\mathcal{B} - i\,\Omega)\,\tilde{F}(z,t) - \frac{\mathcal{A}}{2}\,\tilde{G}(z,t)\tilde{E}(z,t)\right] \\
&\equiv -\frac{\mathcal{B} - i\,\Omega}{\tau_\perp}\left[\tilde{F}(z,t) - \frac{1}{2}\,\mathcal{L}(\Omega)\,\tilde{G}(z,t)\tilde{E}(z,t)\right],
\end{aligned}
\tag{3.48}
$$

where

$$
\mathcal{L}(\Omega) \equiv \frac{\mathcal{A}}{\mathcal{B} - i\,\Omega}
\tag{3.49}
$$

is referred to as the "lineshape function" of the gain medium. In our analysis of homogeneous gain media above, we chose $\mathcal{A} = \mathcal{B} = 1$, leading to the Lorentzian lineshape function

$$
\mathcal{L}(\Omega) = \frac{1}{1 - i\,\Omega} = \frac{1 + i\,\Omega}{1 + \Omega^2}.
\tag{3.50}
$$

In the case of the semiconductor laser discussed in Section 5.5, these coefficients are given by [20]

$$
\mathcal{B} \equiv 1 - i\,\alpha, \text{ and}
\tag{3.51a}
$$

$$
\mathcal{A} = \mathcal{B}^2 = (1 - i\,\alpha)^2,
\tag{3.51b}
$$

with the asymmetric lineshape function

$$
\mathcal{L}_\alpha(\Omega) \equiv \frac{(1 - i\,\alpha)^2}{1 - i\,(\Omega + \alpha)},
\tag{3.52}
$$

where α is known historically as the "linewidth enhancement factor."[3.3] Note that when $\alpha = 0$ this function describes the Lorentzian lineshape, and when $\Omega = 0$ we have $\mathcal{L}(\alpha, 0) = 1 - i\,\alpha$. We defer further discussion of this lineshape function to Section 5.5.

Applying this technique to Eq. (3.48) and Eq. (3.46c), we find the formal solutions

$$
\tilde{F}(z,t) = \frac{1}{2}\,\hat{\partial}_\perp^{-1}\left[\tilde{E}(z,t)\,\tilde{G}(z,t)\right], \text{ and}
\tag{3.53a}
$$

$$
\tilde{G}(z,t) = \hat{\partial}_\parallel^{-1}\,G_0(z,t) - \hat{\partial}_\parallel^{-1}\left[\tilde{E}^*(z,t)\tilde{F}(z,t) + \tilde{E}(z,t)\tilde{F}^*(z,t)\right],
\tag{3.53b}
$$

where

$$
\hat{\partial}_\perp^{-1} \equiv \frac{\mathcal{A}}{\mathcal{B}}\left(1 + \frac{\tau_\perp}{\mathcal{B}}\frac{\partial}{\partial t}\right)^{-1} \equiv \mathcal{L}\left(i\,\tau_\perp\frac{\partial}{\partial t}\right),
\tag{3.54a}
$$

$$
\hat{\partial}_\parallel^{-1} \equiv \left(1 + \tau_\parallel\frac{\partial}{\partial t}\right)^{-1}.
\tag{3.54b}
$$

[3.3]Apologies for the similarity between α, the linewidth enhancement factor, and α_0, the bulk/background absorption coefficient.

Chapter 4

Laser Beams and Resonators: One-Dimensional Models

The approximate description of a laser electromagnetic field as a transverse plane-polarized wave with the complex amplitude function given by Eq. (2.85a) allows us to build simple dynamical models of resonant cavities that are commonly used to build laser oscillators. In this chapter, we will ignore the transverse dimensions of mirrors and other optical components, and rely on the *scattering matrix* [21, 10] to build models of common "two-port" linear optical systems.

Expand on this paragraph to include the discussions of time/frequency properties and quasi-normal modes.

4.1 Scattering Matrices in the Frequency Domain

4.1.1 Dielectric Regions and Waveguides

Let's apply the wave equation in the frequency domain given by the Fourier Transform of Eq. (3.46a) to the linear dielectric region (e.g., free space or a waveguide such as an optical fiber) shown in Fig. 4.1 and recapitulate our treatment of the experiment shown in Fig. 2.2a. For a forward-propagating field (i.e., traveling in the $+\hat{z}$ direction), in one dimension the rapidly-varying complex envelope function has the form of Eq. (2.85a), or in the frequency domain

$$\mathbf{E}^+(\mathbf{r}, \omega) \equiv \hat{\epsilon}\, e^{+i\,k_0(\omega_0)z}\, E^+(z, \omega), \tag{4.1}$$
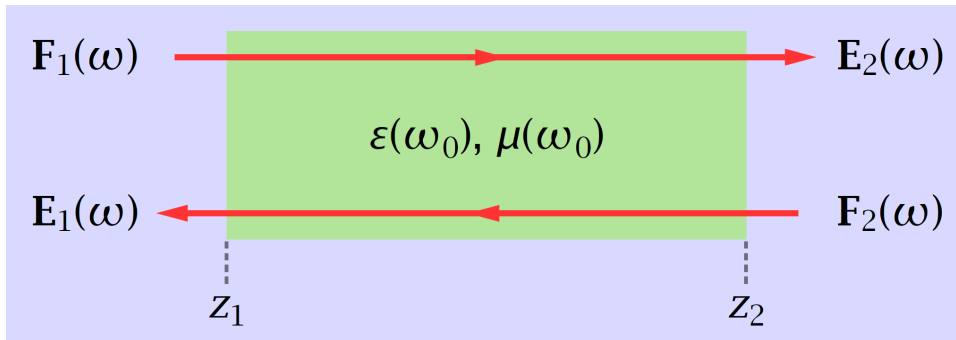

Figure 4.1: Schematic diagram of a linear one-dimensional dielectric propagation region with a constant relative permittivity and permeability. The effective refractive index $n(\omega_0)$, the group refractive index $n'(\omega_0)$, and the linear absorption coefficient $\alpha(\omega_0)$ are defined by Eq. (2.72), Eq. (2.73), and Eq. (2.74), respectively, at the carrier frequency ω_0. In the absence of a macroscopic polarization, we use $\mathbf{F}$ to represent an incident electric field.

where, from Eq. (2.70), $k_0(\omega_0) = \mathrm{Re}\,[\beta(\omega_0)] = (\omega_0/c)n(\omega_0)$. The corresponding wave equation for the complex scalar envelope function that varies slowly in both space and time is therefore given by[4.1]

$$\frac{\partial}{\partial z}E^+(z,\omega) - i\,\omega\,E^+(z,\omega) + \frac{1}{2}\,\alpha(\omega_0)\,E^+(z,\omega) = 0. \tag{4.2}$$

As in Section 2.2, the effective refractive index $n(\omega_0)$, the group refractive index $n'(\omega_0)$, and the linear absorption coefficient $\alpha(\omega_0)$ are defined by Eq. (2.72), Eq. (2.73), and Eq. (2.74), respectively, at the carrier frequency ω_0. In the absence of a macroscopic polarization arising from an internal gain region, in this chapter we use $\mathbf{F}$ to represent an incident electric field. For the wave traveling from a *reference plane* at $z = z_1$ to a reference plane at $z = z_2$, in the case where we can ignore backscattering, we find the solution

$$E^+(z_2,\omega) = \exp\left[i\omega\,(z_2 - z_1) - \frac{1}{2}\alpha(\omega_0)\,(z_2 - z_1)\right]E^+(z_1,\omega). \tag{4.3}$$

Therefore, the one-dimensional complex vector envelope function (that varies rapidly in space but slowly in time) given by Eq. (2.85a) in the frequency domain becomes

$$\mathbf{E}_2(\omega) = \frac{G(z_2,\omega)}{G(z_1,\omega)}\,\mathbf{F}_1(\omega), \tag{4.4}$$

where

$$G(z,\omega) \equiv \exp\left[i\,k_0(\omega_0)z + i\omega z - \frac{1}{2}\alpha(\omega_0)z\right], \tag{4.5}$$

and, as in Fig. 4.1, we have defined the field amplitudes at the reference planes as $E^+(z_1,\omega) \equiv \mathbf{F}_1(\omega)$ and $E^+(z_2,\omega) \equiv \mathbf{E}_2(\omega)$.

For a backward-propagating field traveling in the $-\hat{z}$ direction, in one dimension the complex vector envelope function has the form

$$\mathbf{E}^-(\mathbf{r},t) \equiv \hat{\epsilon}\,e^{-i\,k_0(\omega_0)z}\,E^-(z,t), \tag{4.6}$$

which results in a scalar frequency-domain wave equation similar to that of Eq. (4.2), with a negated spatial derivative:

$$-\frac{\partial}{\partial z}E^-(z,\omega) - i\,\omega\,E^-(z,\omega) + \frac{1}{2}\,\alpha(\omega_0)\,E^-(z,\omega) = 0. \tag{4.7}$$

Integrating this linear differential equation from z_2 to z_1, we find

$$\mathbf{E}_1(\omega) = \frac{G(z_2,\omega)}{G(z_1,\omega)}\,\mathbf{F}_2(\omega), \tag{4.8}$$

where, as above, we have defined the field amplitudes at the reference planes as $\mathbf{E}^-(z_1,\omega) \equiv \mathbf{E}_1(\omega)$ and $\mathbf{E}^-(z_2,\omega) \equiv \mathbf{F}_2(\omega)$. Therefore, in matrix form, we have found that

$$\begin{bmatrix} \mathbf{E}_1(\omega) \\ \mathbf{E}_2(\omega) \end{bmatrix} = \begin{bmatrix} M_{11}(\omega) & M_{12}(\omega) \\ M_{21}(\omega) & M_{22}(\omega) \end{bmatrix} \begin{bmatrix} \mathbf{F}_1(\omega) \\ \mathbf{F}_2(\omega) \end{bmatrix} \equiv \mathbf{M}(\omega)\begin{bmatrix} \mathbf{F}_1(\omega) \\ \mathbf{F}_2(\omega) \end{bmatrix} \tag{4.9}$$

where, in the case of the *two-port* region shown in Fig. 4.1, the *scattering-matrix* $\mathbf{M}(\omega)$ is given by

$$\mathbf{M}(\omega) = \begin{bmatrix} 0 & G(1,\omega) \\ G(1,\omega) & 0 \end{bmatrix} \qquad \text{(Waveguide)}, \tag{4.10}$$
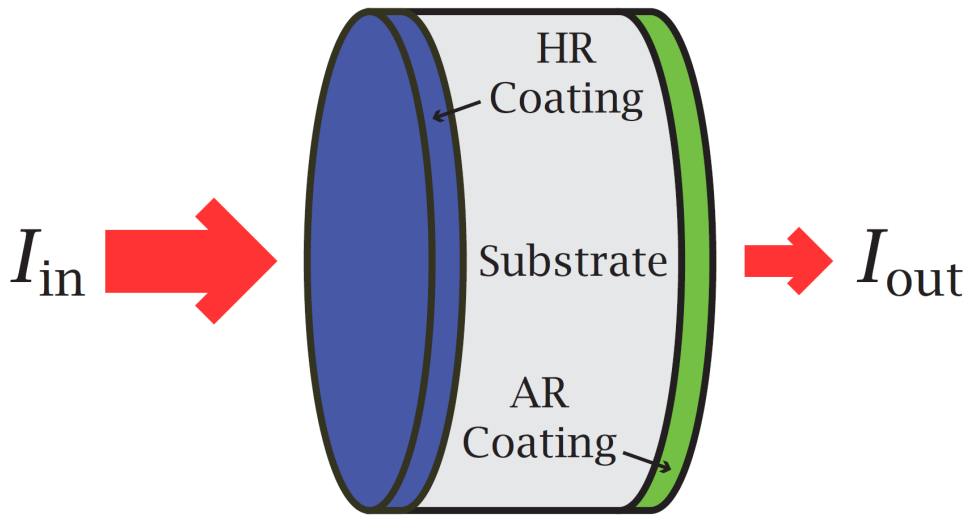
for the case $z_1 = 0$ and $z_2 = 1$[4.2].

Figure 4.2: Schematic diagram of a laser mirror with high-reflection and anti-reflection dielectric coatings on opposite faces.

4.1.2   Mirrors and General Two-Port Components

In modern macroscopic lasers, the mirrors which form the laser resonator resemble the schematic shown in Fig. 4.2. A mirror typically consists of a transparent cylindrical substrate (such as pure fused silica) with a high-reflectance (HR) or partially-reflecting multilayer dielectric coating applied to the inner face of the cylinder; in the partially-reflecting case, transmission through the mirror substrate is usually necessary, so an antireflection (AR) coating will be applied to the outer surface as well. When the mirror is designed, Maxwell's equations are solved for electromagnetic fields propagating from air through the coating to the substrate (and/or vice versa) to optimize the reflectance for a particular application at a target carrier frequency ω_0. However, as we try to build accurate models of laser oscillators, we would like to "abstract" the optical characteristics of a mirror in such a way that our predictions do not depend significantly on the physical details of either the coatings or the substrate. Following the example of the one-dimensional waveguide treated in Section 4.1.1, we'll attempt to find a general relationship between the input fields shown in Fig. 4.3a,

$$\mathbf{F}_1(t) \equiv \hat{\epsilon} \exp\left[+i\,k_1(\omega_0)z_1\right] E^+(z_1, t), \text{ and} \tag{4.11a}$$
$$\mathbf{F}_2(t) \equiv \hat{\epsilon} \exp\left[-i\,k_2(\omega_0)z_2\right] E^-(z_2, t), \tag{4.11b}$$

and the corresponding output fields

$$\mathbf{E}_1(t) \equiv \hat{\epsilon} \exp\left[-i\,k_1(\omega_0)z_1\right] E^-(z_1, t), \text{ and} \tag{4.12a}$$
$$\mathbf{E}_2(t) \equiv \hat{\epsilon} \exp\left[+i\,k_2(\omega_0)z_2\right] E^+(z_2, t), \tag{4.12b}$$

where we have defined $k_j(\omega_0) \equiv (\omega_0/c)n_j(\omega_0)$ for $j \in \{1, 2\}$. Our goal will be to find a relationship between the input and output fields that has a *form* that is independent of the angles of incidence (and polarizations) of the input fields, but we will note that in practice non-normal incidence may convert our simple mirror into the beamsplitter shown in Fig. 4.3b.

Suppose that we have isolated a volume $\mathcal{V}$—bounded by $z_1 \le z \le z_2$ in our one-dimensional example—with a surface S that contains no free charges or currents, and that in principle we can solve

---

[4.1]We recall from Section 3.3 that the coordinate z has been scaled by a physical length L chosen for convenience, and therefore $\alpha(\omega_0)$ and $k_0(\omega_0)$ have been scaled by L^{-1}. Similarly, the time t has been scaled by the corresponding group propagation time $\tau_g \equiv n'(\omega_0)L/c$, and all frequencies by τ_g^{-1}.

[4.2]As we shall see in Section 4.1.2, there are subtleties in the definition of $\mathbf{M}(\omega)$ if $\eta(z_1) \ne \eta(z_2)$.
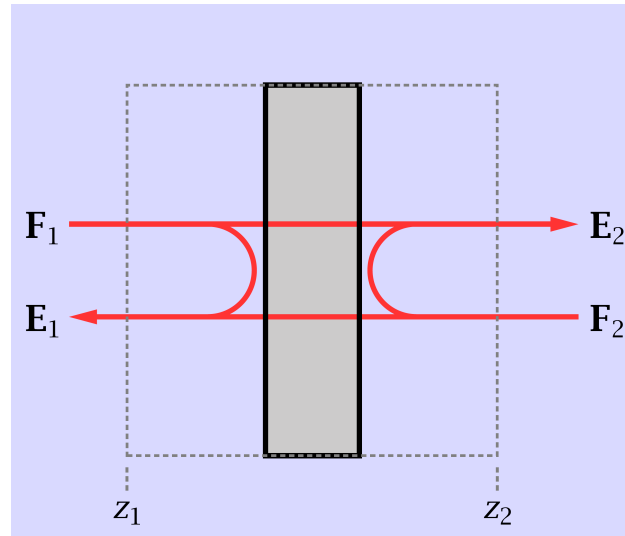
(a) Normal-incidence mirror
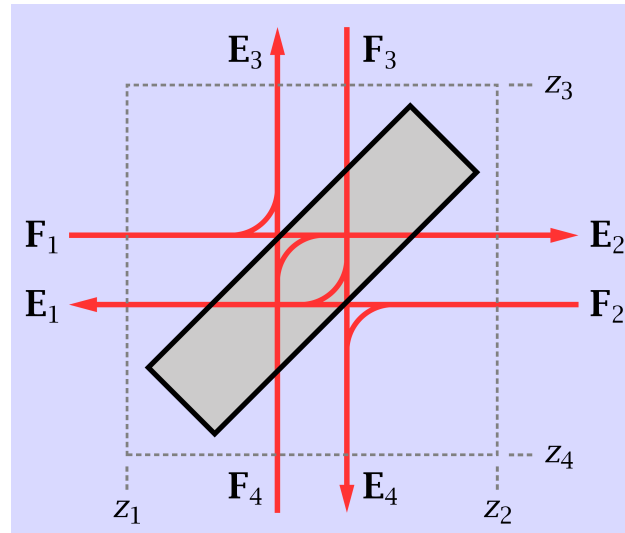
(b) Off-axis mirror (beamsplitter)

Figure 4.3: Common choices of reference planes for (a) simple two-port optical components (like laser mirrors) and (b) four-port optical components (like a tilted laser mirror or beamsplitter).

(a) Schematic of a general two-port element   (b) Time-reversed excitation of a two-port element
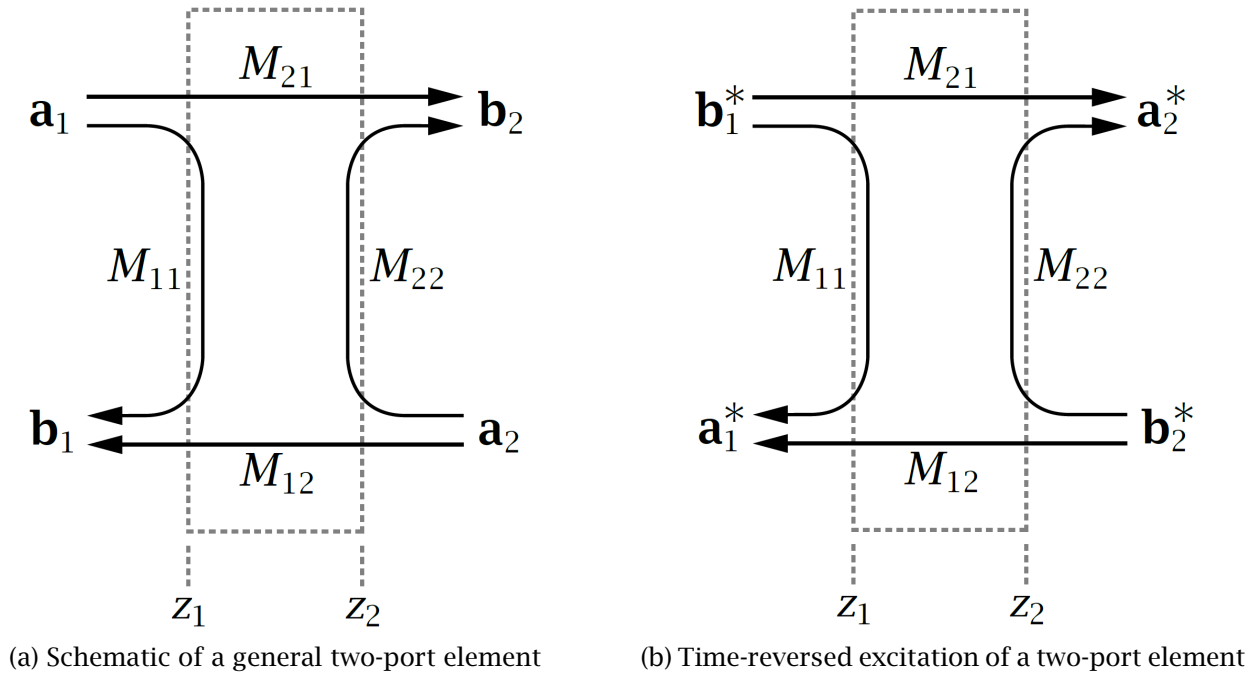
Figure 4.4:   A schematic of a general two-port linear optical element under both forward and time-reversed excitations in the frequency domain.

Maxwell's equations everywhere in $\mathcal{V}$ for some external source configuration (e.g., one or more lasers). Referring to the general two-port component in Fig. 4.4a, we assume that the space in the region $z < z_1$ is filled with a material that has spatially uniform relative permittivity and permeability $\varepsilon_1(\omega_0)$ and $\mu_1(\omega_0)$ at the carrier frequency ω_0, and that the corresponding constants have the values $\varepsilon_2(\omega_0)$ and $\mu_2(\omega_0)$ for $z > z_2$. Then the Poynting vectors evaluated just outside $\mathcal{V}$ at each of the reference planes z_1 and z_2 of S have the values

$$\mathbf{S}(z_1, t) = \hat{z} \left(|\mathbf{a}_1(t)|^2 - |\mathbf{b}_1(t)|^2 \right), \text{ and} \tag{4.13a}$$

$$\mathbf{S}(z_2, t) = \hat{z} \left(|\mathbf{a}_2(t)|^2 - |\mathbf{b}_2(t)|^2 \right), \tag{4.13b}$$

where

$$\mathbf{a}_1(t) = \left[\frac{\varepsilon_0 c}{2\eta_1(\omega_0)} \right]^{\frac{1}{2}} \mathbf{F}_1(t), \tag{4.14a}$$

$$\mathbf{b}_1(t) = \left[\frac{\varepsilon_0 c}{2\eta_1(\omega_0)} \right]^{\frac{1}{2}} \mathbf{E}_1(t), \tag{4.14b}$$

$$\mathbf{a}_2(t) = \left[\frac{\varepsilon_0 c}{2\eta_2(\omega_0)} \right]^{\frac{1}{2}} \mathbf{F}_2(t), \tag{4.14c}$$

$$\mathbf{b}_2(t) = \left[\frac{\varepsilon_0 c}{2\eta_2(\omega_0)} \right]^{\frac{1}{2}} \mathbf{E}_2(t), \tag{4.14d}$$

and $\eta_j(\omega_0) \equiv \text{Re}\left[\mu_j(\omega_0) \right] / n_j(\omega_0)$. Eq. (4.13) may not be obvious to the student, and I probably need to discuss the appropriate spatial averaging concepts in Section 2.2.3 right after Eq. (2.89).

Let's now conduct a *gedanken* ("thought") experiment where we first configure sources to generate input fields with complex vector envelope functions $\mathbf{F}_1(t)$ and $\mathbf{F}_2(t)$, and then we measure the resulting output fields $\mathbf{E}_1(t)$ and $\mathbf{E}_2(t)$. In other words, from Eq. (4.13) and Eq. (4.14), at time t the total energy

flux (intensity) incident on S is $|\mathbf{a}_1(t)|^2 + |\mathbf{a}_2(t)|^2$, and the total intensity emerging from S is $|\mathbf{b}_1(t)|^2 + |\mathbf{b}_2(t)|^2$. Since the two-port optical system under investigation may incorporate resonant elements that cause time delays, these intensities are not necessarily equal at any given time. However, if all fields have amplitudes which approach 0 as $t \longrightarrow \pm\infty$, and $\text{Im}[\epsilon(\omega_0)\mu(\omega_0)] = 0$ everywhere in $\mathcal{V}$, then we can express conservation of *energy fluence* (i.e., energy per unit area) as

$$\int_{-\infty}^{\infty} dt \, \left[|\mathbf{a}_1(t)|^2 + |\mathbf{a}_2(t)|^2 - |\mathbf{b}_1(t)|^2 - |\mathbf{b}_2(t)|^2 \right] = 0. \tag{4.15}$$

We can use the Fourier Power Theorem given by Eq. (A.19) to write this equation in the frequency domain as

$$\int_{-\infty}^{\infty} \frac{d\omega}{2\pi} \, \left[|\mathbf{a}_1(\omega)|^2 + |\mathbf{a}_2(\omega)|^2 - |\mathbf{b}_1(\omega)|^2 - |\mathbf{b}_2(\omega)|^2 \right] = 0, \tag{4.16}$$

where $\mathbf{a}_1(\omega)$, $\mathbf{a}_2(\omega)$, $\mathbf{b}_1(\omega)$, and $\mathbf{b}_2(\omega)$ are the Fourier transforms of their counterparts in Eq. (4.14). But the key difference between the time and frequency domains is that we expect the input and output fields to be coupled by simple constitutive relationships similar to Eq. (2.41), or

$$\mathbf{b}(\omega) = \mathbf{M}(\omega)\,\mathbf{a}(\omega), \tag{4.17}$$

where we have defined the (concatenated) vectors

$$\mathbf{a}(\omega) \equiv \begin{bmatrix} \mathbf{a}_1(\omega) \\ \mathbf{a}_2(\omega) \end{bmatrix} \quad \text{and} \quad \mathbf{b}(\omega) \equiv \begin{bmatrix} \mathbf{b}_1(\omega) \\ \mathbf{b}_2(\omega) \end{bmatrix}, \tag{4.18}$$

and $\mathbf{M}(\omega)$ is the square *scattering* matrix

$$\mathbf{M}(\omega) \equiv \begin{bmatrix} M_{11}(\omega) & M_{12}(\omega) \\ M_{21}(\omega) & M_{22}(\omega) \end{bmatrix}. \tag{4.19}$$

Therefore, in the frequency domain, the *integrand* of Eq. (4.16) should be zero at all values of ω, and we must have

$$\mathbf{a}^\dagger(\omega)\mathbf{a}(\omega) = \mathbf{b}^\dagger(\omega)\mathbf{b}(\omega), \tag{4.20}$$

where $\mathbf{a}^\dagger(\omega) \equiv [\mathbf{a}_1^\dagger(\omega) \;\; \mathbf{a}_2^\dagger(\omega)]$ and $\mathbf{b}^\dagger(\omega) \equiv [\mathbf{b}_1^\dagger(\omega) \;\; \mathbf{b}_2^\dagger(\omega)]$ are the conjugate transposes of $\mathbf{a}(\omega)$ and $\mathbf{b}(\omega)$, respectively[4.3]. Equation (4.20) places a significant constraint on the possible values that the elements of $\mathbf{M}(\omega)$ can have, since

$$\begin{aligned}
\mathbf{b}^\dagger(\omega)\mathbf{b}(\omega) - \mathbf{a}^\dagger(\omega)\mathbf{a}(\omega) &= \left[\mathbf{a}^\dagger(\omega)\,\mathbf{M}^\dagger(\omega)\right][\mathbf{M}(\omega)\,\mathbf{a}(\omega)] - \mathbf{a}^\dagger(\omega)\mathbf{a}(\omega) \\
&= \mathbf{a}^\dagger(\omega)\left[\mathbf{M}^\dagger(\omega)\,\mathbf{M}(\omega) - \mathbf{1}\right]\mathbf{a}(\omega),
\end{aligned} \tag{4.21}$$

or

$$\mathbf{M}^\dagger(\omega) = \mathbf{M}^{-1}(\omega). \tag{4.22}$$

In other words, the scattering matrix $\mathbf{M}(\omega)$ is a unitary matrix, with the properties $|\det[\mathbf{M}(\omega)]| = 1$, and its row (or column) vectors (of length n) form an orthonormal set in $\mathbb{C}^n$. In the two-port case, this means that

$$|M_{11}(\omega)|^2 + |M_{21}(\omega)|^2 = |M_{12}(\omega)|^2 + |M_{22}(\omega)|^2 = 1, \text{ and} \tag{4.23a}$$

$$M_{11}^*(\omega)M_{12}(\omega) + M_{21}^*(\omega)M_{22}(\omega) = M_{11}^*(\omega)M_{21}(\omega) + M_{12}^*(\omega)M_{22}(\omega) = 0. \tag{4.23b}$$

There are additional constraints placed on $\mathbf{M}(\omega)$ by the time-reversal symmetry of Maxwell's equations discussed in Section 2.2.4. Suppose that we have solved Eq. (2.59) for the complex field amplitude functions $[\mathbf{E}(\mathbf{r}, \omega), \mathbf{H}(\mathbf{r}, \omega)]$ in a volume $\mathcal{V}$ for the case where the bounding surface S contains no free charges or currents, as well as no nonlinear polarization $\mathbf{P}(\mathbf{r}, \omega)$. Equation (2.99) and

---

[4.3]In the case where the elements of $\mathbf{a}(\omega)$ are scalars, $\mathbf{a}^\dagger(\omega) \equiv [a_1^*(\omega) \;\; a_2^*(\omega)]$.

Eq. (2.100b) show that, in the frequency domain, the solutions of the time-reversed macroscopic Maxwell equations are $[\mathbf{E}^*(\mathbf{r}, \omega), -\mathbf{H}^*(\mathbf{r}, \omega)]$ given appropriately time-reversed boundary conditions *and* that $\text{Im}[\varepsilon(\mathbf{r}, \omega)] = \text{Im}[\mu(\mathbf{r}, \omega)] = 0$. In this case, Eq. (2.98) and the corresponding analog of Eq. (2.87) show that the solutions to the time-reversed equations will propagate in the reverse direction, and from Eq. (2.101) the Poynting vector will have reversed direction as well. Therefore, as shown in Fig. 4.4b, we can make the replacements $\mathbf{a}(\omega) \longrightarrow \mathbf{b}^*(\omega)$ and $\mathbf{b}(\omega) \longrightarrow \mathbf{a}^*(\omega)$ in Eq. (4.17) and it will remain valid. Therefore

$$\mathbf{a}^*(\omega) = \mathbf{M}(\omega) \, \mathbf{b}^*(\omega), \tag{4.24}$$

or, multiplying both sides of this equation by $\mathbf{M}^{-1}(\omega) = \mathbf{M}^\dagger(\omega)$ and then taking the complex conjugate,

$$\mathbf{b}(\omega) = \mathbf{M}^T(\omega) \, \mathbf{a}(\omega), \tag{4.25}$$

where $\mathbf{M}^T(\omega)$ is the transpose of $\mathbf{M}(\omega)$. If we compare Eq. (4.26) with Eq. (4.17), we see immediately that we must have

$$\mathbf{M}^T(\omega) = \mathbf{M}(\omega), \tag{4.26}$$

so that the scattering matrix is symmetric.[4.4] In the case of our two-port scattering matrix, together with Eq. (4.23a) this condition requires that

$$M_{12}(\omega) = M_{21}(\omega), \quad \text{and} \quad |M_{11}(\omega)| = |M_{22}(\omega)|. \tag{4.27}$$

We are now equipped to find the scattering matrix of a laser mirror by applying Eq. (4.22) and Eq. (4.26) to Eq. (4.19). Let us specify that the mirror has an intensity reflectance R and transmittance T at frequencies near the carrier frequency ω_0 that (in the lossless mirror case) satisfy $R + T = 1$. We choose our reference planes z_1 and z_2 so that $M_{11} = M_{22} = \sqrt{R}$, and we set $M_{12} = M_{21} = e^{i\varphi}\sqrt{T}$ for some real number φ. Comparing $\mathbf{M}^{-1}$ and $\mathbf{M}^\dagger$, we find that

$$R - e^{i2\varphi}T = 1 \quad \text{and} \quad e^{-i\varphi} = -e^{i\varphi},$$

which requires $\varphi = (q + \frac{1}{2})\pi$, where $q \in \mathbb{Z}$. We choose $q = 0$, and find

$$\mathbf{M} = \begin{bmatrix} \sqrt{R} & i\sqrt{T} \\ i\sqrt{T} & \sqrt{R} \end{bmatrix} \qquad \text{(Mirror)} \tag{4.28}$$

at the carrier frequency ω_0. Note that it is straightforward to update $\mathbf{M}$ for the two-port laser mirror when the locations of the reference planes are changed. For example, suppose that we choose the new reference planes $z_1' = z_1 + \Delta z_1$ and $z_2' = z_2 + \Delta z_2$. Then, from Eq. (4.14), with Eq. (4.11) and Eq. (4.12), we find that the input and output fields at the new input planes are

$$\mathbf{a}'(\omega) = \begin{bmatrix} e^{+ik_1\Delta z_1} & 0 \\ 0 & e^{-ik_2\Delta z_2} \end{bmatrix} \mathbf{a}(\omega) \quad \text{and} \quad \mathbf{b}'(\omega) = \begin{bmatrix} e^{-ik_1\Delta z_1} & 0 \\ 0 & e^{+ik_2\Delta z_2} \end{bmatrix} \mathbf{b}(\omega) \tag{4.29}$$

and that the new scattering matrix is given by

$$\begin{aligned} \mathbf{M}' &= \begin{bmatrix} e^{-ik_1\Delta z_1} & 0 \\ 0 & e^{+ik_2\Delta z_2} \end{bmatrix} \mathbf{M} \begin{bmatrix} e^{-ik_1\Delta z_1} & 0 \\ 0 & e^{+ik_2\Delta z_2} \end{bmatrix} \\ &= \begin{bmatrix} e^{-i2k_1\Delta z_1}\sqrt{R} & e^{-i(k_1\Delta z_1 - k_2\Delta z_2)}i\sqrt{T} \\ e^{-i(k_1\Delta z_1 - k_2\Delta z_2)}i\sqrt{T} & e^{i2k_2\Delta z_2}\sqrt{R} \end{bmatrix}. \end{aligned} \tag{4.30}$$

For example, if we choose $k_1\Delta z_1 = k_2\Delta z_2 = \pi/2$, we will change the sign of the $\sqrt{R}$ elements in Eq. (4.28).

[4.4]The principle of fluence conservation and the time-reversal symmetry of Maxwell's equations imply *reciprocity* [21], a relationship between solutions of Maxwell's equations obtained on S for two different arrangements of sources external to S.

Although we developed the fluence conservation and symmetry principles given by Eq. (4.22) and Eq. (4.26) for two-port components, they are generally applicable to lossless, time-reversible systems with any number of ports. For example, the four-port beamsplitter shown in Fig. 4.3b has the scattering matrix

$$
\begin{bmatrix} \mathbf{b}_1(\omega) \\ \mathbf{b}_2(\omega) \\ \mathbf{b}_3(\omega) \\ \mathbf{b}_4(\omega) \end{bmatrix} = \begin{bmatrix} 0 & M_{12} & M_{13} & 0 \\ M_{21} & 0 & 0 & M_{24} \\ M_{31} & 0 & 0 & M_{34} \\ 0 & M_{42} & M_{43} & 0 \end{bmatrix} \begin{bmatrix} \mathbf{a}_1(\omega) \\ \mathbf{a}_2(\omega) \\ \mathbf{a}_3(\omega) \\ \mathbf{a}_4(\omega) \end{bmatrix},
\tag{4.31}
$$

where we have used the schematic in the figure to determine *a priori* which matrix elements are zero. First, we apply Eq. (4.26) to symmetrize the matrix, and then we apply Eq. (4.22) to find

$$
M_{12} = -M_{34}^*, \quad M_{13} = M_{24}^*, \quad \text{and} \quad |M_{12}|^2 + |M_{13}|^2 = 1,
$$

where we have chosen the locations of the four reference planes shown in Fig. 4.3b so that $M_{13}M_{24} - M_{12}M_{34} = 1$, giving $\text{Det}[M] = (M_{13}M_{24} - M_{12}M_{34})^2 = 1$. Following our derivation of the scattering matrix for a laser mirror, we choose $M_{13} = M_{24} = \sqrt{R}$ and $M_{12} = M_{34} = i\sqrt{T}$ (consistent with the lossless condition $R + T = 1$), and obtain

$$
\mathbf{M} = \begin{bmatrix} 0 & i\sqrt{T} & \sqrt{R} & 0 \\ i\sqrt{T} & 0 & 0 & \sqrt{R} \\ \sqrt{R} & 0 & 0 & i\sqrt{T} \\ 0 & \sqrt{R} & i\sqrt{T} & 0 \end{bmatrix} \quad \text{(Beamsplitter)}
\tag{4.32}
$$

at the carrier frequency ω_0.

Finally, we note that no real laser mirror satisfies the lossless requirement that $R + T = 1$. The dielectric coatings applied to the substrate—as well as the substrate itself—generally will absorb a fraction A of incident light and convert it to heat, as well as scatter a fraction S of that light (usually incoherently) into spatial modes that we aren't studying. In practice, then, $R + T + A + S = 1$, and therefore $R + T < 1$. However, when we model systems incorporating mirrors and dielectric propagation regions such as waveguides, we can build scattering matrices as we have above for arbitrary values of (for example) R and T, and then check that these matrices are unitary and symmetric when we assume that all media are lossless.

4.1.3   Resonant Cavities

Consider the schematic representation of the scattering matrices of the resonant cavities shown in Fig. 4.5. We have constructed each resonator using two partially-reflecting mirrors separated by one or more dielectric propagation regions characterized by a uniform relative permeability and a longitudinally-varying relative permittivity. We assume for convenience (consistent with typical macroscopic laser cavities) that $\eta(\omega_0) = 1$ at the external reference plane of each mirror, allowing us to work with electric field amplitudes rather than the scaled amplitudes given by Eq. (4.14), and that the electromagnetic impedance has the same value $\eta(\omega_0) \equiv \eta$ at the internal reference plane of each mirror[4.5]. We will use the scattering matrix of the mirror given by Eq. (4.28) and rely on the discussion of the solutions of the dielectric propagation equation provided in Section 4.1.1 to build a two-port scattering matrix applicable to three different types of one-dimensional resonator:

Standing-Wave Resonator. A special case of the Fabry-Perot Interferometer, the standing-wave resonator shown schematically in Fig. 4.5a is a two-port one-dimensional optical component built
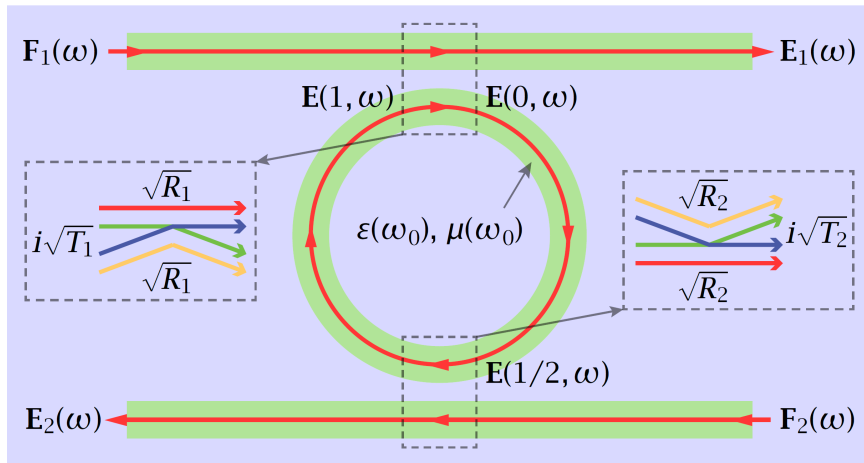

[4.5]These assumptions can be relaxed, but special care must be taken to ensure that—consistent with Maxwell's equations—the transversely-polarized electric field amplitude is preserved across dielectric interfaces, and that intracavity gain dipoles interact with the local laser electric field.
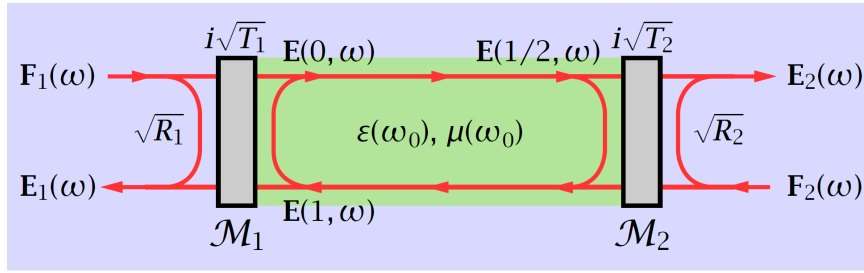
(a) Standing-wave resonator
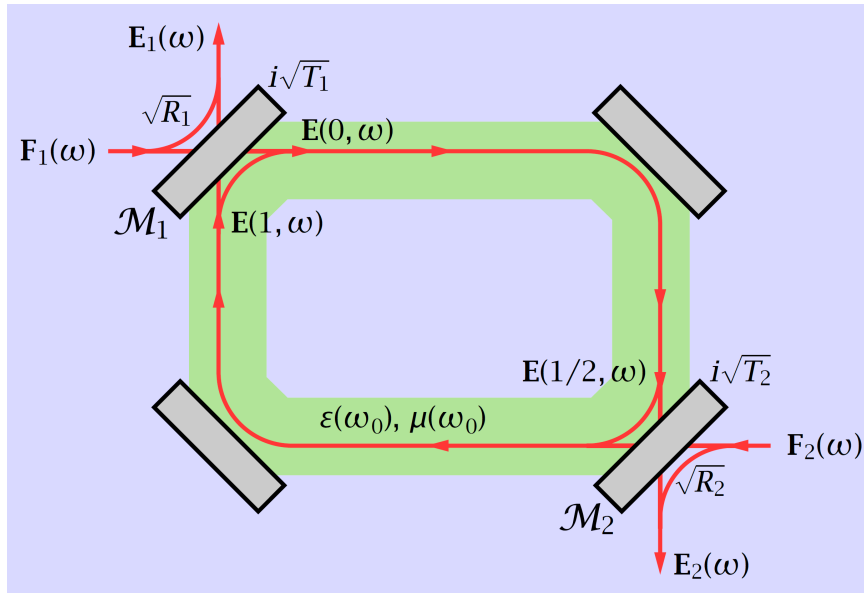
(b) Ring resonator

(c) Microring resonator

Figure 4.5: Schematic diagram of the mirror reflection and transmission coefficients used to determine the intracavity enhancement and output fields of common one-dimensional resonators.

using two laser mirrors and a dielectric propagation region. In this chapter, we adopt the convention that the *round-trip* physical length of the propagation region enclosed within the mirrors is L, rather than the single-pass length, for consistency with both ring resonators and paraxial models of three-dimensional intracavity transverse modes. Toward this end, we calculate a single complex field envelope function $\mathbf{E}(z, \omega)$ as a function of position in the cavity, with $0 < z < 1/2$ as the coordinate for propagation from the reference plane at $\mathcal{M}_1$ (just *after* reflection) to the reference plane at $\mathcal{M}_2$ (just *before* reflection), and $1/2 < z < 1$ as the coordinate for propagation from the reference plane at $\mathcal{M}_2$ (just *after* reflection) to the reference plane at $\mathcal{M}_1$ (just *before* reflection). We note that this approach is completely consistent with the formulation of wave propagation through the dielectric region given in Section 4.1.1, and in particular with Eq. (4.4) and Eq. (4.8). We will link $\mathbf{E}(0, \omega)$ to $\mathbf{E}(1, \omega)$ using the scattering matrix for $\mathcal{M}_1$ given by Eq. (4.28). We will find that the scattering matrix for the standing-wave resonator is symmetric, and (in the lossless case) unitary.

Ring Resonator. We will treat the one-dimensional ring resonator shown schematically in Fig. 4.5b as a two-port optical component, even though (strictly speaking) it is a four-port element with reference planes similar to those of the beamsplitter shown in Fig. 4.3b. Usually, the ring geometry is chosen for laser applications with the intention of operating it unidirectionally by incorporating nonreciprocal elements such as Faraday rotation devices with polarizers. As an interferometer, this configuration is generally excited in only one propagation direction by choosing noncoincident input and output planes at the two mirrors, and we ignore backscattering by mirrors and other intracavity surfaces. In that case, the parameters and reference planes of this system can be treated just as in the case of the standing-wave resonator, but there is no guarantee that the 2×2 scattering matrix will in fact be symmetric (whereas a properly constructed 4×4 scattering matrix for this configuration would be explicitly symmetric.) Although we do not have to place mirror $\mathcal{M}_2$ at $z = 1/2$ (and this certainly is not always the case in practice), we follow this approach here for pedagogical convenience.

Microring Resonator. For completeness, our discussion will necessarily apply to the one-dimensional microring resonator shown schematically in Fig. 4.5c as a two-port optical component, consisting of a ring waveguide adjacent to two bus waveguides. As in the case of the ring resonator, we reduce the 4×4 scattering matrix to a 2×2 matrix by judicious choice of excitation direction. The perimeter of the ring—measured at the center of the curved waveguide—is L. As implied by the insets of Fig. 4.5c, the broadband power reflectances R_j and transmittances T_j at ports 1 and 2 are determined by the dimensions of the waveguides and the separation between them. We assume that the relative (effective) permittivity is uniform in the ring and the adjacent waveguides; thus, the scattering matrix is symmetric, and (again, in the lossless case) unitary.

Let us begin by finding the propagating intracavity field amplitude at the reference planes in the ring resonator shown in Fig. 4.5b; our result will apply to the other two cases in Fig. 4.5 by construction. Using Eq. (4.28), the boundary condition satisfied by $\mathbf{E}(0, \omega)$ and $\mathbf{E}(1, \omega)$ is

$$\mathbf{E}(0, \omega) = \sqrt{R_1}\,\mathbf{E}(1, \omega) + i\sqrt{T_1}\,\sqrt{\eta}\,\mathbf{F}_1(\omega), \tag{4.33}$$

with a similar condition for the field at $z = 1/2$. Propagating $\mathbf{E}(0, \omega)$ to $z = 1/2$ (just prior to reflection at $\mathcal{M}_2$) and then $\mathbf{E}(1/2, \omega)$ to $z = 1$ yields

$$\mathbf{E}(1/2, \omega) = G(1/2, \omega)\mathbf{E}(0, \omega),\ \text{and} \tag{4.34a}$$

$$\mathbf{E}(1, \omega) = \frac{G(1, \omega)}{G(1/2, \omega)} \left[\sqrt{R_2}\,\mathbf{E}(1/2, \omega) + i\sqrt{T_2}\,F_2(\omega) \right], \tag{4.34b}$$

where $G(1/2, \omega)$ and $G(1, \omega)$ are found using Eq. (4.5)[4.6]. These coupled linear equations are readily solved to obtain

$$\begin{bmatrix} \mathbf{E}(1, \omega) \\ \mathbf{E}(1/2, \omega) \end{bmatrix} = \sqrt{\eta}\,\mathbf{H}(\omega) \begin{bmatrix} \mathbf{F}_1(\omega) \\ \mathbf{F}_2(\omega) \end{bmatrix} \tag{4.35}$$

where the *enhancement matrix* for a one-dimensional resonant cavity is given by

$$\mathbf{H}(\omega) = \frac{1}{1 - \sqrt{R_1 R_2}\,G(1, \omega)} \begin{bmatrix} i\sqrt{T_1 R_2}\,G(1, \omega) & i\sqrt{T_2}\,\frac{G(1, \omega)}{G(1/2, \omega)} \\ i\sqrt{T_1}\,G(1/2, \omega) & i\sqrt{R_1 T_2}\,G(1, \omega) \end{bmatrix} \tag{4.36}$$

Applying Eq. (4.28) to the exterior reference planes of mirrors $\mathcal{M}_1$ and $\mathcal{M}_2$ allows us to calculate the output fields $\mathbf{E}_1$ and $\mathbf{E}_2$ as

$$\begin{bmatrix} \mathbf{E}_1(\omega) \\ \mathbf{E}_2(\omega) \end{bmatrix} = \begin{bmatrix} \sqrt{R_1} & 0 \\ 0 & \sqrt{R_2} \end{bmatrix} \begin{bmatrix} \mathbf{F}_1(\omega) \\ \mathbf{F}_2(\omega) \end{bmatrix} + \begin{bmatrix} i\sqrt{T_1} & 0 \\ 0 & i\sqrt{T_2} \end{bmatrix} \frac{1}{\sqrt{\eta}} \begin{bmatrix} \mathbf{E}(1, \omega) \\ \mathbf{E}(1/2, \omega) \end{bmatrix}, \tag{4.37}$$

or, after substitution of Eq. (4.35) and straightforward algebra,

$$\begin{bmatrix} \mathbf{E}_1(\omega) \\ \mathbf{E}_2(\omega) \end{bmatrix} = \mathbf{M}(\omega) \begin{bmatrix} \mathbf{F}_1(\omega) \\ \mathbf{F}_2(\omega) \end{bmatrix}, \tag{4.38}$$

where the two-port scattering matrix for a one-dimensional resonant cavity is

$$\begin{aligned} \mathbf{M}(\omega) &= \begin{bmatrix} \sqrt{R_1} & 0 \\ 0 & \sqrt{R_2} \end{bmatrix} + \begin{bmatrix} i\sqrt{T_1} & 0 \\ 0 & i\sqrt{T_2} \end{bmatrix} \mathbf{H}(\omega) \\ &= \frac{1}{1 - \sqrt{R_1 R_2}\,G(1, \omega)} \begin{bmatrix} \sqrt{R_1} - \sqrt{R_2}\,(R_1 + T_1)\,G(1, \omega) & -\sqrt{T_1 T_2}\,\frac{G(1, \omega)}{G(1/2, \omega)} \\ -\sqrt{T_1 T_2}\,G(1/2, \omega) & \sqrt{R_2} - \sqrt{R_1}\,(R_2 + T_2)\,G(1, \omega) \end{bmatrix}. \end{aligned} \tag{4.39}$$

In the special case where $\varepsilon(1 - z, \omega_0) = \varepsilon(z, \omega_0)$, we have $G(1, \omega)/G(1/2, \omega) = G(1/2, \omega) = \sqrt{G(1, \omega)}$, and the scattering matrix becomes manifestly symmetric. If we also assume that the mirrors are lossless, so that $R_1 + T_1 = R_2 + T_2 = 1$, then we have

$$\mathbf{M}(\omega) = \frac{1}{1 - \sqrt{R_1 R_2}\,G(1, \omega)} \begin{bmatrix} \sqrt{R_1} - \sqrt{R_2}\,G(1, \omega) & -\sqrt{T_1 T_2}\,G(1, \omega) \\ -\sqrt{T_1 T_2}\,G(1, \omega) & \sqrt{R_2} - \sqrt{R_1}\,G(1, \omega) \end{bmatrix}. \tag{4.40}$$

The determinant of this matrix is $-[G(1, \omega) - \sqrt{R_1 R_2}]/[1 - \sqrt{R_1 R_2}\,G(1, \omega))]$, which has an absolute value of unity if $\alpha(z) = 0$ and therefore $|G(1, \omega)| = 1$. In this case, it is also straightforward to show that $\mathbf{M}^\dagger(\omega)\mathbf{M}(\omega) = \mathbf{1}$, demonstrating that $\mathbf{M}(\omega)$ is unitary.

4.2 Properties of Resonant Cavities in the Time and Frequency Domains

4.2.1 Input-Output Relations for Resonant Cavities in the Time Domain

If we define the functions

$$f(\omega) = \frac{1}{1 - \Gamma\,e^{i\omega}}, \tag{4.41a}$$

$$g(\omega) = \frac{\sqrt{\Gamma}\,e^{i\omega/2}}{1 - \Gamma\,e^{i\omega}}, \text{ and} \tag{4.41b}$$

$$h(\omega) = \frac{\Gamma\,e^{i\omega}}{1 - \Gamma\,e^{i\omega}}, \tag{4.41c}$$

[4.6]Since — by assumption — $\eta(z) \equiv \eta$ at each internal mirror reference plane, we can use Eq. (4.5) without modification.

where

$$\Gamma \equiv \sqrt{R_1 R_2} \exp\left[-\frac{1}{2}\alpha(\omega_0) + i\omega_0\tau\right], \tag{4.42}$$

then after straightforward algebra we can rewrite Eq. (4.40) as

$$\mathbf{M}(\omega) = \begin{bmatrix} \sqrt{R_1}f(\omega) - \frac{1}{\sqrt{R_1}}h(\omega) & -\sqrt{\frac{T_1 T_2}{\sqrt{R_1 R_2}}}g(\omega) \\ -\sqrt{\frac{T_1 T_2}{\sqrt{R_1 R_2}}}g(\omega) & \sqrt{R_2}f(\omega) - \frac{1}{\sqrt{R_2}}h(\omega) \end{bmatrix}. \tag{4.43}$$

In Eq. (4.42), we have defined the phase round-trip time

$$\tau \equiv \frac{n(\omega_0)L}{c}, \tag{4.44}$$

which (like ω_0^{-1}) has been scaled by the group round-trip time

$$\tau_g \equiv \frac{n'(\omega_0)L}{c}. \tag{4.45}$$

Now we would like to substitute Eq. (4.43) into Eq. (4.38), and then apply an inverse Fourier transform to find $\mathbf{E}_1(t)$ and $\mathbf{E}_2(t)$. Since $|\Gamma e^{i\omega}| < 1$, we can expand $f(\omega)$ as

$$f(\omega) = \sum_{n=0}^{\infty}\left(\Gamma e^{i\omega}\right)^n, \tag{4.46}$$

giving the inverse transform of $f(\omega)\mathbf{F}(\omega)$ as

$$\int_{-\infty}^{+\infty}\frac{d\omega}{2\pi}e^{-i\omega t}f(\omega)\mathbf{F}(\omega) = \int_{-\infty}^{+\infty}\frac{d\omega}{2\pi}e^{-i\omega t}\sum_{n=0}^{\infty}\Gamma^n e^{in\omega}\mathbf{F}(\omega)$$

$$= \sum_{n=0}^{\infty}\Gamma^n\int_{-\infty}^{+\infty}\frac{d\omega}{2\pi}e^{-i\omega(t-n)}\mathbf{F}(\omega) \tag{4.47a}$$

$$= \sum_{n=0}^{\infty}\Gamma^n\mathbf{F}[t-n],$$

where we have applied the Fourier Shift Theorem given by Eq. (A.15). Following the same approach for both $g(\omega)$ and $h(\omega)$ yields

$$\int_{-\infty}^{+\infty}\frac{d\omega}{2\pi}e^{-i\omega t}g(\omega)\mathbf{F}(\omega) = \sum_{n=0}^{\infty}\Gamma^{\left(n+\frac{1}{2}\right)}\mathbf{F}\left[t-\left(n+\frac{1}{2}\right)\right], \text{ and} \tag{4.47b}$$

$$\int_{-\infty}^{+\infty}\frac{d\omega}{2\pi}e^{-i\omega t}h(\omega)\mathbf{F}(\omega) = \sum_{n=0}^{\infty}\Gamma^{(n+1)}\mathbf{F}[t-(n+1)]. \tag{4.47c}$$

These transform pairs allow us to determine the output fields in the time domain given specified input fields. For example, suppose that $\mathbf{F}_2(t) = 0$; then together Eq. (4.38), Eq. (4.43), and Eq. (4.47) predict that

$$\mathbf{E}_1(t) = \sqrt{R_1}\,\mathbf{F}_1(t) - \frac{T_1}{\sqrt{R_1}}\sum_{n=1}^{\infty}\Gamma^n\mathbf{F}_1[t-n], \text{ and} \tag{4.48}$$

$$\mathbf{E}_2(t) = -\sqrt{\frac{T_1 T_2}{\sqrt{R_1 R_2}}}\sum_{n=0}^{\infty}\Gamma^{\left(n+\frac{1}{2}\right)}\mathbf{F}_1\left[t-\left(n+\frac{1}{2}\right)\right]. \tag{4.49}$$

Both of these input-output relations have a straightforward physical interpretation. $\mathbf{E}_1(t)$ is a coherent superposition of a prompt reflection from mirror $\mathcal{M}_1$ and fields that have experienced an integer number of past resonator round-trips. $\mathbf{E}_2(t)$ is a coherent superposition of past round-trips followed by a final, single propagation step from $\mathcal{M}_1$ to $\mathcal{M}_2$.

Show the $\Theta(t)$ and gaussian pulse examples here.

4.2.2 Input-Output Relations for Resonant Cavities in the Frequency Domain

4.2.2.1 Partial-Fraction Expansion of the Scattering Matrix

Let's allow ω to take on complex values, and seek partial-fraction expansions of $f(\omega)$, $g(\omega)$, and $h(\omega)$ that will guide us to their approximations as finite sums of simple analytic functions. For example, since $1/f(\omega)$ is an analytic function, we can apply the Mittag-Leffler partial-fraction expansion [22]

$$f(\omega) = f(0) + \sum_q r_q \left(\frac{1}{\omega - \nu_q} + \frac{1}{\nu_q} \right), \tag{4.50}$$

where ν_q is a pole of $f(\omega)$ with residue r_q. In the case of Eq. (4.41a), we have

$$\nu_q = 2q\pi + i \ln \Gamma, \text{ and} \tag{4.51a}$$
$$r_q = i, \tag{4.51b}$$

so that

$$f(\omega) = \left[\frac{1}{1-\Gamma} + \sum_{q=-\infty}^{+\infty} \frac{i}{\nu_q} \right] + \sum_{q=-\infty}^{+\infty} \frac{i}{\omega - \nu_q} \tag{4.52a}$$
$$= \frac{1}{2} + \sum_{q=-\infty}^{+\infty} \frac{i}{\omega - \nu_q}.$$

The final right-hand side of this representation of $f(\omega)$ is a superposition of individual *Lorentzian* resonance modes that are each centered at the frequency $\omega = \text{Re}(\nu_q) = 2q\pi$ if $\text{Im}(\Gamma) = 0$. Following the same approach for Eq. (4.41b) and Eq. (4.41c), we find

$$g(\omega) = \sum_{q=-\infty}^{+\infty} \frac{(-1)^q i}{\omega - \nu_q}, \text{ and} \tag{4.52b}$$

$$h(\omega) = -\frac{1}{2} + \sum_{q=-\infty}^{+\infty} \frac{i}{\omega - \nu_q}. \tag{4.52c}$$

Suppose that we have chosen the carrier frequency ω_0 to be aligned with mode $q = 0$ of the unloaded cavity, such that $\exp(\pm i \omega_0 \tau) = 1$. The shape of the magnitude-squared of an individual Lorentzian mode, given by

$$\left| \frac{i}{\omega - \nu_0} \right|^2 = \frac{1}{\omega^2 + (\ln |\Gamma|)^2}, \tag{4.53}$$

is characterized by the full-width at half-maximum (FWHM), or the difference between the positive and negative frequencies that reduce Eq. (4.53) to $1/2 \, (\ln |\Gamma|)^2$. We find

$$\Delta\omega_{\text{FWHM}} \equiv \frac{1}{\tau_p} = \ln\left(\frac{1}{|\Gamma|^2} \right), \tag{4.54}$$

where τ_p is the *photon lifetime* (scaled by the group round-trip time τ_g), or the time duration of light storage in the resonator. A common parameter used to represent this storage time is the cavity "quality factor" Q, defined by

$$Q \equiv \frac{\omega_0}{\Delta\omega_{\text{FWHM}}} = \frac{\omega_0}{\ln(1/|\Gamma|^2)} = \omega_0 \tau_p. \tag{4.55}$$

Therefore, we can express the complex resonance frequency of pole q as

$$\nu_q = 2q\pi - \frac{i}{2\,\tau_p} = 2q\pi - i\frac{\omega_0}{2\,Q}. \tag{4.56}$$

In practice, we will approximate Eq. (4.52) by a finite sum of frequency modes over some range of values of q centered on the carrier frequency (which corresponds to $q = 0$ in our formulation of the wave equation). Truncating the infinite series introduces an error that would ordinarily require many more modes than are needed for a particular representation of a problem of interest, but it is straightforward to include a simple correction term. For example, by calculating the difference between Eq. (4.52a) and the corresponding truncated series to first order in ω, we obtain

$$f(\omega) \approx \frac{1}{2} - \frac{\ln\Gamma + i\omega}{2\pi^2}\, \psi^{(1)}(q_{max} + 1) + \sum_{q=-q_{max}}^{+q_{max}} \frac{i}{(\omega - 2q\pi) - i\ln\Gamma}\,, \tag{4.57}$$

where

$$\psi^{(1)}(n + 1) \approx \frac{2n + 1}{2(n + 0.125)(n + 1)}$$

is the first-order polygamma function. In Fig. 4.6 we have plotted Eq. (4.52a) and Eq. (4.57) for the case $\Gamma = 0.5$ and $q_{max} = 2$. Even for this moderate value of $|\Gamma|$ (i.e., far from unity), Eq. (4.57) is a reasonably good approximation of $f(\omega)$ near $\omega = \mathrm{Re}(\nu_q)$ for $|q| \le q_{max}$.

4.2.2.2   Finesse and Other Properties of Resonant Cavities

Let's explore the optical properties of the simple one-dimensional resonators shown in Fig. 4.5 in the case where $F_2(\omega) = 0$. Relying on Eq. (4.5), Eq. (4.33), Eq. (4.38), and Eq. (4.39), we find

$$E(0, \omega) = \frac{1}{1 - \Gamma\, e^{i\omega}} \left[i\, \sqrt{\eta T_1}\, F(\omega) \right], \tag{4.58}$$

where $\eta \equiv \eta(0) = \eta(1)$ is the dimensionless electromagnetic impedance coefficient at the internal reference plane of $\mathcal{M}_1$, and from Eq. (4.42) we have $\Gamma^2 = R_1 R_2 e^{-\alpha(\omega_0)}$ when ω_0 is chosen such that $\exp(i\omega_0\tau) = 1$. The denominator

$$\mathcal{D}(\omega) \equiv 1 - \Gamma\, e^{i\omega} \tag{4.59}$$

is so common in discussions of optical resonators that we should invest some time to understand its properties in more detail. We begin by defining $\phi(\omega) \equiv \omega/2$, and writing

$$\begin{aligned}
\frac{1}{\mathcal{D}(\omega)} &= \frac{1 - \Gamma\, e^{-i2\phi(\omega)}}{\left(1 - \Gamma\, e^{+i2\phi(\omega)}\right)\left(1 - \Gamma\, e^{-i2\phi(\omega)}\right)} \\
&\equiv \frac{e^{i[\theta(\omega) - \phi(\omega)]}}{|\mathcal{D}(\omega)|}\,,
\end{aligned} \tag{4.60}$$

where $e^{i\theta(\omega)} \equiv [e^{+i\phi(\omega)} - \Gamma\, e^{-i\phi(\omega)}]/|\mathcal{D}(\omega)|$. We note that

$$\begin{aligned}
|\mathcal{D}(\omega)|^2 &= 1 + \Gamma^2 - 2\Gamma\, \cos[2\phi(\omega)] \\
&= (1 - \Gamma)^2 + 4\Gamma\, \sin^2\phi(\omega) \\
&\equiv (1 - \Gamma)^2 \left[1 + \tilde{F}\, \sin^2\phi(\omega)\right],
\end{aligned} \tag{4.61}$$

where

$$\tilde{F} \equiv \frac{4\Gamma}{(1 - \Gamma)^2} \tag{4.62}$$

is known as the coefficient of finesse. Therefore

$$|\mathcal{D}(\omega)| = (1 - \Gamma)\, \sqrt{1 + \tilde{F}\, \sin^2\phi(\omega)}\,, \text{ and} \tag{4.63}$$

$$e^{i\theta(\omega)} = \frac{(1 - \Gamma)\, \cos\phi(\omega) + i\,(1 + \Gamma)\, \sin\phi(\omega)}{(1 - \Gamma)\, \sqrt{1 + \tilde{F}\, \sin^2\phi(\omega)}}\,. \tag{4.64}$$

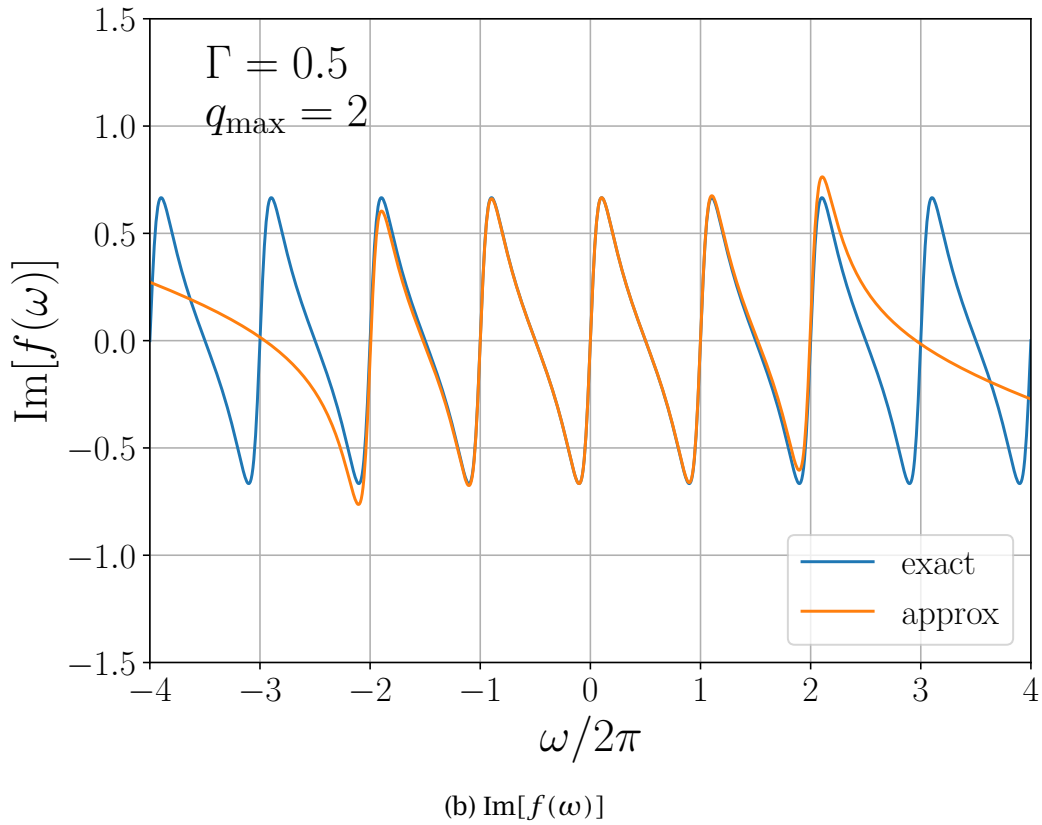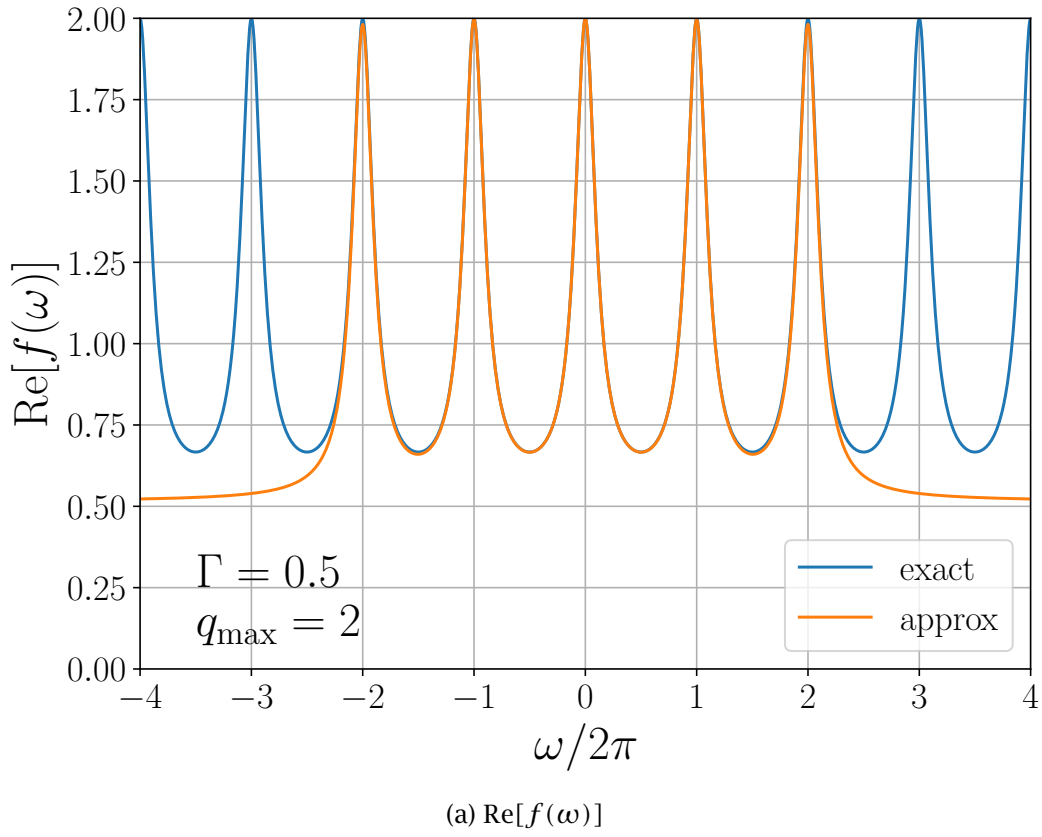(a) $\mathrm{Re}[f(\omega)]$

(b) $\mathrm{Im}[f(\omega)]$

Figure 4.6: A comparison of the value of the resonant function given by Eq. (4.52a) and the Lorentzian approximation defined by Eq. (4.57) for the case where $\Gamma = 0.5$ and $q_{\mathrm{max}} = 2$.

Solving Eq. (4.62) for Γ yields

$$\Gamma = 1 + \frac{2}{\widetilde{F}} - \frac{2}{\widetilde{F}} \sqrt{1 + \widetilde{F}}, \tag{4.65}$$

giving $(1 + \Gamma)/(1 - \Gamma) = \sqrt{1 + \widetilde{F}}$ and

$$E(0, \omega) = \frac{i\sqrt{T_1}}{1 - \Gamma} \frac{e^{i[\theta(\omega) - \phi(\omega)]}}{\sqrt{1 + \widetilde{F}\sin^2\phi(\omega)}} \sqrt{\eta}\, F_1(\omega), \tag{4.66}$$

where now

$$\cos\theta(\omega) \equiv \frac{\cos\phi(\omega)}{\sqrt{1 + \widetilde{F}\sin^2\phi(\omega)}}, \qquad \text{and} \qquad \sin\theta(\omega) \equiv \frac{\sqrt{1 + \widetilde{F}}\,\sin\phi(\omega)}{\sqrt{1 + \widetilde{F}\sin^2\phi(\omega)}}. \tag{4.67}$$

We can use Eq. (4.38) and the same ideas that led us to Eq. (4.66) to solve for the *reflected* field $E_1(\omega)$ and the *transmitted* field $E_2(\omega)$. We find

$$E_1(\omega) = \frac{1}{\sqrt{R_1}(1 - \Gamma)} \frac{R_1 e^{-i\phi(\omega)} - (R_1 + T_1)\,\Gamma\, e^{i\phi(\omega)}}{\sqrt{1 + \widetilde{F}\sin^2\phi(\omega)}} e^{i\theta(\omega)} F_1(\omega), \text{ and} \tag{4.68a}$$

$$E_2(\omega) = -\sqrt{\frac{T_1 T_2 \Gamma}{\sqrt{R_1 R_2}(1 - \Gamma)^2}} \frac{e^{i\theta(\omega)}}{\sqrt{1 + \widetilde{F}\sin^2\phi(\omega)}} F_1(\omega). \tag{4.68b}$$

In the case where $R_1 + T_1 = R_2 + T_2 = 1$ and $\alpha(\omega_0) = 0$, it is straightforward to show that power is conserved for all ω, since $|E_1(\omega)|^2 + |E_2(\omega)|^2 = |F_1(\omega)|^2$.

Whenever the frequency $\omega = \omega_q = 2q\pi$ for some integer q, then $\phi(\omega) = q\pi$, and the magnitudes of both the reflected and transmitted fields reach their maximum values with $\theta(\omega_q) = \phi(\omega_q)$. Restoring the scaling by τ_g^{-1}, these adjacent maxima are separated by the *free spectral range*

$$\Delta\omega_{\text{FSR}} = \frac{2\pi}{\tau_g}. \tag{4.69}$$

The power reflected and transmitted by the cavity is reduced by a factor of two relative to these maxima whenever $\widetilde{F}\sin^2\phi(\omega) = 1$. The corresponding *full width at half-maximum* (FWHM) is therefore

$$\Delta\omega_{\text{FWHM}} = \frac{4}{\tau_g}\sin^{-1}\frac{1}{\sqrt{\widetilde{F}}} \equiv \frac{\Delta\omega_{\text{FSR}}}{\mathcal{F}}, \tag{4.70}$$

where

$$\mathcal{F} \equiv \frac{\pi}{2\sin^{-1}\left(1/\sqrt{\widetilde{F}}\right)} \approx \frac{\pi}{2}\sqrt{\widetilde{F}}, \tag{4.71}$$

is known as the *finesse* of the resonator, with the last approximation valid if $\widetilde{F} \gg 1$. At first glance, Eq. (4.70) does not appear to be completely consistent with that of Eq. (4.54). The difference arises because Eq. (4.66) includes the factor of $1/2$ in Eq. (4.52a), so the way that we have defined "half-maximum" is not the same in the two cases. In the limit $\Gamma \longrightarrow 1$, both methods yield $\Delta\omega_{\text{FWHM}} \approx 2(1 - \Gamma)/\tau_g$. The relationship between Q, defined by Eq. (4.55), and the finesse is

$$Q = \frac{L}{\lambda_g}\mathcal{F}, \tag{4.72}$$

where $\lambda_g \equiv \lambda_0/n'(\omega_0)$ is the "group wavelength" of an input field with vacuum wavelength λ_0. In macroscopic resonators ($L \sim 1$ m), the ratio L/λ_g is so large that Q isn't a particularly useful metric of cavity quality, but Q is routinely chosen to describe the optical quality of microscale and nanoscale resonators.

4.2.2.3 Resonant Cavities as Linear Filters

Comparing Eq. (4.46) and Eq. (4.52a), note that we have demonstrated the identity

$$f(\omega) = \sum_{n=0}^{\infty} \left(\Gamma e^{i\omega}\right)^n = \frac{1}{2} + \sum_{q=-\infty}^{+\infty} \frac{i}{\omega - \nu_q}, \tag{4.73}$$

subject to our usual disclaimers about mathematical rigor. Therefore, taking the Fourier transform of all terms in this expression, we find

$$f(t) = \sum_{n=0}^{\infty} \Gamma^n \delta(t - n) = \frac{1}{2}\delta(t) + \Theta(t) \sum_{q=-\infty}^{+\infty} e^{-i\nu_q t}, \tag{4.74}$$

where we have used the Fourier Shift Theorem given by Eq. (A.15) and the form of the Dirac delta function shown in Eq. (A.35) adapted for the time domain. The sum over n is completely consistent with Eq. (4.47a) in the context of the Fourier Convolution Theorem, Eq. (A.22). The sum over q is easily calculated using contour integration, or by the Mathematica command shown in Listing 4.1. Both series are consistent with the causality requirements [22] discussed in Section A.3.6.

Listing 4.1: Mathematica Command for Inverse Fourier Transform of a Complex Lorentzian

```
FullSimplify[InverseFourierTransform[I/((\[Omega]-\[CapitalOmega]) \[Tau]),
        \[Omega],t,FourierParameters->{1,1}], {\[Tau]>0,Im[\[CapitalOmega]]<0}]
```

Note that the frequency dependence of R_1 and R_2 can be captured by letting $\Gamma \longrightarrow \Gamma_q \equiv \Gamma(\omega_0 + 2q\pi/\tau_g)$. Also, this subsubsection really needs to include a reason to work in the frequency domain at all, given that the time domain is so simple; this is a good place to use the power theorem to estimate the transmitted and reflected power.

4.3 Quasi-Normal Modes

In Eq. (2.9), we have defined the real vector electric field that is rapidly varying in both space and time as

$$\mathcal{E}(\mathbf{r}, t) = \frac{e^{-i\omega_0 t}}{2} \mathbf{E}(\mathbf{r}, t) + \text{c.c.}, \tag{4.75}$$

where $\mathbf{E}(\mathbf{r}, t)$ is a complex vector electric field amplitude that varies rapidly in space but slowly in time. In turn, following Eq. (4.1), we express this vector amplitude for the case of forward and backward propagating waves in one dimension in terms of the complex scalar amplitudes $E^+(z, t)$ and $E^-(z, t)$ of fields that varies slowly in both space and time as

$$\mathbf{E}^+(\mathbf{r}, t) \equiv \hat{\epsilon}\, e^{+i k_0(\omega_0) z} E^+(z, t), \text{ and} \tag{4.76a}$$

$$\mathbf{E}^-(\mathbf{r}, t) \equiv \hat{\epsilon}\, e^{-i k_0(\omega_0) z} E^-(z, t) \tag{4.76b}$$

where $\hat{\epsilon}$ is a complex polarization vector and $k_0(\omega_0) = \text{Re}\,[\beta(\omega_0)] = (\omega_0/c)n(\omega_0)$ is the effective propagation vector magnitude. These slowly-varying envelope functions solve the appropriate homogeneous wave equation, given by Eq. (4.2) and Eq. (4.7) in the frequency domain. In the following discussion, our goal will be to use the solutions to these equations — given in Section 4.1.1 — to find the frequencies of the eigenmodes of Eq. (4.2) and Eq. (4.7) that satisfy the internal boundary conditions appropriate for a laser resonator.

This section needs a better introduction than this. The concept of "modes of the universe" and the history of approaches to this problem should be described, so that the utility of the approach here is highlighted. It would probably be a good idea to move Eq. (4.132) here.

4.3.1   Eigenfunctions of a 1D Unidirectional Ring Resonator

Consider a laser cavity selected from the set of one-dimensional resonators shown in Fig. 4.5 with $R_2 = 1$ and $\mathbf{F}_2(t) = 0$. We will define the reflectivity of the output coupling mirror $\mathcal{M}_1$ as $R \equiv R_1$. In the absence of the injected field $\mathbf{F}_1(t)$, the boundary condition satisfied by the forward-propagating intracavity field amplitude $\mathbf{E}^+(z, \omega)$ is given by Eq. (4.33) as

$$\mathbf{E}^+(0, \omega) = \sqrt{R}\, \mathbf{E}^+(1, \omega), \tag{4.77}$$

As described in Section 4.1.1, the solution to Eq. (4.2) in the frequency domain is given by Eq. (4.3), which when substituted into Eq. (4.1) yields

$$\mathbf{E}^+(1, \omega) = G(1, \omega)\, \mathbf{E}^+(0, \omega), \tag{4.78}$$

as given by Eq. (4.4) for the case where $z_1 = 0$ and $z_2 = 1$. If we substitute Eq. (4.78) into the right-hand side of Eq. (4.77), we obtain the constraint

$$\sqrt{R}\, G(1, \omega) = \sqrt{R}\, \exp\left[i\, \omega_0\, \tau/\tau_g + i\, \omega - \frac{1}{2}\alpha(\omega_0)\right] = \Gamma\, e^{i\omega} = 1, \tag{4.79}$$

where Γ is given by Eq. (4.42) with $R_1 \equiv R$ and $R_2 = 1$. We note that the contribution of $\omega_0\, \tau = k_0(\omega_0)$ in Γ is in fact the result of the rapidly-varying factor $e^{+i\,k_0(\omega_0)\,z}$ accumulating phase over one full cavity round-trip, and should be neglected in our construction of slowly-varying spatial eigenmodes of the cavity. We can do this by modifying the boundary condition given by Eq. (4.77) to include a factor of $e^{i\omega_0\tau}$, or by choosing ω_0 such that $e^{i\omega_0\tau} = 1$.

By comparing this result with Eq. (4.41a) and Eq. (4.50), we see immediately that the eigenfrequencies $\omega \equiv \nu_q$ which satisfy Eq. (4.79) are those of the poles of Eq. (4.41), with the rapidly-varing phase removed. The corresponding complex propagation constant is given by Eq. (4.51a) as

$$\frac{\nu_q}{c} \equiv \frac{2q\pi + i \ln|\Gamma|}{L_g}, \tag{4.80}$$

where the round-trip group cavity length is defined in terms of Eq. (4.45) as

$$L_g \equiv c\tau_g = n'(\omega_0)L. \tag{4.81}$$

The eigenfunctions $u_q(z)$ we seek satisfy Eq. (4.2) with $\omega = \nu_q$ (and $e^{i\omega_0\tau} = 1$), or

$$\frac{d}{dz}u_q(z) - i\,\nu_q\, u_q(z) + \frac{1}{2}\,\alpha(\omega_0)\, u_q(z) = 0, \tag{4.82}$$

which has the solution

$$u_q(z) = C \exp\left[\left(i2q\pi + \ln\frac{1}{\sqrt{R}}\right)z\right], \tag{4.83}$$

where C is a normalization factor. We note that $u_q(0) = C$, and $u_q(1) = C/\sqrt{R}$, so an expansion of $E^+(z, t)$ as a series of these eigenfunctions satisfies the boundary condition given by Eq. (4.77) for the complex vector envelope function.

In fact, we would like to follow the usual eigenfunction expansion approach for a self-adjoint differential operator, where we might expect that $\int_0^1 dz\, u_q(z)\, u_p^*(z) = |C|^2\delta_{qp}$. However, when $u_q(z)$ is given by Eq. (4.83), we find

$$\int_0^1 dz\, u_q(z)\, u_p^*(z) = |C|^2 \int_0^1 dz\, e^{[i2(q-p)\pi + \ln(1/R)]z}$$

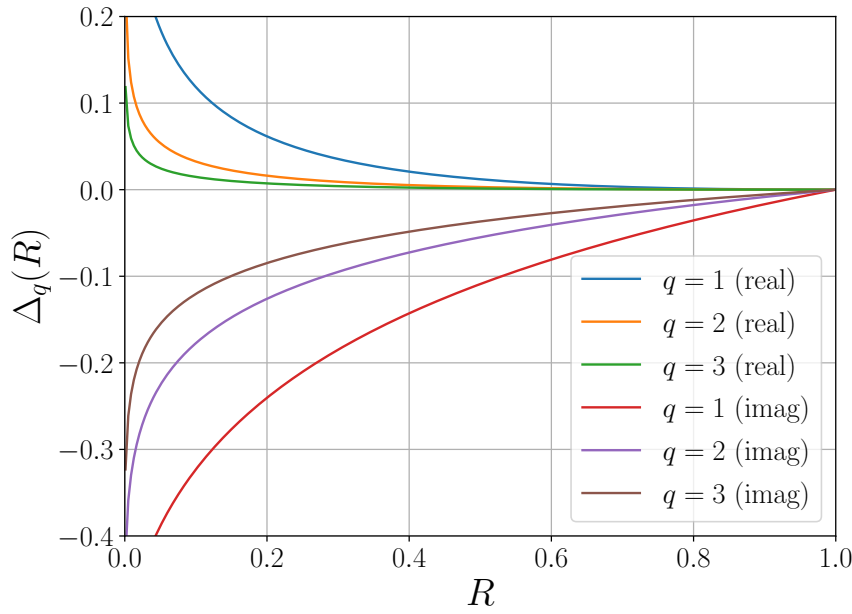$$= |C|^2\, \frac{e^{i2(q-p)\pi + \ln(1/R)} - 1}{i2\,(q - p)\,\pi + \ln(1/R)}, \tag{4.84}$$

Figure 4.7: Plot of the real and imaginary parts of $\Delta_q(R)$, defined by Eq. (4.86), as a function of the output coupler reflectivity R.

giving

$$\int_0^1 dz\, u_q(z)\, u_p^*(z) = \Delta_{q-p}(R),$$ (4.85)

where

$$\Delta_q(R) \equiv \frac{1}{1 + i2q\pi/\ln(1/R)} \approx \begin{cases} 1 & \text{if } q = 0 \\ [\ln(1/R)/(2q\pi)]^2 - i\,[\ln(1/R)/(2q\pi)] & \text{if } q \neq 0 \end{cases}$$ (4.86)

and we have chosen the normalization constant

$$C \equiv \sqrt{\frac{R\ln(1/R)}{1 - R}}.$$ (4.87)

We are forced to conclude that the forward-propagating eigenmodes are not strictly self-orthogonal. As shown in Fig. 4.7, $\Delta_q(R)$ can be reasonably approximated as a Kronecker delta function only as $R \to 1$. This nonorthogonality of the longitudinal eigenmodes has observable physical consequences, such as excess spontaneous emission into each mode of a laser [23].

The difficulty arises because the boundary condition at the output coupler turns the laser resonator into an "open system:" although the differential operator governing our wave equation is self-adjoint, the boundary condition given by Eq. (4.77) breaks this symmetry. We can see this immediately for the simple case where the interior of the cavity is vacuum, so that $n' = 1$ and $\alpha = 0$. If we formally integrate the left-hand side of Eq. (4.2), then we obtain
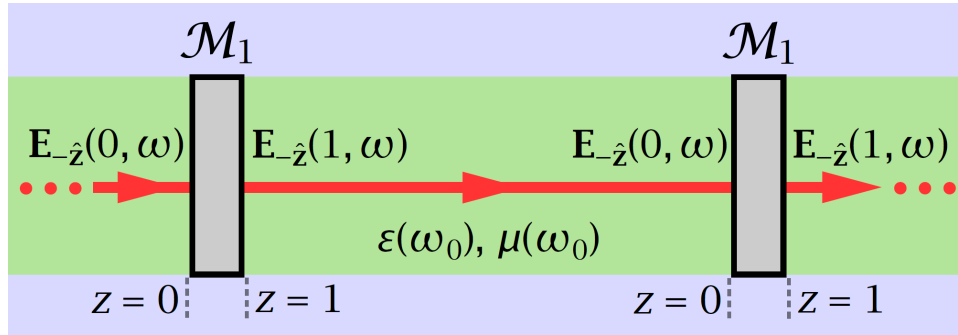
$$E^+(z, \omega) = -i\frac{\omega}{c}\int_0^1 dz'\, K(z, z')\, E^+(z', \omega),$$ (4.88)

where $K(z, z')$ is the Green's function (or *propagator*) that satisfies both the differential equation

$$\frac{\partial}{\partial z}K(z, z') = -\delta(z - z')$$ (4.89)
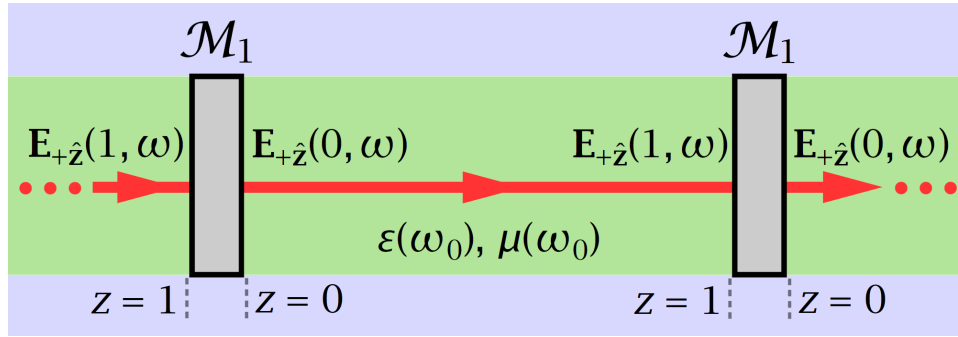
(a) Forward propagation

(b) Backward propagation

Figure 4.8: Diagrams of "unfolded" cavities depicting round-trip propagation in the (a) forward and (b) backward directions. Although each of these pictures resembles a standing-wave cavity, they in fact represent any of the resonator configurations shown in Fig. 4.5.

and the boundary condition $K(0, z') = \sqrt{R}\, K(1, z')$. By inspection, we construct this propagator as

$$K(z, z') = -\frac{\Theta(z - z') + \sqrt{R}\, \Theta(z' - z)}{1 - \sqrt{R}}, \tag{4.90}$$

where $\Theta(z)$ is the Heaviside Theta function. We note immediately that $K(z, z')$ is *not* Hermitian: since $\Theta(z)$ is not even in its argument, $K(z, z') \neq K(z', z)$. This property is ubiquitous in laser physics; we shall see in Chapter 8 that the transverse eigenmodes of open-sided laser resonators are not self-orthogonal.

4.3.2 Biorthogonality and Completeness of the Eigenfunctions

This subsection needs a proper introduction.

$$\mathbf{E}^-(1, \omega) = \sqrt{R}\, \mathbf{E}^-(0, \omega), \tag{4.91}$$

Therefore, the slowly-varying backward-propagating eigenfunctions we seek satisfy Eq. (4.7) with $\omega = \nu_q$, or

$$\frac{d}{dz} v_q(z) + i\, \nu_q\, v_q(z) - \frac{1}{2}\, \alpha(\omega_0)\, v_q(z) = 0, \tag{4.92}$$

which has the solution

$$v_q(z) \equiv C' \exp\left[-\left(i2q\pi + \ln\frac{1}{\sqrt{R}}\right) z\right]. \tag{4.93}$$

In this case, we find that $v_q(0) = C'$, and $v_q(1) = C'\sqrt{R}$, so these eigenfunctions satisfy the same boundary condition given by Eq. (4.91) as the backward-propagating complex vector envelope function. Let us now try to find an integral relationship that allows us to ... If we multiply Eq. (4.82) by $v_p(z)$ and Eq. (4.92) (with $q \to p$) by $u_q(z)$ and then add the results, we obtain

$$\frac{d}{dz}\left[u_q(z)v_p(z)\right] - i\,2\pi\,(q - p)\, u_q(z)v_p(z) = 0. \tag{4.94}$$

Integrating both sides of this equation from $z = 0$ to $z = 1$ yields

$$2\pi\,(q - p) \int_0^1 dz\, u_q(z)\, v_p(z) = -i\left[u_q(1)\, v_p(1) - u_q(0)\, v_p(0)\right] = 0, \tag{4.95}$$

since $u_q(1)v_p(1) = u_q(0)v_p(0) = CC'$. Therefore, if $q \neq p$, the integral on the left-hand side of this equation must vanish. We can verify this explicitly using the functional forms of $u_q(z)$ and $v_q(z)$ given by Eq. (4.83) and Eq. (4.93), respectively; we find that the result of the integral is given by $CC'\delta_{qp}$. If we choose the scaling constant $C' = 1/C$, where C is given by Eq. (4.87), and define

$$u_q(z) \equiv C\, e^{+\left[i2q\pi + \ln(1/\sqrt{R})\right]z}, \text{ and} \tag{4.96a}$$

$$v_q(z) \equiv \frac{1}{C}\, e^{-\left[i2q\pi + \ln(1/\sqrt{R})\right]z}, \tag{4.96b}$$

then $u_q(z)$ and $v_q(z)$ jointly satisfy the weighted *biorthogonality relation*

$$\int_0^1 dz\, u_q(z)\, v_p(z) = \delta_{qp}. \tag{4.97}$$

Before we can develop a self-consistent approach to expanding the intracavity slowly-varying scalar envelope function $E^+(z, t)$, we need to find a relation that establishes the completeness of the eigenfunctions defined by Eq. (4.96). Consider the sum

$$\sum_{q=-\infty}^{\infty} u_q(z)\, v_q(z') = e^{-\ln(\sqrt{R})\,(z-z')} \sum_{q=-\infty}^{\infty} e^{i2q\pi(z-z')}. \tag{4.98}$$

Relying on the definition of the Dirac comb [22],

$$\sum_{q=-\infty}^{\infty} e^{i2q\pi(z-z')} = \sum_{m=-\infty}^{\infty} \delta\left(z - z' + m\right), \tag{4.99}$$

we find

$$\sum_{q=-\infty}^{\infty} u_q(z)\, v_q(z') = \sum_{m=-\infty}^{\infty} R^{m/2}\delta\left(z - z' + m\right). \tag{4.100}$$

If we confine $|z - z'| < 1$, then terms on the right-hand side of this expression with $m \neq 0$ will not contribute, and we have the *completeness relation*

$$\sum_{q=-\infty}^{\infty} u_q(z)\, v_q(z') = \delta\left(z - z'\right), \tag{4.101}$$

valid for $0 < z < 1$ (i.e., everywhere in the cavity *except* at the boundary).

We now have the machinery at our disposal to find a valid expansion of the forward-propagating field $E^+(z,t)$ as a series of time-dependent coefficients multiplied by the functions $u_q(z)$. Dropping the subscript, we have

$$\begin{aligned} E(z,t) &= \int_0^1 dz'\, \delta\left(z - z'\right) E(z',t) \\ &= \sum_{q=-\infty}^{\infty} u_q(z) \int_0^1 dz'\, v_q(z')E(z',t), \end{aligned} \tag{4.102}$$

or

$$E(z,t) = \sum_{q=-\infty}^{\infty} u_q(z)\, E_q(t), \tag{4.103}$$

where

$$E_q(t) \equiv \int_0^1 dz\, v_q(z)E(z,t). \tag{4.104}$$

We make two adjustments to these expressions before choosing the final form of our slowly-varying eigenfunction expansions. The argument $2q\pi \equiv \Delta k_q$ in the exponent of $u_q(z)$ represents a small change in the propagation constant $k_0(\omega_0)$. There must be a corresponding small shift in the carrier frequency ω_0, since

$$\begin{aligned} k_0\left(\omega_0 + \delta\omega\right) &= \frac{\left(\omega_0 + \delta\omega\right) n\left(\omega_0 + \delta\omega\right)}{c} \\ &\cong k_0(\omega_0) + \frac{\delta\omega}{c}\left[n(\omega_0) + \omega_0\frac{dn(\omega_0)}{d\omega_0}\right] \\ &= k_0(\omega_0) + \frac{n'(\omega_0)}{c}\delta\omega \\ &\equiv k_0(\omega_0) + \delta k. \end{aligned} \tag{4.105}$$

If $\delta k = \Delta k_q$, then we must have

$$\delta\omega = \Delta\omega_q \equiv \frac{c}{n'(\omega_0)}\Delta k_q = \frac{2q\pi}{\tau_g} = q\Delta\omega_{\text{FSR}}, \tag{4.106}$$

where $\Delta\omega_{\text{FSR}}$ is defined by Eq. (4.69). Therefore, we can define the effective rapidly-varying propagation vector and frequency of each eigenmode as

$$k_q \equiv k_0(\omega_0) + 2q\pi, \text{ and} \tag{4.107a}$$
$$\omega_q \equiv \omega_0 + 2q\pi, \tag{4.107b}$$

For convenience, then, we make this frequency shift explicit, and write our expansions as

$$E(z,t) = \sum_{q=-\infty}^{\infty} u_q(z)\, e^{-i\Delta\omega_q t}\, E_q(t), \tag{4.108}$$

where

$$E_q(t) \equiv e^{+i\Delta\omega_q t} \int_0^1 dz\, v_q(z) E(z,t). \tag{4.109}$$

The analogs of these two equations in the frequency domain are straightforward.

The output electric field $E_1(t) = \sqrt{1-R}\, E(1,t)$ takes on a particularly elegant form given Eq. (4.96a) and Eq. (4.108). Since $u_q(1) = C/\sqrt{R}$, using Eq. (4.87) we obtain

$$E_1(t) = \sqrt{\ln\left(\frac{1}{R}\right)} \sum_{q=-\infty}^{\infty} e^{-i\Delta\omega_q t}\, E_q(t). \tag{4.110}$$

We close this section with the subtle but important observation that the functions $v_q(z)$ are *not* normalized. Rather, they are scaled to allow us to project field amplitudes such as $E^+(z,t)$ and $P^+(z,t)$ onto the space of functions $u_q(z)$ using Eq. (4.109). Although $v_q(z)$ has the functional form of backward-propagating fields, a bidirectional ring laser would need two properly normalized eigenfunction basis sets, $u_q^+(z)$ and $u_q^-(z)$, with the corresponding biorthogonal projectors, $v_q^+(z)$ and $v_q^-(z)$, to expand the counterpropagating fields within the resonator. We see this explicitly in the next section for the case of a standing-wave resonator.

4.3.3 Eigenfunctions of a 1D Standing-Wave Resonator

Let us now construct a similar set of eigenmodes for the standing-wave laser resonator shown in Fig. 4.5a, where both mirror reflection coefficients differ from unity. When we were analyzing the scattering matrices of resonant cavities in Section 4.1.3, it was convenient to "fold" the coordinate system so that $0 < z < 1/2$ represented the coordinate for propagation from the reference plane at $\mathcal{M}_1$ (just *after* reflection) to the reference plane at $\mathcal{M}_2$ (just *before* reflection), and $1/2 < z < 1$ represented the coordinate for propagation from the reference plane at $\mathcal{M}_2$ (just *after* reflection) to the reference plane at $\mathcal{M}_1$ (just *before* reflection). But this convenience isn't as helpful when we begin to construct physical models of lasers, where the total electric field at each point within the laser amplifier drives the evolution of the local population inversion.

In the absence of the injected fields $\mathbf{F}_1(t)$ and $\mathbf{F}_1(t)$, the boundary conditions satisfied by the intracavity field amplitudes $\mathbf{E}^\pm(z,\omega)$ are given by Eq. (4.33) as

$$\mathbf{E}^+(0,\omega) = -\sqrt{R_1}\,\mathbf{E}^-(0,\omega), \text{ and} \tag{4.111a}$$

$$\mathbf{E}^-(1/2,\omega) = -\sqrt{R_2}\,\mathbf{E}^+(1/2,\omega), \tag{4.111b}$$

where we have repositioned the reference planes using Eq. (4.30) to be consistent with the sign convention chosen in many of the discussions of standing-wave cavities in the literature. Then, in this case, the most convenient choice is to represent the rapidly-varying eigenmodes as a "vector" with components representing the solution of the full wave equations on $0 < z < 1/2$ subject to the boundary conditions. If we write [24]

$$\mathbf{u}_q(z) = \begin{bmatrix} u_q^+(z) \\ u_q^-(z) \end{bmatrix}, \tag{4.112}$$

then, following the analysis of Section 4.3.1, we find

$$u_q^+(z) = C e^{+\left[i2q\pi + \ln\left(1/\sqrt{R_1 R_2}\right)\right]z}, \text{ and} \tag{4.113a}$$

$$u_q^-(z) = -C\sqrt{R_2}\, e^{+\left[i2q\pi + \ln\left(1/\sqrt{R_1 R_2}\right)\right](1-z)}$$

$$= -\frac{C}{\sqrt{R_1}} e^{-\left[i2q\pi + \ln\left(1/\sqrt{R_1 R_2}\right)\right]z}. \tag{4.113b}$$

It is clear that both of the boundary conditions — at $z = 0$ and $z = 1/2$ — are satisfied when we assume that $e^{i\omega_0\tau} = e^{ik_0(\omega_0)} = 1$. The normalization integral

$$\int_0^{1/2} dz\, \mathbf{u}_q(z) \cdot \mathbf{u}_q^*(z) = |C|^2 \left[\int_0^{1/2} dz\, e^{z\ln(1/R_1 R_2)} + \frac{1}{R_1} \int_0^{1/2} dz\, e^{-z\ln(1/R_1 R_2)} \right]$$

$$= |C|^2 \frac{\left(\sqrt{R_1} + \sqrt{R_2}\right)\left(1 - \sqrt{R_1 R_2}\right)}{R_1\sqrt{R_2}\,\ln\left(1/R_1 R_2\right)} \tag{4.114}$$

is unity if we choose the normalization constant

$$C = \left[\frac{2\,R_1\sqrt{R_2}\,\ln\left(1/\sqrt{R_1 R_2}\right)}{\left(\sqrt{R_1} + \sqrt{R_2}\right)\left(1 - \sqrt{R_1 R_2}\right)} \right]^{1/2}. \tag{4.115}$$

Then the nonorthogonality integral is given by

$$\int_0^{1/2} dz\, \mathbf{u}_p(z) \cdot \mathbf{u}_q^*(z) = C^2 \left[\int_0^{1/2} dz\, e^{[i2(p-q)\pi + \ln(1/R_1 R_2)]z} + \frac{1}{R_1} \int_0^{1/2} dz\, e^{-[i2(p-q)\pi + \ln(1/R_1 R_2)]z} \right]$$

$$= \Delta_{p-q}'(R_1 R_2), \tag{4.116}$$

where

$$\Delta_q'(R_1 R_2) \equiv \begin{cases} \Delta_q(R_1 R_2) & \text{if } q \text{ is even} \\ \frac{\left(1+\sqrt{R_1 R_2}\right)\left(\sqrt{R_2}-\sqrt{R_1}\right)}{\left(\sqrt{R_1}+\sqrt{R_2}\right)\left(1-\sqrt{R_1 R_2}\right)}\, \Delta_q(R_1 R_2) & \text{if } q \text{ is odd} \end{cases} \tag{4.117}$$

and $\Delta_q(R)$ is given by Eq. (4.86). Once again, we see that the eigenmodes are not strictly orthogonal unless both R_1 and R_2 approach unity. Note that when $R_1 = R_2$, all the odd-q modes vanish, and when $R_2 = 1$, $\Delta_q'(R_1 R_2) = \Delta_q(R_1 R_2)$ for any value of q.

We define the backward-propagating projection eigenmodes in vector form as

$$\mathbf{v}_q(z) = \begin{bmatrix} v_q^+(z) \\ v_q^-(z) \end{bmatrix}, \tag{4.118}$$

and simply reverse the directions of the standing-wave functions given by Eq. (4.113) to obtain

$$v_q^+(z) = C' e^{-\left[i2q\pi + \ln\left(1/\sqrt{R_1 R_2}\right)\right]z}, \text{ and} \tag{4.119a}$$

$$v_q^-(z) = -\frac{C'}{\sqrt{R_2}} e^{-\left[i2q\pi + \ln\left(1/\sqrt{R_1 R_2}\right)\right](1-z)}$$

$$= -C'\sqrt{R_1}\, e^{+\left[i2q\pi + \ln\left(1/\sqrt{R_1 R_2}\right)\right]z}. \tag{4.119b}$$

It is easy to verify that the two sets of eigenmodes are biorthogonal, since

$$\int_0^{1/2} dz\, \mathbf{u}_q(z) \cdot \mathbf{v}_p(z) = \delta_{qp}, \tag{4.120}$$

where again $C' = 1/C$.

At first glance, it isn't entirely obvious how to craft a completeness relation that would allow us to expand a spatially rapidly-varying, single-transverse-mode field in a series over the eigenfunctions $\mathbf{u}_q(z)$. As a guide, we note that the sum $\sum_q \mathbf{u}_q(z)\mathbf{v}_q^T(z)$ contains diagonal terms proportional to $\sum_q e^{\pm i2q\pi(z-z')}$ that will simplify to $\delta(z-z')$ using Eq. (4.99), and off-diagonal terms proportional to $\sum_q e^{\pm i2q\pi(z+z')}$ that will become $\sum_m \delta(z+z'+m)$. These latter arguments are never zero for any m over the interval $0 < z < 1/2$, so we have

$$\sum_{q=-\infty}^{\infty} \mathbf{u}_q(z)\mathbf{v}_q^T(z') = \begin{bmatrix} \delta(z-z') & 0 \\ 0 & \delta(z-z') \end{bmatrix}, \tag{4.121}$$

Therefore, if we write the coefficients of the total spatially rapidly-varying electric field $\tilde{E}(z,t) = E^+(z,t)e^{+ik_0(\omega_0)z} + E^-(z,t)e^{-ik_0(\omega_0)z}$ in vector form as

$$\mathbf{E}(z,t) = \begin{bmatrix} E^+(z,t) \\ E^-(z,t) \end{bmatrix}, \tag{4.122}$$

then

$$\mathbf{E}(z,t) = \int_0^{1/2} dz' \begin{bmatrix} \delta(z-z') & 0 \\ 0 & \delta(z-z') \end{bmatrix} \mathbf{E}(z',t)$$
$$= \sum_{q=-\infty}^{\infty} \mathbf{u}_q(z) \int_0^{1/2} dz'\, \mathbf{v}_q^T(z') \mathbf{E}(z',t), \tag{4.123}$$

or

$$\mathbf{E}(z,t) = \sum_{q=-\infty}^{\infty} \mathbf{u}_q(z)\, e^{-i\Delta\omega_q t}\, E_q(t), \tag{4.124}$$

where

$$E_q(t) \equiv e^{+i\Delta\omega_q t} \int_0^{1/2} dz\, \mathbf{v}_q(z) \cdot \mathbf{E}(z,t). \tag{4.125}$$

The output fields from each mirror can be calculated given Eq. (4.113) and Eq. (4.124):

$$E_1 = i\sqrt{1-R_1} \sum_q u_q^-(0)\, e^{-i\Delta\omega_q t}\, E_q(t), \text{ and} \tag{4.126a}$$

$$E_2 = i\sqrt{1-R_2} \sum_q u_q^+(1/2)\, e^{-i\Delta\omega_q t}\, E_q(t). \tag{4.126b}$$

Since $u_q^-(0) = -C/\sqrt{R_1}$, and $u_q^+(1/2) = (-1)^q C/(R_1R_2)^{1/4}$, using Eq. (4.115) we find

$$E_1 = -i\left[\frac{2(1-R_1)\sqrt{R_2}\ln(1/\sqrt{R_1R_2})}{(\sqrt{R_1}+\sqrt{R_2})(1-\sqrt{R_1R_2})}\right]^{1/2} \sum_q e^{-i\Delta\omega_q t}\, E_q(t), \text{ and} \tag{4.127a}$$

$$E_2 = i\left[\frac{2\sqrt{R_1}(1-R_2)\ln(1/\sqrt{R_1R_2})}{(\sqrt{R_1}+\sqrt{R_2})(1-\sqrt{R_1R_2})}\right]^{1/2} \sum_q (-1)^q\, e^{-i\Delta\omega_q t}\, E_q(t). \tag{4.127b}$$

Although in general each of these expressions lacks the elegance of Eq. (4.110), they each give exactly the same result in two cases of practical interest:

1. In the limit where one of the mirrors has unit reflectivity — either the substitution $R_1 = R$ and $R_2 = 1$ for E_1, or $R_1 = 1$ and $R_2 = R$ for E_2, will simplify the magnitude of the corresponding coefficient on the left of the sum to $\sqrt{\ln(1/R)}$.

2. When $R_1 = R_2 \equiv R$, the magnitude of each coefficient on the left of the corresponding sum becomes $\sqrt{\ln(1/R)}$.

In fact, it is remarkable that over a wide range of values of R_1 and R_2, we can make the same approximation without significant loss of accuracy. If we write $R_1 \equiv 1 - \delta_1$ and $R_2 \equiv 1 - \delta_2$, then we find as $\{\delta_1, \delta_2\} \longrightarrow \{0, 0\}$ that

$$\left[\frac{2\sqrt{R_1 R_2} \, \ln\left(1/\sqrt{R_1 R_2}\right)}{\left(\sqrt{R_1} + \sqrt{R_2}\right)\left(1 - \sqrt{R_1 R_2}\right)} \right]^{1/2} \approx 1 - \frac{\delta_1^2 - \delta_1 \delta_2 + \delta_2^2}{48}, \tag{4.128}$$

so that we can almost always approximate the product of this coefficient and the factor $\sqrt{(1 - R_j)/R_j}$ as simply $\sqrt{\ln(1/R_j)}$.

In Section 7.4, we will describe the intracavity spatial dependence of the total field of longitudinal mode q as

$$\tilde{u}_q(z) = u_q^+(z) \, e^{+ik_0 z} + u_q^-(z) \, e^{-ik_0 z}$$
$$= C \left\{ e^{+\left[ik_q + \ln\left(1/\sqrt{R_1 R_2}\right)\right] z} - \frac{1}{\sqrt{R_1}} e^{-\left[ik_q + \ln\left(1/\sqrt{R_1 R_2}\right)\right] z} \right\}, \tag{4.129}$$

where k_q is given by Eq. (4.107a). In the case where $R_1 = 1$ and $R_2 \equiv R$, Eq. (4.129) can be approximated quite accurately by assuming that $\ln(1/\sqrt{R}) \ll 1$, and expanding $\exp[\ln(1/\sqrt{R})z]$ linearly in z to obtain

$$\tilde{u}_q(z) \approx i2C \left[\sin\left(k_q z\right) - i \ln\left(\frac{1}{\sqrt{R}}\right) z \cos\left(k_q z\right) \right]. \tag{4.130}$$

In Fig. 4.9, we have plotted Eq. (4.129) with Eq. (4.130) for $k_q = 10\pi$, $R_1 = 1$, and $R_2 \equiv R = 0.3$. We have scaled all functions by a factor of $i2C$ to allow a direct comparison with the simple function $\sin(k_q z)$ that is often chosen in the literature. The relative accuracy of Eq. (4.130) is surprising for a reflectivity this low, but it is clear that the simple approximation fails badly near the output coupler.

4.4   Temporal Coupled-Mode Theory

As an example of the utility of the quasi-normal mode methods discussed above, we expand the intracavity fields of the resonators shown in Fig. 4.5 for the scalar case where $R_2 = 1$ and, therefore, $F_2(\omega) = 0$.

4.4.1   One-Dimensional Unidirectional Ring Resonator

We begin by using Eq. (A.10b) to calculate the Fourier Transform of the expansion coefficient in Eq. (4.109) as

$$E_q(\omega) = \int_{-\infty}^{+\infty} dt \, e^{+i\omega t} E_q(t) = \int_0^1 dz \, v_q(z) \, E(z, \omega + 2q\pi), \tag{4.131}$$

where we have reapplied the Fourier Shift Theorem given by Eq. (A.15) in the frequency domain. From Eq. (4.3),

$$E(z, \omega) = \exp\left[i\omega z - \frac{1}{2}\alpha(\omega_0) z \right] E(0, \omega), \tag{4.132}$$

where $E(0, \omega)$ is given by Eq. (4.58) for the ring resonator under consideration here. Substituting Eq. (4.132) into Eq. (4.131), we find

$$\begin{aligned} E_q(\omega) &= \frac{i\sqrt{\eta T}}{C} \frac{F(\omega + 2q\pi)}{1 - \Gamma \, e^{i\omega}} \int_0^1 dz \, e^{(i\omega + \ln\Gamma) z} \\ &= \frac{i\sqrt{\eta T}}{C} \frac{F(\omega + 2q\pi)}{1 - \Gamma \, e^{i\omega}} \frac{e^{i\omega + \ln\Gamma} - 1}{i\omega + \ln\Gamma} \\ &= -\frac{i\sqrt{\eta T}}{C} \frac{F(\omega + 2q\pi)}{i\omega + \ln\Gamma}. \end{aligned} \tag{4.133}$$

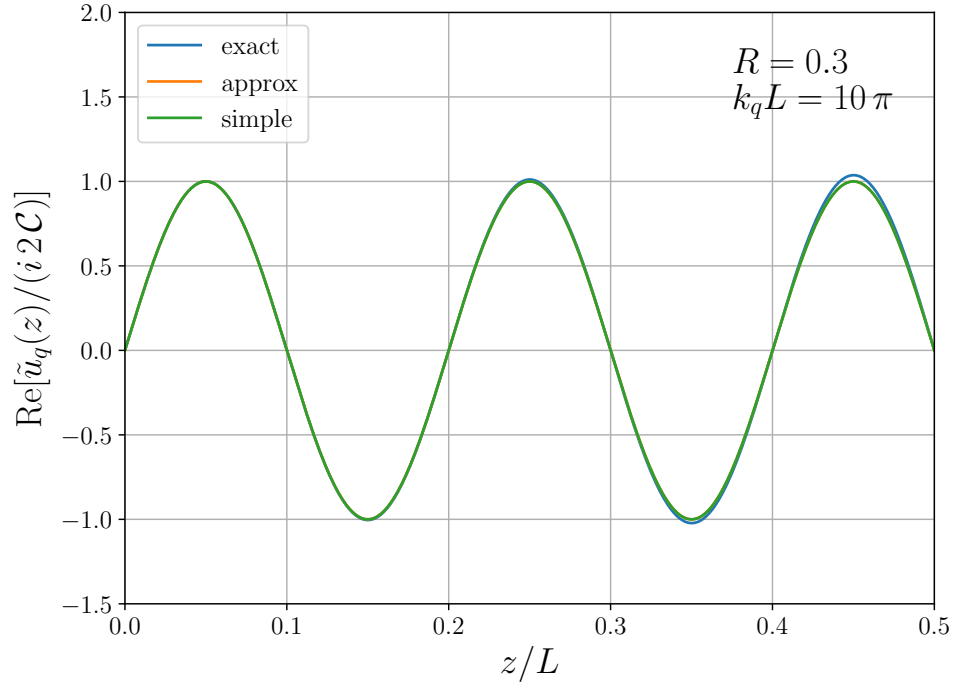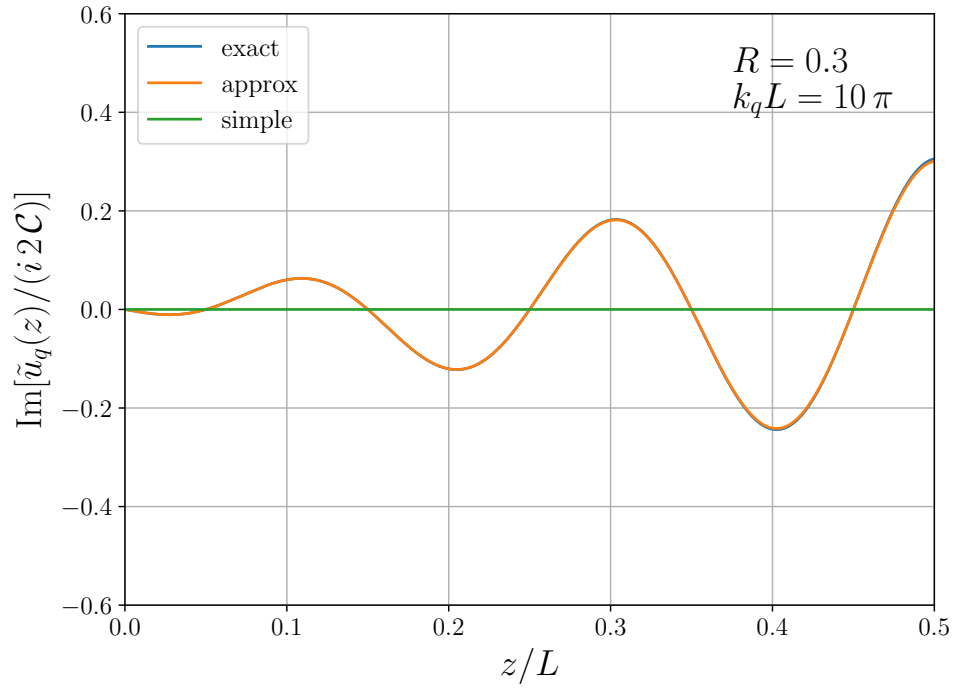(a) Real part of $\tilde{u}_q(z)/(i\,2\,C)$

(b) Imaginary part of $\tilde{u}_q(z)/(i\,2\,C)$

Figure 4.9: Plot of Eq. (4.129) with Eq. (4.130) for $k_q = 10\,\pi$, $R_1 = 1$, and $R_2 \equiv R = 0.3$. We have scaled all functions by a factor of $i\,2\,C$ to allow a direct comparison with the simple function $\sin(k_q z)$ that is often chosen in the literature. The relative accuracy of Eq. (4.130) is surprising for a reflectivity this low, but it is clear that the simple approximation fails badly near the output coupler.

We can follow either of two approaches to determine $E_q(t)$ for general $F(\omega)$. Choosing the method of integration, we can take the Fourier transform of Eq. (4.133) and apply the shift theorem to obtain

$$E_q(t) = \frac{\sqrt{\eta T}}{C} e^{i2q\pi t} \int_{-\infty}^{+\infty} \frac{d\omega}{2\pi} e^{-i\omega t} \frac{F(\omega)}{\nu_q - \omega} , \tag{4.134}$$

where ν_q is defined by Eq. (4.51a). Alternatively, we can multiply both sides of Eq. (4.133) by $i\omega + \ln\Gamma$, take the Fourier transform, and then apply the Fourier derivative theorem to find the ordinary differential equation

$$\dot{E}_q(t) + \frac{1}{2\tau_p} E_q(t) = \frac{i\sqrt{\eta T}}{C} e^{i2q\pi t} F(t) , \tag{4.135}$$

where we have used Eq. (4.54) to write $\ln(1/\Gamma) = 1/2\tau_p$. The damping term on the left-hand side of this equation has two contributions:

$$\frac{1}{2\tau_p} = \frac{1}{2} \alpha(\omega_0) + \frac{1}{2} \ln\left(\frac{1}{1-T}\right) , \tag{4.136}$$

First, $\alpha(\omega_0)/2$ describes the rate (scaled by τ_g^{-1}) at which the intracavity field in Eq. (4.135) decays due to internal dissipative losses. Second, in the limit $T \ll 1$, the term $T/2$ represents the rate at which cavity fields "leak" out of the resonator. The relationship between this leakage rate — proportional to T — and the coupling coefficient for the field incident on the external reference plane of the mirror $\mathcal{M}_1$ — proportional to $\sqrt{T}$ — is consistent with the formulations of temporal coupled-mode theory developed in [21] and [25].

Consider the simple case where $F(\omega)$ describes a single-mode input field, given by

$$F(\omega) = \frac{2\pi}{\sqrt{\eta}} \delta(\omega - \Delta\omega) . \tag{4.137}$$

Direct application of Eq. (4.134) gives

$$E_q(t) = \frac{\sqrt{T}}{C(\nu_q - \Delta\omega)} e^{i(2q\pi - \Delta\omega)t} . \tag{4.138}$$

Therefore, substitution of this expression into Eq. (4.109) yields the time-domain expansion

$$E(z,t) = \sqrt{T} e^{-i\Delta\omega t} \sum_q \frac{e^{[i2q\pi + \ln(1/\sqrt{R})]z}}{\nu_q - \Delta\omega} , \tag{4.139}$$

while the Fourier transform of Eq. (4.132) given the same single-mode input field yields

$$E(z,t) = i\sqrt{T} e^{-i\Delta\omega t} \frac{e^{[i\Delta\omega - \alpha(\omega_0)/2]z}}{1 - \Gamma e^{i\Delta\omega}} . \tag{4.140}$$

In Fig. 4.10, we show a plot of Eq. (4.138) for 11 modes at $t = 0$ with $R = 0.5$, $\alpha(\omega_0) = 0.1$, and $\Delta\omega = 0.5$. Using the same parameters, Fig. 4.11 shows plots of Eq. (4.139) and Eq. (4.140) at $t = 0$, where we have truncated the sum in Eq. (4.139) at three different values of $\pm q_{max}$. Note that the eigenmode expansion for $\text{Re}[E(z,0)]$ is quite accurate even for $q_{max} = 5$, but larger sets of modes improve the estimates of $\text{Im}[E(z,0)]$, particularly near the mirrors.

4.4.2 One-Dimensional Standing-Wave Resonator

For a standing-wave resonator, we compute the expansion coefficient in Eq. (4.125) in the frequency domain as

$$E_q(\omega) = \int_{-\infty}^{+\infty} dt \, e^{+i\omega t} E_q(t) = \int_0^{1/2} dz \, \mathbf{v}_q(z) \cdot \mathbf{E}(z, \omega + 2q\pi) . \tag{4.141}$$
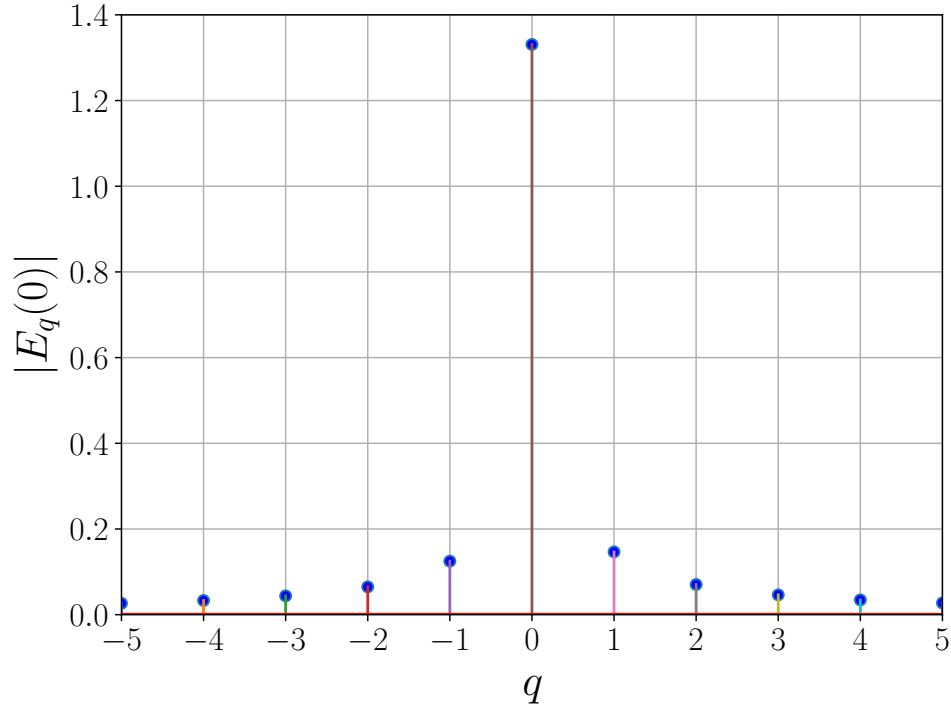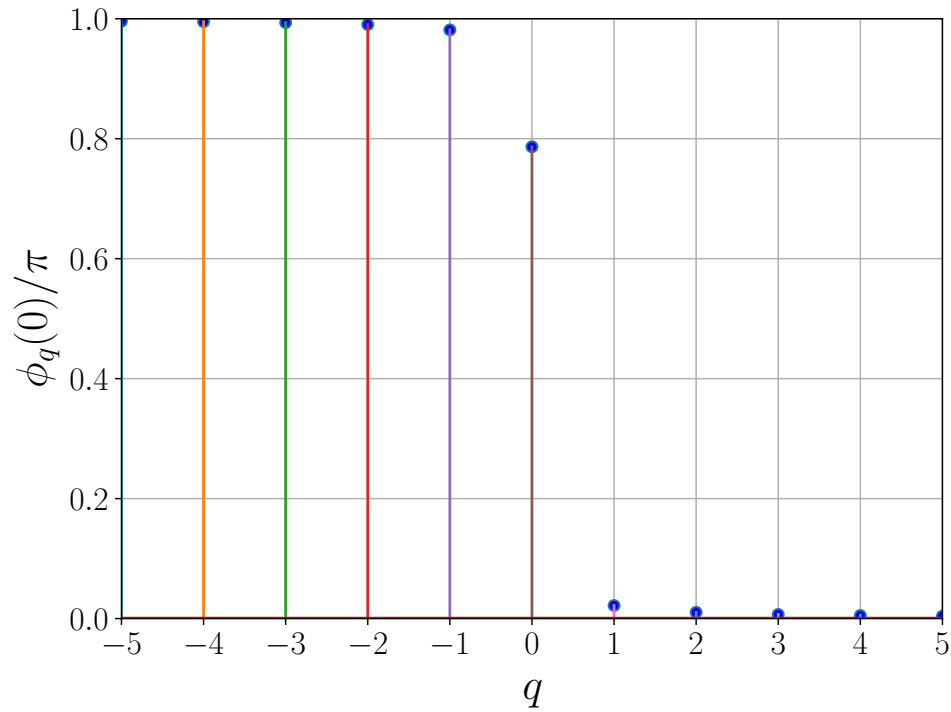
(a) Absolute value of $E_q(0)$

(b) Phase angle of $E_q(0)$

Figure 4.10: Plot of Eq. (4.138) for 11 modes at $t = 0$ with $R = 0.5$, $\alpha(\omega_0) = 0.1$, and $\Delta\omega = 0.5$. We have defined $E_q(t) \equiv |E_q(t)| e^{i\phi_q(t)}$, and graphed $|E_q(0)|$ and $\phi_q(0)$ separately.
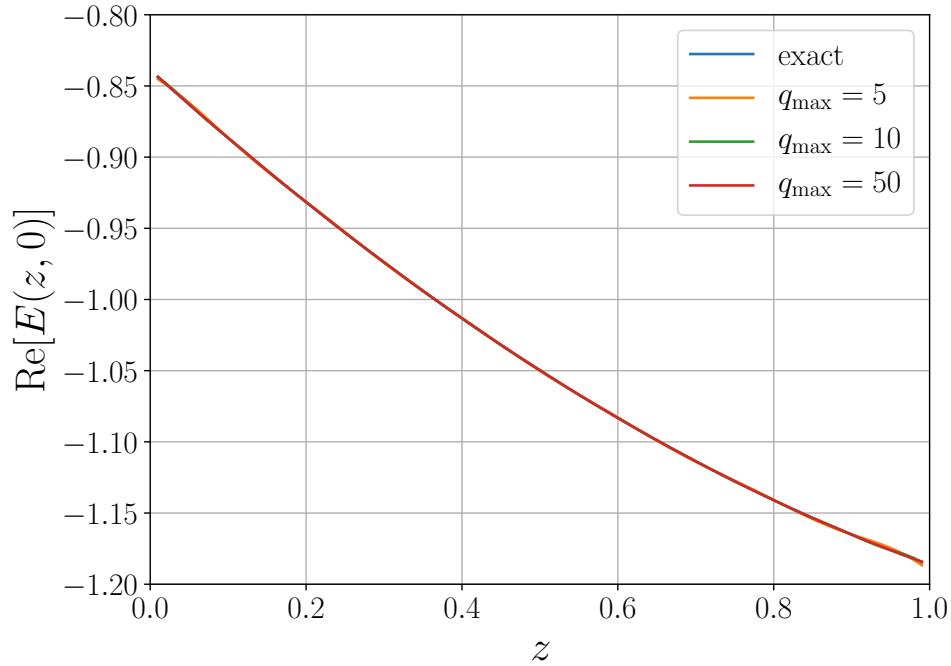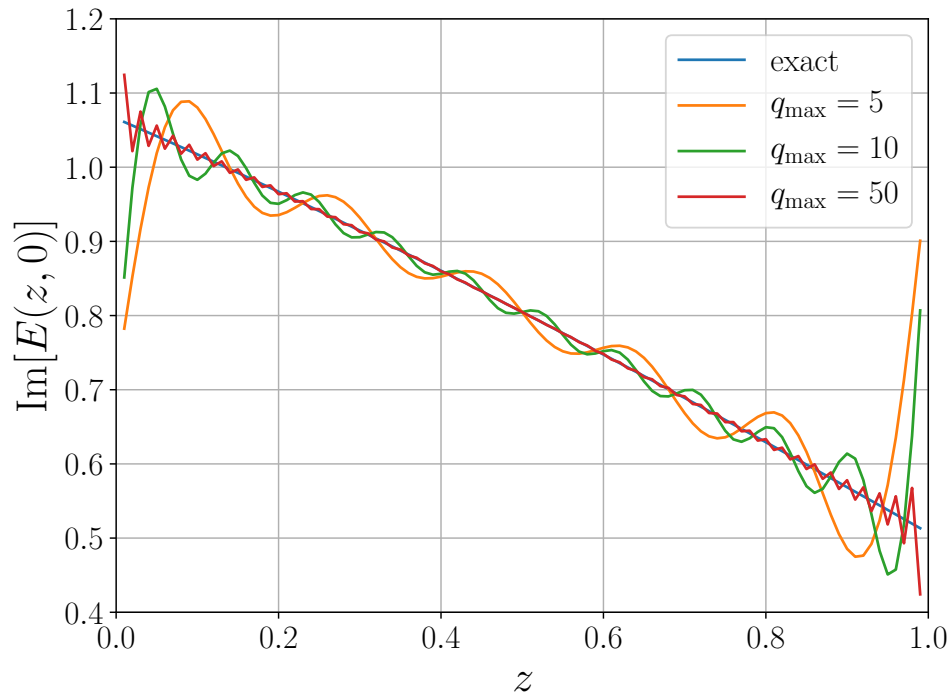
(a) Real part of $E(z,0)$

(b) Imaginary part of $E(z,0)$

Figure 4.11: Plots of Eq. (4.139) and Eq. (4.140) at $t = 0$ using the same values of R, $\alpha(\omega_0)$, and $\Delta\omega$ as in Fig. 4.10. We have truncated the sum in Eq. (4.139) at three different values of $\pm q_{max}$. Note that the eigenmode expansion for $\text{Re}[E(z,0)]$ is quite accurate even for $q_{max} = 5$, but larger sets of modes improve the estimates of $\text{Im}[E(z,0)]$, particularly near the mirrors.

Both Eq. (4.132) and Eq. (4.58) remain valid for $E^+(z, \omega)$ in the standing-wave case where $0 < z < 1/2$, provided that we define $\Gamma^2 = R_1 R_2 e^{-\alpha(\omega_0)}$. Rewriting Eq. (4.33) to be consistent with the sign convention chosen in Eq. (4.111), we calculate the field amplitude just inside the reference plane of mirror $\mathcal{M}_1$ as

$$E^-(0, \omega) = -\frac{1}{\sqrt{R_1}} \left[E^+(0, \omega) - i\sqrt{\eta T_1}\, F(\omega) \right] = -i\sqrt{\frac{\eta T_1}{R_1}} \frac{\Gamma e^{i\omega}}{1 - \Gamma e^{i\omega}} F(\omega), \tag{4.142}$$

and then write $E^-(z, \omega)$ as

$$E^-(z, \omega) = \exp\left[-i\,\omega\,z + \frac{1}{2}\alpha(\omega_0)\,z \right] E^-(0, \omega). \tag{4.143}$$

Substituting this expression and Eq. (4.132) into Eq. (4.141) yields

$$
\begin{aligned}
E_q(\omega) &= \frac{i}{C} \frac{\sqrt{\eta T_1}\, F(\omega + 2q\pi)}{1 - \Gamma e^{i\omega}} \int_0^{1/2} dz \left[e^{(i\omega + \ln\Gamma)z} + \Gamma e^{i\omega} e^{-(i\omega + \ln\Gamma)z} \right] \\
&= \frac{i}{C} \frac{\sqrt{\eta T_1}\, F(\omega + 2q\pi)}{(1 - \Gamma e^{i\omega})(i\omega + \ln\Gamma)} \left\{ \left[e^{(i\omega + \ln\Gamma)/2} - 1 \right] - \Gamma e^{i\omega} \left[e^{-(i\omega + \ln\Gamma)/2} - 1 \right] \right\} \\
&= -\frac{i\sqrt{\eta T_1}}{C} \frac{F(\omega + 2q\pi)}{i\omega + \ln\Gamma},
\end{aligned}
\tag{4.144}
$$

which is identical to Eq. (4.133) with $T \to T_1$ and a properly generalized definition of Γ.

Chapter 5

One-dimensional Single-Mode Continuous-Wave Lasers

In this chapter, our goal will be to understand gain saturation in both unidirectional and standing-wave laser amplifiers, and how it affects continuous-wave (i.e., static) laser oscillator performance. We will work in one dimension only, and begin with Eq. (3.46) to describe a laser amplifier in the steady-state:

$$\pm \frac{d}{dz} E^{\pm}(z) = \left[i\,\delta\omega_0 - \frac{1}{2}\,\alpha_0(z) \right] E^{\pm}(z) + F^{\pm}(z)\,, \tag{5.1a}$$

$$\tilde{F}(z) = \frac{1}{2}\,\mathcal{L}(\Omega)\,\tilde{G}(z)\,\tilde{E}(z)\,, \text{ and} \tag{5.1b}$$

$$\tilde{G}(z) = G_0(z) - 2\,\mathrm{Re}\left[\tilde{E}^*(z)\,\tilde{F}(z) \right]\,, \tag{5.1c}$$

where $\alpha_0 \equiv \alpha(\omega_0)$, and $\tilde{E}(z)$ and $\tilde{P}(z) \equiv -i\,2\,\tilde{F}(z)$ are the rapidly-varying (in space) electric field and macroscopic polarization, respectively; $E^{\pm}(z)$ and $F^{\pm}(z)$ are the corresponding spatially slowly-varying amplitudes; and $\tilde{G}(z)$ is the rapidly-varying dimensionless gain. We have updated Eq. (5.1b) to include the generalized lineshape function $\mathcal{L}(\Omega)$ developed through Eq. (3.48).

If we substitute Eq. (5.1b) into Eq. (5.1c), solve for $\tilde{G}(z)$, and then update Eq. (5.1b) with this result, we obtain

$$\tilde{G}(z) = \frac{G_0(z)}{1 + \mathrm{Re}\left[\mathcal{L}(\Omega)\right]\left|\tilde{E}(z)\right|^2}\,, \text{ and} \tag{5.2a}$$

$$\tilde{F}(z) = \frac{1}{2} \frac{\mathcal{L}(\Omega)}{1 + \mathrm{Re}\left[\mathcal{L}(\Omega)\right]\left|\tilde{E}(z)\right|^2}\,G_0(z)\,\tilde{E}(z)\,, \tag{5.2b}$$

which — in the case of a Lorentzian lineshape — becomes

$$\tilde{G}(z) = \frac{(1 + \Omega^2)\,G_0(z)}{1 + \Omega^2 + \left|\tilde{E}(z)\right|^2}\,, \text{ and} \tag{5.3a}$$

$$\tilde{F}(z) = \frac{1}{2} \frac{1 + i\,\Omega}{1 + \Omega^2 + \left|\tilde{E}(z)\right|^2}\,G_0(z)\,\tilde{E}(z)\,. \tag{5.3b}$$

We will rely primarily on Eq. (5.1a) and Eq. (5.2b) for our descriptions of one-dimensional steady-state laser amplifiers and oscillators.

5.1   Nonlinear Gain and Phase Shifts in Unidirectional Laser Amplifiers

In the case of a unidirectional laser amplifier, $\tilde{E}(z) \equiv E^{\pm}(z) e^{\pm i k_0(\omega_0) z}$, so that both $I(z) \equiv |\tilde{E}(z)|^2 = |E^{\pm}(z)|^2$ and $G(z)$ are slowly-varying in space. Then Eq. (5.1b) shows that the rapid spatial variation of $\tilde{F}(z) \equiv F^{\pm}(z) e^{\pm i k_0(\omega_0) z}$ is given entirely by that of $\tilde{E}(z)$, and the common factor of $e^{\pm i k_0(\omega_0) z}$ can be cancelled. Therefore, defining the slowly-varying field amplitude as

$$E^{\pm}(z) \equiv \sqrt{I^{\pm}(z)}\, e^{-i\phi^{\pm}(z)} \tag{5.4}$$

we rewrite Eq. (5.1a) as

$$\pm \left[\frac{1}{2 I^{\pm}(z)} \frac{d}{dz} I^{\pm}(z) - i \frac{d}{dz}\phi^{\pm}(z) \right] = i\,\delta\omega_0 - \frac{1}{2}\alpha_0(z) + \frac{F^{\pm}(z)}{E^{\pm}(z)} \,. \tag{5.5}$$

Using Eq. (5.2b), the real part of this equation becomes

$$\pm \frac{1}{I^{\pm}(z)} \frac{d}{dz} I^{\pm}(z) = -\alpha_0(z) + \frac{\rho(\Omega)}{1 + \rho(\Omega)\, I^{\pm}(z)}\, G_0(z)\,, \tag{5.6}$$

where

$$\rho(\Omega) \equiv \mathrm{Re}\left[\mathcal{L}(\Omega)\right]\,. \tag{5.7}$$

Let's analyze the forward-propagation intensity $I^{+}(z) \equiv I(z)$ in the case of spatially independent unsaturated gain $G_0(z) \equiv \overline{G}_0$ and nonsaturable background loss $\alpha_0(z) \equiv \overline{\alpha}_0$; we find

$$\frac{d}{dz} I(z) = \frac{\rho(\Omega)\,\overline{G}_0\, I(z)}{1 + \rho(\Omega)\, I(z)} - \overline{\alpha}_0\, I(z) = \frac{\left\{ \rho(\Omega)\,\overline{G}_0 - \overline{\alpha}_0\left[1 + \rho(\Omega)\, I(z)\right] \right\} I(z)}{1 + \rho(\Omega)\, I(z)}\,. \tag{5.8}$$

Noting that

$$\frac{1 + \rho(\Omega)\, I(z)}{\left\{ \rho(\Omega)\,\overline{G}_0 - \overline{\alpha}_0\left[1 + \rho(\Omega)\, I(z)\right] \right\} I(z)} = \frac{1}{\rho(\Omega)\,\overline{G}_0 - \overline{\alpha}_0} \left\{ \frac{1}{I(z)} + \frac{\rho^2(\Omega)\,\overline{G}_0}{\rho(\Omega)\,\overline{G}_0 - \overline{\alpha}_0\left[1 + \rho(\Omega)\, I(z)\right]} \right\}\,,$$

we quickly obtain the transcendental solution for propagation from the reference plane $z = 0$ to the reference plane z, given by

$$\ln \frac{I(z)}{I(0)} - \frac{\rho(\Omega)\,\overline{G}_0}{\overline{\alpha}_0} \ln \left\{ \frac{\rho(\Omega)\,\overline{G}_0 - \overline{\alpha}_0\left[1 + \rho(\Omega)\, I(z)\right]}{\rho(\Omega)\,\overline{G}_0 - \overline{\alpha}_0\left[1 + \rho(\Omega)\, I(0)\right]} \right\} = \left[\rho(\Omega)\,\overline{G}_0 - \overline{\alpha}_0\right] z\,. \tag{5.9}$$

In the limit $\overline{\alpha}_0/\overline{G}_0 \ll 1$, Eq. (5.9) becomes

$$\ln \frac{I(z)}{I(0)} + \rho(\Omega)\left[I(z) - I(0)\right] = \left[\rho(\Omega)\,\overline{G}_0 - \overline{\alpha}_0\right] z\,. \tag{5.10}$$

If in fact $\alpha_0(z) = 0$, then we can relax the constraint that the unsaturated gain be spatially independent, and quickly find

$$\ln \frac{I(z)}{I(0)} + \rho(\Omega)\left[I(z) - I(0)\right] = \rho(\Omega) \int_0^z dz'\, G_0\left(z'\right)\,. \tag{5.11}$$

Suppose that $I(z) \ll 1$ for all z. Then Eq. (5.6) has the solution

$$I(z) \cong I(0)\, \exp\left\{ \int_0^z dz'\, \left[\rho(\Omega)\, G_0\left(z'\right) - \alpha_0\left(z'\right)\right] \right\}\,, \tag{5.12}$$

which is essentially just Beer's Law given by Eq. (2.93). On the other hand, if $I(z) \gg 1$ for all z (corresponding to a heavily saturated amplifier), Eq. (5.8) gives

$$I(z) \cong e^{-\int_0^z dz' \, \alpha_0(z')} \left[I(0) + \rho(\Omega) \int_0^z dz' e^{\int_0^{z'} dz'' \, \alpha_0(z'')} G_0(z') \right]. \tag{5.13}$$

In Fig. 5.1, we plot the effective gain $G_{\text{eff}}(z) \equiv I(z)/I(0)$ and the saturated gain $G(z)$ as a function of position in an amplifier with constant gain $\overline{G}_0 = 1.5$ and absorption $\overline{\alpha}_0 = 0.5$, and a Lorentzian detuning $\Omega = 0.5$. For a relatively small input intensity, the effective gain is exponential in z, and the gain saturation is negligible. However, as the input intensity increases, $G_{\text{eff}}(z)$ becomes more linear, until at very high intensities the saturated gain is *less* than the constant loss, and the net gain drops below 1. Figure 5.1a was obtained using a numerical solution of Eq. (5.9), but a direct initial value integration of Eq. (5.8) yields the same result.

We determine the corresponding phase shift in the amplifier using the imaginary part of Eq. (5.5), which is

$$\mp \frac{d}{dz} \phi^\pm(z) = \delta\omega_0 + \text{Im}\left[\frac{F^\pm(z)}{E^\pm(z)} \right]. \tag{5.14}$$

From Eq. (5.2b), we note that

$$\text{Im}\left[\frac{F^\pm(z)}{E^\pm(z)} \right] = \frac{\mu(\Omega)}{\rho(\Omega)} \, \text{Re}\left[\frac{F^\pm(z)}{E^\pm(z)} \right],$$

where

$$\mu(\Omega) \equiv \text{Im}\left[\mathcal{L}(\Omega)\right]. \tag{5.15}$$

Using Eq. (5.5), we have

$$\frac{d}{dz} \phi^\pm(z) = \mp\delta\omega_0 - \frac{1}{2} \frac{\mu(\Omega)}{\rho(\Omega)} \left[\pm\alpha_0(z) + \frac{1}{I^\pm(z)} \frac{d}{dz} I^\pm(z) \right]. \tag{5.16}$$

Integrating from 0 to z, we obtain the solution

$$\phi^\pm(z) - \phi^\pm(0) = \mp\delta\omega_0 z - \frac{1}{2} \frac{\mu(\Omega)}{\rho(\Omega)} \ln\left[e^{\pm\int_0^z dz' \, \alpha_0(z')} \frac{I^\pm(z)}{I^\pm(0)} \right]. \tag{5.17}$$

We see that the phase shift depends linearly on the ratio of the imaginary part to the real part of the lineshape function $\mathcal{L}(\Omega)$; in the Lorentzian case, this ratio is the net fractional detuning of the laser frequency from the center of the gain distribution, given by Ω. This result is completely general for steady-state one-dimensional laser amplifiers, and will allow us to easily calculate the magnitude of the "frequency pulling" that occurs within continuous-wave laser oscillators. We can also quickly recover the expression for the net phase shift that is commonly found in textbooks[10], valid in the unsaturated-gain forward-propagation case where $\phi^+(z) \equiv \phi(z)$, $\alpha_0(z) = 0$, $G_0(z) \equiv \overline{G}_0 \ll 1$; from Eq. (5.12), for a Lorentzian lineshape we find

$$\phi(z) - \phi(0) = -\left[\delta\omega_0 + \frac{\Omega}{2} \frac{\overline{G}_0}{1 + \Omega^2} \right] z. \tag{5.18}$$

When the gain is low, the phase shift also depends linearly on the length of the laser amplifier.

There's a subtle effect of laser intensity on the gain lineshape known as *power broadening*. From Eq. (5.6), the dependence of the saturated gain on the detuning arising from a Lorentzian lineshape is captured by the expression
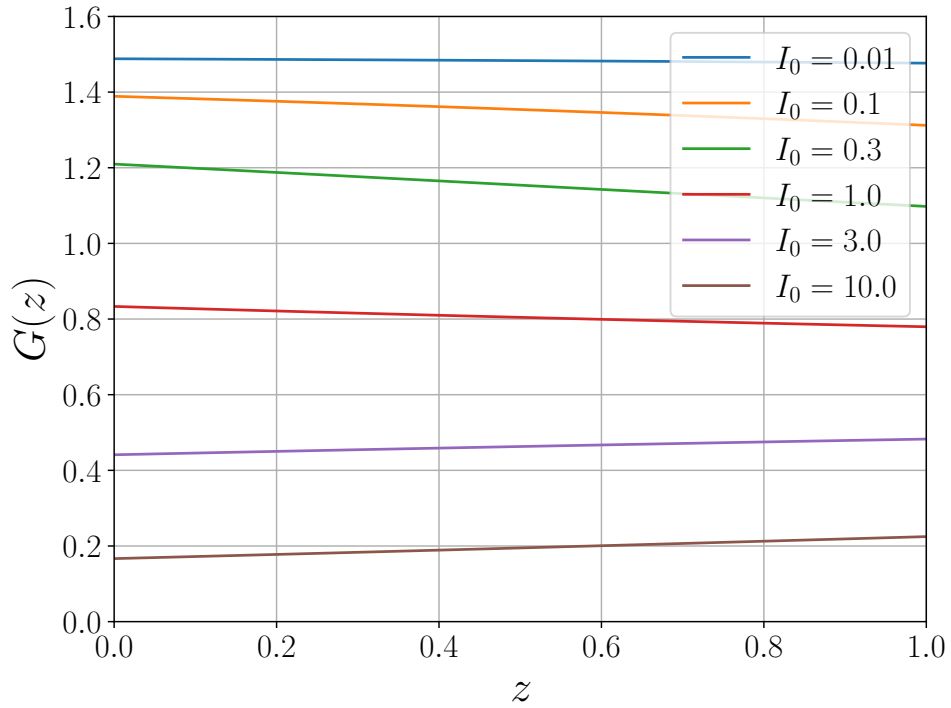
$$L_{\text{sat}}(\Omega) \equiv \frac{1}{1 + I + \Omega^2}, \tag{5.19}$$

where I is the unidirectional intensity at the point of interest within the amplifier. Since $L_{\text{sat}}(0) = 1/(1 + I)$, when $\Omega = \pm\sqrt{1 + I}$ we have $L_{\text{sat}}(\Omega) = L_{\text{sat}}(0)/2$, giving the full width at half-maximum

$$\Omega_{\text{FWHM}} = 2\sqrt{1 + I}, \tag{5.20}$$
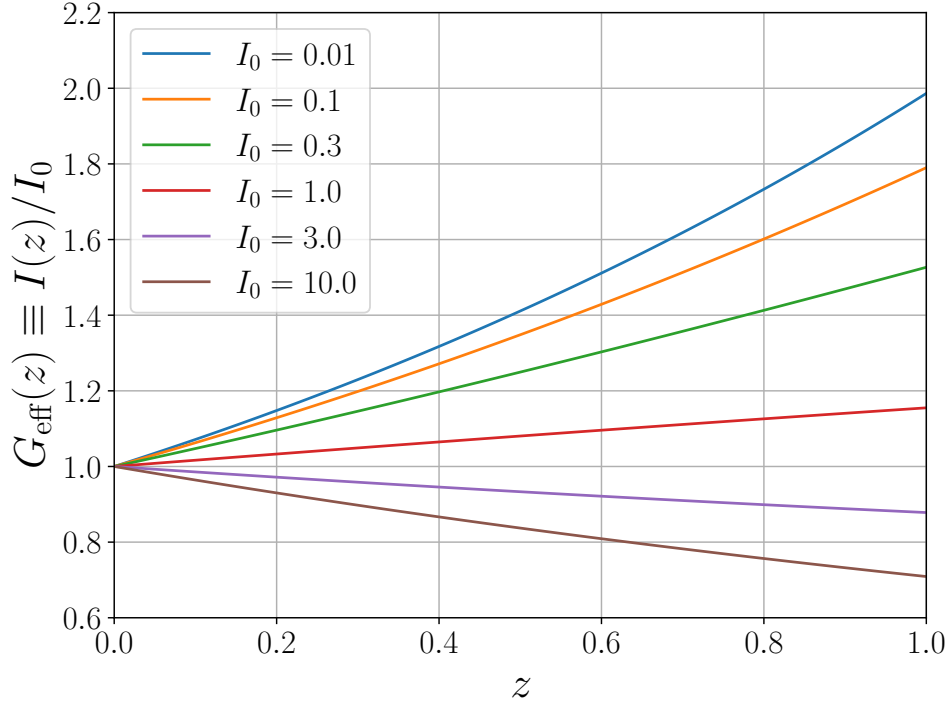
(a) Effective net gain from Eq. (5.9)

(b) Saturated gain from Eq. (5.2a)

Figure 5.1: Plot of the effective gain $G_{\text{eff}}(z)$ and the saturated gain $G(z)$ as a function of position in an amplifier with constant gain $\overline{G}_0 = 1.5$ and absorption $\overline{\alpha}_0 = 0.5$, and a Lorentzian detuning $\Omega = 0.5$.

or, since $\Omega = \Delta\omega\,\tau_\perp$,

$$\Delta\omega_{\text{FWHM}} = \sqrt{1 + I}\,\Delta\omega_g\,,\tag{5.21}$$

where $\Delta\omega_g = 2/\tau_\perp$ is the FWHM when $I = 0$. This increase in the width of the gain lineshape is illustrated in Fig. 5.2a. The effect is difficult to untangle visually from saturation, so in Fig. 5.2b we normalize each lineshape to unity at $\Omega = 0$ to make it clearer. Note that power broadening does *not* increase gain at any frequency detuning; rather, it reduces the "gain curvature"

$$\frac{1}{2}\frac{\partial^2}{\partial\Omega^2}\,L_{\text{sat}}(\Omega) = -\frac{(1 + I - 3\,\Omega^2)}{(1 + I + \Omega^2)^3} \approx -\frac{1}{(1 + I)^2} + \frac{6\,\Omega^2}{(1 + I)^3}\tag{5.22}$$

by a factor of $(1 + I)^2$ near $\Omega = 0$.

5.2   Approximate Continuous-Wave Single-Mode Laser Models

Let's derive a simple single-mode model of continuous-wave laser oscillators based on the quasi-normal modes developed in Section 4.3, applied to Eq. (5.1) in order. We begin with the unidirectional ring laser (URL) shown in Fig. 5.3a, which is the ring resonator of Fig. 4.5b with an incorporated laser amplifier. Note that this amplifier may or may not fill the entire resonator, and that only one pass is made through the amplifier every round trip. We define the spatially slowly-varying field as $E(z) \equiv u_0(z)\,E_0$, where $u_0(z)$ and the corresponding biorthogonal eigenfunction $v_0(z)$ in the range $0 < z < 1$ are given by Eq. (4.83) and Eq. (4.93) with $q = 0$, and the corresponding normalization constant C_{URL} is given by Eq. (4.87). Then

$$u_0(z) = C_{\text{URL}}\,\exp\left[+\left(\ln\frac{1}{\sqrt{R}}\right)z\right],\tag{5.23a}$$

$$v_0(z) = C_{\text{URL}}^{-1}\,\exp\left[-\left(\ln\frac{1}{\sqrt{R}}\right)z\right],\tag{5.23b}$$

We apply the biorthogonality relation given by Eq. (4.97) to Eq. (5.1a) by substituting $E^+(z) = u_0(z)\,E_0$ and $F^+(z) = u_0(z)\,F_0$; multiplying both sides through by $v_0(z)$; and then integrating the result from $z = 0$ to $z = 1$. We find

$$\left(\frac{1}{2\,\tau_\lambda} - i\,\delta\omega_0\right)E_0 = F_0\,,\tag{5.24}$$

where $\tau_\lambda \equiv 1/\ln[1/R\exp(-\overline{\alpha}_0)]$ is the photon lifetime given by Eq. (4.54) and $\overline{\alpha}_0 \equiv \int_0^1 dz\,\alpha_0(z)$.

The appropriate corresponding rapidly-varying biorthogonal eigenfunctions are

$$\tilde{u}_0(z) = C_{\text{URL}}\,\exp\left[+\left(i\,k_0 + \ln\frac{1}{\sqrt{R}}\right)z\right],\tag{5.25a}$$
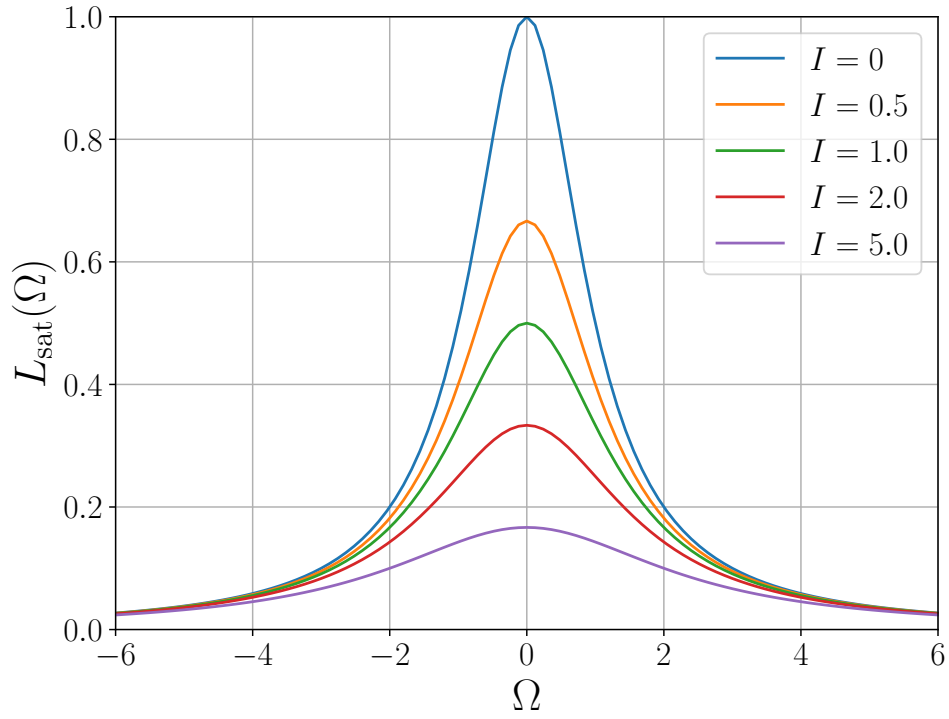
$$\tilde{v}_0(z) = C_{\text{URL}}^{-1}\,\exp\left[-\left(i\,k_0 + \ln\frac{1}{\sqrt{R}}\right)z\right],\tag{5.25b}$$

If we substitute $\tilde{E}(z) = E_0\,\tilde{u}_0(z)$ and $\tilde{F}(z) = F_0\,\tilde{u}_0(z)$ into Eq. (5.1b), multiply through by $\tilde{v}_0(z)$, and integrate from $z = 0$ to $z = 1$, then we obtain
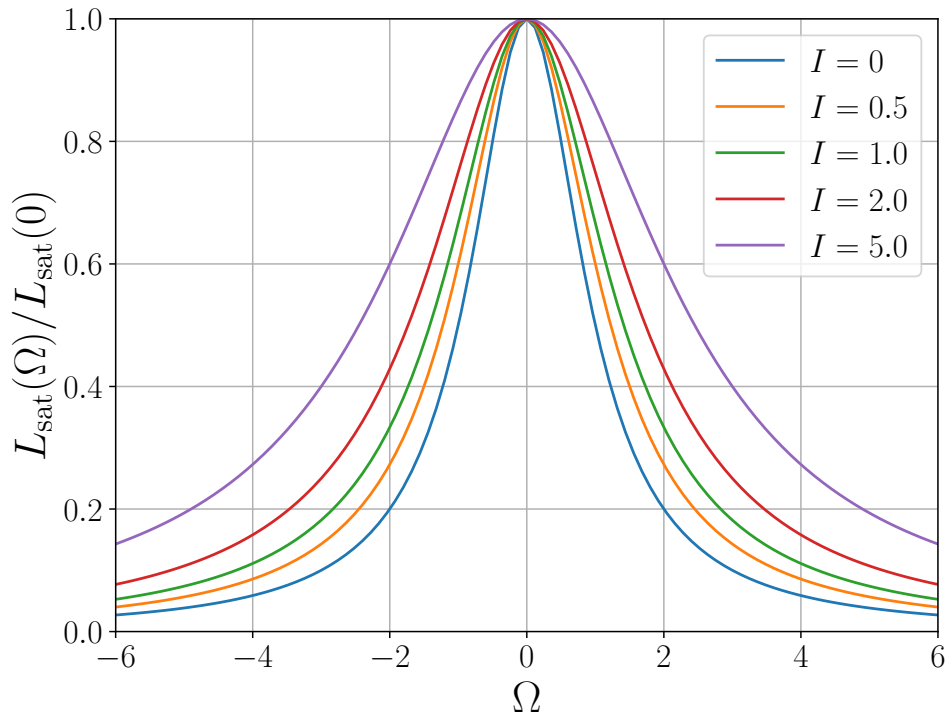
$$F_0 = \frac{1}{2}\,\mathcal{L}(\Omega)\,\overline{G}\,E_0\,,\tag{5.26}$$

where $\overline{G} \equiv \int_0^1 dz\,\tilde{G}(z)$ is the round-trip gain. Then, performing this integral directly on Eq. (5.1c), we obtain

$$\overline{G} = \overline{G}_0 - 2\,\text{Re}\left[\int_0^1 dz\,E^{+\,*}(z)\,F^+(z)\right],\tag{5.27}$$

(a) Saturated and broadened gain lineshape

(b) Normalized and broadened gain lineshape

Figure 5.2: Plot of the effective gain lineshape function $L_{\text{sat}}(\Omega)$ given by Eq. (5.19), including the effects of saturation and detuning.

where $\overline{G}_0 \equiv \int_0^1 dz\, \overline{G}_0(z)$ is the round-trip unsaturated gain. Applying the substitutions we've used above, the integral on the right-hand side of this expression is

$$\int_0^1 dz\, E^{+\,*}(z)\, F^+(z) = E_0^*\, F_0\, C_{\mathrm{URL}}^2 \int_0^1 dz\, e^{\ln(1/R)\, z} = \frac{E_0^*\, F_0\, C_{\mathrm{URL}}^2}{\ln(1/R)} \left(\frac{1}{R} - 1 \right) = \frac{1}{2}\, \mathcal{L}(\Omega)\, \overline{G}\, |E_0|^2 \,, \quad (5.28)$$

yielding

$$\overline{G} = \frac{\overline{G}_0}{1 + \rho(\Omega)\, |E_0|^2} \,. \quad (5.29)$$

The derivation of the model for a standing-wave laser (SWL) proceeds similarly, provided that we consider interference between the counterpropagating fields within the amplifier. The slowly-varying biorthogonal eigenfunctions that we now use for the standing-wave case are $\mathbf{u}_0(z)$ and $\mathbf{v}_0(z)$, given by Eq. (4.112), Eq. (4.113), Eq. (4.118), and Eq. (4.119) with $q = 0$, and the corresponding normalization constant C_{SWL} is given by Eq. (4.115). Then

$$\mathbf{u}_0(z) \equiv \begin{bmatrix} u_0^+(z) \\ u_0^-(z) \end{bmatrix} = C_{\mathrm{SWL}} \begin{bmatrix} e^{+\left[\ln\left(1/\sqrt{R_1 R_2}\right)\right]z} \\ -\frac{1}{\sqrt{R_1}}\, e^{-\left[\ln\left(1/\sqrt{R_1 R_2}\right)\right]z} \end{bmatrix}, \text{ and} \quad (5.30a)$$

$$\mathbf{v}_0(z) \equiv \begin{bmatrix} v_0^+(z) \\ v_0^-(z) \end{bmatrix} = C_{\mathrm{SWL}}^{-1} \begin{bmatrix} e^{-\left[\ln\left(1/\sqrt{R_1 R_2}\right)\right]z} \\ -\sqrt{R_1}\, e^{+\left[\ln\left(1/\sqrt{R_1 R_2}\right)\right]z} \end{bmatrix}, \quad (5.30b)$$

where $0 < z < 1/2$. In this case, we apply the biorthogonality relation given by Eq. (4.120) to Eq. (5.1a) by substituting $E^\pm(z) = u_0^\pm(z)\, E_0$ and $F^\pm(z) = u_0^\pm(z)\, F_0$; forming the inner product of both sides with $\mathbf{v}_0(z)$; and then integrating the result from $z = 0$ to $z = 1/2$. We note that $\mathbf{v}_0(z) \cdot \mathbf{u}_0(z) = 2$ and $\int_0^{1/2} dz\, \mathbf{v}_0(z) \cdot \mathbf{u}_0(z) = 1$. Therefore, Eq. (5.24) remains valid for the standing-wave case with $\tau_\lambda \equiv 1/\ln[1/R_1 R_2 \exp(-\overline{\alpha}_0)]$ and $\overline{\alpha}_0 \equiv 2 \int_0^{1/2} dz\, \alpha_0(z)$.

Because the gain in our amplifier can be sensitive to spatial interference between the counterpropagating fields, we must be careful in how we apply these eigenfunctions to Eq. (5.1b) and Eq. (5.1c). We begin by substituting $\tilde{E}(z) = \tilde{u}_0(z)\, E_0$ and $\tilde{F}(z) = \tilde{u}_0(z)\, F_0$ into Eq. (5.1b), where $\tilde{u}_0(z)$ and the corresponding rapidly-varying standing-wave biorthognal eigenfunction $\tilde{v}_0(z)$ are given by

$$\tilde{u}_0(z) = C_{\mathrm{SWL}} \left\{ e^{+\left[i k_0 + \ln\left(1/\sqrt{R_1 R_2}\right)\right]z} - \frac{1}{\sqrt{R_1}}\, e^{-\left[i k_0 + \ln\left(1/\sqrt{R_1 R_2}\right)\right]z} \right\}, \text{ and} \quad (5.31a)$$

$$\tilde{v}_0(z) = C_{\mathrm{SWL}}^{-1} \left\{ e^{-\left[i k_0 + \ln\left(1/\sqrt{R_1 R_2}\right)\right]z} - \sqrt{R_1}\, e^{+\left[i k_0 + \ln\left(1/\sqrt{R_1 R_2}\right)\right]z} \right\}. \quad (5.31b)$$

Then we multiply both sides of the resulting expression by $\tilde{v}_0(z)$, noting that

$$\tilde{v}_0(z)\, \tilde{u}_0(z) = 2 - \sqrt{R_1}\, e^{+[i\, 2 k_0 + \ln(1/R_1 R_2)]z} - \frac{1}{\sqrt{R_1}}\, e^{-[i\, 2 k_0 + \ln(1/R_1 R_2)]z} \,. \quad (5.32)$$

Using Eq. (2.81) as our guide, we first average this expression over one wavelength $\lambda_0 = 2\pi/k_0$ to eliminate the rapidly-varying terms, and then integrate the result from $z = 0$ to $z = 1/2$. We find
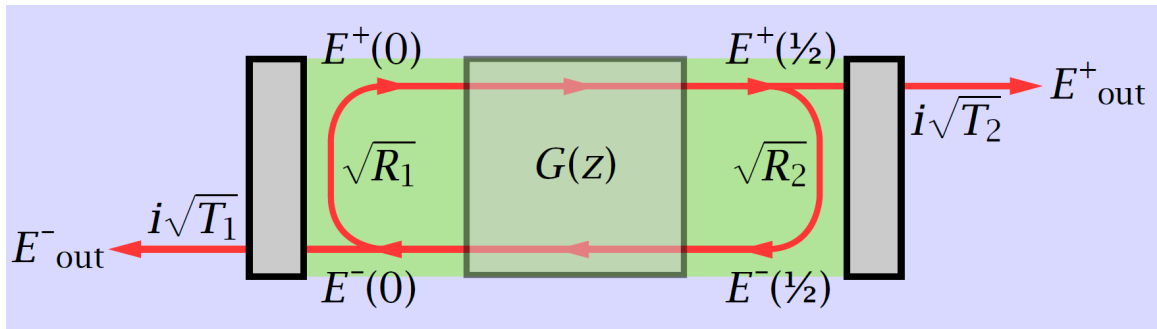
$$F_0 \int_0^{1/2} dz\, \frac{k_0}{2\pi} \int_{z-\pi/k_0}^{z+\pi/k_0} dz'\, \tilde{v}_0(z')\, \tilde{u}_0(z') = F_0 = \frac{1}{2}\, \mathcal{L}(\Omega)\, \overline{G}\, E_0 \,, \quad (5.33)$$

where

$$\overline{G} = \int_0^{1/2} dz\, \frac{k_0}{2\pi} \int_{z-\pi/k_0}^{z+\pi/k_0} dz'\, \tilde{v}_0(z')\, \tilde{u}_0(z')\, \tilde{G}(z') \,, \quad (5.34)$$
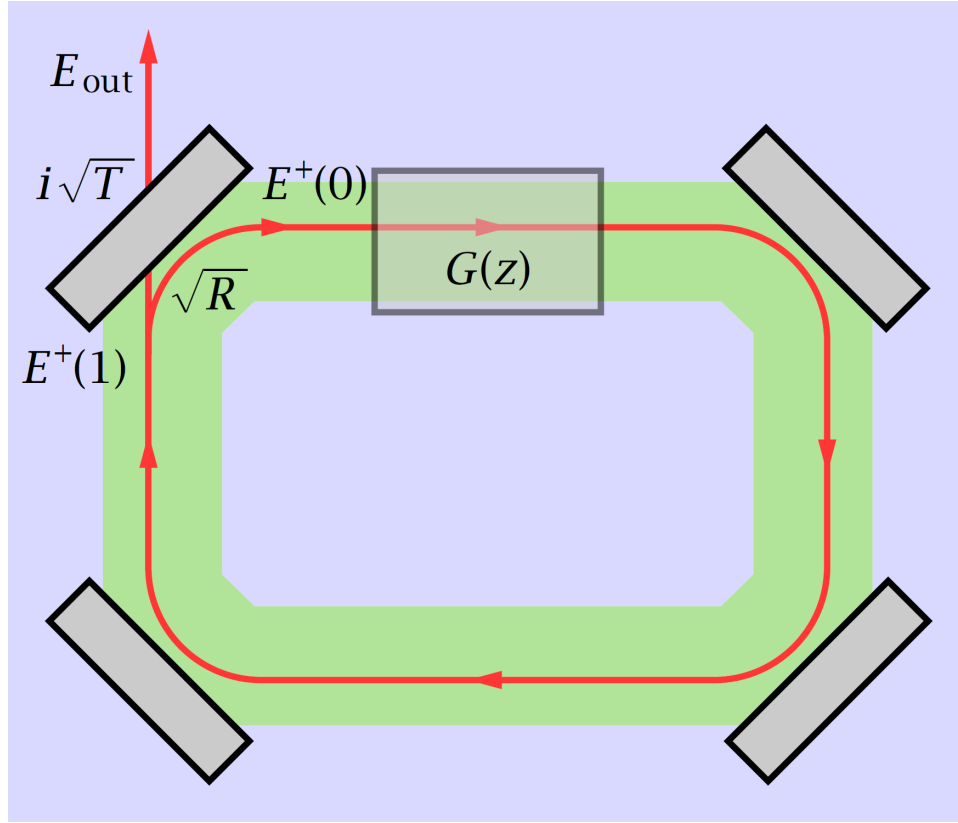
(a) Saturated and broadened gain lineshape

(b) Normalized and broadened gain lineshape

Figure 5.3: Schematics of laser resonators with an incorporated laser amplifier, which may or may not fill the entire resonator. (a) The unidirectional ring resonator of Fig. 4.5b, where only one pass is made through the amplifier every round trip. (b) The standing-wave resonator of Fig. 4.5a, where two passes are made through the amplifier every round trip, and counterpropagating fields are linked by boundary conditions at the two mirrors.

so that we have recovered Eq. (5.26). Performing this integral directly on Eq. (5.1c), we obtain

$$
\overline{G} = \int_0^{1/2} dz \, \frac{k_0}{2\pi} \int_{z-\pi/k_0}^{z+\pi/k_0} dz' \, \tilde{v}_0(z') \, \tilde{u}_0(z') \left\{ G_0(z) - 2 \operatorname{Re} \left[E_0^* F_0 \right] |\tilde{u}_0(z')|^2 \right\}
$$

$$
= \overline{G}_0 - \rho(\Omega) \, |E_0|^2 \, \overline{G} \int_0^{1/2} dz \, \frac{k_0}{2\pi} \int_{z-\pi/k_0}^{z+\pi/k_0} dz' \, \tilde{v}_0(z') \, \tilde{u}_0(z') \, |\tilde{u}_0(z')|^2 \, , \tag{5.35}
$$

where $\overline{G}_0 \equiv 2 \int_0^{1/2} dz \, G_0(z)$ is the round-trip unsaturated gain, and

$$
|\tilde{u}_0(z)|^2 = C_{\mathrm{SWL}}^2 \left[e^{+\ln(1/R_1 R_2) z} + \frac{1}{R_1} e^{-\ln(1/R_1 R_2) z} - \frac{1}{\sqrt{R_1}} \left(e^{+i 2 k_0 z} + e^{-i 2 k_0 z} \right) \right]. \tag{5.36}
$$

When we compute the average over one wavelength in Eq. (5.35), we have the option of either neglecting or including spatial interference between the counterpropagating fields. When gain diffusion is high, and spatial hole-burning (SHB) can be neglected, we can treat the two fields as independent within the amplifier, and completely ignore the rapidly-varying terms in $|\tilde{u}_0(z)|^2$ when performing the average. However, when gain diffusion is low, and SHB effects are important, we must include the full expression for $|\tilde{u}_0(z)|^2$ when performing the average to describe the spatially periodic modulation of the gain within the amplifier. In either case, we find that

$$
\frac{k_0}{2\pi} \int_{z-\pi/k_0}^{z+\pi/k_0} dz' \, \tilde{v}_0(z') \, \tilde{u}_0(z') \, |\tilde{u}_0(z')|^2 = \tilde{\kappa} \, C_{\mathrm{SWL}}^2 \left[e^{+\ln(1/R_1 R_2) z} + \frac{1}{R_1} e^{-\ln(1/R_1 R_2) z} \right], \tag{5.37}
$$

where we use $\tilde{\kappa} = 2$ if we neglect spatial interference between the counterpropagating fields, and $\tilde{\kappa} = 3$ if we include it. The integral over z on the right-hand side of Eq. (5.35) is then

$$
\tilde{\kappa} \, C_{\mathrm{SWL}}^2 \int_0^{1/2} dz \left[e^{+\ln(1/R_1 R_2) z} + \frac{1}{R_1} e^{-\ln(1/R_1 R_2) z} \right] = \tilde{\kappa}. \tag{5.38}
$$

Collecting results, the approximate governing equations for continuous-wave single-mode one-dimensional lasers are

$$
\left(\frac{1}{2 \tau_\lambda} - i \, \delta \omega_0 \right) = \frac{1}{2} \mathcal{L}(\Omega) \, \overline{G}, \text{ and} \tag{5.39a}
$$

$$
\overline{G} = \frac{\overline{G}_0}{1 + \tilde{\kappa} \, \rho(\Omega) \, I_0}, \tag{5.39b}
$$

where $I_0 \equiv |E_0|^2$ is the average intracavity intensity in units of the saturation intensity I_s,

$$
\overline{G}_0 \equiv \begin{cases} \int_0^1 dz \, G_0(z) & \text{(URL)}, \\ 2 \int_0^{1/2} dz \, G_0(z) & \text{(SWL or SHB)}, \end{cases} \tag{5.40}
$$

is the *round-trip unsaturated intensity gain*, and

$$
\tilde{\kappa} \equiv \begin{cases} 1 & \text{(URL)}, \\ 2 & \text{(SWL)}, \\ 3 & \text{(SHB)}, \end{cases} \tag{5.41}
$$

is the *effective saturation parameter*. We will discover in Section 5.4.2 that $\tilde{\kappa} = 3$ is in fact an *overestimate* of the effective saturation parameter, and we'll find an analytic approach that allows us to choose a value that is more accurate.

Applying Eq. (5.39b) to the real part of Eq. (5.39a), we find

$$
I_0 = \frac{\overline{H}_0 - 1}{\tilde{\kappa} \, \rho(\Omega)}, \tag{5.42}
$$

where

$$\overline{H}_0 \equiv \rho(\Omega)\,\tau_\lambda\,\overline{G}_0 \equiv \frac{\overline{G}_0}{G_{\text{th}}}\,, \tag{5.43}$$

and the *threshold* gain is

$$G_{\text{th}} \equiv \frac{1}{\rho(\Omega)\,\tau_\lambda}\,, \tag{5.44}$$

or

$$G_{\text{th}} = \frac{1 + \Omega^2}{\tau_\lambda} \tag{5.45}$$

when the lineshape is Lorentzian.

Note that $I_0 > 0$ only if the pump is strong enough that the round-trip unsaturated gain $\overline{G}_0$ exceeds the threshold gain. If $\overline{G}_0 \le G_{\text{th}}$, then $I \longrightarrow 0$. Remarkably, if we substitute Eq. (5.42) into Eq. (5.39b), we find that — when $\overline{G}_0 > G_{\text{th}}$ — the *saturated* round-trip gain is given by

$$\overline{G} = G_{\text{th}}\,, \tag{5.46}$$

independent of $\overline{G}_0$. Above threshold, the steady-state gain is clamped at the threshold value regardless of the strength of the pump.

Suppose that each mirror has a small absorption/scattering of incident laser intensity A, so that the transmission is given by $T = 1 - A - R$. To find the intensity output from the URL's single mirror, we compute $I_{\text{out}} = (1 - A - R)\,|u_0(1)|^2\,I_0$, giving

$$I_{\text{out}} = \frac{1 - A - R}{1 - R}\,\ln\!\left(\frac{1}{R}\right)\frac{\overline{H}_0 - 1}{\widetilde{\kappa}\,\rho(\Omega)}\,. \tag{5.47}$$

For the SWL, the output fields are $I_{\text{out}}^{+} = (1 - A_2 - R_2)\,\left|u_0^{+}(1/2)\right|^2\,I_0$ and $I_{\text{out}}^{-} = (1 - A_1 - R_1)\,\left|u_0^{-}(0)\right|^2\,I_0$. If either one of the mirrors has an intensity reflectance of 1, then the other mirror is the sole output coupler with reflectance R, and the intensity output through that mirror is also given by Eq. (5.47). In both cases, the threshold gain is

$$G_{\text{th}} = \rho^{-1}(\Omega)\,\ln\!\left(\frac{1}{|\Gamma'|^2 R}\right)\,, \tag{5.48}$$

where $|\Gamma'|^2 = e^{-\overline{\alpha}_0}$. If necessary, we can generalize the definition of Γ' to include all round-trip boundary and background losses in the laser cavity *except* the transmission and absorption of the output coupler.

If the resonator is strictly lossless, so that $\overline{\alpha}_0 = A = 0$, then $G_{\text{th}} = \rho^{-1}(\Omega)\,\ln(1/R)$, and the output intensity becomes

$$I_{\text{out}} = \frac{1}{\widetilde{\kappa}}\left(\overline{G}_0 - G_{\text{th}}\right)\,. \tag{5.49}$$

In this (unphysical) case, the output intensity increases monotonically with R until the threshold gain vanishes as $R \longrightarrow 1$, while the intensity incident on the output coupler increases to $\overline{G}_0/\widetilde{\kappa}\,(1 - R)$ in the same limit. The result would be a damaged mirror reflection coating. In Section 5.4, published models of intracavity intensity distributions in standing-wave lasers assume that $\overline{\alpha}_0 = 0$, so we'll avoid the quandary in the limit $R \longrightarrow 1$ by assuming that the output coupler *always* has a small finite loss and writing

$$I_{\text{out}} = \frac{1 - A - R}{1 - R}\,\frac{\overline{G}_0 - G_{\text{th}}}{\widetilde{\kappa}}\,. \tag{5.50}$$

In the practical case where losses are present, there's an optimum output coupling that maximizes I_{out}. We can optimize Eq. (5.47) numerically to find R_{opt}, but there's a simple trick we can use to obtain an analytic approximation that is quite reasonably accurate. We note in Fig. 5.4 that the reflectance
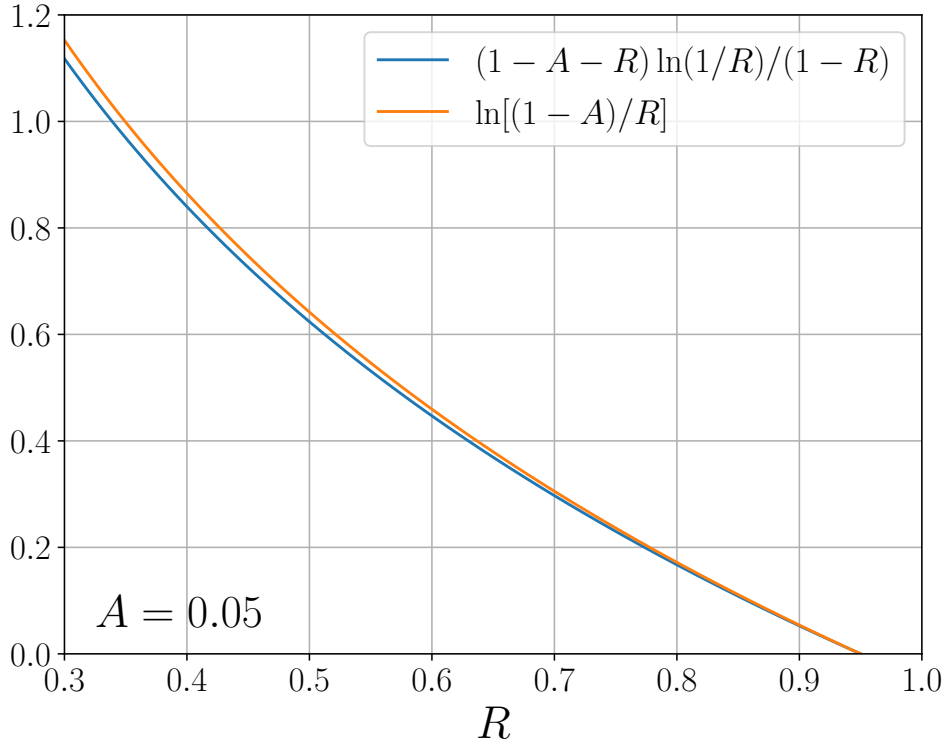
Figure 5.4: A comparison of the exact reflectance normalization given by Eq. (5.47) and the approximation used in Eq. (5.51) for a relatively large value of the mirror intensity scattering and absorption coefficient.

normalization of Eq. (5.47) is only slightly different from the function $\ln[(1-A)/R]$ even when A is very large. Hence, we rewrite I_{out} as

$$I_{\text{out}} = \ln\left(\frac{1-A}{R}\right)\frac{\overline{H}_0 - 1}{\widetilde{\kappa}\,\rho(\Omega)},\tag{5.51}$$

differentiate the right-hand side with respect to R, set the result to 0, and then solve for R_{opt}. We find

$$R_{\text{opt}} = \frac{1}{|\Gamma'|^2}\exp\left\{-\sqrt{\rho(\Omega)\,\overline{G}_0\,\ln\left[\frac{1}{(1-A)\,|\Gamma'|^2}\right]}\right\}.\tag{5.52}$$

The corresponding optimum output intensity is given by

$$I_{\text{opt}} = \frac{1}{\widetilde{\kappa}\,\rho(\Omega)}\left\{\sqrt{\rho(\Omega)\,\overline{G}_0} - \sqrt{\ln\left[\frac{1}{(1-A)\,|\Gamma'|^2}\right]}\right\}^2.\tag{5.53}$$

Note that these equations make sensible predictions only when $(1-A)\,|\Gamma'|^2 < 1$. Also, the maximum value of the reflectance given by $R = 1 - A$ is the "optimum" output coupler reflectance when the gain $\overline{G}_0$ has the minimum value

$$G_{\text{min}} = \rho^{-1}(\Omega)\,\ln\left[\frac{1}{(1-A)\,|\Gamma'|^2}\right],\tag{5.54}$$

corresponding to $I_{\text{opt}} = 0$, as it must.

What happens to the approximate model when the gain and loss are arbitrary functions of z (e.g., they don't fill the resonator)? We can patch the function $u_0(z)$ to take this spatial nonuniformity into account while continuing to satisfy the boundary condition (e.g., for a URL) at $z = 1$:

$$\left|u_0'(z)\right|^2 = C_{\text{URL}}^2 \, K(z), \tag{5.55}$$

where

$$K(z) \equiv \exp\left[\beta \int_0^z dz' \, G_0(z') - \int_0^z dz' \, \alpha_0(z')\right], \text{ and} \tag{5.56a}$$

$$\beta \equiv \frac{\ln(1/R\, e^{-\overline{\alpha}_0})}{\overline{G}_0} = \frac{\rho(\Omega)}{\overline{H}_0}. \tag{5.56b}$$

Similarly, we can extend $u_0^{\pm}(z)$ for the case of standing-wave lasers by defining

$$\left|u_0^{+\prime}(z)\right|^2 = C_{\text{SWL}}^2 \, K(z), \text{ and} \tag{5.57a}$$

$$\left|u_0^{-\prime}(z)\right|^2 = \frac{C_{\text{SWL}}^2}{R_1 \, K(z)} \tag{5.57b}$$

and using $R = R_1 R_2$ in Eq. (5.56b). We'll see that this approach works surprisingly well for both unidirectional ring lasers (URLs) and standing-wave lasers (SWLs) when the gain and loss are not uniform.

Returning to the phase of the field, we take the ratio of the imaginary and real parts of Eq. (5.39a) to find the steady-state frequency shift

$$\delta\omega_0 = -\frac{1}{2\,\tau_\lambda} \frac{\mu(\Omega)}{\rho(\Omega)}. \tag{5.58}$$

Let's define $\Omega_0 \equiv (\omega_0 - \omega_{ab})\,\tau_\perp$. Then the total normalized detuning is

$$\Omega = \Omega_0 + \delta\omega_0\,\tau_\perp, \tag{5.59}$$

and we find $\delta\omega_0$ by substituting this expression into Eq. (5.58) and then solving. For example, if the lineshape is Lorentzian, then $\mu(\Omega)/\rho(\Omega) = \Omega$, and

$$\delta\omega_0 = -\frac{1}{2\,\tau_\lambda} \frac{\Omega_0}{1 + \tau_\perp/2\,\tau_\lambda}. \tag{5.60}$$

Recall that the total angular frequency of the electric field is $\omega_0 + \delta\omega_0$, and that we have chosen the carrier frequency ω_0 to be aligned with one of the modes of the unloaded cavity, such that $\exp(\pm i\,\omega_0\tau) = 1$. If the frequency of that cavity mode does not coincide with the resonance frequency ω_{ab} of the gain medium, then Eq. (5.60) predicts that the total frequency of the laser will be *pulled* away from that of the cavity mode toward the resonance of the medium. Note that the corresponding value of the total normalized frequency detuning Ω is

$$\Omega = \frac{\Omega_0}{1 + \tau_\perp/2\,\tau_\lambda}. \tag{5.61}$$

Therefore, the net result of this frequency-pulling effect is to *reduce* the detuning, and *increase* the unsaturated gain. But Eq. (5.60) indicates that this detuning depends on the total intracavity loss through τ_λ, and *not* the unsaturated gain at all. This apparent contradiction is resolved by Eq. (5.46): the gain is clamped at the threshold value, which is indeed independent of the pump.

5.3 One-Dimensional Unidirectional Ring Lasers

In general, the simple one-dimensional unidirectional ring laser shown in Fig. 5.3a has an amplifier with position-dependent gain and loss distributed from $z = 0$ to $z = 1$. Let's begin to understand the performance characteristics of this laser by assuming that the gain and loss are constant, with the values $G_0(z) \equiv \overline{G}_0$ and $\alpha_0(z) \equiv \overline{\alpha}_0$, so that we can use Eq. (5.9) to determine the intensity $I(1)$ incident on the output coupler. Substituting the boundary condition $I(0) = R\,I(1)$ into Eq. (5.9), we obtain

$$I(1) = \left[\frac{\overline{G}_0}{\overline{\alpha}_0} - \rho^{-1}(\Omega)\right] \frac{1 - e^{-\xi}}{1 - R\,e^{-\xi}}, \tag{5.62}$$

where $\rho(\Omega)$ is defined by Eq. (5.7), and

$$\xi \equiv \frac{\overline{\alpha}_0}{\overline{G}_0}\left(\overline{G}_0 - G_{\text{th}}\right). \tag{5.63}$$

In the limit where $\overline{\alpha}_0/\overline{G}_0 \ll 1$,

$$I(1) \approx \frac{\overline{G}_0 - G_{\text{th}}}{1 - R}\left\{1 - \left[\frac{1 + R}{2(1 - R)}\left(\overline{G}_0 - G_{\text{th}}\right) + \rho^{-1}(\Omega)\right]\frac{\overline{\alpha}_0}{\overline{G}_0}\right\}. \tag{5.64}$$

(Often, when intracavity loss is nonzero, the analytic formulas that we use to drive our intuition tend to become fairly complicated.)

For a lossless cavity with $\overline{\alpha}_0 = 0$, we have $I(1) = (\overline{G}_0 - G_{\text{th}})/(1 - R)$, and an output intensity given by

$$I_{\text{out}} = \frac{1 - A - R}{1 - R}\left(\overline{G}_0 - G_{\text{th}}\right), \tag{5.65}$$

which is identical to Eq. (5.50) with $\kappa = 1$. In Fig. 5.5, we have assumed that $\text{Re}[\mathcal{L}(0)] = 1$ and plotted the intracavity and output intensity for a lossless unidirectional ring laser in one dimension. In Fig. 5.5a, the intracavity intensity is computed using three methods: the direct numerical integration of Eq. (5.8) using the Scientific Python routine `scipy.integrate.solve_bvp`; the numerical solution of Eq. (5.11) using the Scientific Python routine `scipy.optimize.brentq`; and the approximate solution provided by Eq. (5.42) in the form

$$I(z) \approx \frac{\overline{H}_0 - 1}{\kappa\,\rho(\Omega)}\,|u_0(z)|^2 \tag{5.66}$$

with $\kappa = 1$. The approximate laser model described in Section 5.2 essentially assumes that the intracavity gain profile will be exponential, which corresponds to the low-gain limit of Eq. (5.12). But when the gain is significantly above threshold, the intensity becomes a more linear function of z, consistent with the approximation of Eq. (5.13). Nevertheless, for a lossless laser the simple model accurately predicts the values of both $I(0)$ and $I(1)$, so that we can make reliable predictions of the laser output intensity. In Fig. 5.5b, we compare the corresponding output intensity as a function of R using Eq. (5.51) (with $\overline{\alpha}_0 = 0$) and Eq. (5.65). The results are virtually identical.

In the general case of a one-dimensional unidirectional ring laser with intracavity absorption and nonzero scattering and loss in the output coupler, the output intensity is given by

$$I_{\text{out}} = (1 - A - R)\,I(1) = (1 - A - R)\left[\frac{\overline{G}_0}{\overline{\alpha}_0} - \rho^{-1}(\Omega)\right]\frac{1 - e^{-\xi}}{1 - R\,e^{-\xi}}, \tag{5.67}$$

where ξ is defined by Eq. (5.63). In Fig. 5.6, we have plotted the intracavity and output intensity for a unidirectional ring laser in one dimension. Again, we have assumed that $\text{Re}[\mathcal{L}(0)] = 1$. In Fig. 5.6a, our approach is identical to that of Fig. 5.5a. We see that our approximate model slightly overestimates the value of the intensity arriving at the output coupler when $\overline{\alpha}_0 \neq 0$. In Fig. 5.6b, we compare the
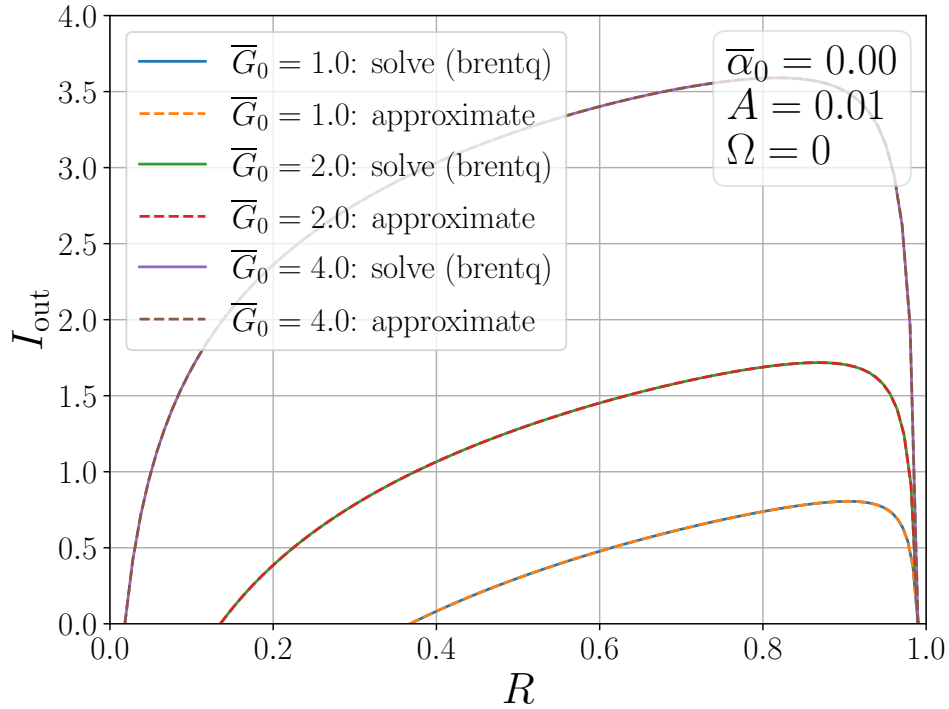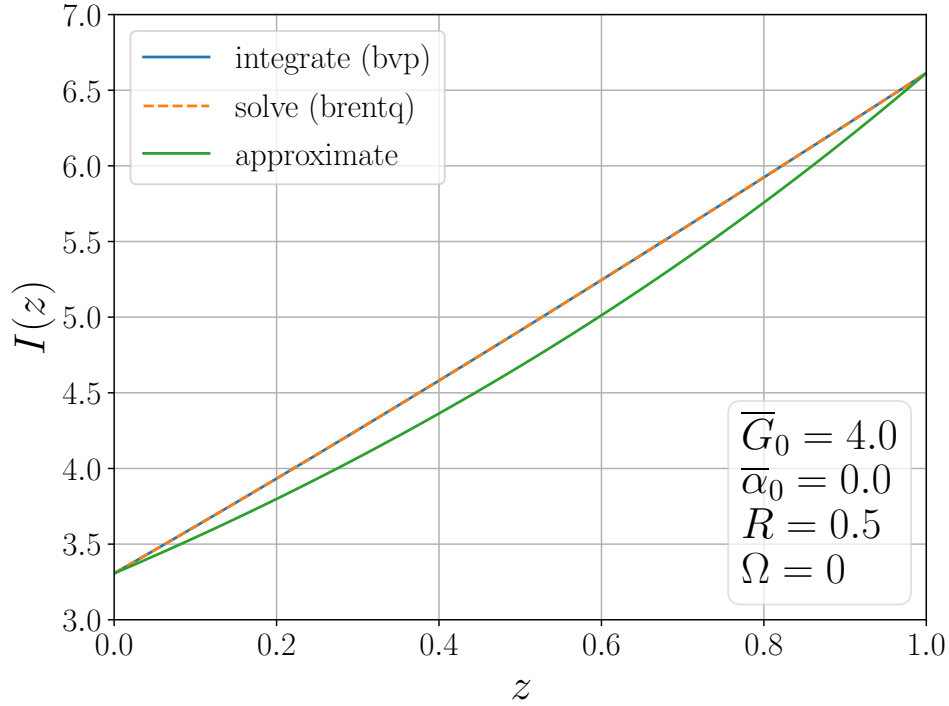
(a) Intracavity intensity

(b) Output intensity

Figure 5.5: Intracavity and output intensity for a lossless unidirectional ring laser in one dimension with $R = 0.5$, $\Omega = 0$, and $\overline{G}_0 = 4$. We have assumed that $\text{Re}[\mathcal{L}(0)] = 1$. (a) The intracavity intensity computed using three methods: direct numerical integration of Eq. (5.8); numerical solution of Eq. (5.11); and the approximate solution provided by Eq. (5.66). (b) Output intensity as a function of R comparing Eq. (5.51) (with $\overline{\alpha}_0 = 0$) and Eq. (5.65).

corresponding output intensity as a function of R using Eq. (5.51) and Eq. (5.67). Even at relatively high gains, our simple model matches the exact analytic result reasonably well. This agreement is echoed by the computations of optimum output coupler reflectance and output intensity shown in Fig. 5.7 for $A = 1\%$, $\Omega = 0$, and $\overline{\alpha}_0 = \ln(1.25)$. In Fig. 5.7a, we compare the optimum output coupler reflectance as a function of $\overline{G}_0$ computed using Eq. (5.52) and a numerical solution of Eq. (5.67). The close agreement of these two predictions is consistent with the corresponding output intensity computed using Eq. (5.53) and Eq. (5.67) shown in Fig. 5.7b.

Suppose that the amplifier in the laser resonator is spatially nonuniform. For example, consider a gain region with constant $\overline{G}_0$ extending from $z = z_1$ to $z = z_2$. Then $G_0(z)$ is given by

$$G_0(z) = \frac{\overline{G}_0}{z_2 - z_1} \tag{5.68}$$

which clearly satisfies $\int_0^1 dz\, G_0(z) = \overline{G}_0$. For our approximate model of this unidirectional ring laser, we use $I(z) = I(0)\,|u_0(z)|^2$, but we replace $|u_0(z)|^2$ with $|u_0'(z)|^2$ defined by Eq. (5.55). The result is shown in Fig. 5.8 for $z_1 = 0.25$ and $z_2 = 0.75$. The numerical solution of Eq. (5.9) fails to predict the correct intensities everywhere except at the mirrors, but our approximate model using Eq. (5.55) does a very reasonable job of matching the result of a direct numerical integration of Eq. (5.8).

Finally, we can use Eq. (5.17) to determine the small phase shift $\delta\omega_0$ that arises when the frequencies of the carrier (ω_0), the center of the gain distribution (ω_{ab}), and the nearest cavity mode are not perfectly aligned. We require that the round-trip phase accumulated by the electric field must be zero, and we apply the boundary condition $I(0) = R\,I(1)$ to obtain

$$0 = \phi(1) - \phi(0) = -\delta\omega_0 - \frac{1}{2}\frac{\mu(\Omega)}{\rho(\Omega)} \ln\left[\frac{1}{e^{-\overline{\alpha}_0}R}\right]. \tag{5.69}$$

Since $e^{-\alpha(\omega_0)}R \equiv |\Gamma|^2$, using Eq. (4.54) we again have

$$\delta\omega_0 = -\frac{1}{2\,\tau_p}\frac{\mu(\Omega)}{\rho(\Omega)}, \tag{5.70}$$

in precise agreement with the frequency shift defined by Eq. (5.58).

5.4   Spatial Interference in One-Dimensional Standing-Wave Lasers

Recall that the general time-independent wave propagation equation is given by Eq. (5.1a), where, from Eq. (2.81) and Eq. (5.2b), $F^{\pm}(z)$ is given by

$$F^{\pm}(z) = \frac{1}{2}\mathcal{L}(\Omega)\,G_0(z)\,\frac{k_0}{2\pi}\int_{z-\pi/k_0}^{z+\pi/k_0} dz'\,e^{\mp i k_0 z'}\,\frac{\tilde{E}(z')}{1 + \rho(\Omega)\left|\tilde{E}(z')\right|^2}, \tag{5.71}$$

where $\rho(\Omega)$ is defined by Eq. (5.7), and the total spatially rapidly-varying electric field envelope function is given in the one-dimensional case by Eq. (2.80) as

$$\tilde{E}(z) = E^{+}(z)\,e^{+i k_0 z} + E^{-}(z)\,e^{-i k_0 z}, \tag{5.72}$$

Here we have assumed that $E^{+}(z)$, $E^{-}(z)$, and the pump, $G_0(z)$, vary slowly over distance scales on the order of a wavelength or less. Again, let $E^{\pm}(z) \equiv \sqrt{I^{\pm}(z)}\,e^{-i\phi^{\pm}(z)}$, and $\phi(z) \equiv \phi^{-}(z) - \phi^{+}(z)$. Then, taking the real part of Eq. (5.1a), we obtain

$$\frac{d}{dz}I^{\pm}(z) = \mp\frac{1}{2}\alpha_0(z)\,I^{\pm}(z) \pm 2\,\mathrm{Re}\left[\frac{F^{\pm}(z)}{E^{\pm}(z)}\right]I^{\pm}(z), \tag{5.73}$$

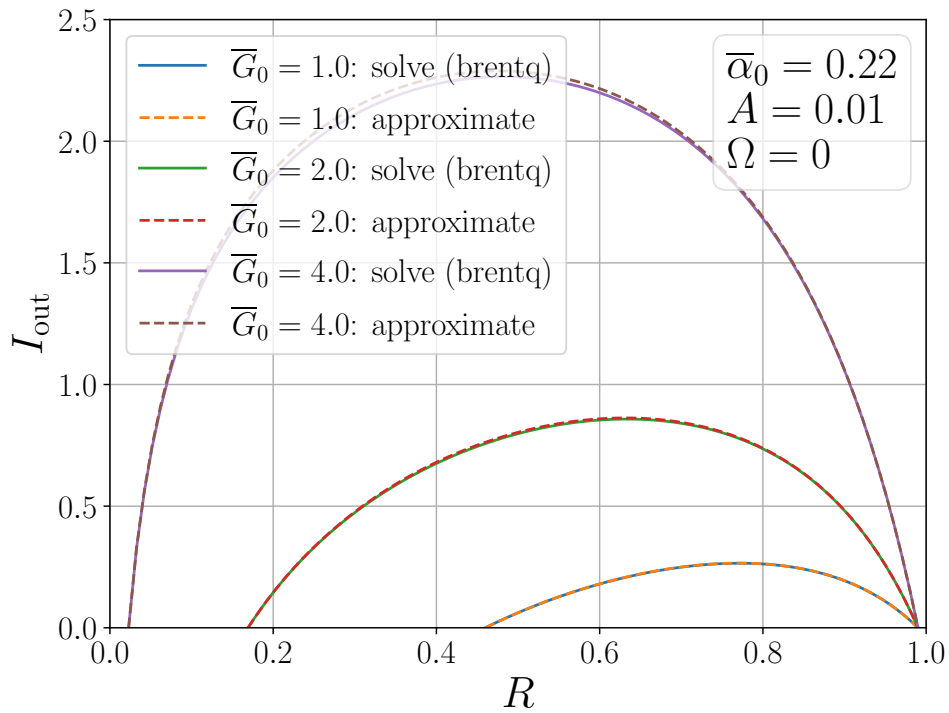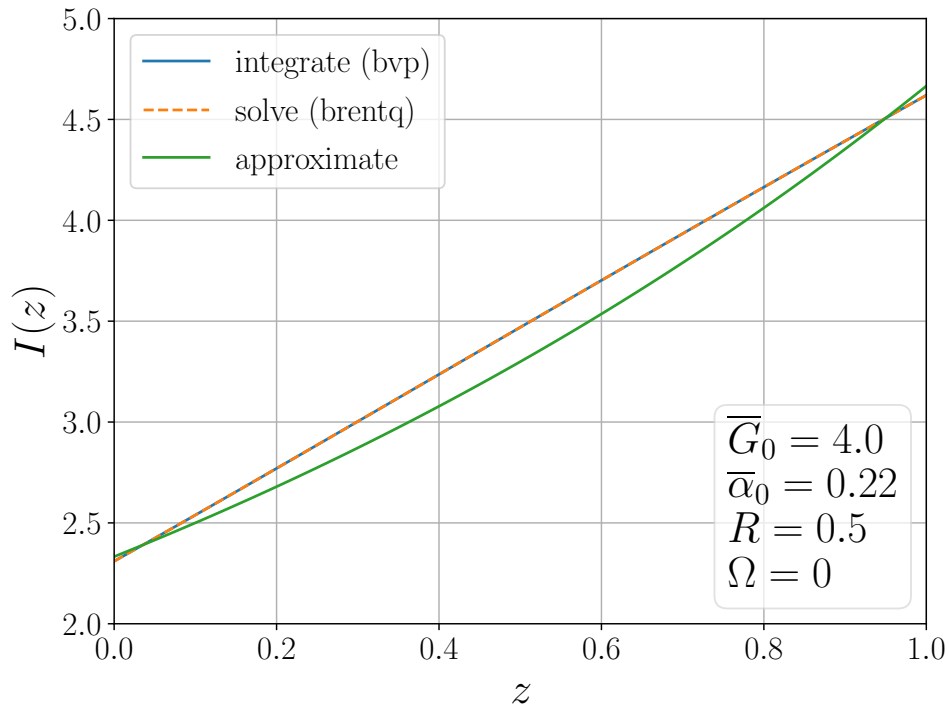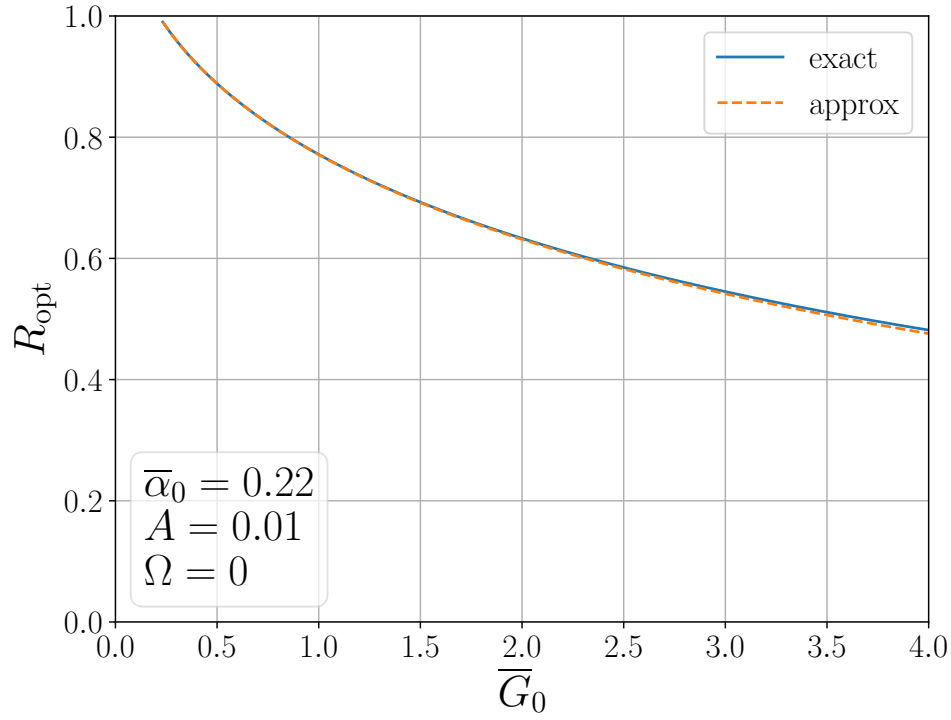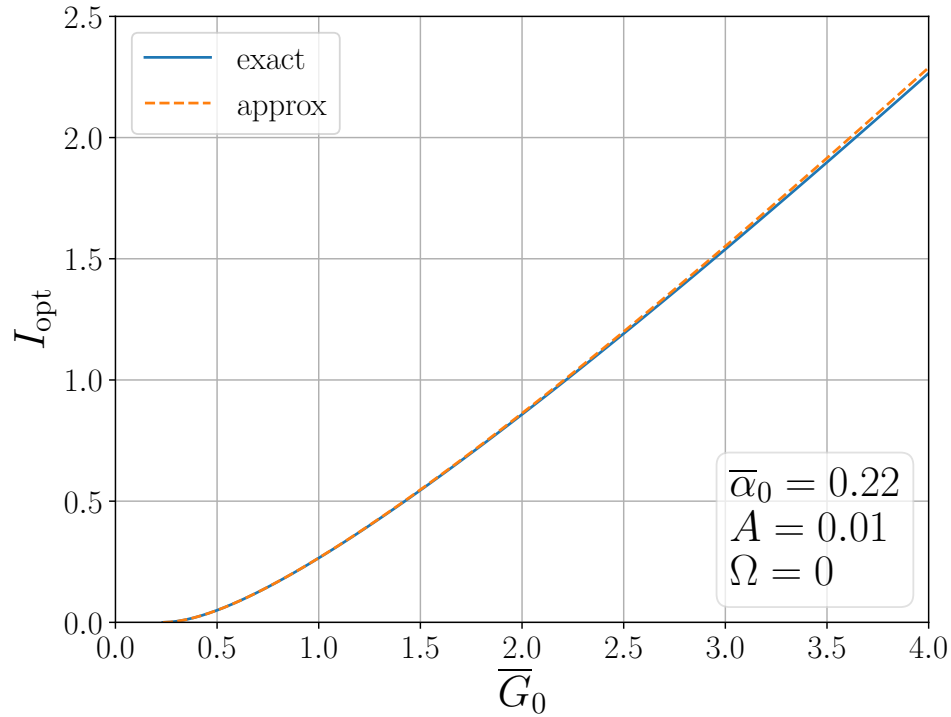(a) Intracavity intensity

(b) Output intensity

Figure 5.6:   Intracavity and output intensity for a unidirectional ring laser in one dimension with $R = 0.5$, $A = 1\%$, $\Omega = 0$, $\overline{\alpha}_0 = \ln(1.25)$, and $\overline{G}_0 = 4$. (a) The intracavity intensity computed using three methods: direct numerical integration of Eq. (5.8); numerical solution of Eq. (5.9); and the approximate solution provided by Eq. (5.66). (b) Output intensity as a function of R comparing Eq. (5.51) and Eq. (5.67).

(a) Intracavity intensity

(b) Output intensity

Figure 5.7: Optimum output coupler reflectance as a function of unsaturated round-trip gain for a unidirectional ring laser in one dimension with $A = 1\%$, $\Omega = 0$, and $\overline{\alpha}_0 = \ln(1.25)$. (a) The optimum output coupler reflectance as a function of $\overline{G}_0$ computed using Eq. (5.52) and a numerical solution of Eq. (5.67). (b) The corresponding output intensity comparing Eq. (5.53) and Eq. (5.67).
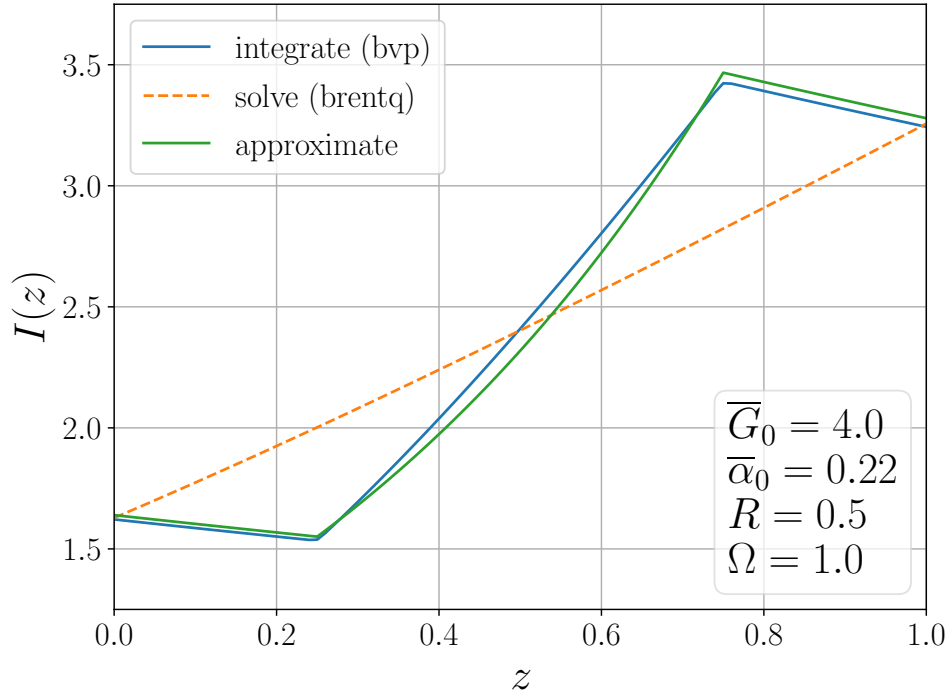
Figure 5.8: Intracavity intensity as a function of z for a constant gain region that extends from $z = 0.25$ to $z = 0.75$. The numerical solution of Eq. (5.9) predicts the correct intensities at the mirrors, but (as it must) otherwise fails. On the other hand, an approximate model using Eq. (5.55) does a credible job of matching the result of a direct numerical integration of Eq. (5.8).

where now

$$
2\,\mathrm{Re}\left[\frac{F^{\pm}(z)}{E^{\pm}(z)}\right] = \rho(\Omega)\,G_0(z)
$$
$$
\times \frac{k_0}{2\pi} \int_{z-\pi/k_0}^{z+\pi/k_0} dz' \frac{1 + \sqrt{I^{\mp}(z)/I^{\pm}(z)}\,e^{-i\,[2\,k_0\,z' + \phi(z)]}}{1 + \rho(\Omega)\left\{I^{+}(z) + I^{-}(z) + 2\,\sqrt{I^{+}(z)\,I^{-}(z)}\,\cos[2\,k_0\,z' + \phi(z)]\right\}}, \tag{5.74}
$$

Since $\phi(z)$ is slowly-varying, we can shift the limits of integration by $\Delta z = -\phi(z)/2k$, eliminating the contribution from $\sin[2\,k\,z' + \phi(z)]$ in the numerator of the integrand, yielding

$$
2\,\mathrm{Re}\left[\frac{F^{\pm}(z)}{E^{\pm}(z)}\right] = G_0(z)\,\frac{1}{2\pi}\int_0^{2\pi} d\theta\,\frac{1 + c^{\pm 1}\cos\theta}{a + b\cos\theta}, \tag{5.75}
$$

where

$$
a = \rho^{-1}(\Omega) + I^{+}(z) + I^{-}(z), \tag{5.76a}
$$
$$
b = 2\sqrt{I^{+}(z)\,I^{-}(z)}, \text{ and} \tag{5.76b}
$$
$$
c = \sqrt{I^{-}(z)/I^{+}(z)}, \tag{5.76c}
$$

and $\rho^{-1}(\Omega) \equiv 1/\rho(\Omega)$. Then substituting Eq. (5.75) into Eq. (5.73) yields

$$
\frac{d}{dz}I^{+}(z) = G_0(z)\,I^{+}(z)\,\frac{1}{2\pi}\int_0^{2\pi} d\theta\,\frac{1 + c\cos\theta}{a + b\cos\theta} - \frac{1}{2}\,\alpha_0(z)\,I^{+}(z), \text{ and} \tag{5.77a}
$$
$$
\frac{d}{dz}I^{-}(z) = -G_0(z)\,I^{-}(z)\,\frac{1}{2\pi}\int_0^{2\pi} d\theta\,\frac{1 + c^{-1}\cos\theta}{a + b\cos\theta} + \frac{1}{2}\,\alpha_0(z)\,I^{-}(z). \tag{5.77b}
$$

Below we will apply Eq. (5.77) to the standing-wave laser resonator in Fig. 5.3b, subject to the boundary conditions

$$I^+(0) = R_1 I^-(0) \quad \text{and} \tag{5.78a}$$

$$I^-(1/2) = R_2 I^+(1/2) \tag{5.78b}$$

at the two mirrors, using two different approaches to the problem of spatial interference between the counterpropagating fields. However, we can follow the same approach as in Section 5.3 to find the amount of frequency pulling that occurs in a stable standing-wave laser. In this case, the total phase accumulated during one round trip is the sum of the phase acquired by the forward-propagating field as it travels from R_1 to R_2, and the phase accrued by the backward-propagating field as it travels from R_2 to R_1. Using Eq. (5.17), we find

$$
\begin{aligned}
0 &= \left[\phi^+\left(\frac{1}{2}\right) - \phi^+(0) \right] + \left[\phi^-(0) - \phi^-\left(\frac{1}{2}\right) \right] \\
&= \delta\omega_0 \left[-\left(\frac{1}{2} - 0\right) + \left(0 - \frac{1}{2}\right) \right] - \frac{1}{2}\frac{\mu(\Omega)}{\rho(\Omega)} \ln\left[e^{+\int_0^{1/2} dz\,\alpha_0(z) - \int_{1/2}^0 dz\,\alpha_0(z)} \frac{I^+\left(\frac{1}{2}\right)}{I^+(0)}\frac{I^-(0)}{I^-\left(\frac{1}{2}\right)} \right] \\
&= -\delta\omega_0 - \frac{1}{2}\frac{\mu(\Omega)}{\rho(\Omega)} \ln\left(\frac{1}{e^{-\overline{\alpha}_0} R_1 R_2} \right),
\end{aligned}
\tag{5.79}
$$

where we have applied Eq. (5.78). Since $e^{-\alpha(\omega_0)} R_1 R_2 \equiv |\Gamma|^2$, using Eq. (4.54) we again have

$$\delta\omega_0 = -\frac{1}{2\tau_p}\frac{\mu(\Omega)}{\rho(\Omega)}, \tag{5.80}$$

in agreement with Eq. (5.58). In other words, we have found that Eq. (5.58) gives a result for a frequency-pulling shift that is true for all single-mode one-dimensional continuous-wave lasers under a variety of approximations and assumptions.

5.4.1 Rigrod's Model

One of the first treatments of saturation effects in standing-wave lasers was reported by Rigrod in [26]. He chose to ignore both intracavity absorption and spatial interference completely, which is equivalent to replacing $\cos\theta$ in Eq. (5.77) with 0, giving

$$\frac{d}{dz}I^+(z) = \frac{G_0(z)\,I^+(z)}{\rho^{-1}(\Omega) + I^+(z) + I^-(z)}, \quad \text{and} \tag{5.81a}$$

$$\frac{d}{dz}I^-(z) = -\frac{G_0(z)\,I^-(z)}{\rho^{-1}(\Omega) + I^+(z) + I^-(z)}. \tag{5.81b}$$

In this simplified case, we see immediately that

$$I^-(z)\frac{d}{dz}I^+(z) + I^+(z)\frac{d}{dz}I^-(z) = \frac{d}{dz}I^+(z)\,I^-(z) = 0,$$

so that

$$I^+(z)\,I^-(z) \equiv \varphi_0^2, \tag{5.82}$$

where φ_0 is a constant of integration to be determined later. Applying Eq. (5.82) to the boundary conditions given by Eq. (5.78), we find

$$I^+(0) = \sqrt{R_1}\,\varphi_0, \tag{5.83a}$$

$$I^+(1/2) = \frac{\varphi_0}{\sqrt{R_2}}, \tag{5.83b}$$

$$I^-(0) = \frac{\varphi_0}{\sqrt{R_1}}, \quad \text{and} \tag{5.83c}$$

$$I^-(1/2) = \sqrt{R_2}\,\varphi_0. \tag{5.83d}$$

Hence, our task is essentially to determine φ_0.

Solving Eq. (5.82) for $I^-(z)$, and substituting the result into Eq. (5.81a), we have

$$\frac{d}{dz} I^+(z) = \frac{G_0(z)\, I^+(z)}{\rho^{-1}(\Omega) + I^+(z) + \varphi_0^2/I^+(z)}\,, \tag{5.84}$$

giving the solution

$$\rho^{-1}(\Omega)\, \ln \frac{I^+(z)}{I^+(0)} + \left[I^+(z) - I^+(0)\right] \left[1 + \frac{\varphi_0^2}{I^+(0)\, I^+(z)}\right] = \int_0^z dz'\, G_0(z')\,. \tag{5.85}$$

Therefore, setting $z = 1/2$ using $I^+(0) = \sqrt{R_1}\, \varphi_0$ and $I^+(1/2) = \varphi_0/\sqrt{R_2}$, we find

$$
\begin{aligned}
\varphi_0 &= \frac{\sqrt{R_1 R_2}}{2\left(\sqrt{R_1} + \sqrt{R_2}\right)\left(1 - \sqrt{R_1 R_2}\right)} \left[\overline{G}_0 - \rho^{-1}(\Omega)\, \ln \frac{1}{R_1 R_2}\right] \\
&= \frac{1}{2\sqrt{R_1}\, \rho(\Omega)}\, C_{\text{SWL}}^2 \left(\overline{H}_0 - 1\right)\,,
\end{aligned}
\tag{5.86}
$$

where again $\overline{H}_0 = \overline{G}_0/G_{\text{th}}$, $G_{\text{th}} = \rho^{-1}(\Omega)\, \ln(1/R_1 R_2)$ when $\overline{\alpha}_0 = 0$, and C_{SWL} is given by Eq. (4.115). In Fig. 5.9, we have assumed that $\rho(0) = 1$ and plotted the intracavity and output intensity for a lossless standing-wave laser in one dimension. The intracavity intensity is computed using three methods: the direct numerical integration of Eq. (5.81) using the Scientific Python routine `scipy.integrate.solve_bvp`; the numerical solution of Eq. (5.85) — with φ_0 computed with Eq. (5.86) — using the Scientific Python routine `scipy.optimize.brentq`; and the approximate solution provided by Eq. (5.42) in the form

$$I^\pm(z) \approx \frac{\overline{H}_0 - 1}{\kappa\, \rho(\Omega)}\, \left|u_0^\pm(z)\right|^2 \tag{5.87}$$

with $\kappa = 2$. (We'll see soon that this expression is valid even when $\overline{\alpha}_0 \neq 0$.) The agreement between the two numerical solvers is expected, but the accuracy of the simple approximation is remarkable and warrants further investigation.

A clue to the relevant physics is provided by the plot shown in Fig. 5.9b. We see that the sum of the counterpropagating intensities is very well approximated by the average value. Let's maintain the presence of the background loss and rewrite Eq. (5.77) in the form

$$\frac{d}{dz} I^+(z) \cong \frac{G_0(z)\, I^+(z)}{\rho^{-1}(\Omega) + \frac{1}{2}\kappa\left[I^+(z) + I^-(z)\right]} - \alpha_0(z)\, I^+(z)\,, \text{ and} \tag{5.88a}$$

$$\frac{d}{dz} I^-(z) \cong -\frac{G_0(z)\, I^-(z)}{\rho^{-1}(\Omega) + \frac{1}{2}\kappa\left[I^+(z) + I^-(z)\right]} + \alpha_0(z)\, I^-(z)\,, \tag{5.88b}$$

where $\kappa = 2$ for the standing-wave laser in the Rigrod case, but we are anticipating the results of Section 5.4.2. We now assume that the gain and absorption functions are constants that fill the resonator, so that $\overline{G}(z) \equiv \overline{G}_0$, and $\alpha_0(z) \equiv \overline{\alpha}_0$. We then make the ansatz that

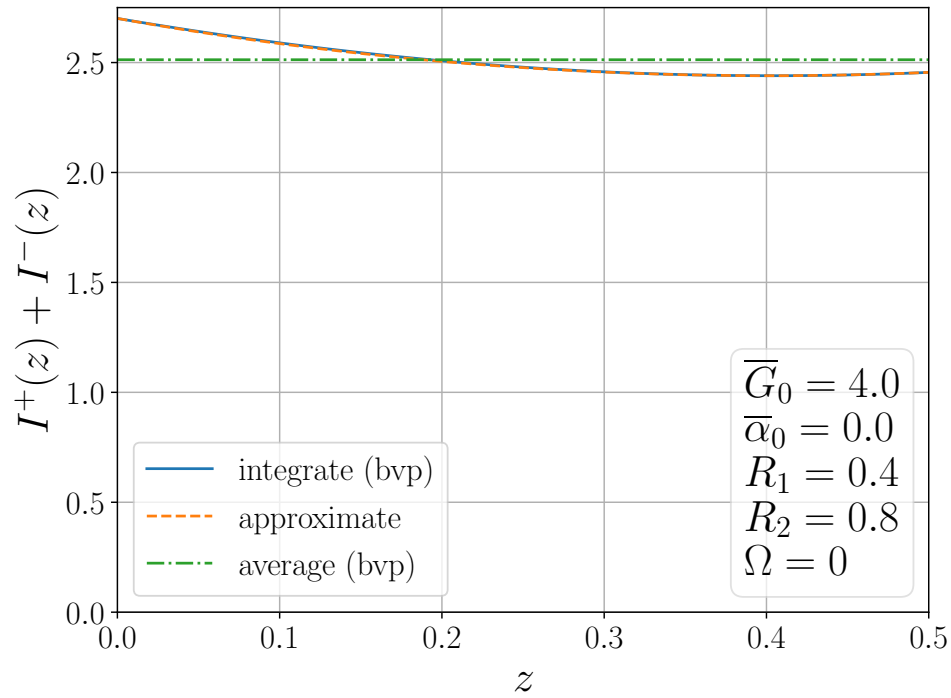$$I^+(z) \approx I^+(0)\, e^{\ln(1/R_1 R_2)z}\,, \text{ and} \tag{5.89a}$$

$$I^-(z) \approx I^-(0)\, e^{-\ln(1/R_1 R_2)z} = \frac{I^+(0)}{R_1}\, e^{-\ln(1/R_1 R_2)z}\,. \tag{5.89b}$$

After substituting these trial functions into Eq. (5.88) and canceling common factors, we obtain

$$\frac{1}{\kappa\, \rho(\Omega)\, I^+(0)} \left(\frac{\overline{G}_0}{G_{\text{th}}} - 1\right) \approx \frac{1}{2} \left[e^{\ln(1/R_1 R_2)z} + \frac{1}{R_1}\, e^{-\ln(1/R_1 R_2)z}\right]\,, \tag{5.90}$$
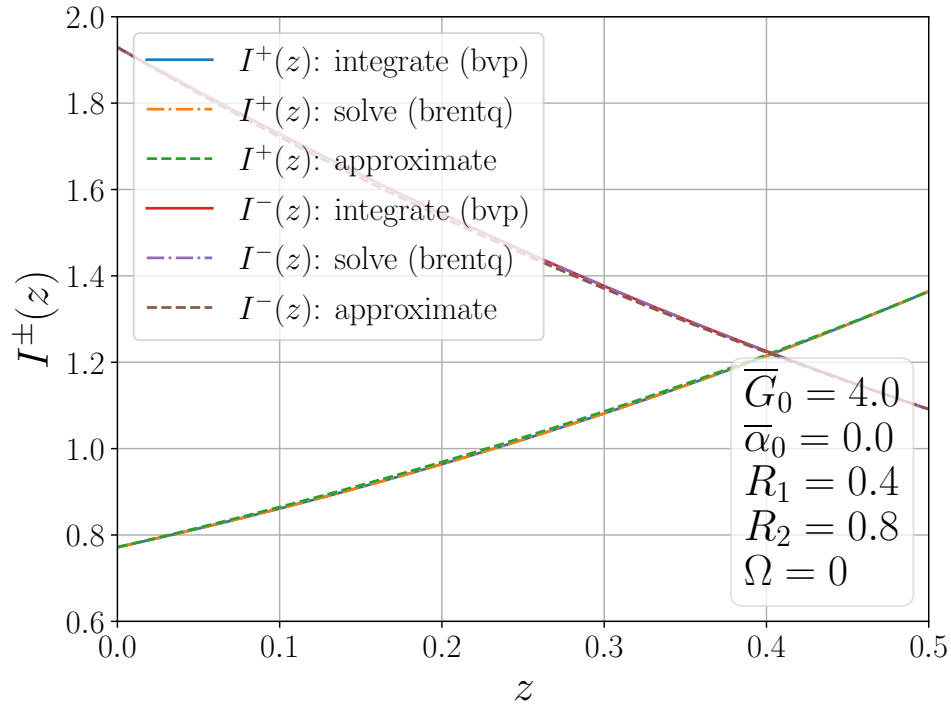
(a) Intracavity intensities

(b) Sum and average of the intracavity intensities

Figure 5.9: Intracavity and total intensities for a lossless standing-wave laser in one dimension with $R_1 = 0.4$, $R_2 = 0.8$, $\Omega = 0$, and $\overline{G}_0 = 4$. We have assumed that $\mathrm{Re}[\mathcal{L}(0)] = 1$. (a) The intracavity intensity computed using three methods: direct numerical integration of Eq. (5.81); numerical solution of Eq. (5.85); and the approximate solution provided by Eq. (5.87). (b) Comparison of the sum of the intracavity intensities using direct numerical integration and approximation.

where now $G_{\text{th}} = \rho^{-1}(\Omega)\ln(1/R_1 R_2 e^{-\overline{\alpha}_0})$. For a suitable value of $I^+(0)$, this expression should become reasonably accurate since we've learned that the right-hand side — the sum of the counterpropagating intensities in a standing-wave laser cavity — doesn't depend strongly on z. Let's estimate $I^+(0)$ by computing the mean value of the right-hand side of this expression over the single-pass length of the resonator. We find

$$2\int_0^{1/2} dz\, \frac{1}{2}\left[e^{\ln(1/R_1 R_2)z} + \frac{1}{R_1}e^{-\ln(1/R_1 R_2)z}\right] = \frac{1}{C_{\text{SWL}}^2}. \tag{5.91}$$

Therefore,

$$I^+(0) = \frac{C_{\text{SWL}}^2}{\kappa\,\rho(\Omega)}\left(\overline{H}_0 - 1\right), \tag{5.92}$$

and

$$I^+(z) \approx C_{\text{SWL}}^2\, e^{\ln(1/R_1 R_2)z}\,\frac{\overline{H}_0 - 1}{\kappa\,\rho(\Omega)} = \frac{\overline{H}_0 - 1}{\kappa\,\rho(\Omega)}\,|u_0^+(z)|^2, \text{ and}$$

$$I^-(z) \approx \frac{C_{\text{SWL}}^2}{R_1}\, e^{-\ln(1/R_1 R_2)z}\,\frac{\overline{H}_0 - 1}{\kappa\,\rho(\Omega)} = \frac{\overline{H}_0 - 1}{\kappa\,\rho(\Omega)}\,|u_0^-(z)|^2,$$

where $u_0^\pm(z)$ are given by Eq. (4.113). This result is identical to Eq. (5.87), with nonzero $\overline{\alpha}_0$ incorporated into G_{th}.

Following the approach to output coupling described in Section 5.2, we define the transmittance of each mirror as $T_j = 1 - A_j - R_j$, $j \in \{1, 2\}$, where A_j represents a small power absorption in mirror j. Using Eq. (5.83), the output intensity through each mirror is therefore

$$I_{\text{out}}^+ = T_2\, I^+(1/2) = (1 - R_2 - A_2)\,\frac{\varphi_0}{\sqrt{R_2}}, \text{ and} \tag{5.93a}$$

$$I_{\text{out}}^- = T_1\, I^-(0) = (1 - R_1 - A_1)\,\frac{\varphi_0}{\sqrt{R_1}}. \tag{5.93b}$$

Suppose that $R_2 = 1$ and therefore $A_2 = 0$, so that mirror $\mathcal{M}_1$ is the only output coupler with $R_1 \equiv R$ and $A_1 \equiv A$. Then we find that

$$I_{\text{out}} = \frac{1 - A - R}{2\,(1 - R)}\left(\overline{G}_0 - G_{\text{th}}\right), \tag{5.94}$$

which is identical to Eq. (5.50) with $\kappa = 2$. As in the case of the lossless unidirectional ring laser in Fig. 5.5b, it is no surprise that the same-gain curves in Fig. 5.10 are virtually identical.

In the general case of a one-dimensional standing-wave laser with intracavity scattering and absorption, when we neglect spatial hole-burning the counterpropagating intensities obey the differential equations

$$\frac{d}{dz}I^\pm(z) = \pm\frac{G_0(z)\,I^\pm(z)}{\rho^{-1}(\Omega) + I^+(z) + I^-(z)} \mp \alpha_0(z)\,I^\pm(z), \tag{5.95}$$

subject to the boundary conditions given by Eq. (5.78). In Fig. 5.11, our approach is identical to that of Fig. 5.9a and Fig. 5.10. We have plotted the intracavity intensities in Fig. 5.11a for the same laser as in Fig. 5.9a, but now with $\overline{\alpha}_0 \neq 0$. We see that the numerical solution of Eq. (5.85) is no longer useful, and that our approximate model does a remarkable job reproducing the values of the counterpropagating intensities computed everywhere in the cavity by direct integration of Eq. (5.95). Once again, this is the result of $I^+(z) + I^-(z)$ maintaining a nearly constant value throughout the cavity. In Fig. 5.11b, we set $R_2 = 1$, $R_1 \equiv R$, and $A_1 \equiv A \neq 0$, and compare the result of direct integration and Eq. (5.51). Even at relatively high gains, our simple model very closely matches the exact numerical result. This agreement is echoed by the computations of optimum output coupler reflectance and output intensity shown in Fig. 5.12. In Fig. 5.12a, we compare the optimum output coupler reflectance as a function of $\overline{G}_0$ computed using Eq. (5.52) and a numerical solution of Eq. (5.95). The close agreement of these
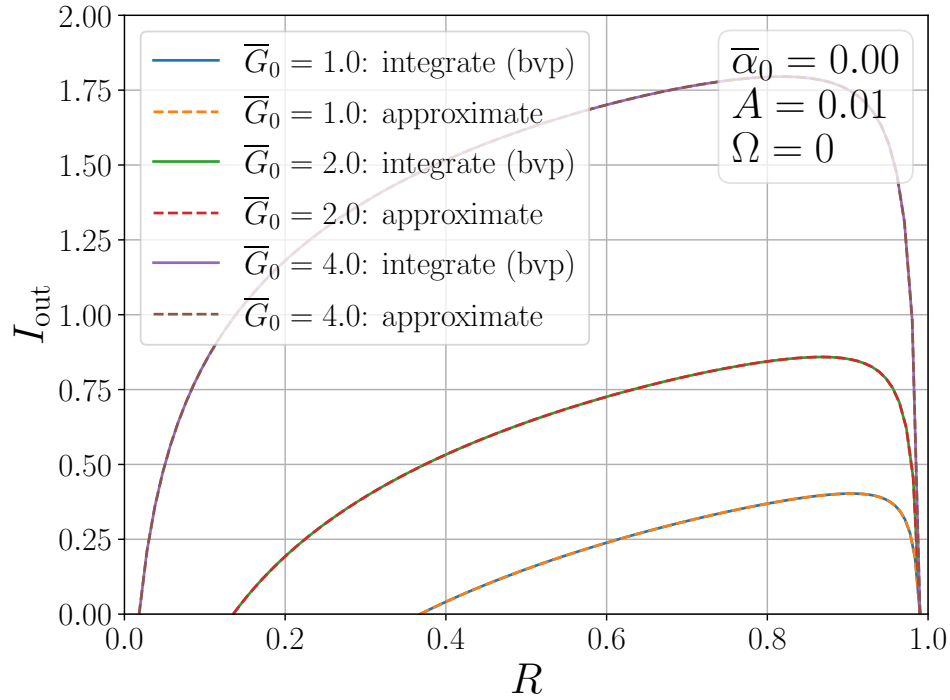
Figure 5.10: Output intensity as a function of R comparing Eq. (5.51) and Eq. (5.94).

two predictions is consistent with the corresponding approximate output intensity computed using Eq. (5.53) shown in Fig. 5.12b.

Suppose that the amplifier in the laser resonator is spatially nonuniform. For example, consider a gain region with constant $\overline{G}_0$ extending from $z = z_1$ to $z = z_2$. Then $G_0(z)$ is given by

$$G_0(z) = \frac{\overline{G}_0}{2\,(z_2 - z_1)} \tag{5.96}$$

which clearly satisfies $2 \int_0^{1/2} dz\, G_0(z) = \overline{G}_0$. For our approximate model of this standing-wave laser, we use $I^\pm(z) = I(0)\,|u_0^\pm(z)|^2$, but we replace $|u_0^\pm(z)|^2$ with $|u_0^{\pm\prime}(z)|^2$ defined by Eq. (5.57). The result is shown in Fig. 5.13 for $z_1 = 0.125$ and $z_2 = 0.375$. The numerical solution of Eq. (5.85) fails to predict the correct intensities everywhere except at the mirrors, but our approximate model using Eq. (5.57) and Eq. (5.87) does a very reasonable job of matching the result of a direct numerical integration of Eq. (5.95).
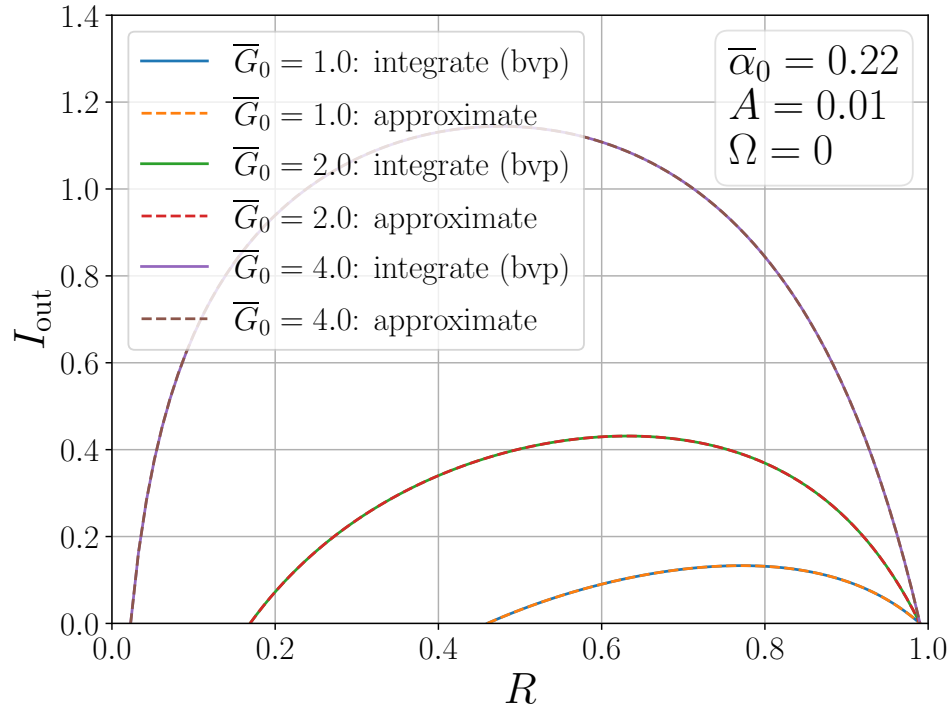
5.4.2   Agrawal and Lax's Model

A more comprehensive analysis of interference effects in standing-wave lasers was published by Agrawal and Lax in [27], but this paper seems to have been largely forgotten in the field. We begin by noting the result of an integral common in quantum optics,

$$\frac{1}{2\pi} \int_0^{2\pi} d\theta\, \frac{1}{a + b\cos\theta} = \frac{1}{\sqrt{a^2 - b^2}}, \tag{5.97}$$
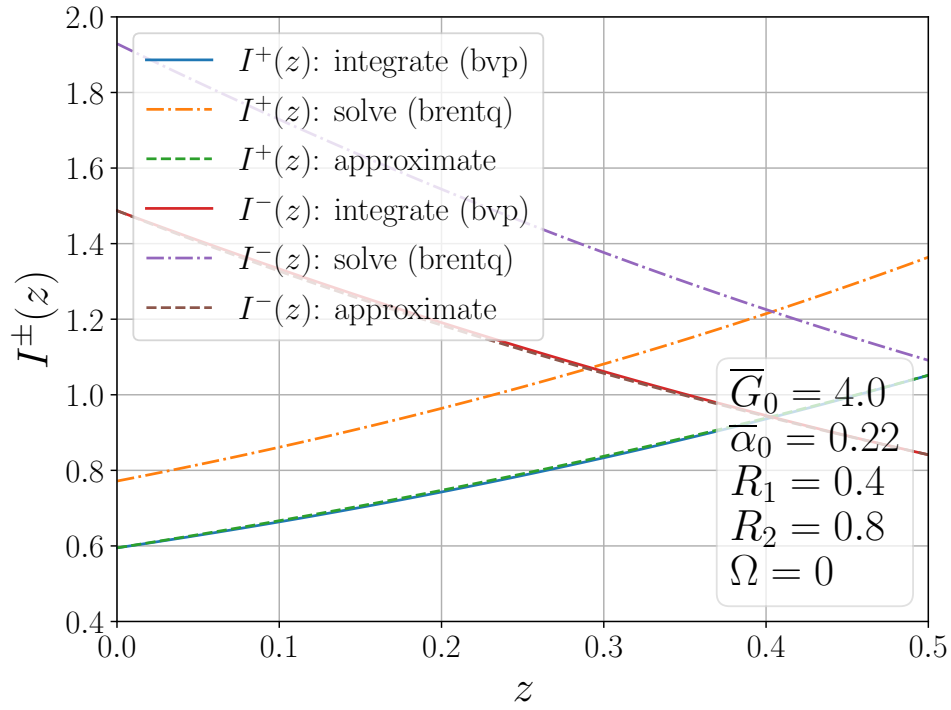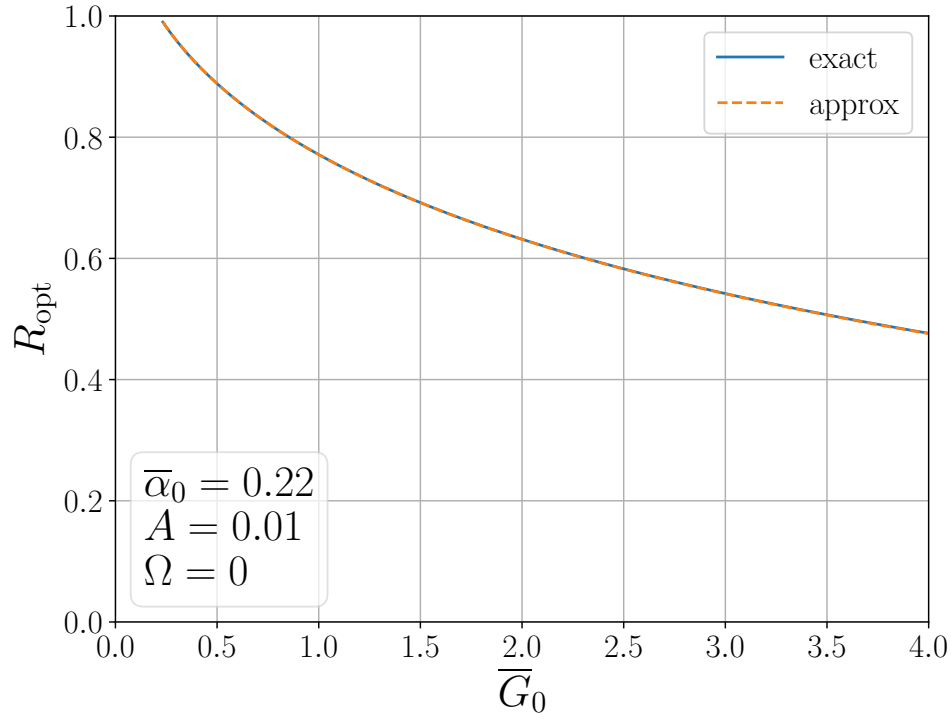
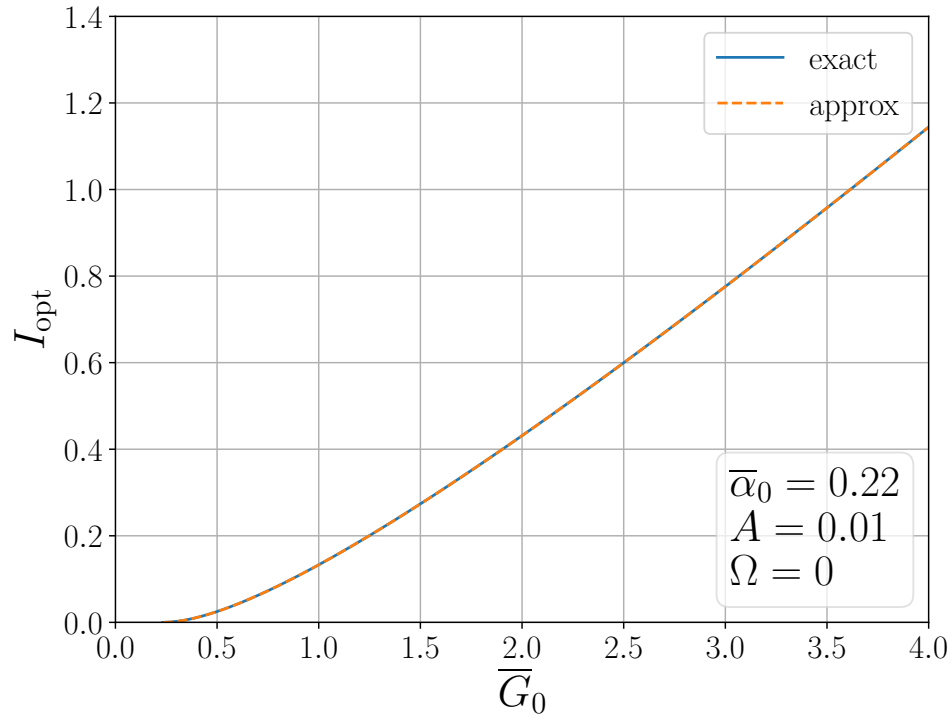(a) Intracavity intensity

(b) Output intensity

Figure 5.11:   Intracavity and output intensity for a standing-wave laser in one dimension with both background and mirror absorption loss. (a) The intracavity intensity is computed using three methods: direct numerical integration of Eq. (5.95); numerical solution of Eq. (5.85); and the approximate solution provided by Eq. (5.87). (b) Output intensity as a function of R comparing the result of direct numerical integration and Eq. (5.51). Here $R_2 = 1$, $R_1 \equiv R$ and $A_1 \equiv A$.

(a) Optimum output coupler reflectance

(b) Optimum output intensity

Figure 5.12: Optimum output coupler reflectance as a function of unsaturated round-trip gain for a standing-wave laser in one dimension with both background and mirror absorption loss. (a) The optimum output coupler reflectance as a function of $\overline{G}_0$ computed using direct numerical optimization of Eq. (5.8) and Eq. (5.52). (b) The corresponding output intensity using Eq. (5.53).
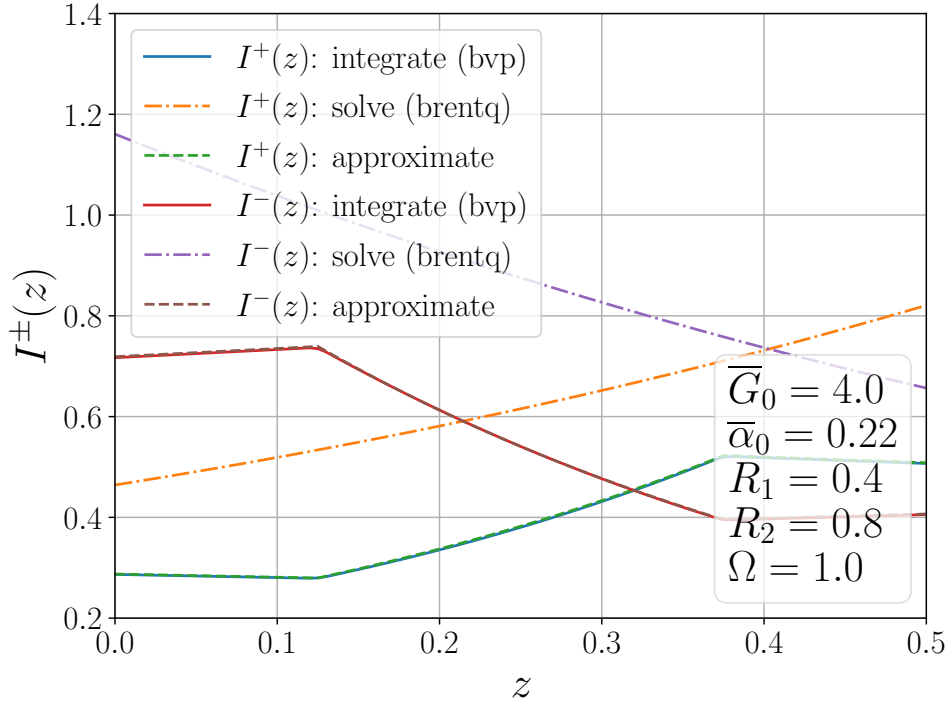
Figure 5.13: Intracavity intensity as a function of z for a standing-wave laser with a constant gain region that extends from $z = 0.125$ to $z = 0.375$. The numerical solution of Eq. (5.85) predicts incorrect intensities everywhere. On the other hand, an approximate model using Eq. (5.57) and Eq. (5.87) does a credible job of matching the result of a direct numerical integration of Eq. (5.95).

and then we find for the integrals on the right-hand side of Eq. (5.77)

$$
\begin{aligned}
\frac{1}{2\pi} \int_0^{2\pi} d\theta \, \frac{1 + c \, \cos\theta}{a + b \, \cos\theta} &= \frac{1}{2\pi} \int_0^{2\pi} d\theta \, \frac{c}{b} \left(1 - \frac{a - b/c}{a + b \, \cos\theta} \right) \\
&= \frac{c}{b} \left(1 - \frac{a - b/c}{\sqrt{a^2 - b^2}} \right) \\
&= \frac{1}{\sqrt{a^2 - b^2}} \left[1 - \frac{c}{b} \left(a - \sqrt{a^2 - b^2} \right) \right]
\end{aligned}
\tag{5.98}
$$

We have $c/b = 1/2 I^+(z)$ and $1/bc = 1/2 I^-(z)$, so averaging Eq. (5.77) over a physical wavelength yields

$$
\frac{d}{dz} I^+(z) = \frac{G_0(z)}{\sqrt{a^2 - b^2}} \left[1 - \frac{a - \sqrt{a^2 - b^2}}{2 \, I^+(z)} \right] I^+(z) - \frac{1}{2} \alpha_0(z) \, I^+(z) \,, \text{ and}
\tag{5.99a}
$$

$$
\frac{d}{dz} I^-(z) = -\frac{G_0(z)}{\sqrt{a^2 - b^2}} \left[1 - \frac{a - \sqrt{a^2 - b^2}}{2 \, I^-(z)} \right] I^-(z) + \frac{1}{2} \alpha_0(z) \, I^-(z) \,.
\tag{5.99b}
$$

We note that in the limit of very small gain and intensities, when $\alpha_0(z) = 0$ these equations become

$$
\frac{d}{dz} I^+(z) \cong G_0(z) \, I^+(z) \left\{ \rho^{-1}(\Omega) - [I^+(z) + 2 \, I^-(z)] \right\} \,, \text{ and}
\tag{5.100a}
$$

$$
\frac{d}{dz} I^-(z) \cong -G_0(z) \, I^-(z) \left\{ \rho^{-1}(\Omega) - [I^-(z) + 2 \, I^+(z)] \right\} \,.
\tag{5.100b}
$$

so that the net effect of the interference is to *increase* the saturation caused by the counterpropagating field by a factor of 2.

Next, we follow Agrawal and Lax by setting $\alpha_0(z) = 0$ and defining $X \equiv I^+ + I^-$ and $Y \equiv I^+ - I^-$; we find

$$\frac{d}{dz}X = \frac{G_0\,Y}{\sqrt{a^2 - b^2}}\,, \text{ and} \tag{5.101a}$$

$$\frac{d}{dz}Y = G_0\left(1 - \frac{1}{\rho\,\sqrt{a^2 - b^2}}\right). \tag{5.101b}$$

Now define $u = \sqrt{a^2 - b^2}$, and note that Eq. (5.76a) gives

$$u^2 = \left(\rho^{-1} + I^+ + I^-\right)^2 - 4I^+I^- = (\rho^{-1} + X)^2 - (X + Y)(X - Y) = \rho^{-2} + 2\,\rho^{-1}\,X + Y^2\,. \tag{5.102}$$

Therefore,

$$2u\frac{du}{dX} = 2 + 2Y\frac{dY}{dX} = 2u\,, \tag{5.103}$$

where we have divided Eq. (5.101b) by Eq. (5.101a) to obtain $dY/dX = (u - \rho^{-1})/Y$. Since $du/dX = 1$, we now have

$$\sqrt{a^2 - b^2} = I^+ + I^- + C\,, \tag{5.104}$$

where C is a constant of integration. With Eq. (5.104) in hand, Eq. (5.99) become

$$\frac{d}{dz}I^+(z) = \frac{G_0(z)}{2}\frac{2I^+(z) + C - \rho^{-1}(\Omega)}{I^+(z) + I^-(z) + C}\,, \text{ and} \tag{5.105a}$$

$$\frac{d}{dz}I^-(z) = -\frac{G_0(z)}{2}\frac{2I^-(z) + C - \rho^{-1}(\Omega)}{I^+(z) + I^-(z) + C}\,. \tag{5.105b}$$

Now we define

$$I_R(z) \equiv I^+(z) - \rho(\Omega)\,\varphi^2\,, \text{ and} \tag{5.106a}$$

$$I_L(z) \equiv I^-(z) - \rho(\Omega)\,\varphi^2\,, \tag{5.106b}$$

where $\varphi^2 \equiv [1 - \rho(\Omega)\,C]/2\,\rho^2(\Omega)$. Then

$$\frac{d}{dz}I_R(z) = \frac{G_0(z)\,I_R(z)}{\rho^{-1}(\Omega) + I_R(z) + I_L(z)}\,, \text{ and} \tag{5.107a}$$

$$\frac{d}{dz}I_L(z) = -\frac{G_0(z)\,I_L(z)}{\rho^{-1}(\Omega) + I_R(z) + I_L(z)}\,. \tag{5.107b}$$

These equations have exactly the same form as those of the Rigrod model, given by Eq. (5.81), but with different boundary conditions.

First, we note that substituting Eq. (5.106) into Eq. (5.104) and then squaring both sides yields

$$I_R(z)\,I_L(z) = \varphi^2\,. \tag{5.108}$$

Then the solution to Eq. (5.107a) follows the same approach as that of Eq. (5.81a), and can be read from Eq. (5.85) as

$$\rho^{-1}(\Omega)\ln\frac{I_R(z)}{I_R(0)} + [I_R(z) - I_R(0)]\left[1 + \frac{\varphi^2}{I_R(0)\,I_R(z)}\right] = \int_0^z dz'\,G_0(z')\,. \tag{5.109}$$

We define $I_1 \equiv I_R(0)$ and $I_2 \equiv I_R(1/2)$, and apply the boundary conditions given by Eq. (5.78) to Eq. (5.106). We find

$$I_1 + \rho\,\varphi^2 = \varphi^2\,(\rho + 1/I_1)\,R_1\,, \text{ and} \tag{5.110}$$

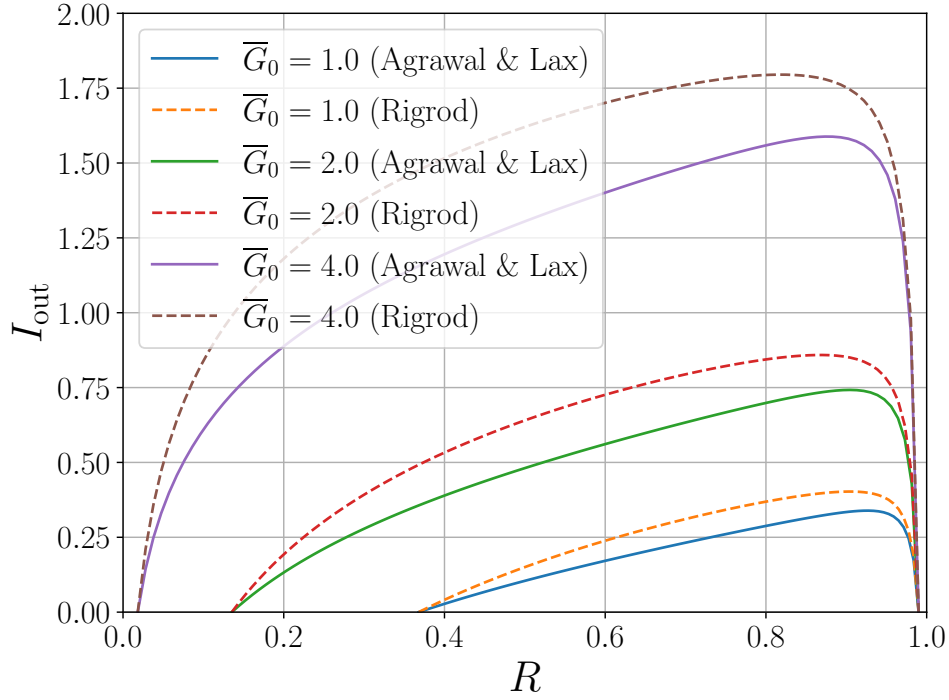$$I_2 + \rho\,\varphi^2 = \frac{\varphi^2\,(\rho + 1/I_2)}{R_2}\,, \tag{5.111}$$

Figure 5.14: Comparison of the output intensity of a laser resonator calculated using Eq. (5.93b) and Eq. (5.114b). Here $R_1 = R$, $R_2 = 1$, $A_1 = 0.01$, $\overline{\alpha}_0 = 0$, and $\Omega = 0$.

or

$$I_1 = \frac{1}{2} \left[\sqrt{4 R_1 \, \varphi^2 + (1 - R_1)^2 \, \rho^2 \, \varphi^4} - (1 - R_1) \, \rho \, \varphi^2 \right] , \text{ and} \tag{5.112a}$$

$$I_2 = \frac{1}{2 R_2} \left[\sqrt{4 R_2 \, \varphi^2 + (1 - R_2)^2 \, \rho^2 \, \varphi^4} + (1 - R_2) \, \rho \, \varphi^2 \right] . \tag{5.112b}$$

By defining $\overline{G}_0 \equiv 2 \int_0^{1/2} dz' \, G_0(z')$ and substituting these expressions into Eq. (5.109) at $z = 1/2$,

$$\rho^{-1}(\Omega) \ln \frac{I_2}{I_1} + (I_2 - I_1) \left(1 + \frac{\varphi^2}{I_1 I_2} \right) = \frac{\overline{G}_0}{2} , \tag{5.113}$$

we can find the value of φ corresponding to particular choices of R_1, R_2, and G_0, and then the values of $I^+(z)$ and $I^-(z)$ everywhere in the laser resonator. If we follow the same approach to output coupling as in Section 5.4.1, leading to Eq. (5.93) in Rigrod's model, we find

$$I_{\text{out}}^+ = T_2 \, I^+(1/2) = (1 - R_2 - A_2) \left[I_2 + \rho(\Omega) \, \varphi^2 \right] , \text{ and} \tag{5.114a}$$

$$I_{\text{out}}^- = T_1 \, I^-(0) = \frac{1 - R_1 - A_1}{R_1} \left[I_1 + \rho(\Omega) \, \varphi^2 \right] . \tag{5.114b}$$

We compare the output intensity of a laser resonator with $R_1 = R$ and $R_2 = 1$ calculated using Eq. (5.93a) and Eq. (5.114b) in Fig. 5.14. It is not surprising that Rigrod's model substantially overestimates the output power of the laser by ignoring the effects of interference in the amplifier.

When interference effects in standing-wave lasers cannot be ignored, to what extent can we continue to rely on the simple approximate model that we constructed in Section 5.2? Let's focus on Eq. (5.47), and seek a modification of the saturation factor κ that will capture the general behavior of a single-mode laser as the gain and losses vary significantly. We begin by defining κ in terms of the intracavity

intensities incident on the output coupler as

$$\kappa \equiv 2 \frac{I_{\mathrm{rr}}}{I_{\mathrm{al}}} = 2 \frac{\sqrt{R_1} \, \varphi_0}{I_1 + \rho \, \varphi^2} \,, \tag{5.115}$$

where the subscripts rr $\equiv$ "Rigrod" and al $\equiv$ "Agrawal and Lax," φ_0 is given by Eq. (5.86), and we have used Eq. (5.83), Eq. (5.106), and Eq. (5.110). Let's find an approximate expression for φ by replacing $1 - R_1$ and $1 - R_2$ (explicitly) with δ_1 and δ_2 in Eq. (5.112), substitute these expressions into Eq. (5.113), and then expand the result to second order in δ_1 and δ_2 to obtain

$$\frac{\rho^2}{4} \left[\left(\frac{1 - R_1}{\sqrt{R_1}} \right)^3 + \left(\frac{1 - R_2}{\sqrt{R_2}} \right)^3 \right] \varphi^3 + \rho \, \frac{(R_1 + R_2) \, (1 - R_1 R_2)}{R_1 R_2} \varphi^2$$
$$+ 3 \left(\frac{1 - R_1}{\sqrt{R_1}} + \frac{1 - R_2}{\sqrt{R_2}} \right) \varphi = \overline{G}_0 - \rho^{-1} \ln \frac{1}{R_1 R_2} \,.$$

Suppose that $R_2 = 1$, and consider values of R_1 greater than 0.2 Then the coefficient of φ^3 is much smaller than those of φ and φ^2, and we can neglect that term. Assuming that this is generally true, after some straightforward algebra, the equation for φ becomes

$$\beta \, \varphi^2 + 3 \, \varphi - 2 \, \varphi_0 = 0 \,, \tag{5.116}$$

where

$$\beta \equiv \rho(\Omega) \, \frac{(R_1 + R_2) \, (1 + \sqrt{R_1 R_2})}{\sqrt{R_1 R_2} \, (\sqrt{R_1} + \sqrt{R_2})} \,. \tag{5.117}$$

Therefore, we find that φ is approximately given by

$$\varphi \cong \frac{3}{2 \beta} \left(\sqrt{1 + \frac{8}{9} \beta \, \varphi_0} - 1 \right) \,. \tag{5.118}$$

Given this analytic approximation for φ, we seek a corresponding expression for I_1 that will allow us to estimate κ using Eq. (5.115). When $\overline{G}_0 \lesssim 4$, then $(1 - R)^2 \varphi^2 / 4 R_1 \ll 1$, and we can approximate Eq. (5.112a) as

$$I_1 \cong \sqrt{R_1} \, \varphi - \frac{1 - R_1}{2} \rho \, \varphi^2 \,. \tag{5.119}$$

When $\overline{G}_0$ is large and R_1 is small, we should expect that our approximation will become less accurate. We note that $\beta = (1 + R) / \sqrt{R}$ in two cases of practical interest ($R_1 = R$, $R_2 = 1$ and $R_1 = R_2 = R$), and use Eq. (5.116) to write

$$\frac{I_1 + \rho \, \varphi^2}{\sqrt{R_1}} \approx \varphi + \frac{\beta}{2} \rho \, \varphi^2 = \varphi_0 - \frac{1}{2} \varphi \,, \tag{5.120}$$

giving

$$\kappa \approx \frac{2 \, \varphi_0}{\varphi_0 - \varphi / 2} \,. \tag{5.121}$$

In the limit $\varphi_0 \longrightarrow 0$,

$$\varphi \longrightarrow \frac{3}{2} \varphi_0 \,, \quad \kappa \longrightarrow 3 \,,$$

which is consistent with the low-intracavity-intensity limit described by Eq. (5.100). On the other hand, if $\varphi_0 \longrightarrow \infty$, then

$$\varphi \longrightarrow \sqrt{\frac{2 \, \varphi_0}{\beta}} \,, \quad \kappa \longrightarrow 2 \,,$$

which allows us to identify Rigrod's model as the very high-intracavity-intensity limit of Agrawal and Lax's result. In Fig. 5.15 we plot the effective saturation parameter defined by Eq. (5.115) and the
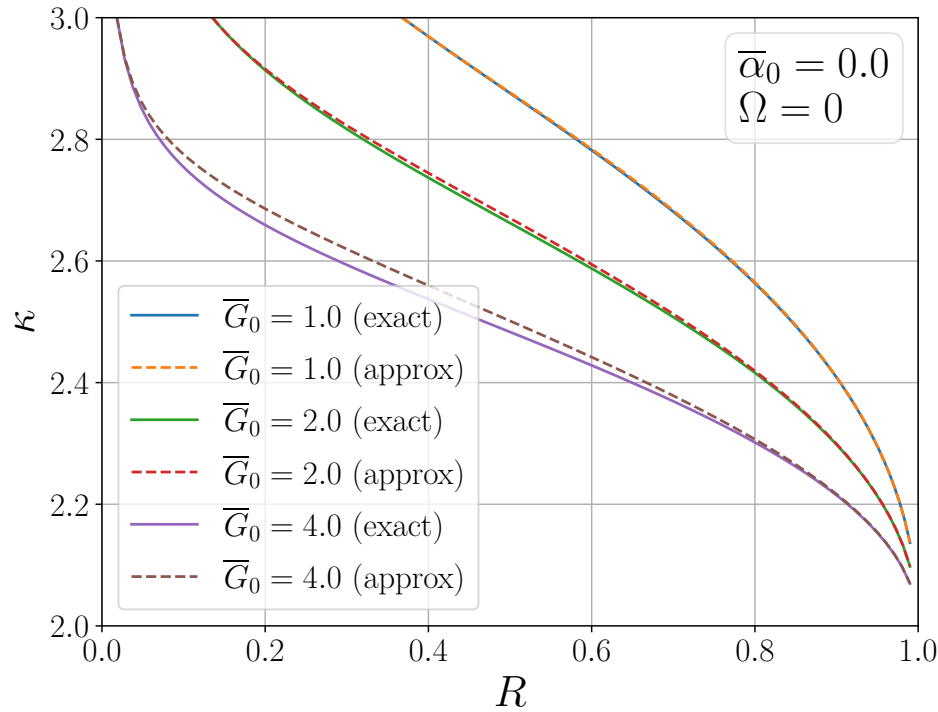
Figure 5.15: Comparison of the effective saturation parameter defined by Eq. (5.115) with the approximation given by Eq. (5.121).

approximation given by Eq. (5.121) for a range of output coupler reflectances $R_1 = R$ (with $R_2 = 1$) and gains. We see that the approximation is quite accurate for a wide range of parameters, and (as we expected) the error is largest for low reflectances and high gains.

In Fig. 5.16a, we have assumed that $\rho(0) = 1$ and plotted the intracavity and output intensity for a lossless standing-wave laser in one dimension. The intracavity intensity is computed using three methods: the direct numerical integration of Eq. (5.99) using the Scientific Python routine `scipy.integrate.solve_bvp`; the numerical solution of Eq. (5.109) and Eq. (5.112) using the Scientific Python routine `scipy.optimize.brentq`; and the approximate solution provided by Eq. (5.87) and Eq. (5.121). The agreement between the two numerical solvers is expected for $\overline{\alpha}_0 = 0$, and the accuracy of the simple approximation is reasonable for high gain and $R_1 R_2 = 0.32$. In Fig. 5.16b, we compare the sum of the intracavity intensities using direct numerical integration and the approximation. We see that the sum of the intensities is nearly constant even when spatial interference is not negligible, and the approximate model does a good job of matching the average value of the counterpropagating intensities. The accuracy of the approximate model for $I^-(0)$ is consistent with the comparison of Eq. (5.51) and Eq. (5.114b) plotted in Fig. 5.17, which shows a significant improvement over Rigrod's model when predicting output intensity as a function of reflectance.

In the general case of a one-dimensional standing-wave laser with intracavity scattering and absorption, when we include spatial hole-burning the counterpropagating intensities obey the differential equations given by Eq. (5.99), subject to the boundary conditions given by Eq. (5.78). In Fig. 5.18, our approach is identical to that of Fig. 5.16a and Fig. 5.17. We have plotted the intracavity intensities in Fig. 5.18a for the same laser as in Fig. 5.16a, but now with $\overline{\alpha}_0 \neq 0$. We see that the numerical solution of Eq. (5.109) is no longer useful, and that using Eq. (5.121) our approximate model does a remarkable job reproducing the values of the counterpropagating intensities computed everywhere in the cavity by direct integration of Eq. (5.99). In Fig. 5.18b, we set $R_2 = 1$, $R_1 \equiv R$, and $A_1 \equiv A \neq 0$, and compare the result of direct integration and Eq. (5.51). Even at relatively high gains, our simple model very closely matches the exact numerical result. In Fig. 5.19a, we compare the optimum output cou-
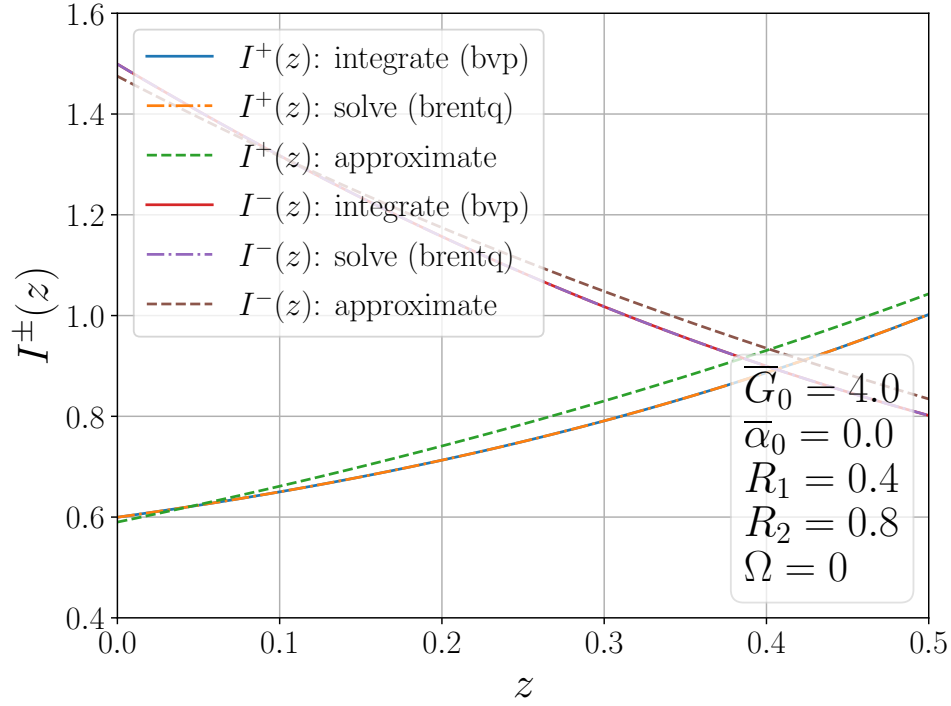
(a) Intracavity intensities
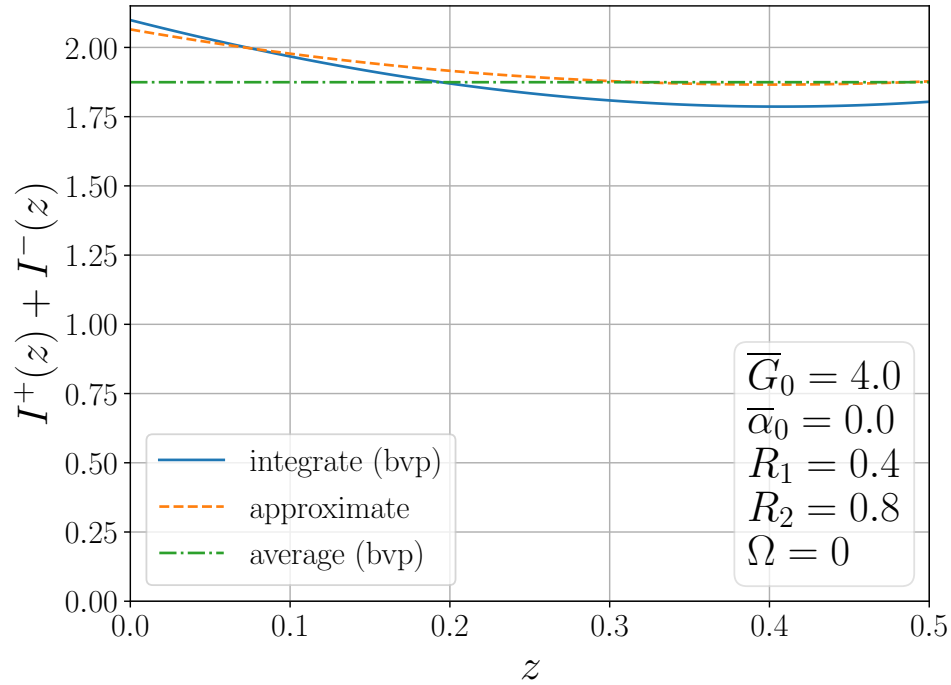
(b) Sum and average of the intracavity intensities

Figure 5.16:   Intracavity and total intensities for a lossless standing-wave laser in one dimension with $R_1 = 0.4$, $R_2 = 0.8$, $\Omega = 0$, and $\overline{G}_0 = 4$. We have assumed that $\mathrm{Re}[\mathcal{L}(0)] = 1$. (a) The intracavity intensity computed using three methods: direct numerical integration of Eq. (5.99); numerical solution of Eq. (5.109); and the approximate solution provided by Eq. (5.87) and Eq. (5.121). (b) Comparison of the sum of the intracavity intensities using direct numerical integration and approximation.
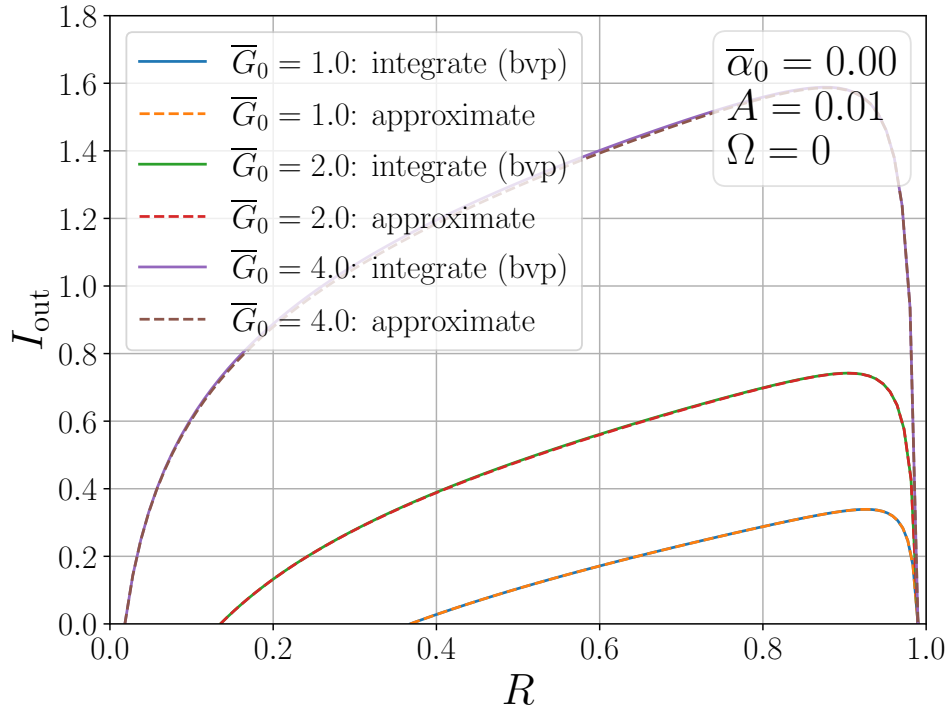
Figure 5.17: Output intensity as a function of R comparing Eq. (5.51) and Eq. (5.114b).

pler reflectance as a function of $\overline{G}_0$ computed using Eq. (5.52) and a numerical solution of Eq. (5.99). Although the approximate model slightly underestimates the value of R_{opt} at high gains, it reliably predicts the output intensity computed using Eq. (5.53) shown in Fig. 5.19b.

Again, let's suppose that the amplifier in the laser resonator is spatially nonuniform with a gain given by Eq. (5.96). As in the case where we neglected interference effects, we replace $|u_0^{\pm}(z)|^2$ with $|u_0^{\pm\prime}(z)|^2$ defined by Eq. (5.57). The result is shown in Fig. 5.20 for $z_1 = 0.125$ and $z_2 = 0.375$, and we rely on κ computed with Eq. (5.121). The numerical solution of Eq. (5.109) fails to predict the correct intensities everywhere, but our approximate model using Eq. (5.57) and Eq. (5.87) does a very reasonable job of matching the result of a direct numerical integration of Eq. (5.99).

5.5   One-Dimensional Single Mode Semiconductor Laser Models

5.5.1   Linewidth Enhancement Factor

In the previous sections of this chapter, we've been careful to allow arbitrary lineshape functions in our single-mode one-dimensional continuous-wave models, but our examples and plots have assumed a symmetric Lorentzian lineshape function $\mathcal{L}(\Omega)$. We can extend these results to the asymmetric lineshapes typical of broad classes of semiconductor lasers by relying on the evolution equation of the macroscopic polarization $\tilde{F}(z,t)$ and the corresponding lineshape function $\mathcal{L}_\alpha(\Omega)$ given by Eq. (3.48)
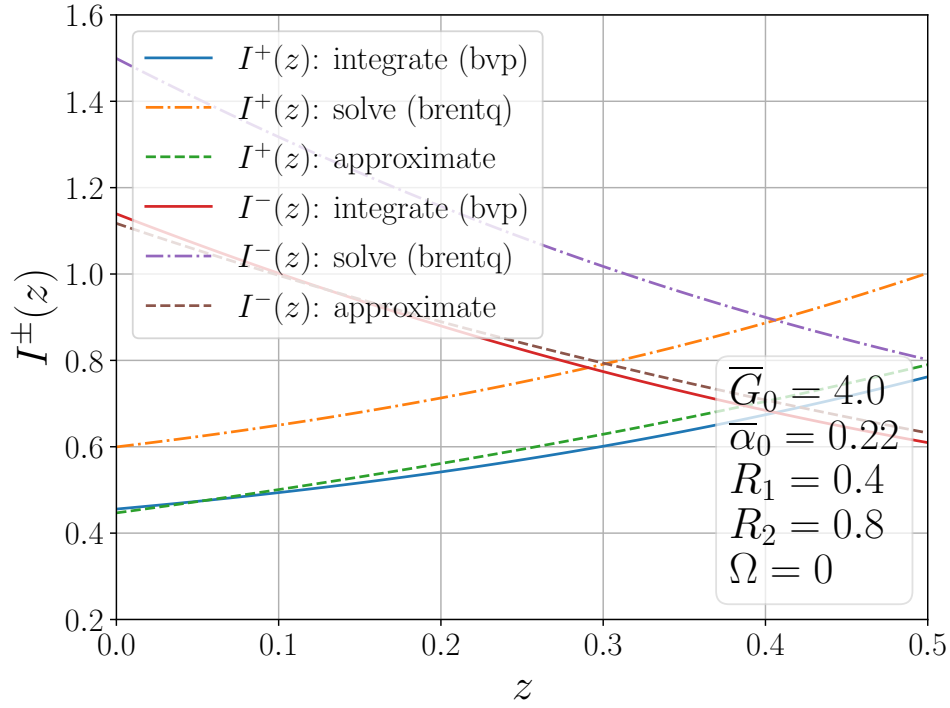
(a) Intracavity intensity
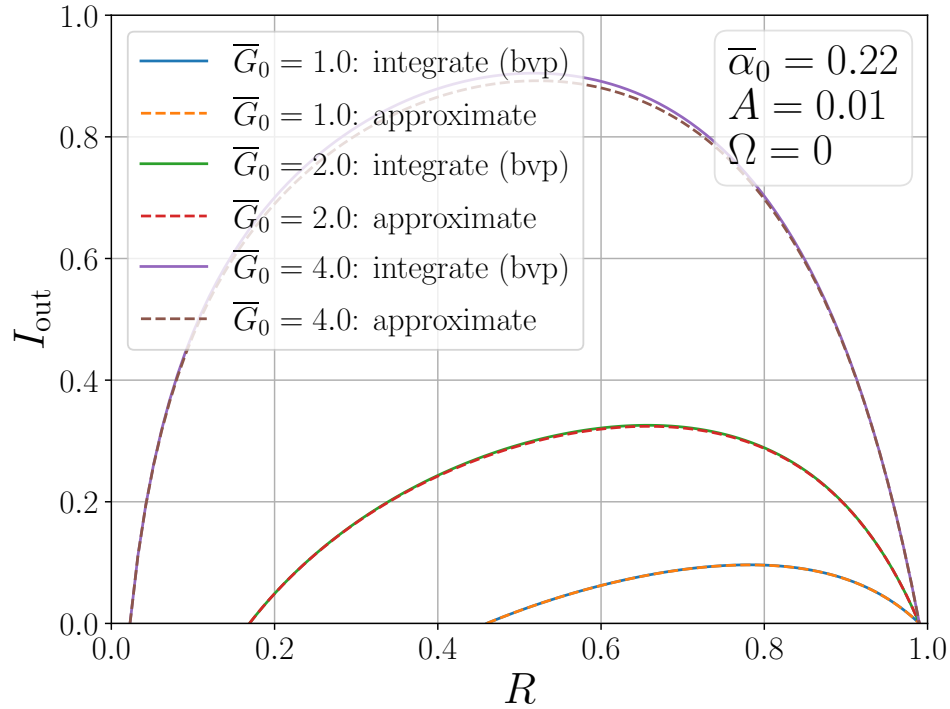
(b) Output intensity

Figure 5.18: Intracavity and output intensity for a standing-wave laser in one dimension with both background and mirror absorption loss. (a) The intracavity intensity is computed using three methods: direct numerical integration of Eq. (5.99); numerical solution of Eq. (5.109); and the approximate solution provided by Eq. (5.87) and Eq. (5.121). (b) Output intensity as a function of R comparing the result of direct numerical integration and Eq. (5.51). Here $R_2 = 1$, $R_1 \equiv R$, and $A_1 \equiv A$.
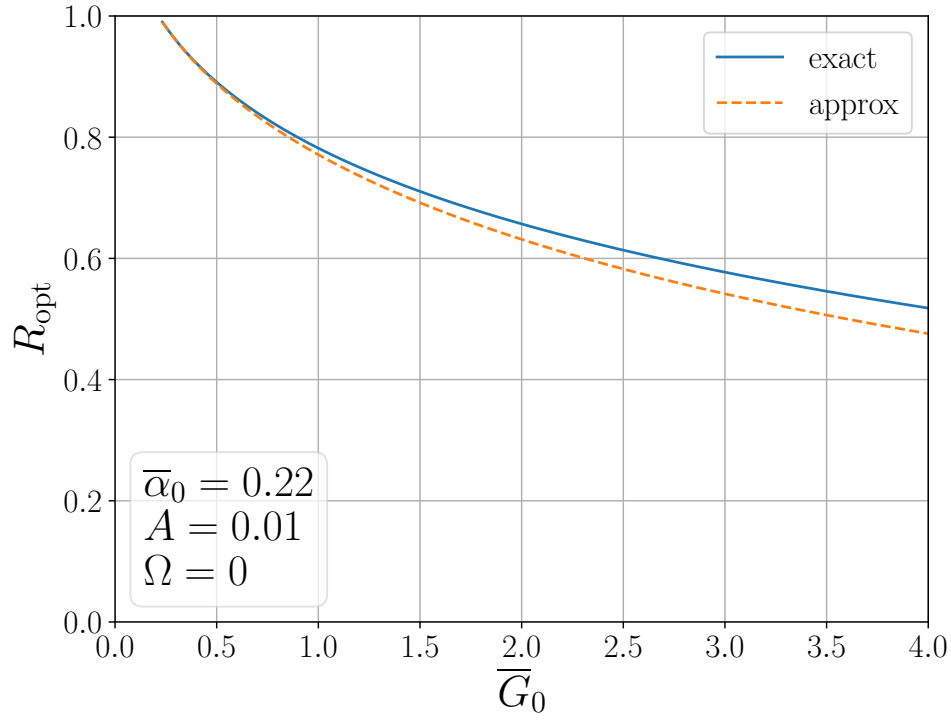
(a) Optimum output coupler reflectance
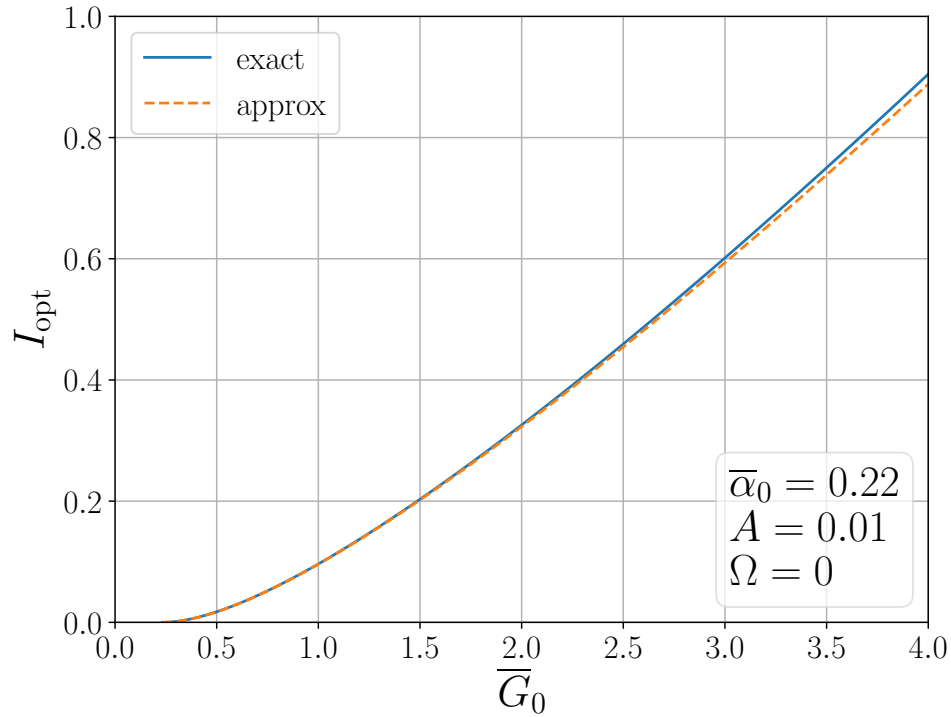
(b) Optimum output intensity

Figure 5.19:   Optimum output coupler reflectance and intensity for a standing-wave laser in one dimension with both background and mirror absorption loss, limited by spatial hole-burning. (a) The optimum reflectance as a function of $\overline{G}_0$ computed using both direct numerical optimization of Eq. (5.99) and Eq. (5.52). (b) The corresponding output intensities, with the approximation using Eq. (5.53).
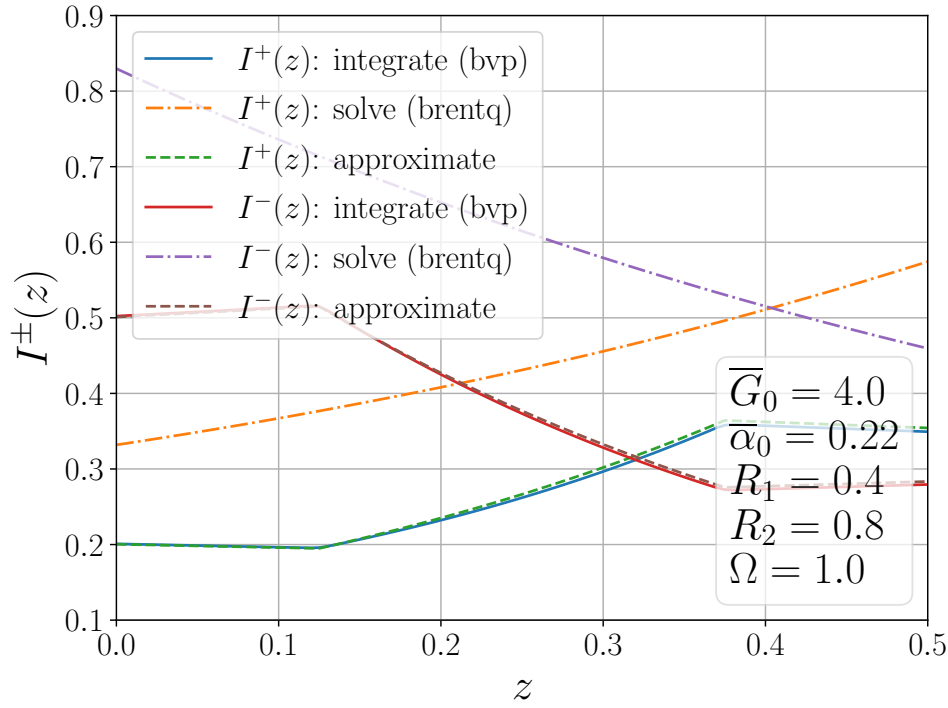
Figure 5.20: Intracavity intensity as a function of z for a standing-wave laser with a constant gain region that extends from $z = 0.125$ to $z = 0.375$. The numerical solution of Eq. (5.109) predicts incorrect intensities everywhere. On the other hand, an approximate model using Eq. (5.57) and Eq. (5.121) does a credible job of matching the result of a direct numerical integration of Eq. (5.99).

and Eq. (3.52), respectively. In general, this function has the real and imaginary parts

$$
\rho(\Omega) = \mathrm{Re}\,[\mathcal{L}_\alpha(\Omega)] = \frac{1 + \alpha^2 + 2\,\alpha\,\Omega}{1 + (\Omega + \alpha)^2}
$$
$$
= 1 - \frac{\Omega^2}{1 + (\Omega + \alpha)^2}, \text{ and}
$$
(5.122a)

$$
\mu(\Omega) = \mathrm{Im}\,[\mathcal{L}_\alpha(\Omega)] = -\frac{\alpha\,(1 + \alpha^2) + (\alpha^2 - 1)\,\Omega}{1 + (\Omega + \alpha)^2}
$$
$$
= -\alpha + \frac{(1 + \alpha^2 + \alpha\,\Omega)\,\Omega}{1 + (\Omega + \alpha)^2}.
$$
(5.122b)

The real part of $\mathcal{L}_\alpha(\Omega)$ is plotted as a function of Ω for two different ranges of α in Fig. 5.21. When $\alpha \lesssim 1$, we observe a dramatic asymmetry for modest detunings, but as α increases the predominant effect becomes a substantial broadening of the lineshape by a factor of $\sqrt{1 + \alpha^2}$. In Fig. 5.22 we plot the imaginary part of $\mathcal{L}_\alpha(\Omega)$ (offset vertically by α) as a function of Ω for the same two ranges of α. Note that at $\Omega = 0$, the slope of $\mathrm{Im}\,\mathcal{L}_\alpha(\Omega)$ is unity.

Consistent with our definition of the macroscopic polarization $\widetilde{F}(z,t)$, we define the *effective linewidth enhancement factor* for a particular detuning Ω as

$$
\alpha_{\mathrm{eff}}(\alpha,\Omega) \equiv -\frac{\mathrm{Im}\,[\mathcal{L}_\alpha(\Omega)]}{\mathrm{Re}\,[\mathcal{L}_\alpha(\Omega)]}
$$
$$
= \alpha - \Omega + \frac{2\,\alpha\,\Omega^2}{1 + \alpha^2 + 2\,\alpha\,\Omega}.
$$
(5.123)

In Fig. 5.23, we show that as α increases, the gain dispersion shifts downward linearly with α, broadens, and maintains a slope of approximately unity near $\Omega = 0$. The corresponding effective linewidth

(a) Real part of the lineshape function for small α

(b) Real part of the lineshape function for large α

Figure 5.21: Real part of the lineshape function given by Eq. (3.52) for $\tau_\perp/\tau_o = 0.0024$ and $\tau_p/\tau_o = 1.0$. When $\alpha \lesssim 1$, the lineshape asymmetry is dramatic, but as α increases $\text{Re}[\mathcal{L}(\Omega, \alpha)]$ is predominantly broadened by a factor of $\sqrt{1 + \alpha^2}$.
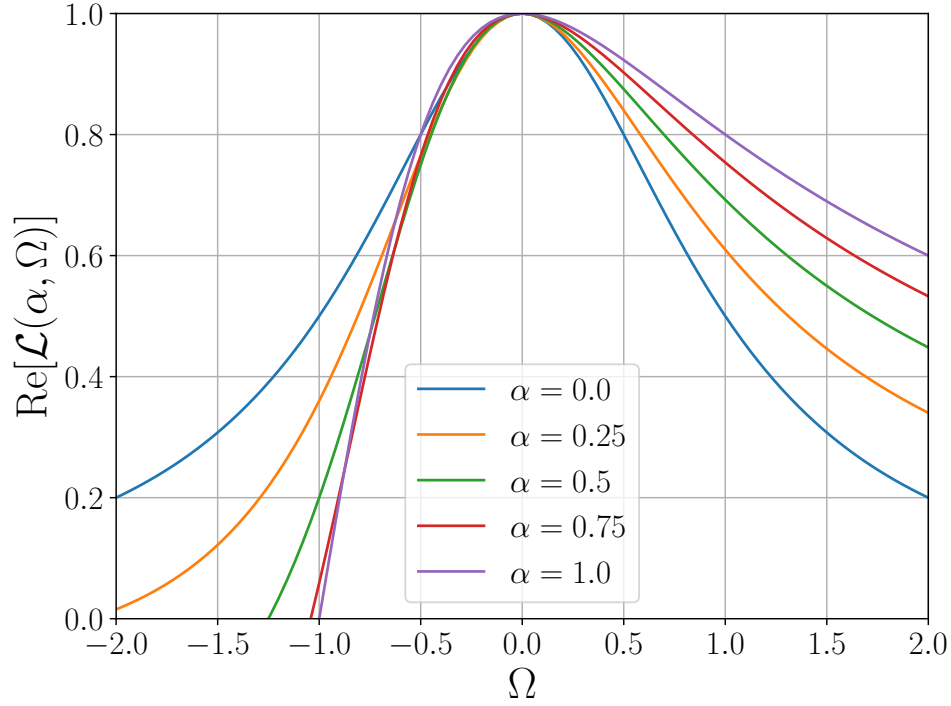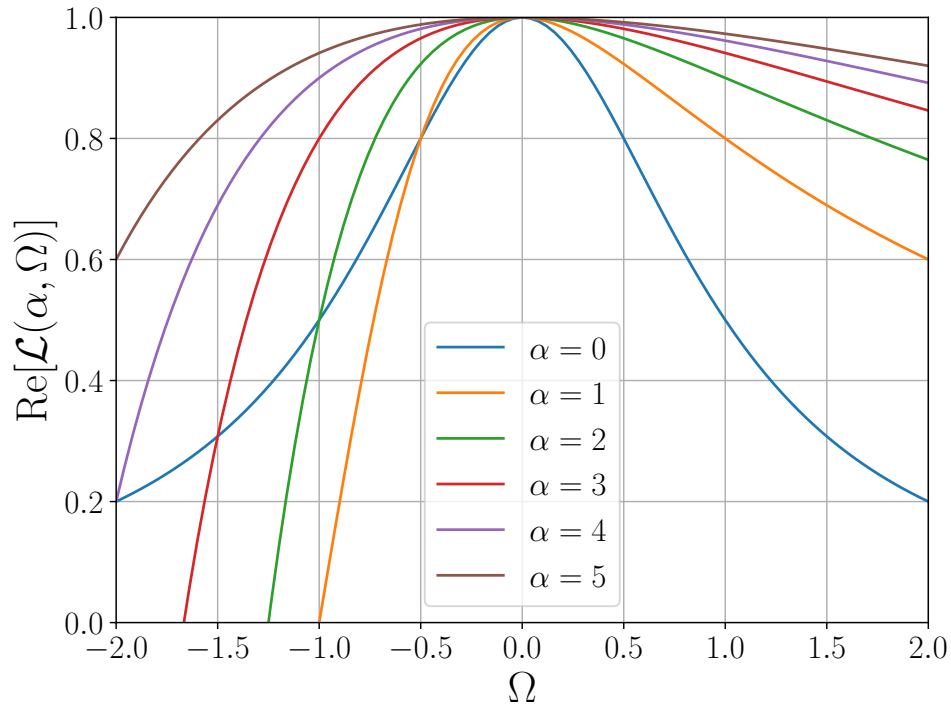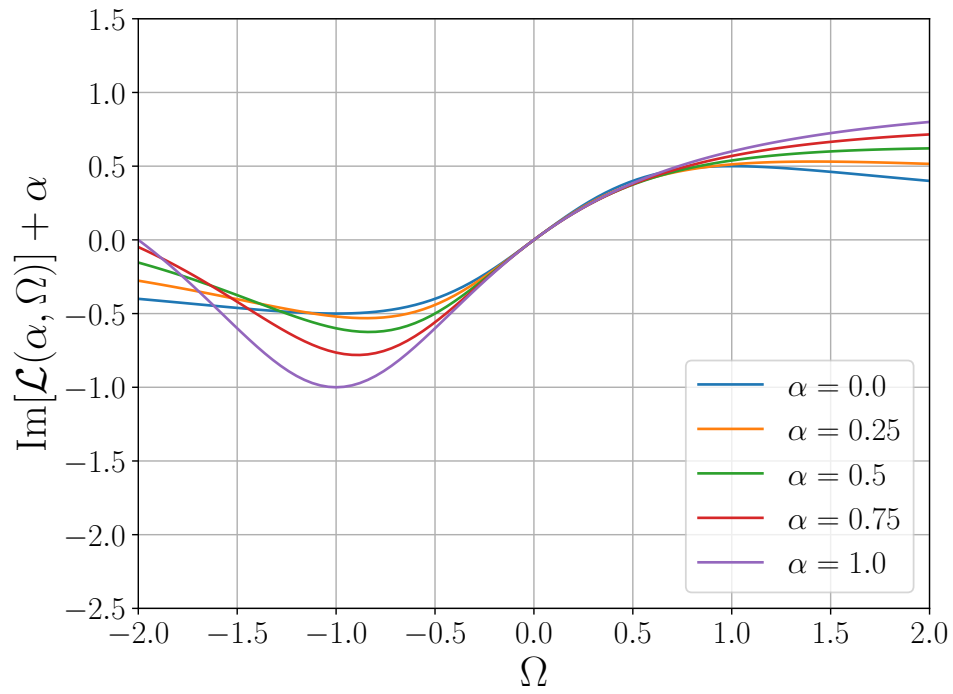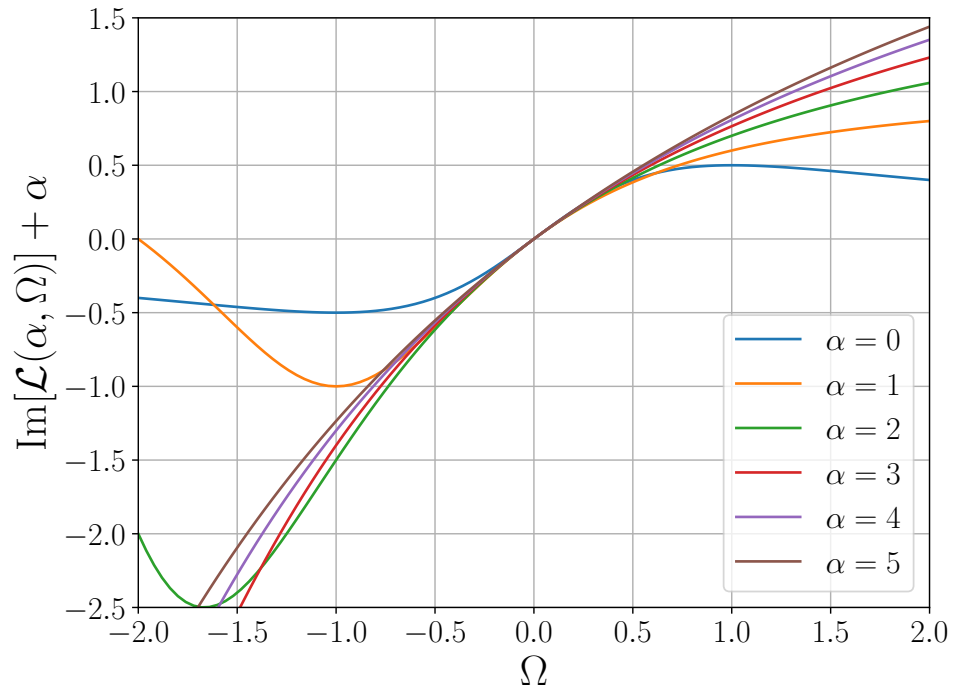
(a) Imaginary part of the lineshape function for small α

(b) Imaginary part of the lineshape function for large α

Figure 5.22: Imaginary part of the lineshape function given by Eq. (3.52). Note that at $\Omega = 0$, the slope of Im $\mathcal{L}_\alpha(\Omega)$ is unity.
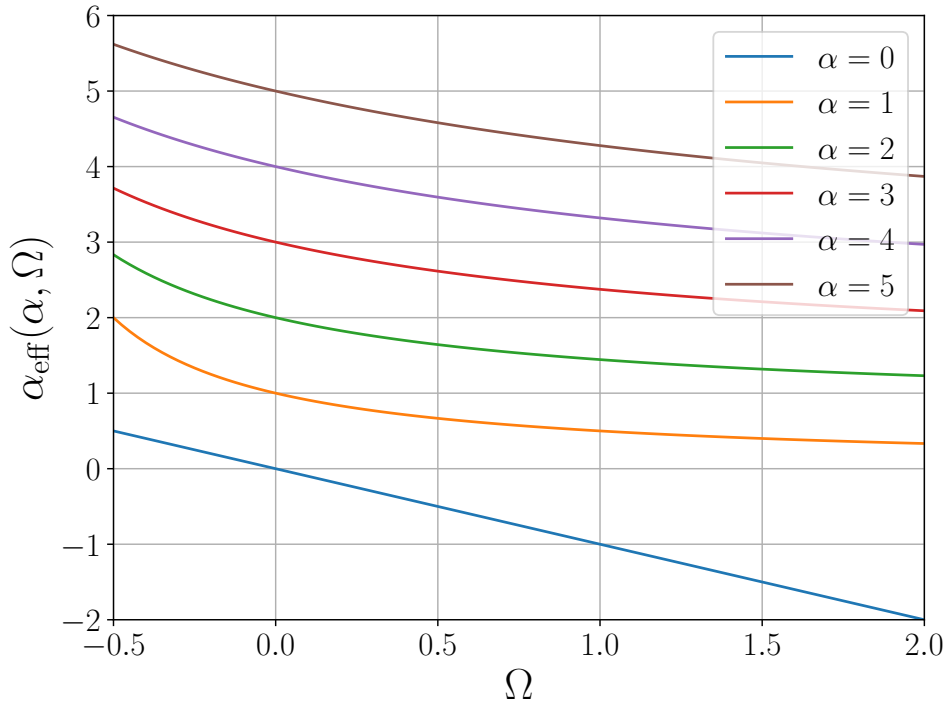
Figure 5.23: Plot of the effective linewidth enhancement factor given by Eq. (5.123) as a function of Ω for the case where $\tau_p/\tau_0 = 1$ and $\tau_\perp/\tau_0 = 2.5 \times 10^{-3}$. The corresponding linewidth — proportional to $1 + \alpha_{\text{eff}}^2(\alpha, \Omega)$ — increases with α, but decreases as the laser is detuned to the blue.

enhancement factor — and therefore the laser linewidth, proportional to $1 + \alpha'^2(\Omega, \alpha)$ — decreases relative to $|\alpha|$ as the laser is detuned to the blue.

5.5.2 Frequency Pulling and Dispersion

Using Eq. (5.58) to determine the presumably small phase shift arising from frequency pulling, we find

$$\delta\omega_0 = -\frac{1}{2\,\tau_p} \frac{\text{Im}\,[\mathcal{L}_\alpha(\Omega)]}{\text{Re}\,[\mathcal{L}_\alpha(\Omega)]}. \tag{5.124}$$

Given that $\Omega = \Omega_0 + \delta\omega_0\,\tau_\perp$, we can solve this equation accurately to second order in $\tau_\perp/\tau_p$ and obtain

$$\begin{aligned}
\delta\omega_0 &\approx \frac{1}{2\,\tau_p + \tau_\perp} \frac{\alpha\,(1 + \alpha^2) + (\alpha^2 - 1)\,\Omega_0}{1 + \alpha^2 + 2\,\alpha\,\Omega_0} \\
&= \frac{1}{2\,\tau_p + \tau_\perp} \left[\alpha - \Omega_0 + \frac{2\,\alpha\,\Omega_0^2}{1 + \alpha^2 + 2\,\alpha\,\Omega_0} \right].
\end{aligned} \tag{5.125}$$

The Lorentzian contribution to the frequency shift — $-\Omega_0/2\,\tau_p$ — is now offset by a large linear shift proportional to α. A plot of Eq. (5.125) — relative to the total linear contribution $(\alpha - \Omega_0)/(2\,\tau_p + \tau_\perp)$ — is shown in Fig. 5.24a.

We're going to treat the *nonlinear* contribution to Eq. (5.125) a little differently. Nonlinear frequency shifts correspond to dispersion, so we're going to replace Ω_0 in this expression with a general frequency $\omega\,\tau_\perp$, expand the result in a series in ω, and then take the inverse Fourier transform. We obtain

$$\frac{1}{2\,\tau_p + \tau_\perp} \frac{2\,\alpha\,\Omega_0^2}{1 + \alpha^2 + 2\,\alpha\,\Omega_0} \longrightarrow \sum_{m=2}^{\infty} \frac{A_m}{m!} \left(i\,\frac{\partial}{\partial t} \right)^m, \tag{5.126}$$

where

$$A_m \equiv \frac{m!}{2\,\tau_p + \tau_\perp} \left(\frac{2\,\alpha}{1+\alpha^2}\right)^{m-1} (-\tau_\perp)^m.$$

(5.127)

A plot of the "effective dispersion" A_m as a function of α for the case where $\tau_p/\tau_0 = 1$ and $\tau_\perp/\tau_0 = 2.5\times10^{-3}$ is shown in Fig. 5.24b. Recall from Section 3.3 that to convert A_m to an equivalent dispersion in units of $\mathrm{fs}^m/\mathrm{mm}$, we multiply by a factor of τ_0^m/L. For a laser cavity with $L = 4$ mm and $\tau_0 = 65$ ps, we obtain (e.g.) $A_2 \approx 4000\ \mathrm{fs}^2/\mathrm{mm}$. The extremum of A_m occurs at $\alpha = \pm 1$, where $2\,|\alpha|/\left(1+\alpha^2\right) = 1$. The full-width at half-maximum of A_m is $2\sqrt{2^{2/(m-1)}-1}$, which approaches $2\sqrt{2\ln(2)/(m-1)}$ as m becomes large.

Collecting the results we've derived using continuous-wave laser models, we'll apply them to dynamic models by updating Eq. (3.46a) to read

$$\frac{\partial}{\partial t}E^\pm(z,t) \pm \frac{\partial}{\partial z}E^\pm(z,t)$$

$$= \left[\frac{i}{2\,\tau_p}\,(\alpha - \Omega_0) + i\sum_{l=2}^{\infty} \frac{A_l + D_l(\omega_0)}{l!}\left(i\frac{\partial}{\partial t}\right)^l E^\pm(z,t) - \frac{1}{2}\,\alpha_0(z)\right]E^\pm(z,t) + F^\pm(z,t).$$

(5.128)

We should remember that in rapidly-varying systems it is likely that α will change with time. Nevertheless, this equation represents a good starting point to understand semiconductor laser systems.
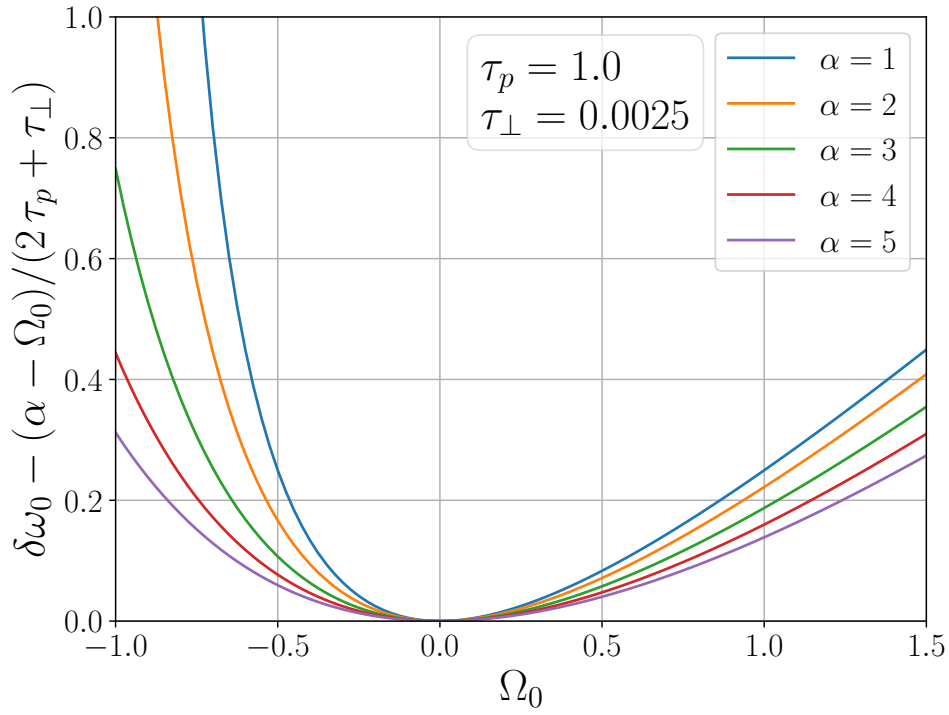
(a) Nonlinear frequency pulling/shift
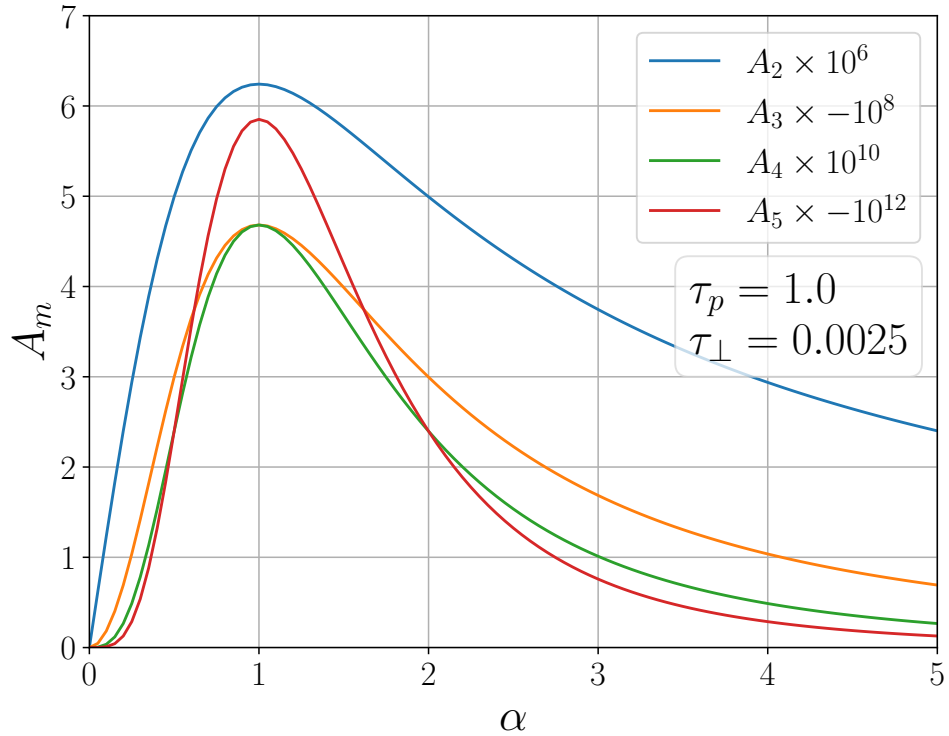
(b) Effective dispersion of nonlinear frequency pulling/shift

Figure 5.24: Nonlinear frequency pulling/shift for the case where $\tau_p/\tau_o = 1$ and $\tau_\perp/\tau_o = 2.5 \times 10^{-3}$. (a) Plot of $\delta\omega_0$ — given by Eq. (5.125) — relative to its linear contribution $(\alpha - \Omega_0)/2\,\tau_p$ as a function of Ω_0. (b) Plot of the corresponding effective dispersion coefficients given by Eq. (5.127) as a function of α.

Chapter 6

One-dimensional Single-Mode Laser Dynamics

In this chapter, we describe the dynamics of one-dimensional laser amplifiers and oscillators by applying the quasi-normal mode expansions derived in Section 4.3 to the wave equation given by Eq. (2.83) and the density matrix evolution equations defined by Eq. (3.35a) and Eq. (3.38). Under the right experimental conditions, these single-mode representations (approximate as they are) can provide remarkably illuminating descriptions of laser behavior, including optimum output coupling, frequency pulling, wave mixing, and mode-locking.

6.1   Laser Amplifiers: Model of One-Dimensional Pulse Propagation

Suppose that we have a laser pulse propagating along the positive z-axis and interacting with a laser amplifier extending from $z = 0$ to $z = 1$. As always, we'll begin with the Optical Maxwell-Bloch Equations given by Eq. (3.46). Let's make some assumptions to simplify these complicated nonlinear coupled equations in this particular case:

1. Since the pulse is traveling in the positive z direction, $E^-(z,t) = 0$ and we can take $E^+(z,t) \longrightarrow E(z,t)$.

2. As in the case of the continuous-wave amplifier treated in Section 5.1, there's a common factor of e^{ik_0z} in both the electric field and the macroscopic polarization, so we can drop it and (e.g.) $\tilde{E}(z,t) \longrightarrow E(z,t)$.

3. We'll neglect both absorption and dispersion, so $D_l(\omega_0) = 0$ and $\alpha(\omega_0) = 0$.

4. Let's assume that $\tau_\perp \longrightarrow 0$, so that we can make the Rate Equation Approximation and set $\partial \tilde{F}(z,t)/\partial t = 0$. Then the macroscopic polarization is given by

$$F(z,t) = \frac{1}{2}\frac{1 + i\Omega}{1 + \Omega^2} G(z,t)\,E(z,t)\,. \tag{6.1}$$

5. We're interested in the problem where the amplifier is pumped into the upper laser level and therefore prepared for the input pulse. This means that the upper laser level has a very long lifetime $\tau_\parallel$ compared to the duration of the laser pulse that we're modeling. Then the first term in the brackets of the gain evolution equation — which corresponds to depopulation due to spontaneous emission — can be ignored. Also, since the pump is no longer active when the pulse arrives at the amplifier, we can neglect the second term as well. Therefore, we retain only the third (nonlinear) term, and we apply the boundary condition: $G(z,-\infty) = G_0(z)$.

6. Finally, we assume that the temporal profile of the input pulse is known, providing the boundary condition $E_0(t) \equiv E(0, t)$.

Under these assumptions, our governing equations become

$$\left(\frac{\partial}{\partial t} + \frac{\partial}{\partial z} \right) E(z, t) = \frac{1}{2} \frac{1 + i\,\Omega}{1 + \Omega^2} G(z, t)\, E(z, t)\,, \text{ and} \tag{6.2a}$$

$$\frac{\partial}{\partial t} G(z, t) = -\frac{1}{\tau_\parallel (1 + \Omega^2)} |E(z, t)|^2 G(z, t)\,. \tag{6.2b}$$

Let's decouple the field intensity from the phase by defining $E(z, t) \equiv \sqrt{I(z, t)}\, e^{i\,\phi(z,t)}$. Then

$$\left(\frac{\partial}{\partial t} + \frac{\partial}{\partial z} \right) I(z, t) = \frac{G(z, t)}{1 + \Omega^2} I(z, t)\,, \tag{6.3a}$$

$$\frac{\partial}{\partial t} G(z, t) = -\frac{I(z, t)}{\tau_\parallel (1 + \Omega^2)} G(z, t)\,, \text{ and} \tag{6.3b}$$

$$\left(\frac{\partial}{\partial t} + \frac{\partial}{\partial z} \right) \phi(z, t) = \frac{\Omega}{2} \left(\frac{\partial}{\partial t} + \frac{\partial}{\partial z} \right) \ln\left[I(z, t) \right]\,. \tag{6.3c}$$

We'll focus on the first two partial differential equations first. We begin by rescaling the intensity and gain to hide the dependence on the detuning Ω:

$$I'(z, t) \equiv \frac{I(z, t)}{\tau_\parallel (1 + \Omega^2)}\,, \text{ and} \tag{6.4a}$$

$$G'(z, t) \equiv \frac{G(z, t)}{1 + \Omega^2}\,. \tag{6.4b}$$

Then we substitute these expressions into Eq. (6.3a) and Eq. (6.3a) to obtain (after temporarily dropping the primes for simplicity) [28]

$$\left(\frac{\partial}{\partial t} + \frac{\partial}{\partial z} \right) I(z, t) = G(z, t)\, I(z, t)\,, \text{ and} \tag{6.5a}$$

$$\frac{\partial}{\partial t} G(z, t) = -I(z, t)\, G(z, t)\,. \tag{6.5b}$$

Next, let us change variables to a coordinate system that follows the forward-propagating field as it travels through the amplifier. We choose $z = \zeta$ and $t = \tau + \zeta$, or

$$\zeta \equiv z\,, \text{ and} \tag{6.6a}$$

$$\tau \equiv t - z\,, \tag{6.6b}$$

where τ is often called the "retarded time." Then

$$\frac{\partial}{\partial z} I(z, t) = \frac{\partial \zeta}{\partial z} \frac{\partial}{\partial \zeta} I(\zeta, \tau) + \frac{\partial \tau}{\partial z} \frac{\partial}{\partial \tau} I(\zeta, \tau) = \left(\frac{\partial}{\partial \zeta} - \frac{\partial}{\partial \tau} \right) I(\zeta, \tau)\,, \tag{6.7a}$$

$$\frac{\partial}{\partial t} I(z, t) = \frac{\partial \zeta}{\partial t} \frac{\partial}{\partial \zeta} I(\zeta, \tau) + \frac{\partial \tau}{\partial t} \frac{\partial}{\partial \tau} I(\zeta, \tau) = \frac{\partial}{\partial \tau} I(\zeta, \tau)\,, \tag{6.7b}$$

and we have

$$\frac{\partial}{\partial \zeta} I(\zeta, \tau) = G(\zeta, \tau)\, I(\zeta, \tau)\,, \text{ and} \tag{6.8a}$$

$$\frac{\partial}{\partial \tau} G(\zeta, \tau) = -I(\zeta, \tau)\, G(\zeta, \tau)\,. \tag{6.8b}$$

These equations seem quite simple now, but we have some work to do to reach general analytic solutions. First, we solve Eq. (6.8a) for $G(\zeta, \tau)$, and substitute the result in Eq. (6.8b) to obtain

$$\frac{\partial}{\partial \tau} \left[\frac{1}{I(\zeta, \tau)} \frac{\partial}{\partial \zeta} I(\zeta, \tau) \right] = -\frac{\partial}{\partial \zeta} I(\zeta, \tau) \text{, or} \tag{6.9}$$

$$\frac{\partial}{\partial \zeta} \left[\frac{\partial}{\partial \tau} \ln I(\zeta, \tau) + I(\zeta, \tau) \right] = 0 . \tag{6.10}$$

Therefore,

$$\frac{\partial}{\partial \tau} \ln I(\zeta, \tau) + I(\zeta, \tau) = f(\tau) , \tag{6.11}$$

where f is an unknown function. Now, let $I(\zeta, \tau) \equiv 1/a(\zeta, \tau)$; then

$$\frac{\partial}{\partial \tau} a(\zeta, \tau) + f(\tau) a(\zeta, \tau) = 1 . \tag{6.12}$$

Multiplying both sides of this equation by $\exp\left[\int d\tau\, f(\tau) \right]$, we find

$$\frac{\partial}{\partial \tau} \left[e^{\int d\tau\, f(\tau)} a(\zeta, \tau) \right] = e^{\int d\tau\, f(\tau)} , \tag{6.13}$$

which has the solution

$$e^{\int d\tau\, f(\tau)} a(\zeta, \tau) = \int d\tau\, e^{\int d\tau'\, f(\tau')} + g(\zeta) , \tag{6.14}$$

where g is *another* unknown function. The corresponding solution for $I(\zeta, \tau)$ is

$$I(\zeta, \tau) = \frac{e^{\int d\tau\, f(\tau)}}{\int d\tau\, e^{\int d\tau'\, f(\tau')} + g(\zeta)} . \tag{6.15}$$

Let's replace the function f with its exponential integral, defining $dh(\tau)/d\tau \equiv \exp[\int d\tau\, f(\tau)]$, and transforming back into our original coordinate system. Then we have

$$I(z, t) = \frac{\frac{\partial}{\partial t} h(t - z)}{h(t - z) + g(z)} . \tag{6.16}$$

To determine $h(\tau)$, we recall that the input pulse provides the boundary condition $I(0, t) \equiv I_0(t)$, so that

$$I_0(t) = \frac{\frac{d}{dt} h(t)}{h(t) + g(0)} = \frac{d}{dt} \left[h(t) + g(0) \right] . \tag{6.17}$$

We assume that $h(t) \longrightarrow 0$ as $t \longrightarrow -\infty$, and we integrate this expression to find

$$h(t) = g(0) \left[e^{J(t)} - 1 \right] , \tag{6.18}$$

where the integrated input fluence is

$$J(t) \equiv \int_{-\infty}^{t} dt'\, I_0(t') . \tag{6.19}$$

Substituting this result into Eq. (6.16), we have an intermediate expression for $I(z, t)$:

$$I(z, t) = \frac{I_0(t - z)}{1 + b(z)\, e^{-J(t-z)}} , \tag{6.20}$$

where $b(z) \equiv g(z)/g(0) - 1$.

Returning to Eq. (6.8), we use Eq. (6.16) to find (in retarded coordinates)

$$G(\zeta, \tau) = -\frac{e^{-J(\tau)}}{1 + b(\zeta)\, e^{-J(\tau)}} \frac{d}{d\zeta} b(\zeta) = -\frac{d}{d\zeta} \ln\left[1 + b(\zeta)\, e^{-J(\tau)}\right]. \tag{6.21}$$

Recall that $G(z, -\infty) = G_0(z)$. Then, since $b(0) = 0$,

$$b(z) = \frac{1}{H(z)} - 1\,, \tag{6.22}$$

where $H(z)$ is the exponential integrated unsaturated single-pass gain given by

$$H(z) \equiv \exp\left[\int_0^z dz'\, G_0\left(z'\right)\right]. \tag{6.23}$$

Collecting results, and restoring the values of the primed variables according to Eq. (6.4), the intensity and population difference are given in general by

$$I(z,t) = \frac{I_0(t - z)}{1 - [1 - 1/H_0(z)]e^{-J(t-z)/(1+\Omega^2)}}\,, \text{ and} \tag{6.24a}$$

$$G(z,t) = \frac{G_0(z)}{1 + \left[e^{J(t-z)/(1+\Omega^2)} - 1\right] H_0(z)}\,, \tag{6.24b}$$

where now

$$J(t) \equiv \int_{-\infty}^t \frac{dt'}{\tau_\parallel} I_0\left(t'\right)\,, \text{ and} \tag{6.25a}$$

$$H_0(z) \equiv \exp\left[\frac{1}{1+\Omega^2} \int_0^z dz'\, G_0\left(z'\right)\right]. \tag{6.25b}$$

Now we can easily calculate the total output fluence

$$J_1 \equiv \int_{-\infty}^{\infty} \frac{dt}{\tau_\parallel} I(1,t) = \int_{-\infty}^{\infty} \frac{dt}{\tau_\parallel} \frac{I_0(t)}{1 - [1 - 1/\overline{H}_0]e^{-J(t)/(1+\Omega^2)}}\,, \tag{6.26}$$

where

$$\overline{H}_0 \equiv H_0(1) = \exp\left(\frac{1}{1+\Omega^2} \overline{G}_0\right), \tag{6.27}$$

and

$$\overline{G}_0 \equiv \int_0^1 dz\, G_0(z)\,. \tag{6.28}$$

Changing the integration variable to $u = 1 - (1 - 1/H_0)e^{-J(t)/(1+\Omega^2)}$, since $u < 1$ we quickly find

$$\begin{aligned}
J_1 &= \left(1 + \Omega^2\right) \int_{u(-\infty)}^{u(\infty)} \frac{du}{u\,(1 - u)} \\
&= \left(1 + \Omega^2\right) \ln\left[\frac{u(\infty)}{u(-\infty)} \frac{1 - u(-\infty)}{1 - u(\infty)}\right] \\
&= \left(1 + \Omega^2\right) \ln\left\{1 + \left[e^{J_0/(1+\Omega^2)} - 1\right] \overline{H}_0\right\},
\end{aligned} \tag{6.29}$$

where $J_0 \equiv J(\infty)$ is the total input fluence. Therefore, the effective net gain is given by

$$G_{\text{eff}} \equiv \frac{J_1}{J_0} = \frac{1 + \Omega^2}{J_0} \ln\left\{1 + \left[e^{J_0/(1+\Omega^2)} - 1\right] \overline{H}_0\right\}. \tag{6.30}$$

Similarly, we can compute the efficiency η_{ext} with which the energy stored in the amplifier has been extracted by the input pulse. The energy added to the input pulse is $J_1 - J_0$, and the energy originally

stored in the amplifier is proportional to $\overline{G}_0$. In fact, because of the choices we've made when scaling the variables, a calculation similar to that of G_{eff} shows that the extraction efficiency is exactly the ratio of these two quantities:

$$\eta_{\text{ext}} = \frac{\overline{G}_0 - \int_0^1 dz\, G(z, \infty)}{\overline{G}_0} = \frac{J_1 - J_0}{\overline{G}_0} . \tag{6.31}$$

Note that both G_{eff} and η_{ext} do not depend on either the temporal profile of the input pulse $I_0(t)$ or the spatial dependence of the initial population inversion $G_0(z)$. If $J_0/(1 + \Omega^2) \ll 1$, then

$$G_{\text{eff}} \longrightarrow \overline{H}_0 \quad \text{and} \quad \eta_{\text{ext}} \longrightarrow \frac{\overline{H}_0 - 1}{\overline{G}_0} J_0 ; \tag{6.32}$$

on the other hand, if $J_0/(1 + \Omega^2) \gg 1$, then

$$J_1 \longrightarrow J_0 + \overline{G}_0 \quad \text{and} \quad \eta_{\text{ext}} \longrightarrow 1 - \frac{1 + \Omega^2}{\overline{G}_0} \left(1 - \frac{1}{\overline{H}_0}\right) e^{-J_0/(1+\Omega^2)} . \tag{6.33}$$

In other words, for weak input fields the gain is exponential in the stored energy, and the efficiency is proportional to the input fluence. When the input fluence is very large, the pulse extracts the energy stored in the amplifier very efficiently and simply adds it to the input.

In Fig. 6.1a, we show a rectangular input pulse with a duration $\tau_p = 1$ and a total fluence $J_0 = 1$ incident on an amplifier with a length $L = 1$ and a stored initial gain $G_0 = 1.5$. The output pulse and the profile of the remaining gain are shown in Fig. 6.1b. The output pulse has a fluence of $J_1 = 2.2$ and has extracted 78% of the energy stored in the amplifier, but the pulse shape is severely distorted. By contrast, in Fig. 6.2a, we show a gaussian input pulse with a duration (at the $1/e^2$ points) $\tau_p = 1$ and a total fluence $J_0 = 1$ incident on the same amplifier. The output pulse and the profile of the remaining gain are shown in Fig. 6.2b. The output fluence and the stored energy extraction efficiency are identical to the case of the rectangular pulse, because Eq. (6.30) and Eq. (6.31) show that these quantities depend only on the total input fluence J_0 and the initial stored energy $\overline{G}_0$. Note also in Fig. 6.3 that the distortion of the output pulse is significantly reduced for the gaussian input profile relative to the case of the rectangular input pulse shape. Finally, we see from Eq. (6.24b) that $G(z, \infty)$ depends only on J_0 and not $I_0(t)$, so it should not be surprising that Fig. 6.4 shows that the final gain distributions in the amplifier are identical for both rectangular and gaussian input pulses.

6.2   Approximate Single-Mode Evolution Equations

We can derive a simple once-dimensional single-mode model of laser oscillators based on the quasi-normal modes developed in Section 4.3 by following an approach similar to that used in Section 5.2 for the case of continuous-wave single-mode lasers. The main differences in the present case are:

1. we replace the constant amplitudes E_0 and F_0 used in Section 5.2 with time-dependent slowly-varying envelope functions $E(t)$ and $F(t)$; and

2. we include the (slowly-varying) time dependence of the population inversion $G(z, t)$.

By following the same steps as in Section 5.2 (and relying on the same integrals), we obtain the approximate evolution equations for single-mode one-dimensional lasers as

$$\dot{E}(t) = \left(-\frac{1}{2\,\tau_\lambda} + i\,\delta\omega_0\right) E(t) + F(t) , \tag{6.34a}$$

$$\dot{F}(t) = -\frac{\mathcal{B}(\Omega)}{\tau_\perp} \left[F(t) - \frac{1}{2}\mathcal{L}(\Omega)\, G(t)\, E(t)\right] , \text{ and} \tag{6.34b}$$

$$\dot{G}(t) = -\frac{1}{\tau_\parallel} \left\{G(t) - \overline{G}_0(t) + 2\tilde{\kappa}\,\text{Re}\left[E^*(t)\,F(t)\right]\right\} , \tag{6.34c}$$
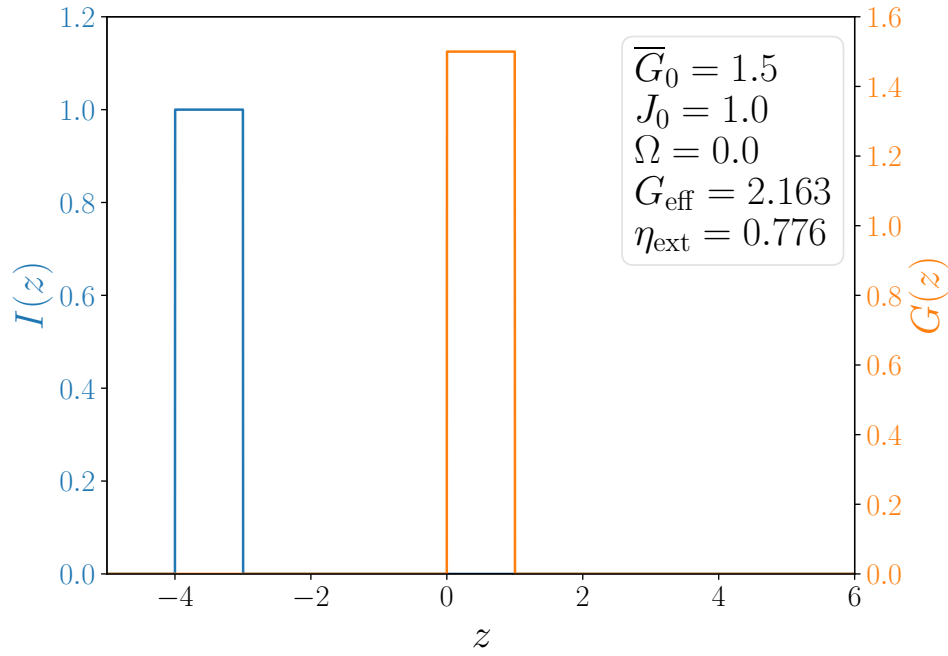
(a) Input pulse and initial gain profiles
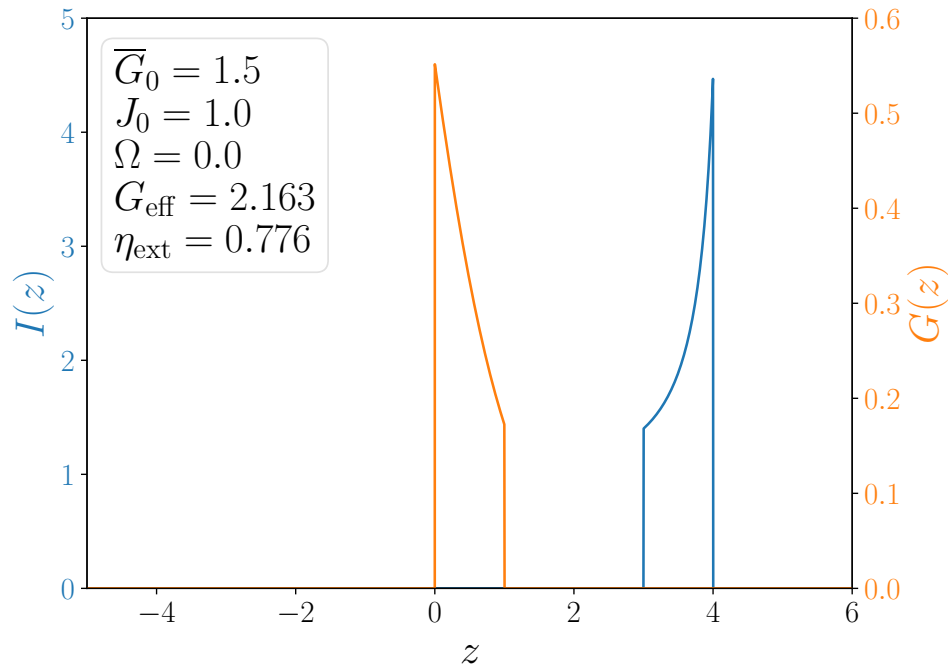
(b) Output pulse and final gain profiles

Figure 6.1: Input and output intensity profiles for a rectangular pulse incident on an amplifier with an initially uniform gain profile.
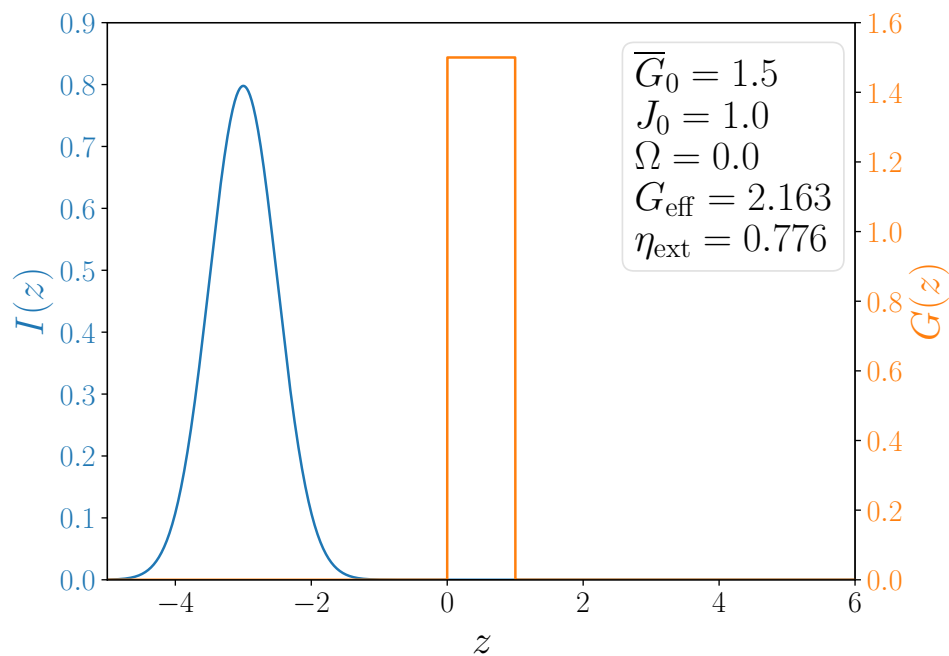
(a) Input pulse and initial gain profiles
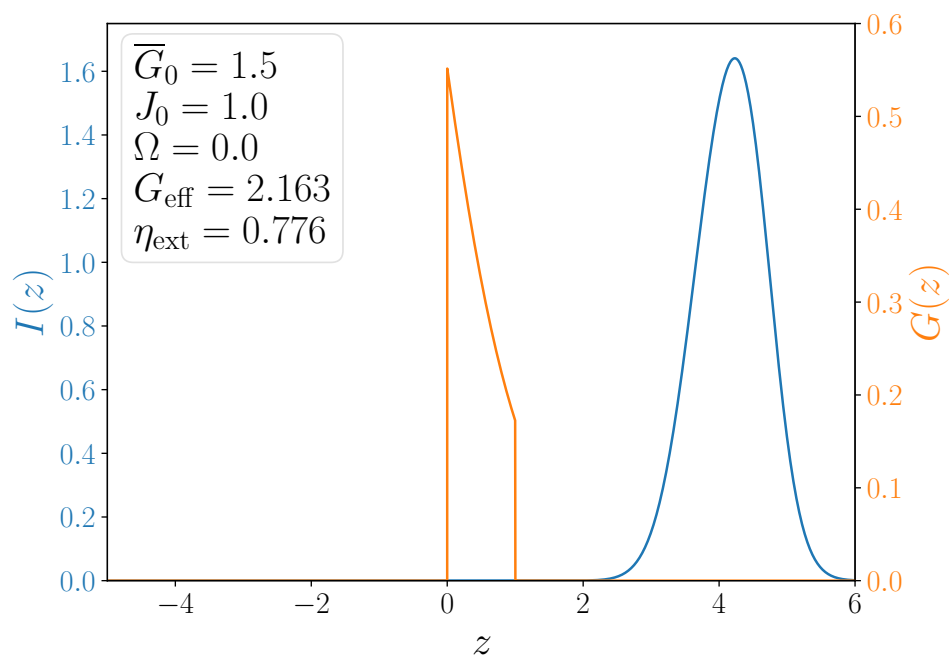
(b) Output pulse and final gain profiles

Figure 6.2: Input and output intensity profiles for a gaussian pulse incident on an amplifier with an initially uniform gain profile.
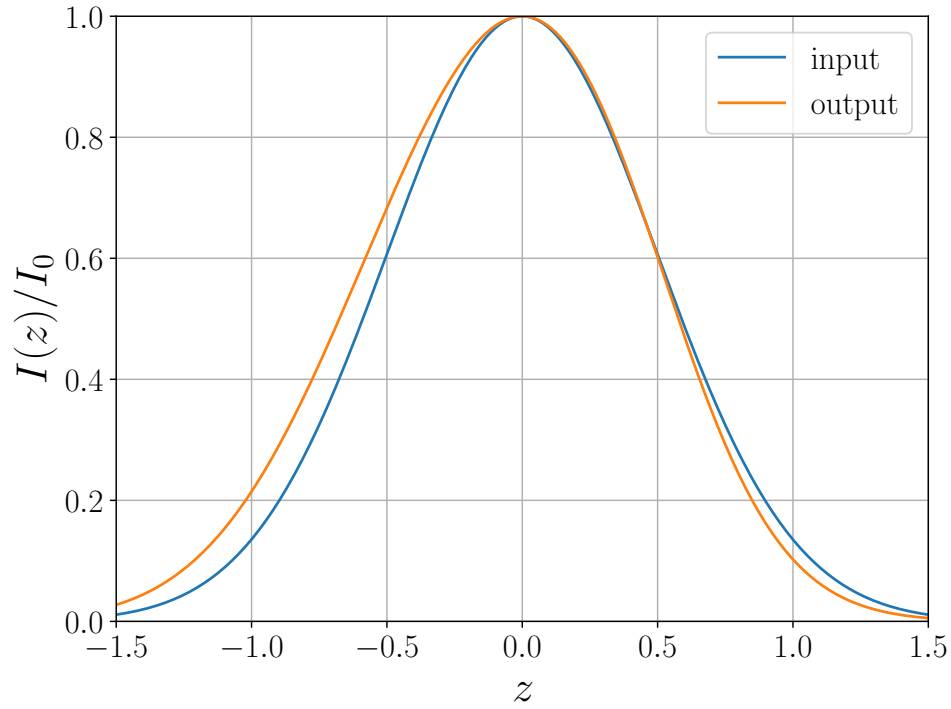
Figure 6.3: A comparison of the input and output pulse profiles shown in Fig. 6.2. The pulse shape distortion is reduced significantly from that of a rectangular pulse.
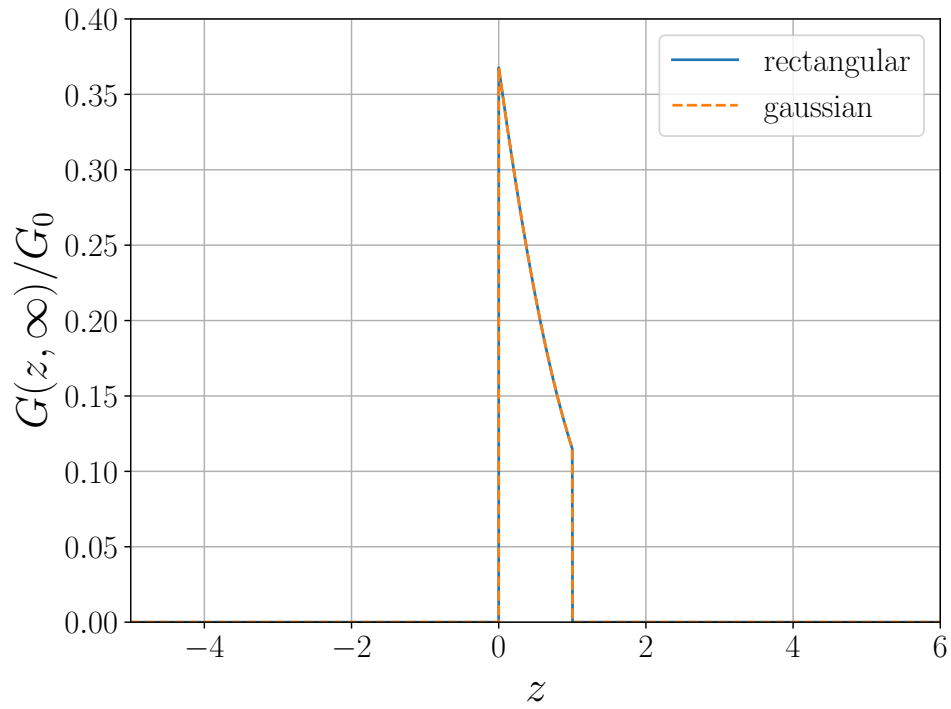
Figure 6.4: A comparison of the final gain profiles shown in Fig. 6.1b and Fig. 6.2b. $G(z, \infty)$ is the same in both cases by Eq. (6.24b).

where now

$$\overline{G}_0(t) \equiv \begin{cases} \int_0^1 dz\, G_0(z,t) & \text{(URL)}, \\ 2 \int_0^{1/2} dz\, G_0(z,t) & \text{(SWL or SHB)}, \end{cases} \tag{6.35}$$

$G(t)$ is the time-dependent generalization of the round-trip gains derived in Section 5.2, and $\widetilde{\kappa}$ is again defined by Eq. (5.41).

6.3 Laser Oscillators: One-Dimensional Single-Mode Dynamical Models

6.3.1 The Rate Equation Approximation

Let's make a few modifications to the approximate evolution equations given by Eq. (6.34) to make the numerical simulations more straightforward. We'll adopt the definitions $\rho(\Omega) \equiv \text{Re}[\mathcal{L}(\Omega)]$ and $\mu(\Omega) \equiv \text{Im}[\mathcal{L}(\Omega)]$ from Section 5.1, express the gain $G(t)$ and the pump $G_0(t)$ in terms of the threshold gain $G_{\text{th}} = 1/\rho(\Omega)\,\tau_\lambda$, and we'll rescale the macroscopic polarization $F(t)$:

$$H(t) \equiv \frac{\overline{G}(t)}{G_{\text{th}}}, \text{ and} \tag{6.36}$$

$$F(t) \longrightarrow \frac{F(t)}{2\,\tau_\lambda}. \tag{6.37}$$

For convenience, we *choose* $2\,\delta\omega_0\,\tau_\lambda = -\mu(\Omega)/\rho(\Omega)$, which is the value we derived for the CW SML. Then our laser evolution equations become

$$\dot{E}(t) = \frac{1}{2\,\tau_\lambda} \left\{ -\left[1 + i\frac{\mu(\Omega)}{\rho(\Omega)} \right] E(t) + F(t) \right\}, \tag{6.38a}$$

$$\dot{F}(t) = \frac{\mathcal{B}(\Omega)}{\tau_\perp} \left\{ -F(t) + \left[1 + i\frac{\mu(\Omega)}{\rho(\Omega)} \right] H(t)\, E(t) \right\}, \text{ and} \tag{6.38b}$$

$$\dot{H}(t) = -\frac{1}{\tau_\parallel} \left\{ H(t) - H_0(t) + \widetilde{\kappa}\,\rho(\Omega)\, \text{Re}\left[E^*(t)\, F(t) \right] \right\}, \tag{6.38c}$$

where $H_0(t) \equiv G_0(t)/G_{\text{th}}$ is the dimensionless scaled pump. If $\mathcal{L}(\Omega)$ is given by Eq. (3.49), then

$$\rho(\Omega) = \frac{\mathcal{A}\,\mathcal{B}}{\mathcal{B}^2 + \Omega^2}, \tag{6.39a}$$

$$\mu(\Omega) = \frac{\mathcal{A}\,\Omega}{\mathcal{B}^2 + \Omega^2}, \tag{6.39b}$$

and $\mu(\Omega)/\rho(\Omega) = \Omega/\mathcal{B}$. Note that implicit in Eq. (6.38) is the spatial dependence of the lowest-order eigenmodes developed in Chapter 4 and used extensively in Chapter 5 to describe single-mode continuous-wave lasers.

Even though Eq. (6.38) are pretty complicated (they're nonlinear ODEs), it's still possible to use them to discover simple properties of lasers. For example, using the third equation, let's calculate the "turn-on time" τ_0 of the laser: if $H(0) = 0$ and $E(0) = 0$, then what value of t_0 satisfies $H(t_0) = 1$? When $t < t_0$, the laser is below threshold and $E(t < t_0) = 0$. In this case,

$$\dot{H}(t) = -\frac{1}{\tau_\parallel} \left[H(t) - H_0(t) \right], \tag{6.40}$$

which has the solution

$$H(t) = H(0)\, e^{-t/\tau_\parallel} + \frac{1}{\tau_\parallel} \int_0^t dt'\, e^{(t'-t)/\tau_\parallel}\, H_0(t'). \tag{6.41}$$

If the pump is constant, so that $H_0(t) \equiv H_0$, then

$$H(t) = H(0) \, e^{-t/\tau_\parallel} + H_0 \left(1 - e^{-t/\tau_\parallel} \right) \tag{6.42}$$

Suppose that $H(0) = 0$, and that $H_0 > 1$. Then $H(t_0) = 1$ for

$$t_0 = \tau_\parallel \, \ln \left(\frac{H_0}{H_0 - 1} \right) . \tag{6.43}$$

In the limit $H_0 \gg 1$, $t_0 \approx \tau_\parallel / H_0$. However, as $H_0 \to 1$, the turn-on time lengthens to $t_0 \approx \tau_\parallel \, \ln[1/(H_0 - 1)]$.

The formal solution to Eq. (6.38b) is given by Eq. (A.28) as

$$F(t) = \left[1 + i \, \frac{\mu(\Omega)}{\rho(\Omega)} \right] \sum_{m=0}^{\infty} \left(-\frac{\tau_\perp}{\mathcal{B}(\Omega)} \right)^m \frac{d^m}{dt^m} \left[H(t) \, E(t) \right] . \tag{6.44}$$

Simply stated, the Rate Equation Approximation (REA) assumes that $\tau_\perp$ is small enough that we can neglect all the terms in the Taylor series with $m > 0$. In this case,

$$F(t) = \left[1 + i \, \frac{\mu(\Omega)}{\rho(\Omega)} \right] H(t) \, E(t) , \tag{6.45}$$

and

$$\dot{E}(t) = \frac{1}{2 \, \tau_\lambda} \left[1 + i \, \frac{\mu(\Omega)}{\rho(\Omega)} \right] [H(t) - 1] \, E(t) , \text{ and} \tag{6.46}$$

$$\dot{H}(t) = \frac{1}{\tau_\parallel} \left\{ H_0(t) - \left[1 + \tilde{\kappa} \, \rho(\Omega) \, |E(t)|^2 \right] H(t) \right\} . \tag{6.47}$$

If the REA is valid, then the difference between the phases of $F(t)$ and $E(t)$ is just the constant value

$$\phi_F - \phi_E = -i \, \ln \left\{ \frac{1 + i \, \mu(\Omega)/\rho(\Omega)}{\sqrt{1 + [\mu(\Omega)/\rho(\Omega)]^2}} \right\} . \tag{6.48}$$

In this case, the phase of $E(t)$ is not interesting, so instead we calculate the derivative of the laser intensity $I(t) \equiv |E(t)|^2$. Then

$$\dot{I}(t) = \frac{1}{\tau_\lambda} \, [H(t) - 1] \, I(t) , \text{ and} \tag{6.49}$$

$$\dot{H}(t) = \frac{1}{\tau_\parallel} \left\{ H_0(t) - \left[1 + \tilde{\kappa} \, \rho(\Omega) \, I(t) \right] H(t) \right\} . \tag{6.50}$$

These simplified equations are the mainstay of almost all laser models in electrical engineering.

6.3.2 Gain-Switched Lasers

6.3.3 Q-Switched Lasers

Chapter 7

One-dimensional Multi-Mode Laser Dynamics

In this chapter, we describe the dynamics of one-dimensional laser amplifiers and oscillators by applying the quasi-normal mode expansions derived in Section 4.3 to the wave equation given by Eq. (2.83) and the density matrix evolution equations defined by Eq. (3.35a) and Eq. (3.38). Under the right experimental conditions, these multimode representations (approximate as they are) can provide remarkably illuminating descriptions of laser behavior, including optimum output coupling, frequency pulling, wave mixing, and mode-locking.

When multiple modes oscillate in a laser, they give rise to coherent modulations of the populations in the nonlinear gain medium that create interactions between those modes. The frequencies of these modulations are integer multiples of the free spectral range $\Delta\omega_{\mathrm{FSR}}$ — defined by Eq. (4.69) — between adjacent intracavity field modes. In Fig. 7.1, we show a plot of a gain medium with a peak at frequency $\omega_0 = \omega_{ab}$ as a function of the frequency detuning. We have superimposed the frequency modal structure — over several free-spectral ranges — of a cavity containing that medium. In the following sections, we will find that for a particular frequency $\Delta\omega_q \equiv 2q\pi$, fluctuations in the gain medium at frequency $2(q-p)\pi$ couple the electric field amplitude with frequency $2p\pi$ to the macroscopic polarization component at frequency $2q\pi$.

7.1   One-Dimensional Multi-Mode Laser Evolution Equations

We begin by developing evolution equations for the complex longitudinal modal amplitudes of unidirectional and standing-wave intracavity laser fields based on the four-level Maxwell-Bloch equations given by Eq. (3.46) and Eq. (3.48). We have

$$\frac{\partial}{\partial t}E^\pm(z,t) \pm \frac{\partial}{\partial z}E^\pm(z,t) = \left[i\,\widehat{\mathcal{D}}_0 - \frac{1}{2}\,\alpha_0\right]E^\pm(z,t) + F^\pm(z,t)\,, \tag{7.1a}$$

$$\frac{\partial}{\partial t}\widetilde{F}(z,t) = -\frac{1}{\tau_\perp}\left[\mathcal{B}\,\widetilde{F}(z,t) - \frac{\mathcal{A}}{2}\,\widetilde{G}(z,t)\widetilde{E}(z,t)\right]\,, \text{ and} \tag{7.1b}$$

$$\frac{\partial}{\partial t}\widetilde{G}(z,t) = -\frac{1}{\tau_\parallel}\left\{\widetilde{G}(z,t) - G_0(z,t) + 2\,\mathrm{Re}\left[\widetilde{E}^*(z,t)\widetilde{F}(z,t)\right]\right\}\,, \tag{7.1c}$$

where $\widehat{\mathcal{D}}_0$ is the differential operator defined by Eq. (3.47a). Here we will defer the effects of frequency dispersion to Section 7.2.2 by setting $\widehat{\mathcal{D}}_0 = 0$ in Eq. (7.1a).

Our goal will be to develop a set of nonlinear ordinary differential equations representing the time evolution of modal amplitudes of the electromagnetic field. Let's follow an approach similar to that used in Section 5.2 and use the results of Section 4.3 to expand $E^\pm(z,t)$ in terms of the quasi-normal modes of the laser resonator. For example, in the case of the one-dimensional unidirectional ring laser shown in Fig. 5.3a, $E^-(z,t) = 0$, and we can write the slowly-varying forward-propagating electric field
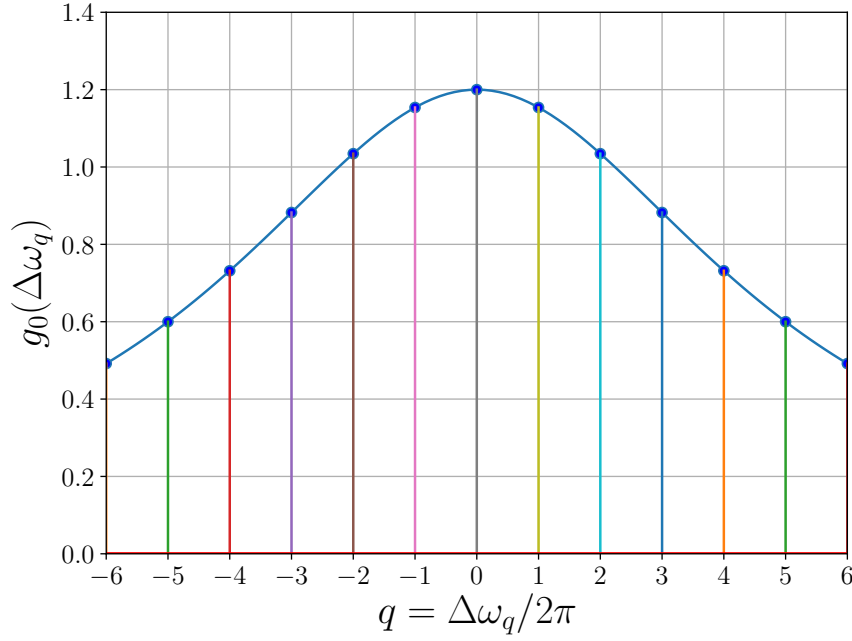
Figure 7.1: Plot of a gain medium with a peak at frequency $\omega_0 = \omega_{ab}$ as a function of the frequency detuning. We have superimposed the frequency modal structure — over several free-spectral ranges — of a cavity containing the medium. We will find that for a particular frequency $\Delta\omega_q \equiv 2q\pi$, fluctuations in the gain medium at frequency $2(q-p)\pi$ couple the electric field amplitude with frequency $2p\pi$ to the macroscopic polarization component at frequency $2q\pi$.

amplitude as

$$E^+(z,t) \equiv \sum_{q=-\infty}^{\infty} u_q(z)\, e^{-i\,\Delta\omega_q t}\, E_q(t)\,, \tag{7.2}$$

where $u_q(z)$ and the corresponding biorthogonal eigenfunction $v_q(z)$ in the range $0 < z < 1$ are given by Eq. (4.83) and Eq. (4.93) as

$$u_q(z) = C_{\text{URL}} \exp\left[+\left(i\,2q\pi + \ln\frac{1}{\sqrt{R}} \right) z \right]\,, \tag{7.3a}$$

$$v_q(z) = C_{\text{URL}}^{-1} \exp\left[-\left(i\,2q\pi + \ln\frac{1}{\sqrt{R}} \right) z \right]\,, \tag{7.3b}$$

C_{URL} is given by Eq. (4.87), and

$$\Delta\omega_q = 2q\pi + \delta\omega_q\,, \tag{7.4}$$

consistent with both Eq. (3.46a) and Eq. (4.106). We apply the biorthogonality relation given by Eq. (4.97) to Eq. (7.1a) by substituting Eq. (7.2) (with $q \rightarrow p$) and a similar expression for $F^+(z,t)$; multiplying both sides through by $e^{+i\,\Delta\omega_q t}\, v_q(z)$; and then integrating the result from $z = 0$ to $z = 1$. We find

$$\dot{E}_q(t) = \left(-\frac{1}{2\tau_\lambda} + i\,\delta\omega_q \right) E_q(t) + F_q(t)\,, \tag{7.5}$$

where $\tau_\lambda \equiv 1/\ln[1/R \exp(-\overline{\alpha}_0)]$ is the photon lifetime given by Eq. (4.54) and $\overline{\alpha}_0 \equiv \int_0^1 dz\, \alpha_0(z)$.

We shouldn't apply the rate-equation approximation (REA) to Eq. (7.1b) just yet, because a laser operating with q_{max} longitudinal modes such that $q_{\text{max}} \Delta\omega_{\text{FSR}} \gtrsim 1/\tau_\perp$ will exhibit a significant dependence of the unsaturated gain on the value of q. Instead, we will first substitute

because we want to keep the macroscopic polarization term $F_q(t)$ general for now. In the unidirectional ring laser case, we define $F_q(t)$ as

For the one-dimensional standing-wave laser shown in Fig. 5.3b, the slowly-varying biorthogonal eigenfunctions are $\mathbf{u}_q(z)$ and $\mathbf{v}_q(z)$, given by Eq. (4.112), Eq. (4.113), Eq. (4.118), and Eq. (4.119), and the corresponding normalization constant C_{SWL} is given by Eq. (4.115). Then

$$\mathbf{u}_q(z) \equiv \begin{bmatrix} u_q^+(z) \\ u_q^-(z) \end{bmatrix} = C_{SWL} \begin{bmatrix} e^{+\left[i\,2q\pi+\ln\left(1/\sqrt{R_1R_2}\right)\right]z} \\ -\frac{1}{\sqrt{R_1}}\,e^{-\left[i\,2q\pi+\ln\left(1/\sqrt{R_1R_2}\right)\right]z} \end{bmatrix}, \text{ and} \tag{7.6a}$$

$$\mathbf{v}_q(z) \equiv \begin{bmatrix} v_q^+(z) \\ v_q^-(z) \end{bmatrix} = C_{SWL}^{-1} \begin{bmatrix} e^{-\left[i\,2q\pi+\ln\left(1/\sqrt{R_1R_2}\right)\right]z} \\ -\sqrt{R_1}\,e^{+\left[i\,2q\pi+\ln\left(1/\sqrt{R_1R_2}\right)\right]z} \end{bmatrix}, \tag{7.6b}$$

where $0 < z < 1/2$ In this case, we apply the biorthogonality relation given by Eq. (4.120) to Eq. (5.1a) by substituting $E^\pm(z) = \sum_p u_p^\pm(z)\,e^{-i\Delta\omega_p t}\,E_p(t)$ and $F^\pm(z) = \sum_p u_p^\pm(z)\,e^{-i\Delta\omega_p t}\,F_p(t)$; forming the inner product of both sides with $e^{i\Delta\omega_q t}\,\mathbf{v}_q(z)$; and then integrating the result from $z = 0$ to $z = 1/2$. Therefore, Eq. (5.24) remains valid for the standing-wave case with $\tau_\lambda \equiv 1/\ln[1/R_1R_2\exp(-\overline{\alpha}_0)]$ and $\overline{\alpha}_0 \equiv 2\int_0^{1/2} dz\,\alpha_0(z)$.

As a general representation of the spatially rapidly-varying fields in both unidirectional ring and standing-wave resonator configurations, we follow Section 4.3.3 and represent the electric field amplitude function as

$$\tilde{E}(z,t) \equiv \sum_{q=-\infty}^{\infty} \tilde{u}_q(z)\,e^{-i\Delta\omega_q t}\,E_q(t). \tag{7.7}$$

In the unidirectional ring laser case,

$$\tilde{u}_q(z) = u_q^+(z)\,e^{+ik_0z}, \text{ and} \tag{7.8a}$$

$$\tilde{v}_q(z) = v_q^+(z)\,e^{-ik_0z}, \tag{7.8b}$$

where k_0 is the propagation constant associated with the carrier frequency ω_0. For a standing-wave resonator,

$$\tilde{u}_q(z) = u_q^+(z)\,e^{+ik_0z} + u_q^-(z)\,e^{-ik_0z}, \text{ and} \tag{7.9a}$$

$$\tilde{v}_q(z) = v_q^+(z)\,e^{-ik_0z} + v_q^-(z)\,e^{+ik_0z}. \tag{7.9b}$$

We use a similar approach to the expansion of the amplitude of the macroscopic polarization.

$$\sum_p \left[\dot{F}_p(t) - i\Delta\omega_p F_p(t)\right]\tilde{u}_p(z)\,e^{-i\Delta\omega_p t}$$

$$= -\frac{1}{\tau_\perp}\sum_p \left[\mathcal{B}F_p(t) - \frac{1}{2}\mathcal{A}\,\tilde{G}(z,t)\,E_p(t)\right]\tilde{u}_p(z)\,e^{-i\Delta\omega_p t}. \tag{7.10}$$

Now, rather than the rate-equation approximation (REA), we will apply the *slowly-varying envelope approximation* (SVEA) to Eq. (7.10) by assuming that $|\dot{F}_p(t)| \ll |\Delta\omega_p F_p(t)|$ and neglecting the terms $\dot{F}_p(t)$ on the left-hand side . This is valid when the time scale for changes in the modal polarization amplitudes $F_p(t)$ is long compared to the polarization relaxation time $\tau_\perp$.

$$\int dz \equiv \begin{cases} \int_0^1 dz & \text{(URL)}, \\ \int_0^{1/2} dz\,\frac{k_0}{2\pi}\int_{z-\pi/k_0}^{z+\pi/k_0} dz' & \text{(SWL or SHB)}, \end{cases} \tag{7.11}$$

$$\sum_p \mathcal{N}_{qp} F_p(t) = \frac{1}{2}\mathcal{L}(\Omega_q)\sum_p e^{i(\Delta\omega_q-\Delta\omega_p)t}\,G_{qp}(t)\,E_p(t), \tag{7.12}$$

$$\sum_p \mathcal{N}_{qp} \left(\mathcal{B} - i\Omega_p \right) F_p(t) = \frac{1}{2} \mathcal{A} \sum_p e^{i(\Delta\omega_q - \Delta\omega_p)t} G_{qp}(t) E_p(t) , \tag{7.13}$$

where $\Omega_p \equiv \Delta\omega_q \tau_\perp$,

$$\mathcal{N}_{qp} \equiv \int dz\, \tilde{v}_q(z)\, \tilde{u}_p(z) \text{ and} \tag{7.14}$$

$$G_{qp}(t) \equiv \int dz\, \tilde{v}_q(z)\, \tilde{u}_p(z)\, \tilde{G}(z,t) . \tag{7.15}$$

Applying Eq. (7.11) to Eq. (7.14), we find that for both unidirectional ring and standing-wave resonators, $\mathcal{N}_{qp} = \delta_{qp}$, and Eq. (7.13) simplifies to

$$F_q(t) = \frac{1}{2} \mathcal{L}(\Omega_q) \sum_p e^{i(\Delta\omega_q - \Delta\omega_p)t} G_{qp}(t) E_p(t) , \tag{7.16}$$

where

$$\mathcal{L}(\Omega_q) \equiv \frac{\mathcal{A}}{\mathcal{B} - i\Omega_q} . \tag{7.17}$$

Let's now determine the evolution equation for $G_{qp}(t)$ by applying Eq. (7.15) and Eq. (7.11) to Eq. (7.1c). Using Eq. (7.7) and the corresponding representation for the macroscopic polarization, the nonlinear term on the right-hand side can be written as

$$2\,\mathrm{Re}\left[\tilde{E}^*(z,t)\, \tilde{F}(z,t) \right] = \tilde{E}^*(z,t)\, \tilde{F}(z,t) + c.c.$$

$$= \sum_{mn} e^{-i(\Delta\omega_m - \Delta\omega_n)t}\, \tilde{u}_m(z)\, \tilde{u}_n^*(z) \left[E_m(t) F_n^*(t) + F_m(t) E_n^*(t) \right] .$$

We obtain

$$\dot{G}_{qp}(t) = -\frac{1}{\tau_\parallel} \left\{ G_{qp}(t) - \overline{G}_{qp}(t) + \sum_{mn} e^{-i(\Delta\omega_m - \Delta\omega_n)t} \kappa_{qpmn} \left[E_m(t) F_n^*(t) + F_m(t) E_n^*(t) \right] \right\} , \tag{7.18}$$

where

$$\overline{G}_{qp}(t) \equiv \int dz\, \tilde{v}_q(z)\, \tilde{u}_p(z)\, G_0(z,t) , \tag{7.19}$$

and

$$\kappa_{qpmn} \equiv \int dz\, \tilde{v}_q(z)\, \tilde{u}_p(z)\, \tilde{u}_m(z)\, \tilde{u}_n^*(z) . \tag{7.20}$$

Let's evaluate $\overline{G}_{qp}(t)$ and κ_{qpmn} for the unidirectional ring resonator. Using Eq. (7.8) and Eq. (7.11), we find

$$\overline{G}_{qp}(t) = \int_0^1 dz\, e^{i\,2(p-q)\,\pi z}\, G_0(z,t) , \tag{7.21}$$

and we see that $\overline{G}_{qp}(t)$ is the complex exponential Fourier series coefficient of order $p - q$ for $G_0(z,t)$ in the resonator. Suppose that $G_0(z,t) = \overline{G}_0(t)/(z_2 - z_1)$ for $0 < z_1 \le z \le z_2 < 1$, and is zero otherwise. In this (common) special case, when $q \ne p$ we have

$$\overline{G}_{qp}(t) = \frac{\overline{G}_0(t)}{z_2 - z_1} \int_{z_1}^{z_2} dz\, e^{i\,2(p-q)\,\pi z} = \frac{\exp[i\,2\,(p-q)\,\pi z_2] - \exp[i\,2\,(p-q)\,\pi z_1]}{i\,2\,(p-q)\,\pi\,(z_2 - z_1)}\, \overline{G}_0(t) , \tag{7.22}$$

and $\overline{G}_{qq}(t) = \overline{G}_0(t)$. Note that when $\{z_1, z_2\} \to \{0,1\}$, $\overline{G}_{qp}(t) \to \delta_{qp}\, \overline{G}_0(t)$. For the URL, the spatial mode coupling coefficient defined by Eq. (7.20) becomes

$$\kappa_{qpmn} = C_{\mathrm{URL}}^2 \int_0^1 dz\, e^{i\,2\,(-q+p+m-n)\,\pi z} = \Delta_{-q+p+m-n}(R) . \tag{7.23}$$

In the case of the standing-wave resonator, we use Eq. (7.9) and Eq. (7.11) to find

$$
\overline{G}_{qp}(t) = \int_0^{1/2} dz \, \mathbf{v}_q(z) \cdot \mathbf{u}_p(z) \, G_0(z,t) = 2 \int_0^{1/2} dz \, \cos\left[2\,(q-p)\,\pi\,z\right] G_0(z,t) \,, \tag{7.24}
$$

showing that $\overline{G}_{qp}(t)$ is the cosine Fourier series coefficient of order $q - p$ for $G_0(z,t)$ in the SWL resonator. As we did above for the URL case, let's suppose that $G_0(z,t) = \overline{G}_0(t)/2(z_2 - z_1)$ for $0 < z_1 \le z \le z_2 < 1/2$, and is zero otherwise. Then for $p \neq q$

$$
\overline{G}_{qp}(t) = \frac{\sin[2\,(q-p)\,\pi\,z_2] - \sin[2\,(q-p)\,\pi\,z_1]}{2\,(q-p)\,\pi\,(z_2 - z_1)} \overline{G}_0(t) \,. \tag{7.25}
$$

When $\{z_1, z_2\} \longrightarrow \{0, 1/2\}$, $\overline{G}_{qp}(t) \longrightarrow \delta_{qp}\overline{G}_0(t)$. For the SWL, the spatial mode coupling coefficient defined by Eq. (7.20) becomes

$$
\begin{aligned}
\kappa_{qpmn} &= \int_0^{1/2} dz \, \frac{k_0}{2\pi} \int_{z-\pi/k_0}^{z+\pi/k_0} dz' \, \tilde{v}_q(z') \, \tilde{u}_p(z') \, \tilde{u}_m(z') \, \tilde{u}_n^*(z') \\
&= \int_0^{1/2} dz \, \Big\{ \big[v_q^+(z) \, u_p^+(z) \, u_m^+(z) \, u_n^{+*}(z) + v_q^-(z) \, u_p^-(z) \, u_m^-(z) \, u_n^{-*}(z) \big] \\
&\qquad\qquad + \big[v_q^+(z) \, u_p^+(z) \, u_m^-(z) \, u_n^{-*}(z) + v_q^-(z) \, u_p^-(z) \, u_m^+(z) \, u_n^{+*}(z) \big] \\
&\qquad\qquad + \big[v_q^+(z) \, u_p^-(z) \, u_m^+(z) \, u_n^{-*}(z) + v_q^-(z) \, u_p^+(z) \, u_m^-(z) \, u_n^{+*}(z) \big] \Big\} \\
&= C_{\mathrm{SWL}}^2 \int_0^{1/2} dz \, \Big\{ \Big[e^{[i\,2(-q+p+m-n)\pi z + \ln(1/R_1R_2)]z} + \frac{1}{R_1} e^{-[i\,2(-q+p+m-n)\pi z + \ln(1/R_1R_2)]z} \Big] \\
&\qquad\qquad + \Big[e^{[i\,2(q-p+m-n)\pi z + \ln(1/R_1R_2)]z} + \frac{1}{R_1} e^{-[i\,2(q-p+m-n)\pi z + \ln(1/R_1R_2)]z} \Big] \\
&\qquad\qquad + \Big[e^{[i\,2(q+p-m-n)\pi z + \ln(1/R_1R_2)]z} + \frac{1}{R_1} e^{-[i\,2(q+p-m-n)\pi z + \ln(1/R_1R_2)]z} \Big] \Big\} \,,
\end{aligned}
$$

or

$$
\kappa_{qpmn} = \Delta'_{-q+p+m-n}\,(R_1\,R_2) + \Delta'_{q-p+m-n}\,(R_1\,R_2) + \Delta'_{q+p-m-n}\,(R_1\,R_2) \,, \tag{7.26}
$$

where $\Delta'_q\,(R_1\,R_2)$ is defined by Eq. (4.117). The first term on the right of this equation couples co-propagating spatial modes (and is identical to the URL coupling term given by Eq. (7.23) when $R_2 = 1$), the second term couples counter-propagating spatial modes neglecting interference, and the third term couples modes incorporating spatial interference.

In the next two sections, we use these multimode evolution equations to study the dynamics of *injection-seeded gain-switched* and *passively mode-locked* lasers. In Section 7.3, we will apply the *strong* rate-equation approximation (REA) to construct a non-perturbative theory of a high-intensity pulsed laser that is driven by a short-duration pump and "primed" by a slowly-varying input field. In Section 7.4, we will relax the REA to allow rapid intermodal interactions and build a weak-field perturbative model of *coherent population pulsations*[29] that lead to passive *mode-locking* in either the time or the frequency domain.

7.2 Frequency Shifts in One-Dimensional Multimode Lasers

7.2.1 Frequency Pulling

As an example of a particular choice of $\delta\omega_q$, we will attempt to capture the bulk of the final frequency-pulling effects we expect in a multimode laser by applying the approximate single-longitudinal-mode laser theory developed in Section 5.2. We define the complex amplitude $E_q(t)$ in terms of a real amplitude $A_q(t)$ and a real phase $\phi_q(t)$ as

$$
E_q(t) \equiv A_q(t) \, e^{-i\,\phi_q(t)} \,. \tag{7.27}
$$

Following Section 5.2, we assume that $\dot{A}_q(t) = 0$ and $\dot{\phi}_q(t) = 0$, so that application of Eq. (7.5) gives

$$\delta\omega_q = -\frac{1}{2\,\tau_p}\frac{\mathrm{Im}[f_q]}{\mathrm{Re}[f_q]}. \tag{7.28}$$

where $f_q(t) \equiv e^{i\,\phi_q(t)}F_q(t)$. In Section 5.2, we found that $\mathrm{Im}[f_0]/\mathrm{Re}[f_0] = \mathrm{Im}[\mathcal{L}_0]/\mathrm{Re}[\mathcal{L}_0]$, where $\mathcal{L}_0$ is the lineshape function, and we assume that this condition is approximately valid in the multimode case. That is,

$$\frac{\mathrm{Im}[f_q]}{\mathrm{Re}[f_q]} \approx \frac{\mathrm{Im}[\mathcal{L}_q]}{\mathrm{Re}[\mathcal{L}_q]} = \Omega_q\,, \tag{7.29}$$

where in the Lorentzian case

$$\mathcal{L}_q \equiv \frac{1}{1 - i\,\Omega_q}\,. \tag{7.30}$$

Therefore, choosing $\delta\omega_q \equiv -\Omega_q/2\,\tau_p$ should give $\dot{\phi}_q(t) \approx 0$ when $\dot{A}_q(t) = 0$. If we assume that $\omega_0 = \omega_{ab}$, then

$$\Omega_q = \Delta\omega_q\,\tau_\perp = \left(2q\pi + \delta\omega_q\right)\tau_\perp\,, \tag{7.31}$$

and we can solve for $\delta\omega_q$ to obtain

$$\delta\omega_q = -\frac{\tau_\perp}{2\,\tau_p}\frac{2q\pi}{1 + \tau_\perp/2\,\tau_p}\,, \quad\text{and} \tag{7.32a}$$

$$\Delta\omega_q = \frac{2q\pi}{1 + \tau_\perp/2\,\tau_p}\,. \tag{7.32b}$$

Finally, substituting $\delta\omega_q = -\Omega_q/2\,\tau_p$ into Eq. (7.5) and simplifying, we find

$$\dot{E}_q(t) = -\frac{1}{2\tau_p}\left(1 + i\,\Omega_q\right)E_q(t) + F_q(t). \tag{7.33}$$

7.2.2 Dispersion

In Section 3.3, we derived the normalized wave equation in the time domain given by Eq. (3.46a) for a particular transverse mode of the electromagnetic field. Our goal here is to update Eq. (7.5) to include the effects of dispersion. The relevant term in Eq. (3.46a) is

$$i\sum_{l=2}^{\infty}\frac{D_l(\omega_0)}{l!}\left(i\frac{\partial}{\partial t}\right)^l E^{\pm}(z,t)\,,$$

where $D_l(\omega_0)$ is given by Eq. (3.47b). Let's consider the unidirectional case — the result for the standing-wave laser will be the same — and use the one-dimensional single-mode expansion of the slowly-varying complex field envelope function given by Eq. (4.108). We find

$$\begin{aligned}
i\sum_{l=2}^{\infty}\frac{D_l(\omega_0)}{l!}\left(i\frac{\partial}{\partial t}\right)^l E(z,t) &= i\sum_{l=2}^{\infty}\frac{D_l(\omega_0)}{l!}\left(i\frac{\partial}{\partial t}\right)^l \sum_p u_p(z)\,e^{-i\Delta\omega_p t}\,E_p(t) \\
&= i\sum_{lp} i^l\frac{D_l(\omega_0)}{l!}\,u_p(z)\,e^{-i\Delta\omega_p t}\sum_{j=0}^{l}\binom{l}{j}(-i\Delta\omega_p)^j\frac{\partial^{l-j}}{\partial t^{l-j}}E_p(t)\,.
\end{aligned} \tag{7.34}$$

If we keep only those terms proportional to $E_p(t)$ and $\dot{E}_p(t)$, then

$$\sum_{j=0}^{l}\binom{l}{j}(-i\Delta\omega_p)^j\frac{\partial^{l-j}}{\partial t^{l-j}}E_p(t) \approx (-i\Delta\omega_p)^l E_p(t) + l\,(-i\Delta\omega_p)^{l-1}\dot{E}_p(t)\,,$$

and then

$$i \sum_{l=2}^{\infty} \frac{D_l(\omega_0)}{l!} \left(i \frac{\partial}{\partial t} \right)^l E(z,t) = i \sum_p u_p(z) e^{-i \Delta \omega_p t} \left[\delta D_p(\omega_0) E_p(t) + i \delta \tau_p(\omega_0) \dot{E}_p(t) \right] , \qquad (7.35)$$

where

$$\delta D_p(\omega_0) \equiv \sum_{l=2}^{\infty} \frac{(2p\pi)^l}{l!} D_l(\omega_0) , \qquad (7.36a)$$

$$\delta \tau_p(\omega_0) \equiv \sum_{l=2}^{\infty} \frac{(2p\pi)^{l-1}}{(l-1)!} D_l(\omega_0) , \qquad (7.36b)$$

and we've used Eq. (7.4) to make the approximation $\Delta \omega_p \approx 2p\pi$.

We follow the approach we used to derive Eq. (7.5), and multiply both sides of Eq. (7.35) by $v_q(z)$ and then integrate the result over the cavity length. Collecting the resulting dispersion terms allow us to obtain the updated field coefficient equation of motion

$$\dot{E}_q(t) = \frac{1}{1 + \delta \tau_q(\omega_0)} \left\{ \left[-\frac{1}{2 \tau_p} \left(1 + i \Omega_q \right) + i \delta D_q(\omega_0) \right] E_q(t) + F_q(t) \right\} , \qquad (7.37)$$

where $F_q(t)$ is again given by Eq. (7.16). We see two primary effects of dispersion. First, there is an additional frequency shift for each mode that increases (in magnitude) nonlinearly with mode number q. Second, the group round-trip time is slightly different for each mode, changing with q by a factor of $1 + \delta \tau_q(\omega_0)$.

7.3 Injection-Seeded Gain-Switched Lasers

We consider the ideal four-level laser dynamical equations developed in Section 3.3, and we assume that $\gamma_\perp \longrightarrow \infty$, so that $\Omega = 0$. The formal integral of Eq. (3.48) becomes

$$\tilde{F}(z,t) = \frac{\gamma_\perp}{2} e^{-\gamma_\perp t} \int_{-\infty}^{t} dt' e^{\gamma_\perp t'} \tilde{G}(z,t') \tilde{E}(z,t') . \qquad (7.38)$$

We now apply the strong REA in the same limit, and assume that $|\partial \tilde{E}(z,t)/\partial t| \ll \gamma_\perp |\tilde{E}(z,t)|$, and $|\partial \tilde{G}(z,t)/\partial t| \ll \gamma_\perp |\tilde{G}(z,t)|$. In this case, both $\tilde{E}(z,t')$ and $\tilde{G}(z,t')$ can be moved outside of the integral, yielding

$$\tilde{F}(z,t) = \frac{1}{2} \tilde{G}(z,t) \tilde{E}(z,t) . \qquad (7.39)$$

Substituting this result into Eq. (3.46c) gives

$$\frac{\partial}{\partial t} \tilde{G}(z,t) = \frac{1}{\tau_{\parallel}} \left[\overline{G}(z,t) - \tilde{G}(z,t) - \tilde{G}(z,t) \left| \tilde{E}(z,t) \right|^2 \right] , \qquad (7.40)$$

Let's allow the intracavity field to be supplemented by a quantity $\tilde{J}(z,t)$ arising from a very weak input $F_1(t)$ injected through the output coupler mirror $\mathcal{M}_1$, as shown in Fig. 4.5. This additional field will contribute to the total macroscopic polarization, so that

$$\tilde{F}(z,t) = \frac{1}{2} \tilde{G}(z,t) \left[\tilde{E}(z,t) + \tilde{J}(z,t) \right] . \qquad (7.41)$$

In Section 4.4, we learned how to expand $\tilde{J}(z,t)$ as a series of quasi-normal spatial modes in both the unidirectional ring and standing-wave resonator cases. Because the injected field is so weak, we do not need to include it in the saturation term in Eq. (7.40).

7.3.1 Unidirectional Ring Lasers

As discussed in the introduction to Chapter 7, in the case of the URL the rapidly-varying spatial function $\exp(+ik_0 z)$ is common to both $\widetilde{E}(z,t)$ and $\widehat{F}(z,t)$, and can therefore be ignored in Eq. (7.39) and Eq. (7.40). Therefore, we find $F_q(t)$ in Eq. (7.5) by substituting Eq. (??) — and the corresponding expression for $J(z,t)$ — into Eq. (7.41), and then the result into Eq. (??). We obtain

$$F_q(t) = \frac{1}{2} \sum_p e^{i2(q-p)\pi t} G_{q-p}(t) \left[E_p(t) + J_p(t) \right],\tag{7.42}$$

where

$$G_{q-p}(t) \equiv \int_0^1 dz\, v_q(z)\, u_p(z)\, G(z,t) = \int_0^1 dz\, e^{-i2(q-p)\pi z}\, G(z,t),\tag{7.43}$$

and $J_p(t)$ is given by Eq. (4.138). Equation (7.42) and the slowly-spatially-varying partial differential equation

$$\frac{\partial}{\partial t} G(z,t) = \frac{1}{\tau_\parallel} \left[\overline{G}(z,t) - G(z,t) - G(z,t)\, |E(z,t)|^2 \right]\tag{7.44}$$

are the only tools we'll need to solve numerically a wide variety of gain-switched URL problems.

7.3.2 Standing-Wave Lasers

The calculation of the macroscopic polarization for a multimode standing-wave laser requires that we pay attention to the interference between the counterpropagating fields. We'll follow a strategy similar to that of the continuous-wave case described in Section 5.4. We begin with an explicit expression for the spatially rapidly-varying polarization of Eq. (7.41), written as

$$F^+(z,t)\, e^{+ik_0 z} + F^-(z,t)\, e^{-ik_0 z} =$$
$$\frac{1}{2}\, \widetilde{G}(z,t) \left\{ \left[E^+(z,t) + J^+(z,t) \right] e^{+ik_0 z} + \left[E^-(z,t) + J^-(z,t) \right] e^{-ik_0 z} \right\}.\tag{7.45}$$

The envelope functions $F^\pm(z,t)$, $E^\pm(z,t)$, and $J^\pm(z,t)$ are spatially slowly varying, but we will need to average $\widetilde{G}(z,t)$ over a physical wavelength. Following the procedure outlined in Eq. (5.74), we find

$$F^+(z,t) = \frac{1}{2}\, G^{[0]}(z,t) \left[E^+(z,t) + J^+(z,t) \right] + \frac{1}{2}\, G^{[-2]}(z,t) \left[E^-(z,t) + J^-(z,t) \right], \text{ and}\tag{7.46a}$$

$$F^-(z,t) = \frac{1}{2}\, G^{[+2]}(z,t) \left[E^+(z,t) + J^+(z,t) \right] + \frac{1}{2}\, G^{[0]}(z,t) \left[E^-(z,t) + J^-(z,t) \right],\tag{7.46b}$$

where

$$G^{[n]}(z,t) \equiv \frac{k_0}{2\pi} \int_{z-\pi/k_0}^{z+\pi/k_0} dz'\, e^{+ink_0 z'}\, \widetilde{G}(z',t).\tag{7.47}$$

Substituting Eq. (7.46) into Eq. (??) yields

$$F_q(t) = \frac{1}{2} \sum_p e^{i2(q-p)\pi t} \left[E_p(t) + J_p(t) \right] \int_0^{1/2} dz \left[\mathbf{v}_q(z) \cdot \mathbf{u}_p(z)\, G^{[0]}(z,t) \right.$$
$$\left. + v_q^+(z)\, u_p^-(z)\, G^{[-2]}(z,t) + v_q^-(z)\, u_p^+(z)\, G^{[+2]}(z,t) \right].\tag{7.48}$$

We'll need to construct partial differential equations for $G^{[0]}(z,t)$ and $G^{[\pm 2]}(z,t)$. We expand $|\widetilde{E}(z,t)|^2$ as

$$\left| \widetilde{E}(z,t) \right|^2 = \left| E^+(z,t) \right|^2 + \left| E^-(z,t) \right|^2 + E^+(z,t)\, E^{-*}(z,t)\, e^{+i2k_0 z} + E^-(z,t)\, E^{+*}(z,t)\, e^{-i2k_0 z},\tag{7.49}$$

substitute this expression into Eq. (7.40), and then apply the average specified by Eq. (7.47) to obtain

$$
\begin{aligned}
\frac{\partial}{\partial t} G^{[n]}(z,t) = \frac{1}{\tau_{\parallel}} \Big\{ & \delta_{n,0} \overline{G}(z,t) - G^{[n]}(z,t) - G^{[n]}(z,t) \left[|E^+(z,t)|^2 + |E^-(z,t)|^2 \right] \\
& - G^{[n+2]}(z,t) E^+(z,t) E^{-*}(z,t) - G^{[n-2]}(z,t) E^-(z,t) E^{+*}(z,t) \Big\} .
\end{aligned}
\tag{7.50}
$$

If the pump has a short duration compared to $\tau_{\parallel}$, then rapid temporal oscillations in $E^{\pm}(z,t) E^{\mp *}(z,t)$ will diminish the contributions of higher-order spatial averages and allow us to neglect $G^{[\pm 4]}(z,t)$.

7.4 Passively Mode-Locked Lasers

As in the case of the Q-switched laser discussed in Section 7.3, intermodal coupling through nonlinearities in the macroscopic polarization $\tilde{F}(z,t)$ add dynamics to the gain and saturation of each mode that can lead to novel dynamical behavior. In a mode-locked laser, the amplitude and phases of the longitudinal modes are fixed in such a way that the output of the laser has particularly desirable properties, such as very short pulses or very stable (quasi-continuous-wave) behavior. We can understand this behavior through formal expansions of $\tilde{F}(z,t)$ and $\tilde{G}(z,t)$ in the Fourier frequency domain, but we must relax the rate-equation approximation that led to Eq. (7.39) to allow fluctuations in the polarization and gain that occur at integer multiples of the cavity free-spectral range $2\pi/\tau_g$.

$$
G_{qp}(t) = \overline{G}_{qp} - \sum_{mn} e^{-i\Delta\omega_{m-n} t} \kappa_{qpmn} C_{m-n} \left(E_m F_n^* + F_m E_n^* \right) ,
\tag{7.51}
$$

where

$$
C_q \equiv \left(1 - i \Delta\omega_q \tau_{\parallel} \right)^{-1} .
\tag{7.52}
$$

$$
\begin{aligned}
F_q = & \frac{1}{2} \mathcal{L}(\Omega_q) \sum_p e^{i\Delta\omega_{q-p} t} \overline{G}_{qp} E_p \\
& - \frac{1}{2} \mathcal{L}(\Omega_q) \sum_{mnp} e^{i\Delta\omega_{q-p-m+n} t} \kappa_{qpmn} C_{m-n} \left(E_m F_n^* + F_m E_n^* \right) E_p ,
\end{aligned}
\tag{7.53}
$$

Referring to Eq. (7.37), when $\dot{E}_q(t) = 0$, we find that F_q must also satisfy the expression

$$
F_q = B_q E_q ,
\tag{7.54}
$$

where

$$
B_q \equiv \frac{1}{2\,\tau_\lambda} \left(1 + i\,\Omega_q \right) - i\,\delta D_q .
\tag{7.55}
$$

Therefore,

$$
\sum_p e^{i\Delta\omega_{q-p} t} \overline{G}_{qp} E_p - 2 \mathcal{L}^{-1}(\Omega_q) B_q E_q = \sum_{mnp} e^{i\Delta\omega_{q-p-m+n} t} \kappa_{qpmn} C_{m-n} \left(B_m + B_n^* \right) E_m E_n^* E_p
\tag{7.56}
$$

This expression must be true at all times, so for convenience, let's use it to calculate E_q at $t = 0$. We obtain

$$
\sum_p \overline{G}_{qp} E_p - 2 \mathcal{L}^{-1}(\Omega_q) B_q E_q = \sum_{mnp} \kappa_{qpmn} C_{mn} \left(B_m + B_n^* \right) E_m E_n^* E_p
\tag{7.57}
$$

7.4.1   Numerics

Let's assume that in all cases of practical interest the transverse coherence time $\tau_\perp$ (which has been scaled by the group round-trip time τ_g) is small enough that we can ignore the corresponding differential operators on the right-hand side of Eq. (??), giving

$$F_q(t) = \frac{1}{2} \mathcal{L}_q\, G_0\, E_q(t) - \frac{1}{2} \mathcal{L}_q \sum_{mn} \kappa_{qmn}\, E_{q-m+n}(t)$$
$$\times \left(1 - i\,\Delta\omega_{m-n}\, \tau_\| + \tau_\| \frac{d}{dt} \right)^{-1} \left[E_m(t)\, F_n^*(t) + F_m(t)\, E_n^*(t) \right], \tag{7.58}$$

where $\mathcal{L}_q$ is defined by Eq. (7.30). In general, we can't make assumptions about the scaled value of $\tau_\|$; it could be smaller or larger than unity. In the case of a single-mode laser with no dispersion, our incorporation of frequency pulling into Eq. (7.33) means that a constant pump will eventually result in $\dot{E}_q(t) = 0$. One approach to estimating the impact of the differential operator on the right-hand side of Eq. (7.58) to a multimode laser is to expand the nonlinear contribution to $F_q(t)$ to third order in the electric field coefficients. Using

$$F_q^{(1)}(t) = \frac{1}{2} \mathcal{L}_q\, G_0\, E_q(t), \tag{7.59}$$

we obtain

$$F_q(t) \cong \frac{1}{2} \mathcal{L}_q\, G_0 E_q(t)$$
$$- \frac{1}{2} \mathcal{L}_q\, G_0 \sum_{mn} \kappa_{qmn}\, B_{mn}\, E_{q-m+n}(t) \left(1 - i\,\Delta\omega_{m-n}\, \tau_\| + \tau_\| \frac{d}{dt} \right)^{-1} E_m(t)\, E_n^*(t), \tag{7.60}$$

where

$$B_{mn} \equiv \frac{1}{2} \left(\mathcal{L}_m + \mathcal{L}_n^* \right). \tag{7.61}$$

From Eq. (??), we note that

$$\left(1 - i\,\Delta\omega_{m-n}\, \tau_\| + \tau_\| \frac{d}{dt} \right)^{-1} \left[E_m(t)\, E_n^*(t) \right] = \sum_{l=0}^{\infty} \left(i\,\Delta\omega_{m-n}\, \tau_\| - \tau_\| \frac{d}{dt} \right)^l \left[E_m(t)\, E_n^*(t) \right]. \tag{7.62}$$

The $l = 1$ term of the sum on the right-hand side has the form

$$\left(i\,\Delta\omega_{m-n}\, \tau_\| - \tau_\| \frac{d}{dt} \right) \left[E_m(t)\, E_n^*(t) \right] = i\,\Delta\omega_{m-n}\, \tau_\| \left[E_m(t)\, E_n^*(t) \right]$$
$$- \tau_\| \left[E_n^*(t)\, \dot{E}_m(t) + E_m(t)\, \dot{E}_n^*(t) \right]. \tag{7.63}$$

Consistent with our third-order expansion of $F_q(t)$, we use Eq. (7.37) to estimate $\dot{E}_q(t)$ to first order in $E_q(t)$. We obtain

$$\dot{E}_q(t) \approx \gamma_q\, E_q(t), \tag{7.64}$$

where

$$\gamma_q \equiv \frac{1}{1 + \delta\tau_q(\omega_0)} \left[\frac{1}{2} \left(1 + i\,\Omega_q \right) \left(\frac{G_0}{1 + \Omega_q^2} - \frac{1}{\tau_p} \right) + i\,\delta D_q(\omega_0) \right]. \tag{7.65}$$

Therefore

$$\left(i\,\Delta\omega_{m-n}\, \tau_\| - \tau_\| \frac{d}{dt} \right) \left[E_m(t)\, E_n^*(t) \right] \approx \left[i\,\Delta\omega_{m-n} - \left(\gamma_m + \gamma_n^* \right) \right] \tau_\|\, E_m(t)\, E_n^*(t), \tag{7.66}$$

and

$$\left(1 - i\,\Delta\omega_{m-n}\, \tau_\| + \tau_\| \frac{d}{dt} \right)^{-1} E_m(t)\, E_n^*(t) = \sum_{l=0}^{\infty} \left\{ \left[i\,\Delta\omega_{m-n} - \left(\gamma_m + \gamma_n^* \right) \right] \tau_\| \right\}^l \left[E_m(t)\, E_n^*(t) \right]$$
$$\equiv C_{mn}\, E_m(t)\, E_n^*(t), \tag{7.67}$$

where

$$C_{mn} \equiv \frac{1}{1 + (\gamma_m + \gamma_n^* - i\,\Delta\omega_{m-n})\,\tau_\parallel}. \tag{7.68}$$

Suppose that $\tau_\parallel \lesssim 1$, and that G_0 is only moderately above threshold, so that $\gamma_0 < 1$. Then $\gamma_m + \gamma_n^*$ can be neglected in favor of $\Delta\omega_{m-n}$. If $\tau_\parallel \gg 1$, then even at moderate gains C_{mn} will be strongly suppressed; we have

$$C_{mn} \approx \frac{\delta_{mn}}{1 + 2\,\mathrm{Re}(\gamma_n)\,\tau_\parallel}. \tag{7.69}$$

This effect is even more pronounced for multimode systems well above threshold. Note that modes *below* threshold should have $C_{nn} = 1$.

Let's now investigate numerical solutions of Eq. (7.37) after replacing the differential operator in Eq. (7.58) with C_{mn} in our computations of $F_q(t)$. First, in the "all-wave-mixing" (AWM) case, we choose

$$F_q(t) \cong \frac{1}{2}\,\mathcal{L}_q\,\left\{ G_0\,E_q(t) - \sum_{mn} \kappa_{qmn}\,C_{mn}\,E_{q-m+n}(t)\,\left[E_m(t)\,F_n^*(t) + F_m(t)\,E_n^*(t)\right]\right\}. \tag{7.70}$$

This equation can be rewritten as a matrix equation for $F_q(t)$ in the form

$$\sum_m \left[A_{qm}(t)\,F_m(t) + B_{qm}(t)\,F_m^*(t)\right] = H_q(t), \tag{7.71}$$

where

$$A_{qm}(t) \equiv \delta_{q,m} + \sum_n \mathcal{K}_{qmn}\,E_{q-m+n}(t)\,E_n^*(t),$$

$$B_{qm}(t) \equiv \sum_n \mathcal{K}_{qnm}\,E_{q-n+m}(t)\,E_n(t),$$

$$\mathcal{K}_{qmn} \equiv \frac{1}{2}\,\mathcal{L}_q\,\kappa_{qmn}\,C_{mn}, \text{ and}$$

$$H_q(t) \equiv \frac{1}{2}\,G_0\,\mathcal{L}_q\,E_q(t).$$

Suppose that the total number of modes in our simulation is $\mathcal{N} \equiv 2q_{\max} + 1$. Then we can think of $A_{qm}(t)$ and $B_{qm}(t)$ as $\mathcal{N} \times \mathcal{N}$ complex square matrices, and $F_q(t)$ and $H_q(t)$ as $\mathcal{N} \times 1$ complex column vectors. Separating all of these variables into their real and imaginary parts, we can rewrite Eq. (7.71) as the $(2\mathcal{N} \times 2\mathcal{N}) \cdot (2\mathcal{N} \times 1)$ real matrix equation

$$\begin{bmatrix} \mathrm{Re}[A(t) + B(t)] & -\mathrm{Im}[A(t) - B(t)] \\ \mathrm{Im}[A(t) + B(t)] & \mathrm{Re}[A(t) - B(t)] \end{bmatrix} \begin{bmatrix} \mathrm{Re}[\mathbf{F}(t)] \\ \mathrm{Im}[\mathbf{F}(t)] \end{bmatrix} = \begin{bmatrix} \mathrm{Re}[\mathbf{H}(t)] \\ \mathrm{Im}[\mathbf{H}(t)] \end{bmatrix}, \tag{7.72}$$

which can be solved using standard numerical linear algebra techniques.

In the low-gain, weak-field case, we can use the expansion of $F_q(t)$ to third-order in the electric field amplitude — the "four-wave mixing" (FWM) case:

$$F_q(t) \cong \frac{1}{2}\,\mathcal{L}_q\,G_0\,\left[E_q(t) - \sum_{mn} \kappa_{qmn}\,B_{mn}\,C_{mn}\,E_{q-m+n}(t)\,E_m(t)\,E_n^*(t)\right]. \tag{7.73}$$

In principle, Eq. (7.37) can be solved much more efficiently with $F_q(t)$ obtained from Eq. (7.73) than with Eq. (7.72).

7.4.1.1   Preliminary Solver

$$\left| E_q(t) \right|^2 - 2 \operatorname{Re}\left[E_q^*(t)\, F_q(t) \right] = 0\,. \tag{7.74}$$

In our code, we scale the time variable by the photon lifetime τ_p, and compute the derivative using

$$\dot{E}_q(t) = \left[-\frac{1}{2} + i \left(\delta\omega_q\, \tau_p + \delta D_q \right) \right] E_q(t) + F_q(t)\,, \tag{7.75}$$

where $\delta\omega_q$ and δD_q are given by Eq. (7.32) and Eq. (7.36a), respectively. Therefore,

$$E_q^*(t)\, \dot{E}_q(t) = \left[-\frac{1}{2} + i \left(\delta\omega_q\, \tau_p + \delta D_q \right) \right] \left| E_q(t) \right|^2 + E_q^*(t)\, F_q(t)\,, \tag{7.76}$$

giving

$$\operatorname{Re}\left[\frac{\dot{E}_q(t)}{E_q(t)} \right] = -\frac{1}{2} + \operatorname{Re}\left[\frac{F_q(t)}{E_q(t)} \right]\,, \quad \text{and} \tag{7.77}$$

$$\operatorname{Im}\left[\frac{\dot{E}_q(t)}{E_q(t)} \right] = \delta\omega_q\, \tau_p + \delta D_q + \operatorname{Im}\left[\frac{F_q(t)}{E_q(t)} \right]\,. \tag{7.78}$$

We see in the top two plots that $\operatorname{Re}[\dot{E}_q(t)/E_q(t)] \longrightarrow 0$ as $t \longrightarrow t_f$, and that in the same limit $\operatorname{Im}[\dot{E}_q(t)/E_q(t)] \longrightarrow \delta\nu_q\, \tau_p$, where

$$\delta\nu_q \equiv \delta\omega_q + \frac{\delta D_q}{\tau_p} + \frac{1}{\tau_p} \operatorname{Im}\left[\frac{F_q(t)}{E_q(t)} \right] \equiv \text{constant}\,. \tag{7.79}$$

So we can use as our FOM the equations

$$\operatorname{Re}\left[\frac{2\, F_q(t_f)}{E_q(t_f)} \right] = 1\,, \quad \text{and} \tag{7.80}$$

$$\operatorname{Im}\left[\frac{\ddot{E}_q(t_f)}{E_q(t_f)} \right] = 0\,; \tag{7.81}$$

but how do we estimate $\ddot{E}_q(t_f)$?

7.4.1.2   Power Spectral Density

Suppose that we have a numerically stable (steady-state) solution to Eq. (7.5), and we wish to compute the frequency content of the output intensity, defined as the square of the absolute value of an output field given by one of Eq. (4.127). Neglecting the overall normalization constant, we have

$$I_{\text{out}}(t) = \left| \sum_p e^{-i2p\pi t} E_p \right|^2 = \sum_{p,p'} e^{-i2(p-p')\pi t} E_p E_{p'}^* \tag{7.82}$$

$$\equiv \sum_q A_q\, e^{-i2\pi q t}\,, \tag{7.83}$$

where

$$A_q \equiv \sum_p E_p E_{p-q}^*\,. \tag{7.84}$$

If $p \in \{-p_{\max}, \ldots, +p_{\max}\}$, then, since $I_{\text{out}}(t)$ is real,

$$I_{\text{out}}(t) = A_0 + 2 \sum_{q=1}^{2\,p_{\max}} \text{Re}\left[A_q\, e^{-i\,2\,\pi\,q\,t} \right] \tag{7.85}$$

$$= A_0 + 2 \sum_{q=1}^{2\,p_{\max}} \left[\text{Re}(A_q) \cos(2\,\pi\,q\,t) + \text{Im}(A_q) \sin(2\,\pi\,q\,t) \right]. \tag{7.86}$$

Therefore, following standard practice[7.1], we define the *power spectral density* at each frequency as

$$P_q \equiv \frac{\sqrt{\text{Re}(A_q)^2 + \text{Im}(A_q)^2}}{A_0} = \frac{|A_q|}{A_0}, \tag{7.87}$$

valid for $q \in \{0, \ldots, 2\,p_{\max}\}$.

7.4.1.3   Chaotic Behavior

7.4.1.4   Passive Temporal Mode-Locking with a Saturable Absorber

7.4.1.5   Passive Frequency Mode-Locking

7.5   Mean-Field Laser Theory

Experimental observations of passively frequency mode-locked lasers show that they exhibit quasi-continuous-wave output field amplitudes and linear frequency chirps that reset after one mode-locked time interval (roughly the group round-trip time of the unloaded laser resonator). Let's represent the most general form of such a field with the time-dependent quadratic exponential function

$$E(t) = \exp\left[(-\gamma + i\,\lambda)\,t - \frac{1}{2}\,(a + i\,b)\,t^2 \right]$$
$$\equiv \sum_{q=-\infty}^{\infty} E_q\, e^{i\,2\,q\,\pi\,t} \tag{7.88}$$

where $\gamma > 0$, λ, $a > 0$, and b are real constants, and the frequency chirp is therefore $b\,t$. We assume that this function is periodic over the time interval $t \in \{-1/2, 1/2\}$, and then we obtain the Fourier series coefficients

$$E_q = \int_{-1/2}^{1/2} dt\, e^{-i\,2\,q\,\pi\,t}\, E(t)$$
$$= \sqrt{\frac{\pi}{2\,(a + i\,b)}}\, \exp\left[\frac{(\gamma - i\,\lambda_q)^2}{2\,(a + i\,b)} \right] \tag{7.89}$$
$$\times \left\{ \text{erf}\left[\frac{\frac{1}{2}(a + i\,b) + (\gamma - i\,\lambda_q)}{\sqrt{2\,(a + i\,b)}} \right] + \text{erf}\left[\frac{\frac{1}{2}(a + i\,b) - (\gamma - i\,\lambda_q)}{\sqrt{2\,(a + i\,b)}} \right] \right\},$$

where $\lambda_0 = \lambda$ and $\lambda_q \equiv \lambda_0 - 2\,q\,\pi$. The properties of these coefficients require some computational exploration to discover. For example, let's assume that $\gamma = a = \lambda_0 = 0$. Then

$$E_q = \sqrt{\frac{\pi}{i\,2\,b}}\, \exp\left(i\,\frac{2\,\pi^2}{b}\,q^2 \right) \left\{ \text{erf}\left[\sqrt{\frac{i}{8\,b}}\,(b - 4\,q\,\pi) \right] + \text{erf}\left[\sqrt{\frac{i}{8\,b}}\,(b + 4\,q\,\pi) \right] \right\}. \tag{7.90}$$

[7.1]Although both the in-phase and quadrature components are included in the definition given by Eq. (7.87), the factor of 2 in the sum of Eq. (7.85) is ignored for essentially the same reason we neglect the negative frequencies when plotting the digital Fourier transform of a real signal.

The imaginary parts of the two error functions are negligible. Therefore, in this case the phase of the Fourier coefficients is given by the exponential argument $(2\pi^2/b)q^2$. When both q and b are positive, the first error function oscillates around the value 1 until $q \approx b/2$, where it rapidly transitions to oscillations around the value -1. The second error function oscillates around the value 1 for all q. Therefore, the sum of the two error functions oscillates around the value 2 for $0 \le q \lesssim b/2$ and 0 for $q \gtrsim b/2$, implying that the comb is composed of approximately $|b|/2\pi$ nonzero components. We confirm these two observations in Fig. 7.2, where we have also allowed a small value of γ to represent the photon lifetime of the cavity. Similar computational experiments show that when $a \gtrsim 1$, the comb narrows and the output field develops ripples that become pulses when $a \gg 1$.

In the remainder of this section, our primary tools will be the formal solutions of Eq. (3.48) and Eq. (3.46c), obtained through Fourier transform expansions. For example, consider the ordinary differential equation

$$\frac{d}{dt}y(t) = -\frac{1}{\tau}\left[y(t) + s(t)\right],\tag{7.91}$$

for some function $y(t)$ driven by $s(t)$. Applying the Fourier Transform and using Eq. (A.10b) and Eq. (A.17), we find

$$y(\omega) = \frac{s(\omega)}{1 - i\omega\tau} = \sum_{l=0}^{\infty}(i\omega\tau)^l s(\omega).\tag{7.92}$$

Returning to the time domain with Eq. (A.17), we obtain

$$y(t) = \left(1 + \tau\frac{d}{dt}\right)^{-1}s(t),\tag{7.93}$$

where for convenience we have defined the differential operator

$$\left(1 + \tau\frac{d}{dt}\right)^{-1} \equiv \sum_{l=0}^{\infty}\left(-\tau\frac{d}{dt}\right)^l.\tag{7.94}$$

Applying this technique to Eq. (3.48) (with $\Omega = 0$) and Eq. (3.46c), we find the formal solutions

$$\tilde{F}(z,t) = \frac{1}{2}\hat{\partial}_{\perp}^{-1}\left[\tilde{E}(z,t)\,\tilde{G}(z,t)\right],\text{ and}\tag{7.95a}$$

$$\tilde{G}(z,t) = \hat{\partial}_{\parallel}^{-1}G_0(z,t) - \hat{\partial}_{\parallel}^{-1}\left[\tilde{E}^*(z,t)\tilde{F}(z,t) + \tilde{E}(z,t)\tilde{F}^*(z,t)\right],\tag{7.95b}$$

where

$$\hat{\partial}_{\perp}^{-1} \equiv (1 - i\alpha)\left(1 + \frac{\tau_{\perp}}{1 - i\alpha}\partial/\partial t\right)^{-1},\text{ and}\tag{7.96a}$$

$$\hat{\partial}_{\parallel}^{-1} \equiv (1 + \tau_{\parallel}\partial/\partial t)^{-1}.\tag{7.96b}$$
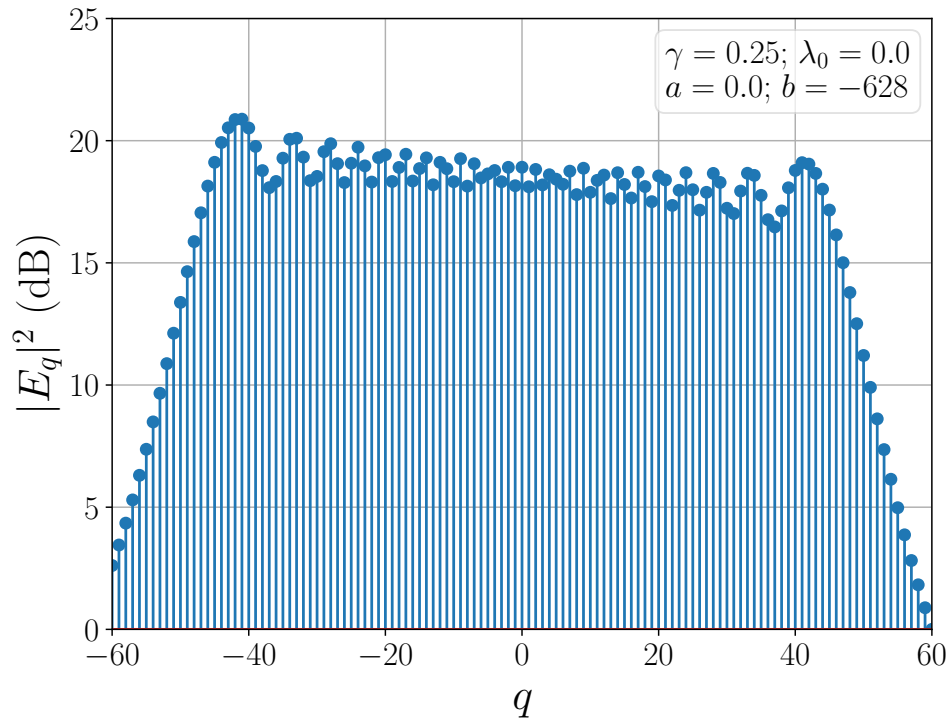
Now, using Eq. (7.94), we can rewrite Eq. (3.53a) as

$$\tilde{F}(z,t) = \frac{1}{2}(1 - i\alpha)\sum_{l=0}^{\infty}\left(-\frac{\tau_{\perp}}{1 - i\alpha}\frac{\partial}{\partial t}\right)^l\left[\tilde{E}(z,t)\,\tilde{G}(z,t)\right] \equiv \frac{1}{2}\widehat{\mathcal{D}}\left[\tilde{E}(z,t)\right]\tilde{G}(z,t),\tag{7.97}$$

where

$$\widehat{\mathcal{D}}\left[\tilde{E}(z,t)\right] \equiv (1 - i\alpha)\sum_{l=0}^{\infty}\left(-\frac{\tau_{\perp}}{1 - i\alpha}\right)^l\sum_{j=0}^{l}\binom{l}{j}\frac{\partial^{l-j}}{\partial t^{l-j}}\tilde{E}(z,t)\frac{\partial^j}{\partial t^j}.\tag{7.98}$$

Substituting Eq. (7.97) into Eq. (3.53b) and gathering terms, we obtain the general formal expression

$$\tilde{G}(z,t) = \frac{1}{1 + \frac{1}{2}\hat{\partial}_{\parallel}^{-1}\left\{\tilde{E}^*(z,t)\,\widehat{\mathcal{D}}\left[\tilde{E}(z,t)\right] + \tilde{E}(z,t)\,\widehat{\mathcal{D}}^*\left[\tilde{E}^*(z,t)\right]\right\}}\hat{\partial}_{\parallel}^{-1}G_0(z,t)\tag{7.99}$$

(a) Fourier coefficient amplitude
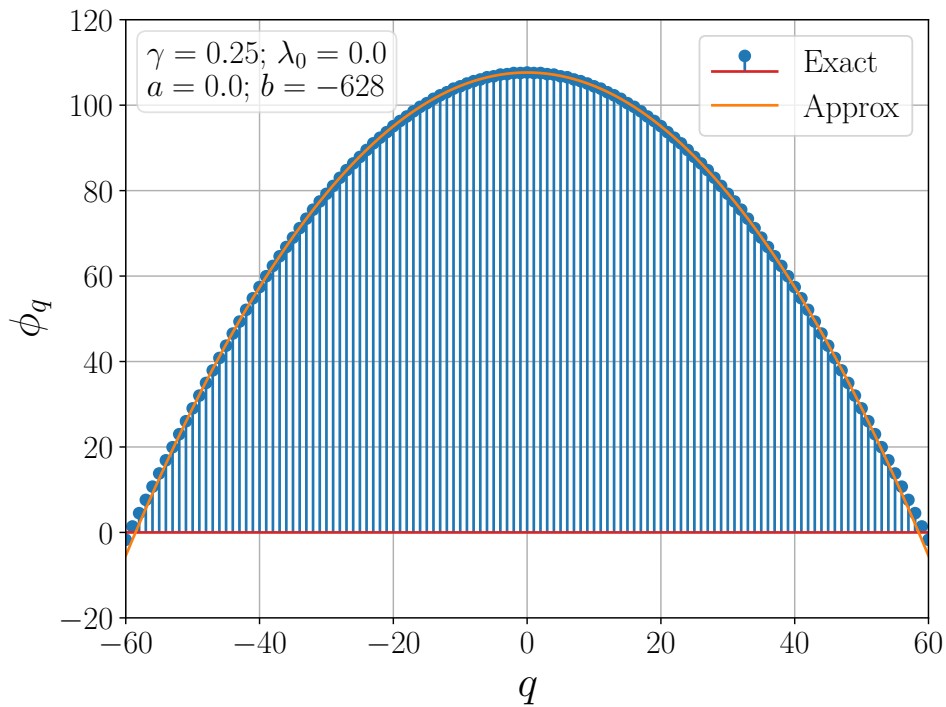
(b) Fourier coefficient phase

Figure 7.2: Squared amplitude and phase of the Fourier series coefficient given by Eq. (7.89). (a) The absolute value squared of the Fourier series coefficient. In our units, the number of comb lines within 3 dB of the maximum value is given approximately by $|b|/2\pi$. (b) The phase of the Fourier series coefficient, as well as the approximate value $\phi_0 + 2\pi^2 q^2/b$, plotted as a function of the mode number.

Suppose now that $G_0(z,t) \equiv \overline{G}(z)$ is constant in time. Then $\partial^j G_0(z,t)/\partial t^j = \delta_{j0}\overline{G}(z)$, and (for example) $\widehat{\mathcal{D}}\left[\tilde{E}(z,t)\right] \longrightarrow \hat{\partial}_\perp^{-1}\tilde{E}(z,t)$, giving

$$\tilde{G}(z,t) = \frac{G_0(z)}{1 + \frac{1}{2}\hat{\partial}_\parallel^{-1}\left[\tilde{E}^*(z,t)\,\hat{\partial}_\perp^{-1}\tilde{E}(z,t) + \tilde{E}(z,t)\left(\hat{\partial}_\perp^{-1}\right)^*\tilde{E}^*(z,t)\right]} \text{, and} \tag{7.100a}$$

$$\tilde{F}(z,t) = \frac{G_0(z)}{2}\hat{\partial}_\perp^{-1}\frac{\tilde{E}(z,t)}{1 + \frac{1}{2}\hat{\partial}_\parallel^{-1}\left[\tilde{E}^*(z,t)\,\hat{\partial}_\perp^{-1}\tilde{E}(z,t) + \tilde{E}(z,t)\left(\hat{\partial}_\perp^{-1}\right)^*\tilde{E}^*(z,t)\right]}\,. \tag{7.100b}$$

Note that the denominator of Eq. (7.100b) is self-contained; those differential operators are not applied to $\tilde{E}(z,t)$ in the numerator. But the differential operator $\hat{\partial}_\perp^{-1}$ preceding the fraction applies to all occurrences of $\tilde{E}(z,t)$ and its complex conjugate. Also, if the complex electric field envelope function is constant in time, then Eq. (7.100) are identical to Eq. (5.2) with $\Omega = 0$.

In this section, we are particularly interested in the case where the field amplitude $|\tilde{E}(z,t)|$ is relatively slowly-varying in time and the output of the laser is passively mode-locked in the frequency domain. Our intermediate goal is to derive a master equation based on Eq. (5.128) that incorporates a form of the macroscopic polarization tailored for frequency mode-locking. We'll begin by expanding Eq. (7.100b) as a Taylor Series in powers of the partial time derivative $\partial/\partial t$. We will keep only the first-order time derivative term that represents the nonlinear interaction between the counterpropagating electric fields. In this case, while temporarily ignoring the spatiotemporal coordinates (z,t), we have

$$\begin{aligned}\tilde{F} &\approx \frac{G_0}{2}L_{\text{sat}}\left(i\,\tau_\perp\frac{\partial}{\partial t}\right)\tilde{E} + \frac{G_0\chi}{4\left[1 + \left|\tilde{E}\right|^2\right]^2}\tilde{E}\frac{\partial}{\partial t}\left|\tilde{E}\right|^2 \\ &= \frac{G_0}{2}\sum_{l=0}^{\infty}\frac{1}{l!}\frac{d^l}{d\Omega^l}L_{\text{sat}}(\Omega)\bigg|_{\Omega=0}\left(i\,\tau_\perp\frac{\partial}{\partial t}\right)^l\tilde{E} + \frac{G_0\chi}{4\left[1 + \left|\tilde{E}\right|^2\right]^2}\tilde{E}\frac{\partial}{\partial t}\left|\tilde{E}\right|^2\,,\end{aligned} \tag{7.101}$$

where we have defined

$$\chi \equiv (2\tau_\parallel + 3\tau_\perp) - i\,\alpha\,(2\tau_\parallel + \tau_\perp) \approx (1 - i\,\alpha)\,(2\tau_\parallel + 3\tau_\perp)\,, \tag{7.102}$$

$$L_{\text{sat}}(\Omega) \equiv \frac{\mathcal{L}(\Omega)}{1 + \text{Re}[\mathcal{L}(\Omega)]\left|\tilde{E}\right|^2}\,, \tag{7.103}$$

and in this case $\mathcal{L}(\Omega)$ is given by Eq. (3.52). The first term on the right-hand side of this equation allows us to sample the frequency dependence of the complex gain of the material medium. If we limit ourselves to second order in the time derivative, then we can write the macroscopic polarization as

$$\begin{aligned}\tilde{F} &\approx \frac{(1 - i\,\alpha)\,G_0}{2\left[1 + \left|\tilde{E}\right|^2\right]}\tilde{E} - \frac{G_0\,\tau_\perp}{2\left[1 + \left|\tilde{E}\right|^2\right]^2}\frac{\partial}{\partial t}\tilde{E} + \frac{G_0\,\tau_\perp^2}{2\,(1 + \alpha^2)\left[1 + \left|\tilde{E}\right|^2\right]^2}\frac{\partial^2}{\partial t^2}\tilde{E} \\ &\quad + \frac{G_0\chi}{4\left[1 + \left|\tilde{E}\right|^2\right]^2}\tilde{E}\frac{\partial}{\partial t}\left|\tilde{E}\right|^2\,,\end{aligned} \tag{7.104}$$

where we have retained only the real part of the coefficient of the second-order time derivative, which represents the power-broadened "gain curvature" and is simply the Fourier transform of the real part of Eq. (5.2b) to second order in $\omega \equiv \Omega/\tau_\perp$. As we shall see, the fourth term in this expression describes the spatial interaction of the counterpropagating intracavity fields and four-wave mixing effects.

Let's now decouple the forward-propagating and backward-propagating fields in the macroscopic polarization. Following Section 5.4, we define

$$\tilde{F} \equiv F_+(z,t)\, e^{+i\,k_0\,z} + F_-(z,t)\, e^{-i\,k_0\,z}, \tag{7.105}$$

apply Eq. (2.80) in the case $m = 0$, and use Eq. (7.104) as a guide to extract $F_\pm$ and establish the right-hand side of Eq. (5.128). The primary difference between the approach we used in Section 5.4 and the one we are using here is that there is no static pattern of (in space or time) spatial hole burning; as shown above, in the case of a frequency mode-locked laser, the total intracavity field is chirped and flows back and forth between the mirrors. In principle, could follow the method we briefly considered in Section 5.4 in the limit where the unsaturated gain is infinitesimally above threshold — so that $|E_\pm| \ll 1$ — and write the saturation factor to first order in $e^{\pm i\,k_0\,z}$ as

$$\frac{\tilde{E}}{1 + \left|\tilde{E}\right|^2} \approx \left[1 - \left(|E_+|^2 + 2\,|E_-|^2\right)\right] E_+\, e^{+i\,k_0\,z} + \left[1 - \left(|E_-|^2 + 2\,|E_+|^2\right)\right] E_-\, e^{-i\,k_0\,z}, \tag{7.106}$$

consistent with Eq. (5.100). However, as we discovered in Section 5.4.2, this expansion is very inaccurate for gains even 10% above threshold. Instead, we'll note that when averaged over one round trip in time, as we learned above for a highly multimode laser the total saturation factor can be approximated by

$$\left[1 + \left|\tilde{E}(z,t)\right|^2\right]^{-1} \approx \frac{1}{1 + |E_+|^2 + |E_-|^2} \equiv S\,[E_\pm]. \tag{7.107}$$

Decoupling the counterpropagating terms in Eq. (7.104) is now straightforward, and they resolve to

$$
\begin{aligned}
F_\pm \approx & \;\frac{(1 - i\,\alpha)\,G_0}{2}\, S\,[E_\pm]\, E_\pm - \frac{G_0\,\tau_\perp}{2}\, S\,[E_\pm]\, \frac{\partial}{\partial t} E_\pm + \frac{G_0\,\tau_\perp^2}{2\,(1 + \alpha^2)}\, S^2\,[E_\pm]\, \frac{\partial^2}{\partial t^2} E_\pm \\
& + \frac{G_0\,\chi}{4}\, S^2\,[E_\pm]\, \left[E_\pm \frac{\partial}{\partial t}\left(|E_+|^2 + |E_-|^2\right) + |E_\mp|^2\, \frac{\partial}{\partial t} E_\pm + E_+\, E_-\, \frac{\partial}{\partial t} E_\mp^*\right].
\end{aligned}
\tag{7.108}
$$

We now make the assumptions that $G_0\,\tau_\perp \ll 1$ and $G_0\,\tau_\parallel\,|E_\pm|^2 \ll 1$, and therefore we neglect terms proportional to $\partial E_\pm / \partial t$ and $|E_\pm|^2\, \partial E_\pm^* / \partial t$ because they are much smaller than the time derivative on the left-hand side of the field evolution equation given by Eq. (5.128).

$$
\begin{aligned}
F_\pm \approx & \;\frac{(1 - i\,\alpha)\,G_0}{2}\, S\,[E_\pm]\, E_\pm + \frac{G_0\,\tau_\perp^2}{2\,(1 + \alpha^2)}\, S^2\,[E_\pm]\, \frac{\partial^2}{\partial t^2} E_\pm \\
& + \frac{G_0\,\chi}{4}\, S^2\,[E_\pm]\, \left[i\,\mathrm{Im}\left(E_\mp\, \frac{\partial}{\partial t} E_\mp^*\right) + \frac{3}{2}\, \frac{\partial}{\partial t}|E_\mp|^2\right] E_\pm.
\end{aligned}
\tag{7.109}
$$

Substituting this expression into Eq. (5.128) gives us the master equation for the passively mode-locked laser in the form

$$
\begin{aligned}
\frac{\partial}{\partial t} E_\pm \pm \frac{\partial}{\partial z} E_\pm \approx & \;\frac{1}{2}\left\{-\alpha_0 + \left[\frac{G_0\,\tau_\perp^2}{1 + \alpha^2}\, S^2\,[E_\pm] - i\,D_2'\right]\frac{\partial^2}{\partial t^2}\right\} E_\pm \\
& + \frac{1}{2}\left\{(1 - i\,\alpha)\,G_0\, S\,[E_\pm] + i\,\alpha\, G_{\text{th}}\right\} E_\pm \\
& + \frac{G_0\,\chi}{4}\, S^2\,[E_\pm]\left[i\,\mathrm{Im}\left(E_\mp\, \frac{\partial}{\partial t} E_\mp^*\right) + \frac{3}{2}\, \frac{\partial}{\partial t}|E_\mp|^2\right] E_\pm,
\end{aligned}
\tag{7.110}
$$

where we have retained only the second-order dispersion term $D_2' \equiv D_2 + A_2$ from Eq. (5.128) and $G_{\text{th}} = 1/\tau_p = \ln(1/R_1\,R_2\,e^{-\alpha_0})$.

Our goal now is to recast Eq. (7.110) as a nonlinear Schrödinger equation (NLSE) that can be solved using numerical techniques such as the Fourier split-step method. First we'll unfold the standing-wave

cavity so that $E_-(z,t)$ is continued from $\{0, 1/2\}$ to $\{1/2, 1\}$. We then map $E_-(1/2-,t)$ to $E_+(1/2+,t)$ and $E_-(0+,t)$ to $E_+(1-,t)$. If we follow this procedure for the counterpropagating steady-state intensities shown in Fig. 5.16 and Fig. 7.3a, we obtain the steady-state forward-propagating intensity in the unfolded cavity shown in Fig. 7.3b. Note that $I(1+z) = I(z)$ in the unfolded case, with the boundary conditions $I(0) = R_1 I(1)$ and $I(1/2+) = R_2 I(1/2-)$.

This approach eliminates $E_-(z,t)$ from the left-hand side of Eq. (7.110), but there is a corresponding subtlety on the right-hand side: the nonlinear terms require that we replace $E_-(z,t)$ with $E_+(1-z,t)$. With this procedure in mind, the saturation function becomes

$$S[E_\pm] \longrightarrow \left(1 + |E_+(z,t)|^2 + |E_+(1-z.t)|^2\right)^{-1}, \tag{7.111}$$

and we introduce the steady-state effective gain function $K(z)$ and the single-mode steady-state forward-propagating intensity $I(z) = K(z) I(0) \equiv K(z) I_0$, such that

$$K(z) \equiv \exp\left(\int_0^z dz' \left\{G_0(z') S[I(z'), I(1-z')] - \alpha_0(z')\right\}\right)$$
$$\approx \exp\left[\int_0^z dz' \, g_{\text{eff}}(z')\right], \tag{7.112}$$

where we have followed the discussion in Section 5.2 and defined $g_{\text{eff}}(z)$ for the *unwrapped* cavity as

$$g_{\text{eff}}(z) \equiv \beta G_0(z) - \alpha_0(z) + \ln(R_2)\delta(z - 1/2) + \ln(R_1)\delta(z - 1), \tag{7.113}$$

with β given by Eq. (5.56b) for $R = R_1 R_2$ in the standing-wave cavity case. We note that $G_0(1-z) = G_0(z)$ because $G_0(z)$ is symmetric about $z = 1/2$ in the unfolded cavity, and that $G_0(1+z) = G_0(z)$ because the gain is also periodic. Then we define the forward-propagating electric-field amplitude function $E(z,t)$ in terms of the single-mode steady-state intensity as

$$E_+(z,t) \equiv I^{1/2}(z) E(z,t) = K^{1/2}(z) \sqrt{I_0} E(z,t). \tag{7.114}$$

Since $K(z)$ — and therefore $I(z)$ — is periodic and consistent with the boundary conditions, $E(z,t)$ is both periodic and continuous. With these modifications, we substitute Eq. (7.112) and Eq. (7.114) into Eq. (7.110) to obtain

$$\left(\frac{\partial}{\partial t} + \frac{\partial}{\partial z}\right)E(z,t) = \frac{1}{2}\left\{\frac{G_0(z)\tau_\perp^2}{1+\alpha^2}S^2[E] - i D_2'\right\}\frac{\partial^2}{\partial t^2}E(z,t)$$
$$+ \frac{G_0(z)}{2}\left\{S[E] - S[1]\right\}E(z,t) + i\frac{\alpha}{2}\left\{G_0(z)S[E] - G_{\text{th}}\right\}E(z,t)$$
$$+ \frac{G_0(z)\chi}{4}S^2[E] I_0 K(-z)\left\{i\,\text{Im}\left[E(-z,t)\frac{\partial}{\partial t}E^*(-z,t)\right] + \frac{3}{2}\frac{\partial}{\partial t}|E(-z,t)|^2\right\}E(z,t), \tag{7.115}$$

where

$$S[E] \equiv \frac{1}{1 + I_0\left[K(z)|E(z,t)|^2 + K(-z)|E(-z,t)|^2\right]}. \tag{7.116}$$

and we have used the periodicity of $K(z)$ and $E(z,t)$ for the counterpropagating fields.

Next, anticipating our mean-field theory, let us change variables to a coordinate system that follows the forward-propagating field as it propagates around the cavity. We choose $z = \zeta$ and $t = \tau + \zeta$, or

$$\zeta \equiv z, \text{ and} \tag{7.117a}$$
$$\tau \equiv t - z, \tag{7.117b}$$

(a) Folded standing-wave cavity

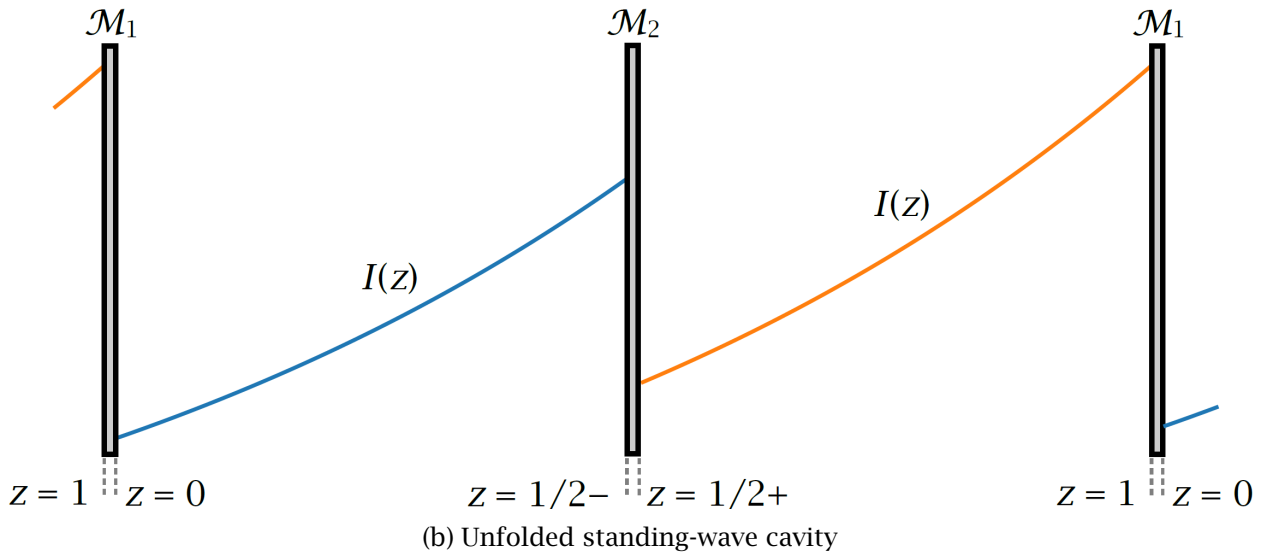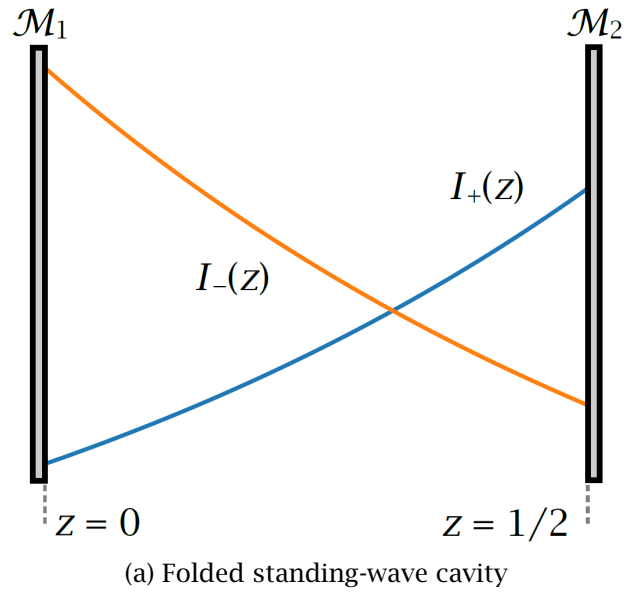(b) Unfolded standing-wave cavity

Figure 7.3:   (a) Counterpropagating steady-state intensities in a folded standing-wave cavity. (b) Forward-propagating steady-state intensities in an unfolded standing-wave cavity. The intensity is periodic (with unit period) but discontinuous.

where τ is called the "retarded time." Then

$$\frac{\partial}{\partial z} E(z,t) = \frac{\partial \zeta}{\partial z} \frac{\partial}{\partial \zeta} E(\zeta,\tau) + \frac{\partial \tau}{\partial z} \frac{\partial}{\partial \tau} E(\zeta,\tau) = \left(\frac{\partial}{\partial \zeta} - \frac{\partial}{\partial \tau} \right) E(\zeta,\tau) \,, \text{ and} \qquad (7.118a)$$

$$\frac{\partial}{\partial t} E(z,t) = \frac{\partial \zeta}{\partial t} \frac{\partial}{\partial \zeta} E(\zeta,\tau) + \frac{\partial \tau}{\partial t} \frac{\partial}{\partial \tau} E(\zeta,\tau) = \frac{\partial}{\partial \tau} E(\zeta,\tau) \,. \qquad (7.118b)$$

In Eq. (7.115), we can immediately update $E(z,t) \longrightarrow E(\zeta,\tau)$ and $K(-z) \longrightarrow K(-\zeta)$. But terms including $E(-z,t)$ are slightly more complicated: we'll have $E(-z,t) \longrightarrow E(\zeta',\tau')$, where $\zeta' = -\zeta$, and $\tau' = t + z = \tau + 2\zeta$. Therefore, our forward-propagating equation of motion becomes

$$\frac{\partial}{\partial \zeta} E(\zeta,\tau) = \frac{1}{2} \left\{ \frac{G_0(\zeta)\,\tau_\perp^2}{1+\alpha^2} S^2[E] - i\,D_2' \right\} \frac{\partial^2}{\partial \tau^2} E(\zeta,\tau)$$

$$+ \frac{G_0(\zeta)}{2} [S[E] - S[1]]\,E(\zeta,\tau) + i\,\frac{\alpha}{2} [G_0(\zeta)\,S[E] - G_{\text{th}}]\,E(\zeta,\tau) + \frac{G_0(\zeta)\,\chi}{4} S^2[E]\,I_0\,K(-\zeta)$$

$$\times \left\{ i\,\text{Im} \left[E(-\zeta,\tau+2\zeta) \frac{\partial}{\partial \tau} E^*(-\zeta,\tau+2\zeta) \right] + \frac{3}{2} \frac{\partial}{\partial \tau} |E(-\zeta,\tau+2\zeta)|^2 \right\} E(\zeta,\tau)\,, \quad (7.119)$$

where now

$$S[E] \equiv \frac{1}{1 + I_0 \left[K(\zeta)\,|E(\zeta,\tau)|^2 + K(-\zeta)\,|E(\zeta,\tau+2\zeta)|^2 \right]} \,. \qquad (7.120)$$

Let's try to simplify this ponderous partial differential equation before we take its average over one round trip. First, since we are now working in a coordinate system that follows a particular point on $E(z,t)$ through the retarded time τ, we assume that on the right-hand side the dependence of the field on ζ is captured by $K(\pm\zeta)$, and we can replace $E(\pm\zeta,\tau)$ with $E(\tau)$. Second, in Section 5.4.2, we learned that in a wide variety of cases of practical interest — including spatially varying gain and loss regions within the laser cavity — the sum of the single-mode counterpropagating intensities depends only weakly on position, and we can approximate $S(1)$ in this expression as

$$S[1] = \frac{1}{1 + I_0 \left[K(\zeta) + K(-\zeta) \right]} \approx \frac{1}{\overline{H}_0} \,, \qquad (7.121)$$

where

$$\overline{H}_0 \equiv \frac{\overline{G}_0}{G_{\text{th}}} \,, \qquad (7.122)$$

and the unsaturated round trip gain (through the unfolded cavity) is defined as

$$\overline{G}_0 \equiv \int_0^1 dz\, G_0(z) \,. \qquad (7.123)$$

Next, we'll average our equation of motion spatially over one round trip to obtain an expression for the mean field. For example, on the left-hand side ,

$$\int_0^1 d\zeta\, \frac{\partial}{\partial \zeta} E(\zeta,\tau) = E(1,\tau) - E(0,\tau) \equiv \frac{\Delta E(\tau)}{T_{\text{rt}}} \,, \qquad (7.124)$$

where T_{rt} is the group round-trip propagation time. Let's define

$$\overline{K} \equiv \frac{1}{\overline{G}_0} \int_0^1 d\zeta\, G_0(\zeta)\,K(\zeta) \qquad (7.125)$$

and the convolution integral

$$\hat{K}(B) \equiv \frac{1}{\overline{G_0}} \int_0^1 d\zeta \, G_0(\zeta) \, K(-\zeta) \, B(\tau + 2\zeta)$$

$$= \frac{1}{\overline{G_0}} \int_0^1 du \, G_0(1 - u) \, K(u) \, B(\tau - 2u) \qquad (7.126)$$

$$= \frac{1}{\overline{G_0}} \int_0^1 du \, G_0(u) \, K(u) \, B(\tau - 2u) \,,$$

where in the final expression we have noted again that $G_0(1 - u) = G_0(u)$ because $G_0(z)$ is symmetric about $z = 1/2$ in the unfolded cavity.

Let's set aside the first term on the right-hand side of Eq. (7.119), and focus on the average of the first two terms on the next line. We have

$$\int_0^1 d\zeta \left\{ \frac{G_0(\zeta)}{2} \left[S[E] - \frac{G_{\text{th}}}{\overline{G_0}} \right] + i \frac{\alpha}{2} \left[G_0(\zeta) \, S[E] - G_{\text{th}} \right] \right\} E(\tau)$$

$$= \frac{1}{2} (1 - i\alpha) \int_0^1 d\zeta \, G_0(\zeta) \left[S[E] - \frac{1}{\overline{H_0}} \right] E(\tau)$$

$$\equiv \frac{1}{2} (1 - i\alpha) \frac{1}{\overline{H_0}} \int_0^1 d\zeta \, G_0(\zeta) \, [\mathcal{R}[E] - 1] \, E(\tau), \quad (7.127)$$

where $\mathcal{R}[E] \equiv \overline{H_0} \, S[E]$. In Section 5.4, we found that

$$I_0 \approx \frac{C^2}{2} \left(\overline{H_0} - 1 \right), \qquad (7.128)$$

where C is defined by Eq. (4.115). Then

$$\mathcal{R}[E] - 1 = \overline{H_0} \, \frac{1}{1 + I_0 \left[K(\zeta) \, |E(\zeta, \tau)|^2 + K(-\zeta) \, |E(\zeta, \tau + 2\zeta)|^2 \right]} - 1$$

$$= \left(\overline{H_0} - 1 \right) \frac{1 - \frac{1}{2} C^2 \left[K(\zeta) \, |E(\tau)|^2 + K(-\zeta) \, |E(\tau + 2\zeta)|^2 \right]}{1 + \frac{1}{2} C^2 \left(\overline{H_0} - 1 \right) \left[K(\zeta) \, |E(\tau)|^2 + K(-\zeta) \, |E(\tau + 2\zeta)|^2 \right]}. \quad (7.129)$$

To third order in $E(\tau)$, we can replace $E(\tau + 2\zeta)$ in the denominator with $E(\tau)$, and we make the same approximation for $K(\zeta) + K(-\zeta) \approx 2/C^2$ as we did for our estimate of $S[1]$ above. Then the average over ζ only applies to the numerator, and we obtain

$$\int_0^1 d\zeta \left\{ \frac{G_0(\zeta)}{2} \left[S(E) - \frac{G_{\text{th}}}{\overline{G_0}} \right] + i \frac{\alpha}{2} \left[G_0(\zeta) \, S(E) - G_{\text{th}} \right] \right\} E(\tau)$$

$$\approx -(1 - i\alpha) \, \rho \, \mathcal{R}[E] \left\{ \frac{1}{2} C^2 \left[\overline{K} \, |E(\tau)|^2 + \hat{K} \left(|E|^2 \right) \right] - 1 \right\} E(\tau), \quad (7.130)$$

where

$$\mathcal{R}[E] \approx \frac{\overline{H_0}}{1 + \left(\overline{H_0} - 1 \right) |E(\tau)|^2} \equiv \frac{1}{1 + \sigma \left[|E(\tau)|^2 - 1 \right]}, \qquad (7.131)$$

$$\sigma \equiv \frac{\overline{H_0} - 1}{\overline{H_0}}, \text{ and} \qquad (7.132a)$$

$$\rho \equiv \frac{\sigma}{2\tau_p}. \qquad (7.132b)$$

Following the same procedure with all other terms in Eq. (7.119), we find

$$
\frac{\partial}{\partial T} E(\tau) \approx \frac{1}{2} \left(\frac{G_{\text{th}}^2}{\overline{G}_0} \frac{\tau_\perp^2}{1+\alpha^2} \mathcal{R}^2[E] - i D_2' \right) \frac{\partial^2}{\partial \tau^2} E(\tau)
$$

$$
- (1 - i\alpha) \rho \, \mathcal{R}[E] \left\{ \frac{C^2}{2} \left[\overline{K} |E(\tau)|^2 + \hat{K} \left(|E|^2 \right) \right] - 1 \right\} E(\tau)
$$

$$
+ \frac{\chi}{8} \rho \, \mathcal{R}^2[E] \, C^2 \left\{ i \hat{K} \left[\operatorname{Im} \left(E \frac{\partial}{\partial \tau} E^* \right) \right] + \frac{3}{2} \hat{K} \left[\frac{\partial}{\partial \tau} |E|^2 \right] \right\} E(\tau). \quad (7.133)
$$

In this form, our nonlinear Schrödinger equation (NLSE) can be solved numerically using (for example) the Fourier split-step method.

Our next task is to derive an approximate analytic solution to the NLSE by estimating the integrals in Eq. (7.133). When we solve our NLSE analytically, we will write the mean-field envelope function E in a form similar to that of Eq. (7.88), i.e., in terms of a positive real amplitude $A e^{\psi(\tau)}$ and real phase angle ϕ as

$$
E(T, \tau) \equiv A e^{\psi(\tau) + i \phi(T, \tau)}. \quad (7.134)
$$

Passive frequency mode-locking primarily arises from the phase of the field, and the second term on the right-hand side of Eq. (7.133) shows that the saturated gain acts as a restoring force that tries to drive $|E(T, \tau)|^2$ to a constant value. If $|\psi(\tau)| \ll 1$ for all τ during one round trip through the unfolded cavity, we can approximate $\hat{K}\left[|E|^2 \right]$ with $\overline{K} |E(\tau)|^2$, and therefore

$$
\frac{C^2}{2} \left[\overline{K} |E(\tau)|^2 + \hat{K} \left(|E|^2 \right) \right] - 1 \approx C^2 \overline{K} |E(\tau)|^2 - 1. \quad (7.135)
$$

Now let's look at the first nonlinear differential convolution term, given by

$$
i C^2 \hat{K} \left[\operatorname{Im} \left(E \frac{\partial}{\partial \tau} E^* \right) \right] = -i |E(\tau)|^2 \frac{C^2}{\overline{G}_0} \int_0^1 du \, G_0(u) \, K(u) \frac{\partial}{\partial \tau} \phi(\tau - 2u). \quad (7.136)
$$

Using integration by parts, the integral can be rewritten as

$$
\frac{C^2}{\overline{G}_0} \int_0^1 du \, G_0(u) \, K(u) \frac{\partial}{\partial \tau} \phi(\tau - 2u)
$$

$$
= -\frac{C^2}{2\overline{G}_0} \int_0^1 du \, G_0(u) \, K(u) \frac{\partial}{\partial u} \phi(\tau - 2u)
$$

$$
= -\frac{C^2}{2\overline{G}_0} G_0(u) \, K(u) \, \phi(\tau - 2u) \Big|_0^1 + \frac{C^2}{2\overline{G}_0} \int_0^1 du \, \phi(\tau - 2u) \frac{d}{du} \left[G_0(u) \, K(u) \right] \quad (7.137)
$$

$$
= \frac{C^2}{2\overline{G}_0} \int_0^1 du \, \phi(\tau - 2u) \frac{d}{du} \left[G_0(u) \, K(u) \right]
$$

since G_0, K, and ϕ are periodic in the unfolded cavity.

For the time being, let's assume that the unsaturated gain and the background loss are constants and fill the resonator, so that $G_0(z) = \overline{G}_0$. In this case, the approximate expression given by the second line of Eq. (7.112) becomes

$$
K(z) \approx \left[\theta(z) \, \theta(1/2 - z) + \theta(z - 1/2) \, \theta(1 - z) R_2 \right] \exp \left[\ln \left(\frac{1}{R_1 R_2} \right) z \right]. \quad (7.138)
$$

We can immediately calculate the average value of the effective gain from Eq. (7.125) as

$$
\overline{K} = \int_0^{1/2} d\zeta \, \exp \left[\ln \left(1/R_1 R_2 \right) \zeta \right] + R_2 \int_{1/2}^1 d\zeta \, \exp \left[\ln \left(1/R_1 R_2 \right) \zeta \right]
$$

$$
= \left(1 + \sqrt{\frac{R_2}{R_1}} \right) \int_0^{1/2} d\zeta \, \exp \left[\ln \left(1/R_1 R_2 \right) \zeta \right] \quad (7.139)
$$

$$
= \frac{1}{C^2}.
$$

Next, differentiating Eq. (7.138), we find

$$\frac{d}{du} K(u) = \delta(u) - \frac{\delta(u-1)}{R_1} - \frac{(1-R_2)\,\delta(u-1/2)}{\sqrt{R_1 R_2}}$$
$$+ [\theta(u)\,\theta(1/2-u) + \theta(u-1/2)\,\theta(1-u)\,R_2]\frac{d}{du}\exp\left[\ln\left(\frac{1}{R_1 R_2}\right)u\right], \tag{7.140}$$

and then we substitute this result into the convolution integral given by Eq. (7.137) to obtain

$$\frac{C^2}{2\,\overline{G_0}}\int_0^1 du\,\phi(\tau-2u)\frac{d}{du}\left[G_0(u)\,K(u)\right] = -\ln\left(1/\sqrt{R_1 R_2}\right)\phi(\tau)$$
$$+ \frac{C^2}{2}\left(1+\sqrt{\frac{R_2}{R_1}}\right)\int_0^{1/2}du\,\phi(\tau-2u)\frac{d}{du}\exp\left[\ln\left(\frac{1}{R_1 R_2}\right)u\right] \tag{7.141}$$

To simplify the remaining integral on the right-hand side of this expression, we cheat and approximate the exponential with a linear function that has the same values at the limits of integration:

$$\exp\left[\ln\left(\frac{1}{R_1 R_2}\right)u\right] \approx 1 + 2\left(\frac{1}{\sqrt{R_1 R_2}}-1\right)u. \tag{7.142}$$

The final nonlinear differential convolution integral is therefore

$$i\,C^2\,\hat{K}\left[\mathrm{Im}\left(E\,\frac{\partial}{\partial\tau}E^*\right)\right] \approx i\,\ln\left(\frac{1}{\sqrt{R_1 R_2}}\right)|E(\tau)|^2\left[\phi(\tau)-\overline{\phi}\right], \tag{7.143}$$

where we have used Eq. (A.9) and defined

$$\overline{\phi} \equiv \int_0^1 d\tau\,\phi(\tau). \tag{7.144}$$

We can follow exactly the same procedure for the second nonlinear convolution term. We find that

$$\frac{3}{2}C^2\,\hat{K}\left[\frac{\partial}{\partial\tau}|E|^2\right] = 3\,|E(\tau)|^2\frac{C^2}{\overline{G_0}}\int_0^1 du\,G_0(u)\,K(u)\frac{\partial}{\partial\tau}\psi(\tau-2u)$$
$$= -3\,\ln\left(\frac{1}{\sqrt{R_1 R_2}}\right)|E(\tau)|^2\left[\psi(\tau)-\overline{\psi}\right]. \tag{7.145}$$

Therefore, after collecting results Eq. (7.133) becomes

$$-i\frac{\partial}{\partial T}E(\tau) = -\frac{1}{2}\left[D_2' + i\frac{G_{\mathrm{th}}\,\tau_\perp^2}{(1+\alpha^2)\,\overline{H_0}}\mathcal{R}^2[E]]\right]\frac{\partial^2}{\partial\tau^2}E(\tau)$$
$$+ (1-i\,\alpha)\,\rho\,\mathcal{R}[E]\left(i\left[|E(\tau)|^2-1\right] + \mu\,\mathcal{R}[E]\,|E(\tau)|^2\left\{\left[\phi(\tau)-\overline{\phi}\right]+i\,3\left[\psi(\tau)-\overline{\psi}\right]\right\}\right)E(\tau), \tag{7.146}$$

where

$$\mu \equiv \frac{2\,\tau_\parallel + 3\,\tau_\perp}{8}\ln\left(\frac{1}{\sqrt{R_1 R_2}}\right). \tag{7.147}$$

This is the final form of our approximate complex NLSE.

We can obtain an approximate analytic solution by making the ansatz Eq. (7.134) with

$$\psi(\tau) \equiv -\frac{1}{2}a\,\tau^2, \text{ and} \tag{7.148}$$

$$\phi(T,\tau) \equiv \lambda\,T - \frac{1}{2}b\,\tau^2. \tag{7.149}$$

We seek estimates of the four parameters A, λ, a, and b, but — in contrast to Burghoff — we will assume that $a \ll 1$, rather than $G_0 \longrightarrow G_{\text{th}}$. Let's initially take $\alpha = 0$ and substitute Eq. (7.134) into Eq. (7.133), expand the result to first order in a, and compare the coefficients of terms of order zero and 2 in τ. Then we obtain the coupled parametric equations

$$-\lambda - \frac{b}{4\,\tau_p}\,\mathcal{R}^2(A)\left(\frac{\tau_\perp^2}{\overline{\overline{H}}_0} - \frac{\mu\,\sigma}{3}\,A^2\right) = -\frac{1}{2}\,a\,D_2\,, \tag{7.150a}$$

$$b\,D_2\,\tau_p - \mu\,\sigma\,\mathcal{R}^2(A)\,A^2 = a\,\mathcal{R}^3(A)\left\{\frac{\mu\,\sigma}{6}\left[1 - \sigma\,(A^2+1)\right]A^2 - (1-\sigma)\,\frac{\tau_\perp^2}{\overline{\overline{H}}_0}\right\}\,, \tag{7.150b}$$

$$b\,D_2\,\tau_p + \sigma\,\mathcal{R}(A)\left(A^2 - 1\right) = -\frac{1}{2}\,a\,\mathcal{R}^2(A)\left(\frac{\tau_\perp^2}{\overline{\overline{H}}_0} + \mu\,\sigma\,A^2\right)\,,\ \text{and} \tag{7.150c}$$

$$\mathcal{R}^2(A)\,b^2\,\frac{\tau_\perp^2}{\overline{\overline{H}}_0} = a\left[(2+3\,\mu)\,\sigma\,\mathcal{R}^2(A)\,A^2 + 4\,b\,D_2\,\tau_p\right]\,, \tag{7.150d}$$

where $\mathcal{R}(A) = 1/[1 + \sigma\,(A^2 - 1)]$. Now we can develop estimates of the four unknown parameters in Eq. (7.134) by solving these equations in turn:

1. Solve Eq. (7.150a) and Eq. (7.150b) for λ and b with $a = 0$.

2. Use these order-zero estimates to solve Eq. (7.150c) for A with $a = 0$.

3. Substitute these results into Eq. (7.150d) to solve for a.

4. Find perturbative first-order (in a) corrections to A and b using Eq. (7.150a) and Eq. (7.150c). Keep only contributions that are first order in the dispersion and gain curvature.

If we define

$$A_0^2 \equiv 1 - \frac{2 + \mu - \sqrt{(2+\mu)^2 - 8\,\mu\,\sigma}}{4\,\sigma} \approx 1 - \frac{\mu}{2} + (1-\sigma)\,\frac{\mu^2}{4} \tag{7.151}$$

so that

$$\mathcal{R}(A_0) = \frac{1}{4}\left[2 - \mu + \sqrt{(2+\mu)^2 - 8\,\mu\,\sigma}\right] \approx 1 + \sigma\,\frac{\mu}{2} - \sigma\,(1 - 2\,\sigma)\,\frac{\mu^2}{4}\,, \tag{7.152}$$

then we finally obtain

$$A^2 \approx A_0^2 - \frac{\mu\,(2-\sigma)}{3}\,a\,, \tag{7.153a}$$

$$\lambda \approx A_0^4\,\mathcal{R}^4(A_0)\,\frac{\mu^2\,\sigma^2}{24\,D_2\,\tau_p^2}\,, \tag{7.153b}$$

$$a \approx A_0^2\,\mathcal{R}^4(A_0)\,\frac{\mu^2\,\sigma}{2\,(2+5\,\mu)}\left(\frac{1}{D_2\,\tau_p}\right)^2 \frac{\tau_\perp^2}{\overline{\overline{H}}_0}\,,\ \text{and} \tag{7.153c}$$

$$b \approx A_0^2\,\mathcal{R}^2(A_0)\,\frac{\mu\,\sigma}{2\,D_2\,\tau_p} + \frac{\mu\,\sigma\,(1 - 2\,\sigma)}{6\,D_2\,\tau_p}\,a\,. \tag{7.153d}$$

Expressions for $A^2 - 1$, λ, a, and b have been plotted in Fig. 7.4 and Fig. 7.5 as a function of the ratio of the unsaturated round-trip gain to the threshold gain for several dispersion coefficients. Here (in units of the group round-trip time) $\tau_\perp = 0.000769$, $\tau_\parallel = 10\,\tau_\perp$, $R_1 = R_2 = 0.3$, $\mu = 0.00266$, and the round-trip loss is 14 dB. Because μ is so small, A^2 differs negligibly from 1 for all pump and dispersion values. We see that a peaks near an unsaturated gain that is twice the threshold. For the selected input values, dispersions with $D_2 < 5 \times 10^{-6}$ are likely to lead to unstable combs. Nevertheless, output fields with $b/2\pi > 200$ are achievable for even modest gains.
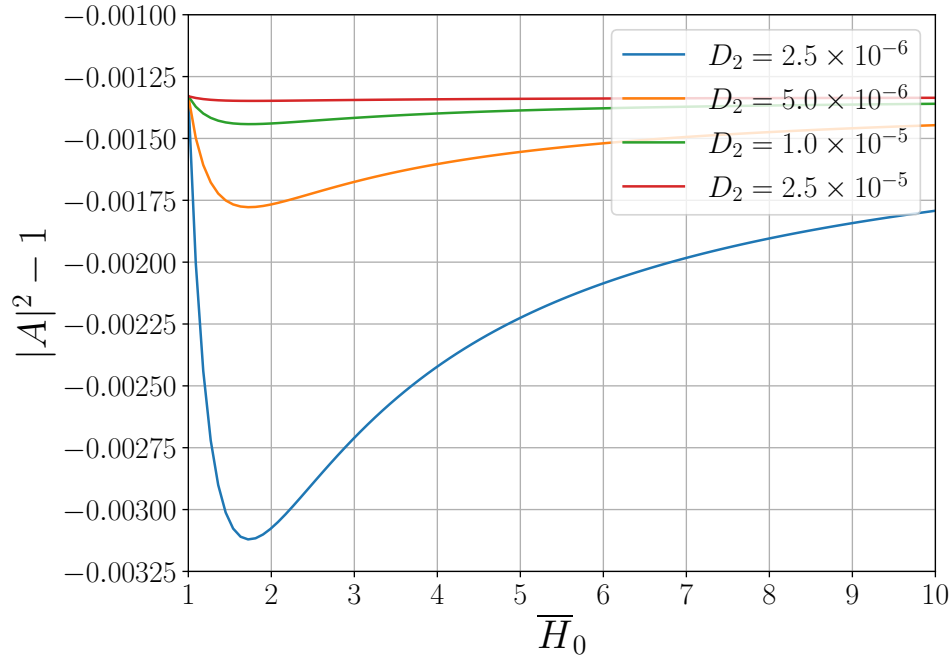
(a) Approximate analytic squared amplitude
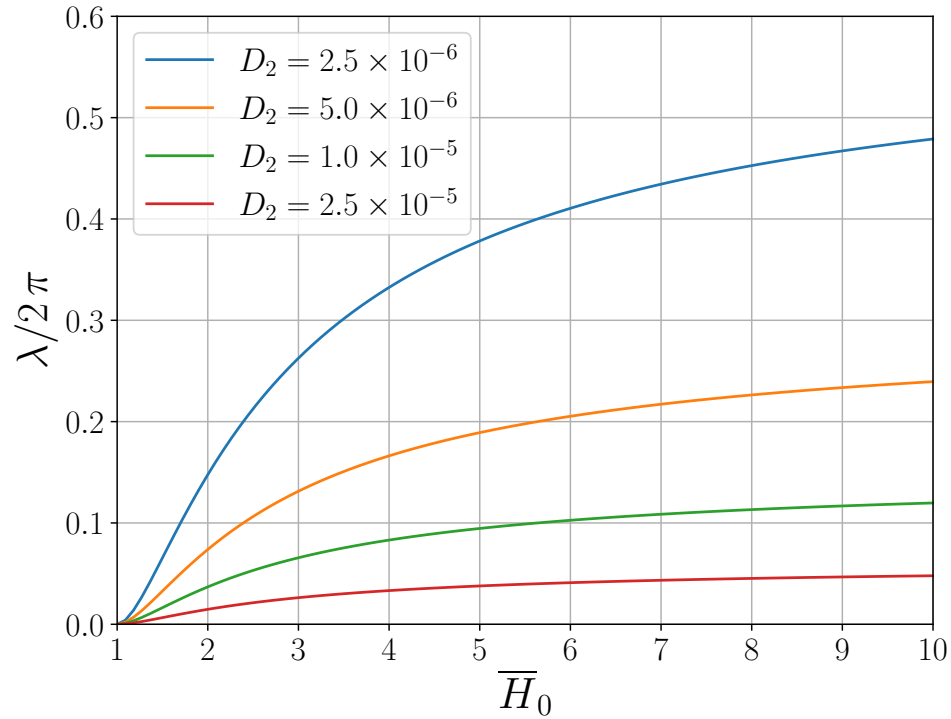
(b) Approximate analytic mean-field eigenvalue (shift)

Figure 7.4: Approximate analytic solutions for the mean-field squared amplitude and shift as functions of $\overline{H}_0$ for various second-order dispersion coefficients. (a) Approximate analytic solution for the mean-field amplitude given by Eq. (7.153a). (b) Approximate analytic solution for the mean-field eigenvalue/shift given by Eq. (7.153b).
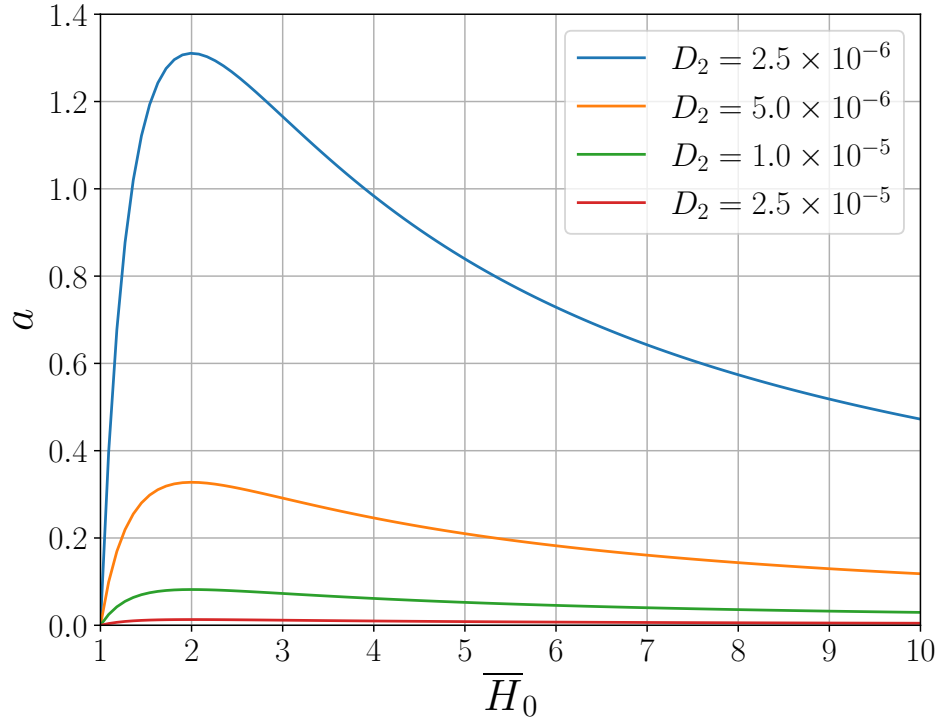
(a) Approximate analytic mean-field quadratic decay coefficient
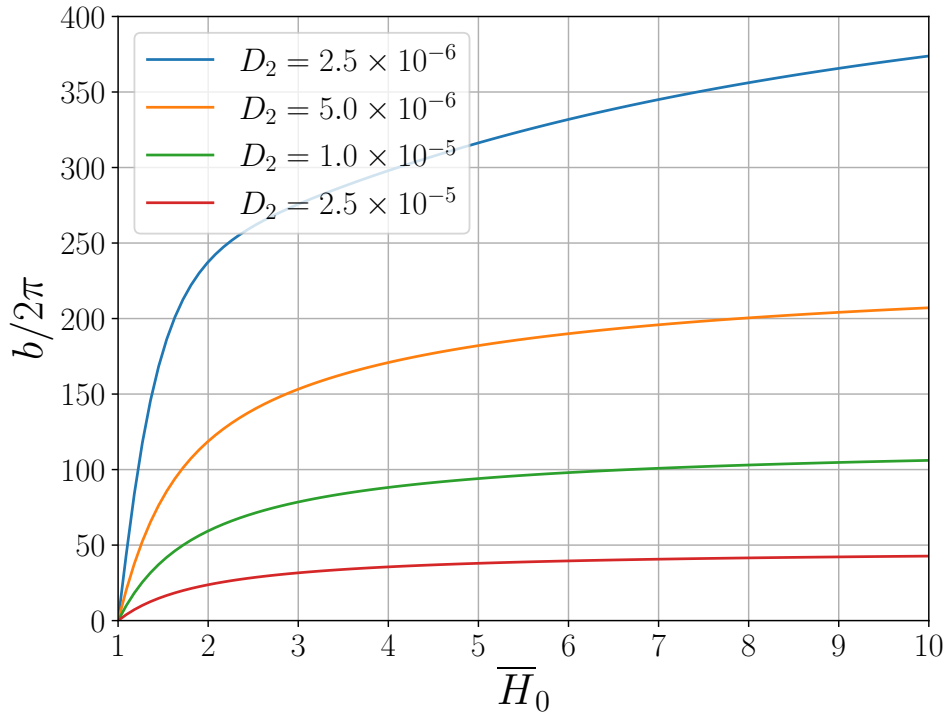
(b) Approximate analytic mean-field frequency chirp coefficient

Figure 7.5: Approximate analytic solutions for the mean-field quadratic coefficients as functions of $\overline{H}_0$ for various second-order dispersion coefficients. (a) Approximate analytic solution for the mean-field quadratic decay coefficient given by Eq. (7.153c). (b) Approximate analytic solution for the mean-field frequency chirp coefficient given by Eq. (7.153d).

Note that the requirement that a remain small (say, less than unity) places a constraint on the number of lines $|b|/2\pi$ comprising the laser comb. Let's restore the scaling of $\tau_\perp$ by the group round-trip travel time τ_0, and write

$$
\begin{aligned}
a &= \frac{b^2}{\overline{H}_0 - 1} \left(\frac{\tau_\perp}{\tau_0}\right)^2 \\
&= \frac{b^2}{\overline{H}_0 - 1} \left(\frac{2}{\Delta\omega_g \tau_0}\right)^2 \\
&< 1 ,
\end{aligned}
\tag{7.154}
$$

where — as in Section 5.1 — $\Delta\omega_g = 2\tau_0/\tau_\perp$ is the unsaturated FWHM of the gain curve. The comb bandwidth is given by $\Delta\omega_c = (|b|/2\pi)(2\pi/\tau_0)$, so we have

$$
\Delta\omega_c < \frac{1}{2} \left(\overline{H}_0 - 1\right)^{1/2} \Delta\omega_g .
\tag{7.155}
$$

This scaling of the comb bandwidth by the square-root of the unsaturated round-trip gain above threshold is a direct result of the reduction of the gain curvature by power broadening discussed in Section 5.1. Substituting Eq. (5.42) into Eq. (5.21), we find for the power-broadened laser gain bandwidth

$$
\Delta\omega_{\text{FWHM}} = (1 + \kappa I)^{1/2} \Delta\omega_g = \overline{H}_0^{1/2} \Delta\omega_g ,
\tag{7.156}
$$

consistent with our result for the comb bandwidth.

When the linewidth enhancement factor $\alpha \neq 0$, there are three primary modifications to Eq. (7.153):

1. As we learned in Section 5.5.1, the asymmetric unsaturated gain curve is broadened when $|\alpha| > 0$, resulting in the replacement $\tau_\perp^2 \longrightarrow \tau_\perp^2/(1 + \alpha^2)$.

2. In Section 5.5.2 we found that the dispersion is modified to include a contribution from the imaginary part of the lineshape function, such that

$$
D_2 \longrightarrow D_2' = D_2 + A_2 = D_2 + \frac{4\tau_\perp^2}{2\tau_p + \tau_\perp} \frac{\alpha}{1 + \alpha^2} .
\tag{7.157}
$$

Whether the magnitude of the net dispersion $|D_2'|$ is greater or less than that of $|D_2|$ depends on the relative sign of D_2 and α.

3. The evolution of the phase $\phi(\tau)$ is coupled to both the field amplitude A and the quadratic time coefficient a through the nonlinear terms in the approximate NLSE given by Eq. (7.146). Following the same procedure that led to Eq. (7.153), we find

$$
A^2 \approx 1 - \frac{\mu}{2} + (1 - \sigma)\frac{\mu^2}{4}\left(1 + \frac{\alpha}{3 D_2' \tau_p}\right) , \text{ and}
\tag{7.158a}
$$

$$
a \approx A_0^2 \mathcal{R}^4(A_0) \frac{\mu^2 \sigma}{2(2 + 5\mu)} \left(\frac{1}{D_2' \tau_p}\right)^2 \left[\frac{\tau_\perp^2}{(1 + \alpha^2)\overline{H}_0} + 2\alpha D_2' \tau_p\right] .
\tag{7.158b}
$$

As shown in Fig. 7.6, there will be significant changes to the dynamics when $\alpha \gtrsim \tau_\perp^2/2\overline{H}_0 D_2' \tau_p$, which is much less than 1 for the parameters we've been considering here. In this case, we'll need to rely on Eq. (7.133) to study the evolution of our mode-locked laser.
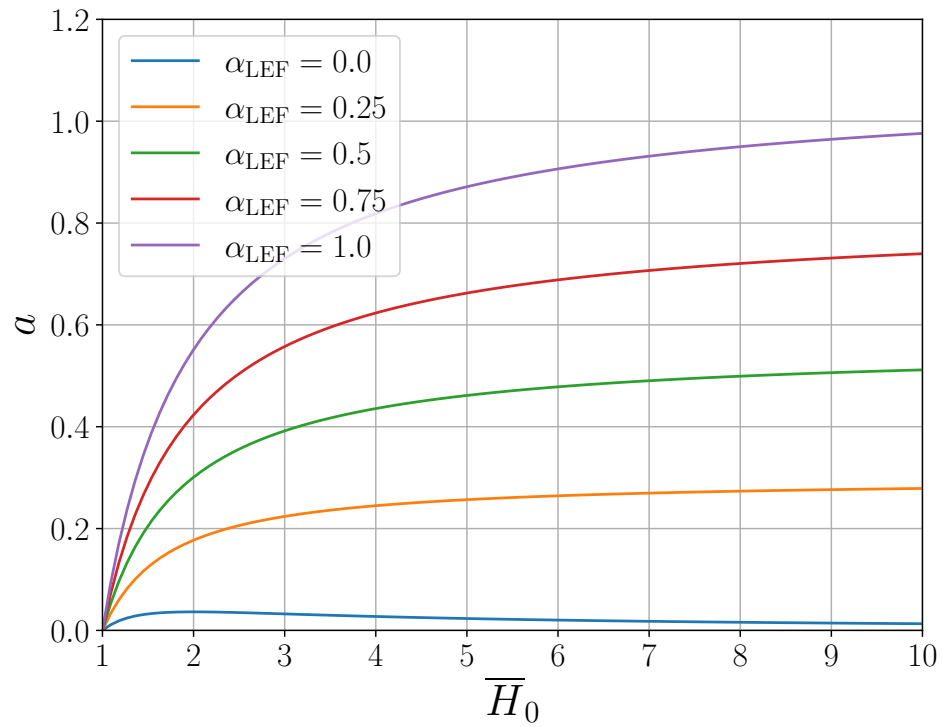
Figure 7.6: Approximate analytic solution for the mean-field quadratic decay coefficient given by Eq. (7.158b) as a function of $\overline{H}_0$ for various linewidth enhancement factors. Here $D_2 = 1.5 \times 10^{-5}$.

Chapter 8

Laser Beams and Resonators: Three-Dimensional Models

Appendix A

Mathematical Preliminaries

A.1 Time Averaging Nearly Harmonic Variables

We define the time average at some time t of any product of two time-varying quantities as

$$\overline{\mathcal{A}(t)\mathcal{B}(t)} \equiv \frac{1}{T}\int_{t-T/2}^{t+T/2} dt'\,\mathcal{A}(t')\mathcal{B}(t') = \frac{1}{T}\int_{-T/2}^{+T/2} d\tau\,\mathcal{A}(t+\tau)\mathcal{B}(t+\tau), \tag{A.1}$$

where T is the duration — to be specified later — of the time interval over which we're averaging. Let us assume that both $\mathcal{A}(t)$ and $\mathcal{B}(t)$ vary approximately sinusoidally with angular frequencies $\omega_a > 0$ and $\omega_b > 0$, respectively, such that

$$\mathcal{A}(t) \equiv \text{Re}\left[A(t)e^{-i\omega_a t}\right] = \frac{1}{2}A(t)e^{-i\omega_a t} + c.c., \text{ and} \tag{A.2a}$$

$$\mathcal{B}(t) \equiv \text{Re}\left[B(t)e^{-i\omega_b t}\right] = \frac{1}{2}B(t)e^{-i\omega_b t} + c.c., \tag{A.2b}$$

where $A(t)$ and $B(t)$ are complex envelope functions. If we substitute Eq. (A.2) into Eq. (A.1), then we obtain

$$\begin{aligned}
\overline{\mathcal{A}(t)\mathcal{B}(t)} &= \frac{e^{-i(\omega_a-\omega_b)t}}{4T}\int_{-T/2}^{+T/2} d\tau\, e^{-i(\omega_a-\omega_b)\tau} A(t+\tau)B^*(t+\tau) + c.c. \\
&+ \frac{e^{-i(\omega_a+\omega_b)t}}{4T}\int_{-T/2}^{+T/2} d\tau\, e^{-i(\omega_a+\omega_b)\tau} A(t+\tau)B(t+\tau) + c.c.
\end{aligned} \tag{A.3}$$

Note that in deriving Eq. (A.3) we haven't made any assumptions about the value of T or the properties of $A(t)$ and $B(t)$. But now let's assume that T is small enough that $A(t)$ and $B(t)$ change so little during the time interval $\{t - T/2, t + T/2\}$ that we can approximate variations in $A(t+\tau)B^*(t+\tau)$ using the first-order term of the Taylor series expansion

$$A(t+\tau)B^*(t+\tau) = A(t)B^*(t) + \tau\frac{d}{dt}\left[A(t)B^*(t)\right] + \ldots, \tag{A.4}$$

with a similar approximation for $A(t+\tau)B(t+\tau)$. Since neither the product $A(t)B^*(t)$ nor its derivatives depend on τ, substituting Eq. (A.4) into Eq. (A.3) yields

$$\begin{aligned}
\overline{\mathcal{A}(t)\mathcal{B}(t)} &\approx \frac{e^{-i(\omega_a-\omega_b)t}}{4}\left\{A(t)B^*(t)j_0\left[\frac{1}{2}(\omega_a-\omega_b)T\right]\right.\\
&\left.-\frac{i}{2}j_1\left[\frac{1}{2}(\omega_a-\omega_b)T\right]T\frac{d}{dt}\left[A(t)B^*(t)\right]\right\} + c.c. \\
&+ \frac{e^{-i(\omega_a+\omega_b)t}}{4}\left\{A(t)B(t)j_0\left[\frac{1}{2}(\omega_a+\omega_b)T\right]\right.\\
&\left.-\frac{i}{2}j_1\left[\frac{1}{2}(\omega_a+\omega_b)T\right]T\frac{d}{dt}\left[A(t)B(t)\right]\right\} + c.c.,
\end{aligned} \tag{A.5}$$

where $j_0(x) = \text{sinc}(x) = \sin(x)/x$, and $j_1(x) \equiv \sin(x)/x^2 - \cos(x)/x$.

Now we choose the value of the averaging time T to be consistent with most cases of practical interest. Let us assume that the angular frequencies ω_a and ω_b are approximately equal, so that we can choose a T that satisfies the inequality

$$|\omega_a - \omega_b|T \ll 1 \ll (\omega_a + \omega_b)T.$$

In other words, we intend to average for a long enough time interval that we won't observe Fourier components at optical frequencies ($\omega \approx 2\pi \cdot 5 \times 10^{14}$ Hz), but for a short enough interval that we will detect beat notes and laser pulses ($\lesssim 10^{12}$ Hz). Given this constraint on T, and that $j_0(x) \longrightarrow 1$ as $x \longrightarrow 0$, we find that

$$\left| \frac{j_0\left[(\omega_a - \omega_b)\,T/2\right]}{j_0\left[(\omega_a + \omega_b)\,T/2\right]} \right| \sim \left| \frac{j_0\left[(\omega_a - \omega_b)\,T/2\right]}{j_1\left[(\omega_a + \omega_b)\,T/2\right]} \right| \gtrsim |\omega_a + \omega_b|\,T \gg 1.$$

Therefore, we can neglect the terms proportional to $j_0\left[(\omega_a + \omega_b)\,T/2\right]$ and $j_1\left[(\omega_a + \omega_b)\,T/2\right]$. Similarly, since $j_1(x) \longrightarrow x/3$ as $x \longrightarrow 0$, and the contribution of $T\,d\left[A(t)B^*(t)\right]/dt$ to Eq. (A.5) is at best no greater than that of $A(t)B^*(t)$, the second term in curly brackets of Eq. (A.5) is smaller than the first by at least a factor of $|\omega_a - \omega_b|\,T$ and can be ignored.

Finally, then, we have

$$\overline{\mathcal{A}(t)\mathcal{B}(t)} \cong \frac{1}{4}A(t)B^*(t)e^{-i(\omega_a - \omega_b)t} + c.c. = \frac{1}{2}\,\text{Re}\left[A(t)B^*(t)e^{-i(\omega_a - \omega_b)t}\right]. \tag{A.6}$$

Similar results apply for cases where $\mathcal{A}$ and $\mathcal{B}$ are vectors, such as $\boldsymbol{\mathcal{A}}(t)\cdot\boldsymbol{\mathcal{B}}(t)$ and $\boldsymbol{\mathcal{A}}(t)\times\boldsymbol{\mathcal{B}}(t)$. Then $A(t)B^*(t) \rightarrow \boldsymbol{\mathcal{A}}(t)\cdot\boldsymbol{\mathcal{B}}^*(t)$ or $\boldsymbol{\mathcal{A}}(t)\times\boldsymbol{\mathcal{B}}^*(t)$.

A.2   Integrating Periodic Functions

Given a function $f(x)$ for real x that has period p such that $f(x + p) = f(x)$, we have for $m \in \mathbb{Z}$

$$\begin{aligned}
\int_0^{mp} dx\, f(x) &= \sum_{k=1}^{m} \int_{(k-1)p}^{kp} dx\, f(x) \\
&= \sum_{k=1}^{m} \int_0^{p} du\, f\left[u + (k-1)p\right] \\
&= \sum_{k=1}^{m} \int_0^{p} dx\, f(x) \\
&= m \int_0^{p} dx\, f(x).
\end{aligned} \tag{A.7}$$

Therefore, for $\{a, b\} \in \mathbb{R}$,

$$
\begin{aligned}
\int_a^{b+mp} dx\, f(x) &= \int_a^b dx\, f(x) + \int_b^{b+mp} dx\, f(x) \\
&= \int_a^b dx\, f(x) + \int_0^b dx\, f(x) + \int_b^{b+mp} dx\, f(x) - \int_0^b dx\, f(x) \\
&= \int_a^b dx\, f(x) + \int_0^b dx\, f(x) + \int_b^{b+mp} dx\, f(x) - \int_0^b dx\, f(x+mp) \\
&= \int_a^b dx\, f(x) + \int_0^b dx\, f(x) + \int_b^{b+mp} dx\, f(x) - \int_{mp}^{b+mp} du\, f(u) \\
&= \int_a^b dx\, f(x) + \int_0^b dx\, f(x) + \int_b^{mp} dx\, f(x) \\
&= \int_a^b dx\, f(x) + \int_0^{mp} dx\, f(x),
\end{aligned}
\tag{A.8}
$$

or, using Eq. (A.7),

$$
\int_a^{b+mp} dx\, f(x) = \int_a^b dx\, f(x) + m \int_0^p dx\, f(x).
\tag{A.9}
$$

A.3   Fourier Transforms

A.3.1   Definition of Spatiotemporal Fourier Transforms

In these notes, we'll often rely on the temporal Fourier transformation [30], defined for an integrable function $f(t)$ by

$$
f(t) \equiv \int_{-\infty}^{+\infty} \frac{d\omega}{2\pi} e^{-i\omega t} \tilde{f}(\omega), \text{ and}
\tag{A.10a}
$$

$$
\tilde{f}(\omega) \equiv \int_{-\infty}^{+\infty} dt\, e^{+i\omega t} f(t),
\tag{A.10b}
$$

as well as the three-dimensional spatial transforms

$$
g(\mathbf{r}) \equiv \int \frac{d^3 k}{(2\pi)^3} e^{+i\mathbf{k}\cdot\mathbf{r}} \tilde{g}(\mathbf{k}), \text{ and}
\tag{A.11a}
$$

$$
\tilde{g}(\mathbf{k}) \equiv \int d^3 r\, e^{-i\mathbf{k}\cdot\mathbf{r}} g(\mathbf{r}),
\tag{A.11b}
$$

where the integrals in Eq. (A.11) are to be taken over all momentum or coordinate space.[A.1] Taken together, these spatiotemporal transforms allow us to represent an arbitrary complex field in space and time as an integral over a collection of plane waves $e^{+i(\mathbf{k}\cdot\mathbf{r}-\omega t)}$:

$$
h(\mathbf{r}, t) \equiv \int \frac{d^3 k}{(2\pi)^3} \frac{d\omega}{2\pi} e^{+i(\mathbf{k}\cdot\mathbf{r}-\omega t)} \tilde{h}(\mathbf{k}, \omega), \text{ and}
\tag{A.12a}
$$

$$
\tilde{h}(\mathbf{k}, \omega) \equiv \int d^3 r\, dt\, e^{-i(\mathbf{k}\cdot\mathbf{r}-\omega t)} h(\mathbf{r}, t),
\tag{A.12b}
$$

[A.1]Note that we will not follow the conventions of those authors who scale both temporal transforms by $(2\pi)^{-1/2}$, or both spatial transforms by $(2\pi)^{-3/2}$. This mathematical egalitarianism — designed to establish unitarity — doesn't pay off when we define the Dirac delta function in terms of its Fourier transform, and is especially inconvenient when we follow the electrical engineers and regain unitarity in Eq. (A.10) using $\nu = \omega/2\pi$ as our frequency variable. In Mathematica, we can use the commands `FourierTransform[…]` and `InverseFourierTransform[…]` with the option `FourierParameters → {1, 1}` to conform to our convention.

A.3.2   Complex Conjugates

Complex conjugating both sides of Eq. (A.10a) and performing the change of variable $\omega \longrightarrow -\omega$ yields

$$f^*(t) = \int_{-\infty}^{+\infty} \frac{d\omega}{2\pi} \, e^{-i\omega t} \tilde{f}^*(-\omega). \tag{A.13}$$

Therefore, if $f(t)$ is real,

$$\tilde{f}^*(-\omega) = \tilde{f}(\omega). \tag{A.14}$$

A.3.3   Shift Theorem

The inverse Fourier transform of the function $\tilde{g}(\omega) \equiv e^{i\omega\tau}\tilde{f}(\omega)$ is

$$\begin{aligned}
g(t) &= \int_{-\infty}^{+\infty} \frac{d\omega}{2\pi} \, e^{-i\omega t} \tilde{g}(\omega) \\
&= \int_{-\infty}^{+\infty} \frac{d\omega}{2\pi} \, e^{-i\omega(t-\tau)} \tilde{f}(\omega) \\
&= f(t - \tau),
\end{aligned} \tag{A.15}$$

where $f(t)$ is the inverse Fourier transform of $\tilde{f}(\omega)$.

A.3.4   Derivative Theorem

If Eq. (A.10) are valid, then we can differentiate Eq. (A.10a) n times to establish that

$$\begin{aligned}
\frac{d^n}{dt^n} f(t) &= \frac{d^n}{dt^n} \int_{-\infty}^{+\infty} \frac{d\omega}{2\pi} \, e^{-i\omega t} \tilde{f}(\omega) \\
&= \int_{-\infty}^{+\infty} \frac{d\omega}{2\pi} \frac{d^n e^{-i\omega t}}{dt^n} \tilde{f}(\omega) \\
&= \int_{-\infty}^{+\infty} \frac{d\omega}{2\pi} \, (-i\omega)^n \, e^{-i\omega t} \tilde{f}(\omega),
\end{aligned} \tag{A.16}$$

or

$$\left(i\frac{d}{dt}\right)^n f(t) = \int_{-\infty}^{+\infty} \frac{d\omega}{2\pi} \, e^{-i\omega t} \omega^n \tilde{f}(\omega), \tag{A.17}$$

where the notation $(id/dt)^n$ represents the operator id/dt applied n consecutive times. In other words, the Fourier transform of $d^n f(t)/dt^n$ is $(-i\omega)^n \tilde{f}(\omega)$.

A.3.5   Power Theorem

Suppose that some signal $f(t)$ is well defined over all time, and that the integral of $|f(t)|^2 \equiv f^*(t)f(t)$ represents the power carried by that signal. Using Eq. (A.13), the total signal power is then

$$\begin{aligned}
\int_{-\infty}^{+\infty} dt \, |f(t)|^2 &= \int_{-\infty}^{+\infty} dt \, f^*(t)f(t) \\
&= \int_{-\infty}^{+\infty} dt \int_{-\infty}^{+\infty} \frac{d\omega'}{2\pi} e^{-i\omega' t} \tilde{f}^*(-\omega') \int_{-\infty}^{+\infty} \frac{d\omega}{2\pi} e^{-i\omega t} \tilde{f}(\omega) \\
&= \int_{-\infty}^{+\infty} \frac{d\omega'}{2\pi} \tilde{f}^*(-\omega') \int_{-\infty}^{+\infty} \frac{d\omega}{2\pi} \tilde{f}(\omega) \int_{-\infty}^{+\infty} dt \, e^{-i(\omega+\omega')t},
\end{aligned} \tag{A.18}$$

or, using Eq. (A.35) to find $\int_{-\infty}^{+\infty} dt \, \exp[-i(\omega + \omega')t] = 2\pi\delta(\omega + \omega')$,

$$\int_{-\infty}^{+\infty} dt \, |f(t)|^2 = \int_{-\infty}^{+\infty} \frac{d\omega}{2\pi} \, \left|\tilde{f}(\omega)\right|^2, \tag{A.19}$$

where $|\tilde{f}(\omega)|^2 \equiv \tilde{f}^*(\omega)\tilde{f}(\omega)$.

A.3.6 Convolution Theorem

Suppose that we apply a filter with Fourier Transform $\tilde{h}(\omega)$ to an input signal $\tilde{x}(\omega)$ to obtain the output $\tilde{y}(\omega)$, given by

$$\tilde{y}(\omega) = \tilde{h}(\omega)\tilde{x}(\omega). \tag{A.20}$$

We wish to compute the output signal $y(t)$ given the input signal $x(t)$, which is

$$
\begin{aligned}
y(t) &= \int_{-\infty}^{+\infty} \frac{d\omega}{2\pi} e^{-i\omega t}\, \tilde{h}(\omega)\tilde{x}(\omega) \\
&= \int_{-\infty}^{+\infty} \frac{d\omega}{2\pi} e^{-i\omega t} \int_{-\infty}^{+\infty} dt'' e^{i\omega t''} h(t'') \int_{-\infty}^{+\infty} dt' e^{i\omega t'} x(t') \\
&= \int_{-\infty}^{+\infty} dt' \int_{-\infty}^{+\infty} dt'' h(t'') x(t') \int_{-\infty}^{+\infty} \frac{d\omega}{2\pi} e^{-i\omega(t-t'-t'')},
\end{aligned}
\tag{A.21}
$$

or, using Eq. (A.35) to find $\int_{-\infty}^{+\infty} \frac{d\omega}{2\pi} e^{-i\omega(t-t'-t'')} = \delta(t - t' - t'')$, we obtain the Fourier Convolution Theorem

$$y(t) = \int_{-\infty}^{+\infty} dt'\, h(t-t')x(t') = \int_{-\infty}^{+\infty} dt'\, h(t')x(t-t'). \tag{A.22}$$

Consistent with the principle of causality in physical systems [22], we generally require that no effect precede its cause, or $h(t) = 0$ for $t < 0$. Equivalently, the function $\tilde{h}(\omega)$ must be analytic everywhere in the upper-half frequency plane.

We can follow a different line of reasoning if we expect that $\tilde{x}(\omega)$ will have significant values only near $\omega = 0$; in this case, let's formally expand $\tilde{h}(\omega)$ in a Taylor series about $\omega = 0$ as

$$\tilde{h}(\omega) = \sum_{n=0}^{\infty} \frac{\omega^n}{n!} \left[\frac{d^n}{d\omega^n} \tilde{h}(\omega) \right]_{\omega=0}, \tag{A.23}$$

giving the output signal

$$
\begin{aligned}
y(t) &= \sum_{n=0}^{\infty} \frac{1}{n!} \left[\frac{d^n}{d\omega^n} \tilde{h}(\omega) \right]_{\omega=0} \int_{-\infty}^{\infty} \frac{d\omega}{2\pi} e^{-i\omega t} \omega^m \tilde{x}(\omega) \\
&= \sum_{n=0}^{\infty} \frac{1}{n!} \left[\frac{d^n}{d\omega^n} \tilde{h}(\omega) \right]_{\omega=0} \left(i\frac{\partial}{\partial t} \right)^n x(t),
\end{aligned}
\tag{A.24}
$$

where in the last step we have applied the Fourier differentiation theorem given by Eq. (A.17). If we adopt the somewhat odd-looking but nevertheless convenient short-hand notation

$$\tilde{h}\left(i\frac{d}{dt} \right) \equiv \sum_{n=0}^{\infty} \frac{1}{n!} \left[\frac{d^n}{d\omega^n} \tilde{h}(\omega) \right]_{\omega=0} \left(i\frac{\partial}{\partial t} \right)^n, \tag{A.25}$$

then we find

$$y(t) = \tilde{h}\left(i\frac{d}{dt} \right) x(t). \tag{A.26}$$

Depending on the temporal behavior of $x(t)$, we choose how many orders of $dx(t)/dt$ to retain in the expansion.

A.4 First-Order Ordinary Differential Equations

In Chapter 6 and Chapter 7, we will rely on the formal solutions of Eq. (3.48) and Eq. (3.46c) (as well as their inhomogeneous counterparts), in both integral and differential Taylor-series forms. For example, consider the ordinary differential equation

$$\frac{d}{dt} y(t) = \frac{1}{\tau} \left[-y(t) + s(t) \right], \tag{A.27}$$

for some function $y(t)$ driven by $s(t)$. The formal integral solution for $y(t)$ when $y(-\infty) \to 0$ is

$$y(t) = \int_{-\infty}^{t} \frac{dt'}{\tau} \, e^{(t'-t)/\tau} \, s(t') \,. \tag{A.28}$$

We can develop a corresponding Taylor-series differential solution in two different ways. First, if we assume that $\tau \ll 1$, then the exponential factor in the integral is very small unless $t' \to t$. This suggests that we can write $s(t')$ as the Taylor series

$$s(t') = \sum_{m=0}^{\infty} \frac{(t'-t)^m}{m!} \frac{d^m}{dt^m} s(t) \,. \tag{A.29}$$

We note that

$$\frac{1}{m!} \int_{-\infty}^{t} \frac{dt'}{\tau} \, e^{(t'-t)/\tau} \, (t'-t)^m = \frac{(-\tau)^m}{m!} \int_{0}^{\infty} du \, e^u \, u^m = (-\tau)^m \,, \tag{A.30}$$

and therefore

$$y(t) = \hat{\partial}_{\tau}^{-1} s(t) \,, \tag{A.31}$$

where for convenience we have defined the differential operator

$$\hat{\partial}_{\tau}^{-1} \equiv \sum_{l=0}^{\infty} \left(-\tau \frac{d}{dt} \right)^l \equiv \left(1 + \tau \frac{d}{dt} \right)^{-1} \,. \tag{A.32}$$

Second, we can derive the same result more directly by applying the Fourier Transform to Eq. (A.27) and using Eq. (A.10b) and Eq. (A.17) to find

$$\tilde{y}(\omega) = \frac{\tilde{s}(\omega)}{1 - i\omega\tau} = \sum_{l=0}^{\infty} (i\omega\tau)^l \, \tilde{s}(\omega) \,. \tag{A.33}$$

Returning to the time domain with Eq. (A.17), we again obtain Eq. (A.31). Note that when $s(t) = e^{-i\nu t}$, both approaches yield the same result:

$$y(t) = \frac{e^{-i\nu t}}{1 - i\nu\tau} \,. \tag{A.34}$$

A.5   The Dirac Delta Function

A.5.1   Fourier Transform

The Fourier transform of the one-dimensional Dirac delta function is given by

$$\delta(x - x_0) = \int_{-\infty}^{+\infty} \frac{dk}{2\pi} e^{ik(x-x_0)} \,, \tag{A.35}$$

with the straightforward extension to three dimensions written as

$$\delta(\mathbf{r} - \mathbf{r}_0) = \int_{-\infty}^{+\infty} \frac{d^3k}{(2\pi)^3} e^{i\mathbf{k}\cdot(\mathbf{r}-\mathbf{r}_0)} \,. \tag{A.36}$$

A.5.2 Composition with a Function

If $g(x)$ is a continuously differentiable function with a set $\{x_k\}$ of simple roots, and it's derivative $g'(x) \neq 0$ everywhere in the domain of interest, then

$$\delta\left[g(x)\right] = \sum_k \frac{\delta\left(x - x_k\right)}{\left|g'(x_k)\right|}. \tag{A.37}$$

For example,

$$\delta(ax) = \frac{\delta(x)}{|a|},$$

and

$$\delta\left(x^2 - b^2\right) = \frac{1}{2|b|}\left[\delta(x + b) + \delta(x - b)\right].$$

A.6 Vector Identities

In the following [2], $\mathbf{r}$ is the three-dimensional coordinate of some point in space (measured with respect to some origin), f and g are well-behaved (i.e., differentiable and integrable) scalar functions of $\mathbf{r}$, and $\mathbf{A}$, $\mathbf{B}$, and $\mathbf{C}$ are well-behaved vector functions of $\mathbf{r}$.

$$\mathbf{A} \cdot (\mathbf{B} \times \mathbf{C}) = \mathbf{B} \cdot (\mathbf{C} \times \mathbf{A}) = \mathbf{C} \cdot (\mathbf{A} \times \mathbf{B}) \tag{A.38}$$

$$\mathbf{A} \times (\mathbf{B} \times \mathbf{C}) = (\mathbf{A} \cdot \mathbf{C})\,\mathbf{B} - (\mathbf{A} \cdot \mathbf{B})\,\mathbf{C} \tag{A.39}$$

$$(\mathbf{A} \times \mathbf{B}) \cdot (\mathbf{C} \times \mathbf{D}) = (\mathbf{A} \cdot \mathbf{C})\,(\mathbf{B} \cdot \mathbf{D}) - (\mathbf{A} \cdot \mathbf{D})\,(\mathbf{B} \cdot \mathbf{C}) \tag{A.40}$$

$$\nabla \times \nabla f = 0 \tag{A.41}$$

$$\nabla \cdot (\nabla \times \mathbf{A}) = 0 \tag{A.42}$$

$$\nabla \times (\nabla \times \mathbf{A}) = \nabla (\nabla \cdot \mathbf{A}) - \nabla^2 \mathbf{A} \tag{A.43}$$

$$\nabla \cdot (f\mathbf{A}) = f\,\nabla \cdot \mathbf{A} + \mathbf{A} \cdot \nabla f \tag{A.44}$$

$$\nabla \times (f\mathbf{A}) = f\,\nabla \times \mathbf{A} + \nabla f \times \mathbf{A} \tag{A.45}$$

$$\nabla^2 (f\mathbf{A}) = f\,\nabla^2 \mathbf{A} + \mathbf{A}\,\nabla^2 f + 2\,(\nabla f \cdot \nabla)\,\mathbf{A} \tag{A.46}$$

$$\nabla (\mathbf{A} \cdot \mathbf{B}) = (\mathbf{A} \cdot \nabla)\,\mathbf{B} + (\mathbf{B} \cdot \nabla)\,\mathbf{A} + \mathbf{A} \times (\nabla \times \mathbf{B}) + \mathbf{B} \times (\nabla \times \mathbf{A}) \tag{A.47}$$

$$\nabla \cdot (\mathbf{A} \times \mathbf{B}) = \mathbf{B} \cdot (\nabla \times \mathbf{A}) - \mathbf{A} \cdot (\nabla \times \mathbf{B}) \tag{A.48}$$

$$\nabla \times (\mathbf{A} \times \mathbf{B}) = \mathbf{A}\,(\nabla \cdot \mathbf{B}) - \mathbf{B}\,(\nabla \cdot \mathbf{A}) - (\mathbf{A} \cdot \nabla)\,\mathbf{B} + (\mathbf{B} \cdot \nabla)\,\mathbf{A} \tag{A.49}$$

In the special case where $\mathbf{k}$ is a constant vector, we have

$$\nabla\left(e^{i\mathbf{k}\cdot\mathbf{r}}f\right) = e^{i\mathbf{k}\cdot\mathbf{r}}\left(\nabla + i\,\mathbf{k}\right)f, \tag{A.50}$$

$$\nabla \cdot \left(e^{i\mathbf{k}\cdot\mathbf{r}}\mathbf{A}\right) = e^{i\mathbf{k}\cdot\mathbf{r}}\left(\nabla + i\,\mathbf{k}\right) \cdot \mathbf{A}, \tag{A.51}$$

$$\nabla \times \left(e^{i\mathbf{k}\cdot\mathbf{r}}\mathbf{A}\right) = e^{i\mathbf{k}\cdot\mathbf{r}}\left(\nabla + i\,\mathbf{k}\right) \times \mathbf{A}, \text{ and} \tag{A.52}$$

$$\nabla^2\left(e^{i\mathbf{k}\cdot\mathbf{r}}\mathbf{A}\right) = e^{i\mathbf{k}\cdot\mathbf{r}}\left(\nabla^2 + i\,2\,\mathbf{k}\cdot\nabla - k^2\right)\mathbf{A}, \tag{A.53}$$

where $k^2 = \mathbf{k} \cdot \mathbf{k} = |\mathbf{k}|^2$.

In the following [2], $\mathcal{V}$ is a three-dimensional volume with volume element d^3r, and $\mathcal{S}$ is a two-dimensional closed surface bounding $\mathcal{V}$ with surface normal element $d\mathbf{a}$.

$$\int_{\mathcal{V}} d^3r\, \boldsymbol{\nabla} f = \int_S d\mathbf{a}\, f \qquad\qquad \text{Gradient Theorem} \qquad (A.54)$$

$$\int_{\mathcal{V}} d^3r\, \boldsymbol{\nabla} \cdot \mathbf{A} = \int_S d\mathbf{a} \cdot \mathbf{A} \qquad\qquad \text{Divergence Theorem} \qquad (A.55)$$

$$\int_{\mathcal{V}} d^3r\, \boldsymbol{\nabla} \times \mathbf{A} = \int_S d\mathbf{a} \times \mathbf{A} \qquad\qquad \text{Curl Theorem} \qquad (A.56)$$

$$\int_{\mathcal{V}} d^3r\, \left(f\, \nabla^2 g + \boldsymbol{\nabla} f \cdot \boldsymbol{\nabla} g \right) = \int_S d\mathbf{a} \cdot (f\, \boldsymbol{\nabla} g) \qquad\qquad \text{Green's First Identity} \qquad (A.57)$$

$$\int_{\mathcal{V}} d^3r\, \left(f\, \nabla^2 g - g\, \nabla^2 f \right) = \int_S d\mathbf{a}\, (f\, \boldsymbol{\nabla} g - g\, \boldsymbol{\nabla} f) \qquad\qquad \text{Green's Theorem} \qquad (A.58)$$

In the following [2], S is a two-dimensional open surface with surface normal element $d\mathbf{a}$, and C is the contour bounding S with curve element $d\mathbf{l}$. The direction of $d\mathbf{a}$ is defined relative to that of $d\mathbf{l}$ by the right-hand rule.

$$\int_S d\mathbf{a} \cdot (\boldsymbol{\nabla} \times \mathbf{A}) = \oint_C d\mathbf{l} \cdot \mathbf{A} \qquad\qquad \text{Stokes' Theorem} \qquad (A.59)$$

$$\int_S d\mathbf{a} \times \boldsymbol{\nabla} f = \oint_C d\mathbf{l}\, f \qquad\qquad (A.60)$$

$$\boldsymbol{\nabla} f = \hat{\boldsymbol{x}}\, \frac{\partial f}{\partial x} + \hat{\boldsymbol{y}}\, \frac{\partial f}{\partial y} + \hat{\boldsymbol{z}}\, \frac{\partial f}{\partial z} \qquad\qquad (A.61)$$

$$\boldsymbol{\nabla} \cdot \mathbf{A} = \frac{\partial A_x}{\partial x} + \frac{\partial A_y}{\partial y} + \frac{\partial A_z}{\partial z} \qquad\qquad (A.62)$$

$$\boldsymbol{\nabla} \times \mathbf{A} = \hat{\boldsymbol{x}}\left(\frac{\partial A_z}{\partial y} - \frac{\partial A_y}{\partial z} \right) + \hat{\boldsymbol{y}}\left(\frac{\partial A_x}{\partial z} - \frac{\partial A_z}{\partial x} \right) + \hat{\boldsymbol{z}}\left(\frac{\partial A_y}{\partial x} - \frac{\partial A_x}{\partial y} \right) \qquad (A.63)$$

$$\nabla^2 f = \frac{\partial^2 f}{\partial x^2} + \frac{\partial^2 f}{\partial y^2} + \frac{\partial^2 f}{\partial z^2} \qquad\qquad (A.64)$$

$$\boldsymbol{\nabla} f = \hat{\boldsymbol{\rho}}\, \frac{\partial f}{\partial \rho} + \hat{\boldsymbol{\phi}}\, \frac{1}{\rho}\frac{\partial f}{\partial \phi} + \hat{\boldsymbol{z}}\, \frac{\partial f}{\partial z} \qquad\qquad (A.65)$$

$$\boldsymbol{\nabla} \cdot \mathbf{A} = \frac{1}{\rho}\frac{\partial}{\partial \rho}\left(\rho A_\rho \right) + \frac{1}{\rho}\frac{\partial A_\phi}{\partial \phi} + \frac{\partial A_z}{\partial z} \qquad\qquad (A.66)$$

$$\boldsymbol{\nabla} \times \mathbf{A} = \hat{\boldsymbol{\rho}}\left(\frac{1}{\rho}\frac{\partial A_z}{\partial \phi} - \frac{\partial A_\phi}{\partial z} \right) + \hat{\boldsymbol{\phi}}\left(\frac{\partial A_\rho}{\partial z} - \frac{\partial A_z}{\partial \rho} \right) + \hat{\boldsymbol{z}}\, \frac{1}{\rho}\left(\frac{\partial}{\partial \rho}\left[\rho A_\phi \right] - \frac{\partial A_\rho}{\partial \phi} \right) \qquad (A.67)$$

$$\nabla^2 f = \frac{1}{\rho}\frac{\partial}{\partial \rho}\left(\rho\frac{\partial f}{\partial \rho} \right) + \frac{1}{\rho^2}\frac{\partial^2 f}{\partial \phi^2} + \frac{\partial^2 f}{\partial z^2} \qquad\qquad (A.68)$$

$$\boldsymbol{\nabla} f = \hat{\boldsymbol{r}}\, \frac{\partial f}{\partial r} + \hat{\boldsymbol{\theta}}\, \frac{1}{r}\frac{\partial f}{\partial \theta} + \hat{\boldsymbol{\phi}}\, \frac{1}{r\sin\theta}\frac{\partial f}{\partial \phi} \qquad\qquad (A.69)$$

$$\boldsymbol{\nabla} \cdot \mathbf{A} = \frac{1}{r^2}\frac{\partial}{\partial r}\left(r^2 A_r \right) + \frac{1}{r\sin\theta}\frac{\partial}{\partial \theta}\left[\sin\theta A_\theta \right] + \frac{1}{r\sin\theta}\frac{\partial A_\phi}{\partial \phi} \qquad (A.70)$$

$$\boldsymbol{\nabla} \times \mathbf{A} = \hat{\boldsymbol{r}}\, \frac{1}{r\sin\theta}\left[\frac{\partial}{\partial \theta}\left(\sin\theta A_\phi \right) - \frac{\partial A_\theta}{\partial \phi} \right] + \hat{\boldsymbol{\theta}}\left[\frac{1}{r\sin\theta}\frac{\partial A_r}{\partial \phi} - \frac{1}{r}\frac{\partial}{\partial r}\left(r A_\phi \right) \right]$$

$$+ \hat{\boldsymbol{\phi}}\, \frac{1}{r}\left[\frac{\partial}{\partial r}\left(r A_\theta \right) - \frac{\partial A_r}{\partial \theta} \right] \qquad\qquad (A.71)$$

$$\nabla^2 f = \frac{1}{r}\frac{\partial^2}{\partial r^2}\left(r f \right) + \frac{1}{r^2\sin\theta}\frac{\partial}{\partial \theta}\left(\sin\theta\frac{\partial f}{\partial \theta} \right) + \frac{1}{r^2\sin^2\theta}\frac{\partial^2 f}{\partial \phi^2} \qquad (A.72)$$

Appendix B

Numerical Preliminaries

B.1 Gaussian Quadrature

For a given weight function $W(x)$ specified on the interval $[a, b]$, we can define a set of polynomials with the orthogonality relation

$$\int_a^b dx\, W(x) P_n(x) P_{n'}(x) = 0 \quad \text{if} \quad n \neq n'. \tag{B.1}$$

The polynomial $P_n(x)$ has n real roots such that $a < x_1 < x_2 < ... < x_{n-1} < x_n < b$, and satisfies the three-term recurrence relation

$$P_{k+1}(x) = (A_k x + B_k) P_k(x) - C_k P_{k-1}(x), \tag{B.2}$$

with $P_{-1}(x) \equiv 0$ and $P_0(x) \equiv 1$. The essential idea of Gaussian Quadrature [31] is that armed with the n zeros of the orthogonal polynomial $P_n(x)$, we can approximate an integral of a real function $f(x)$ over the domain $[a, b]$ by

$$\int_a^b dx\, W(x) f(x) \cong \sum_{j=1}^n w_j f(x_j), \tag{B.3}$$

where $w_j \propto -[P_{n+1}(x_j) P_n'(x_j)]^{-1}$, and $P_n'(x) \equiv dP_n(x)/dx$.

Golub and Welsch [32] have shown that—given the weight function and three-term recurrence relation for a particular orthogonal polynomial—the abscissae and weights needed to estimate an integral using the quadrature rule given by Eq. (B.3) can be found from the eigenvalues and eigenvectors of the symmetric tridiagonal Jacobi matrix

$$J = \begin{bmatrix} \alpha_1 & \beta_1 & 0 & \cdots & 0 & 0 \\ \beta_1 & \alpha_2 & \beta_2 & \cdots & 0 & 0 \\ 0 & \beta_2 & \alpha_3 & \ddots & 0 & 0 \\ \vdots & \vdots & \ddots & \ddots & \beta_{n-2} & 0 \\ 0 & 0 & 0 & \beta_{n-2} & \alpha_{n-1} & \beta_{n-1} \\ 0 & 0 & 0 & 0 & \beta_{n-1} & \alpha_n \end{bmatrix}, \tag{B.4}$$

where the matrix elements α_j and β_j are given by

$$\alpha_j \equiv -\frac{B_{j-1}}{A_{j-1}}, \text{ and} \tag{B.5a}$$

$$\beta_j \equiv \left(\frac{C_j}{A_j A_{j-1}} \right)^{\frac{1}{2}}. \tag{B.5b}$$

The abscissae x_j are the eigenvalues of J, and the weights are found from the first elements of the corresponding eigenvector using[B.1]

$$w_j = \mu_0\, v_j^2(1),\tag{B.6}$$

where

$$\mu_0 \equiv \int_a^b dx\, W(x).\tag{B.7}$$

B.1.1 Legendre Polynomials

The weight function of the Legendre polynomials is $W(x) = 1$ over the domain $x = [-1, +1]$, and the corresponding recursion relation is given by

$$P_{k+1}(x) = \left(\frac{2k+1}{k+1}\right) x\, P_k(x) - \left(\frac{k}{k+1}\right) P_{k-1}(x).\tag{B.8}$$

Using Eq. (B.5), we find

$$\alpha_j = 0,\ \text{and}\tag{B.9a}$$

$$\beta_j = \frac{j}{\sqrt{4j^2 - 1}},\tag{B.9b}$$

and, from Eq. (B.7),

$$\mu_0 = 2.\tag{B.10}$$

Since the more general integral

$$\int_a^b dx\, f(x) = \frac{b-a}{2} \int_{-1}^{+1} dx\, f\left(\frac{b-a}{2}x + \frac{a+b}{2}\right),\tag{B.11}$$

we can use Gauss-Legendre quadrature to estimate its value if we apply the transformations

$$x \longrightarrow \frac{b-a}{2}x + \frac{a+b}{2},\ \text{and}\tag{B.12a}$$

$$w \longrightarrow \frac{b-a}{2}w.\tag{B.12b}$$

A MATLAB R2011b function that returns abscissae and weights for Gauss-Legendre quadrature is shown in Listing B.1.

Listing B.1: MATLAB Function `gauss_legendre`

```
%% gauss_legendre
% Compute the abscissae (x) and weights (w) for Gauss-Legendre quadrature.
%% Syntax
%# [x, w] = gauss_legendre(n);
%# [x, w] = gauss_legendre(n, a, b);
%% Description
% The function gauss_legendre computes the abscissae (x) and weights (w)
% needed for Gauss-Legendre quadrature using the symmetric tridiagonal
% Jacobi matrix J of the Legendre polynomials. The values of x are derived
% from the eigenvalues of J, and the weights from the first elements of the
% eigenvectors. This method is numerically more reliable than using the
% MATLAB function roots(...), since the symmetry of J guarantees that the
% abscissae and weights will be real even for large n.
% * n - An integer > 0 giving the number of abscissae and weights; if n is
```

[B.1]Here the notation $v_j(1)$ indicates the first element of the vector v_j, consistent with MATLAB's convention for array indices.

```
% odd, the midpoint of the interval will be included.
% * a, b - Real numbers giving the integration interval [a, b]; if these
% arguments are absent, then the default interval [-1, +1] is used.
% * x - A column vector containing the abscissae.
% * w - A row vector containing the weights.
%% Example
% Integral over [-1, 1] with W(x) = 1; analytic result computed using Mma.
%# npts = 15;
%# f = inline('1./(1 + x.^2)', 'x');
%# analytic = 1.570796326794897;
%# [x, w] = gauss_legendre(npts);
%# quad = w * f(x);
%# fprintf('Gauss-Legendre Result = %f; error = %e\n', quad, quad - analytic);
%% References
% * G. H. Golub and J. H. Welsch, "Calculation of Gauss Quadrature Rules,"
% Mathematics of Computation 23, 221 (1969).
% * W. H. Press, S. A. Teukolsky, W. T. Vetterling, and B. P. Flannery,
% Numerical Recipes: The Art of Scientific Computing (Cambridge University
% Press, 2007), Sections 4.6.1 and 4.6.2.
%
function [x, w] = gauss_legendre(n, a, b)

% Construct the symmetric tridiagonal Jacobi matrix J.
j = 1:n-1;
beta = j./sqrt(4*j.^2-1);
J = diag(beta,1) + diag(beta,-1);

% Specify the integral of the weight function W(x) over the exact interval.
mu_0 = 2;

% The abscissae will be the (sorted) real eigenvalues of J, and the weights
% can be found from the first element of the corresponding eigenvectors.
[v, lambda] = eig(J);
[x, ix] = sort(diag(lambda));
v = v(:,ix);
w = mu_0 * v(1,:).^2;

% If the interval was specified, then rescale both the abscissae and
% weights.
if nargin > 1
    x = (b - a)*x/2 + (a + b)/2;
    w = (b - a)*w/2;
end
```

B.1.2 Hermite Polynomials

The weight function of the Hermite polynomials is $W(x) = e^{-x^2}$ over the domain $x = [-\infty, +\infty]$, and the corresponding recursion relation is given by

$$H_{k+1}(x) = 2x\,H_k(x) - 2n\,H_{k-1}(x). \tag{B.13}$$

Using Eq. (B.5), we find

$$\alpha_j = 0, \text{ and} \tag{B.14a}$$

$$\beta_j = \sqrt{\frac{j}{2}}, \tag{B.14b}$$

and, from Eq. (B.7),

$$\mu_0 = \sqrt{\pi}. \tag{B.15}$$

Since the more general integral

$$\int_{-\infty}^{\infty} dx \, e^{-(x-m)^2/\sigma^2} f(x) = \sigma \int_{-\infty}^{\infty} dx \, e^{-x^2} f(\sigma x + m), \tag{B.16}$$

we can use Gauss-Hermite quadrature to estimate its value if we apply the transformations

$$x \longrightarrow \sigma x + m, \text{ and} \tag{B.17a}$$
$$w \longrightarrow \sigma w. \tag{B.17b}$$

A MATLAB R2011b function that returns abscissae and weights for Gauss-Hermite quadrature is shown in Listing B.2.

Listing B.2: MATLAB Function `gauss_hermite`

```matlab
%% gauss_hermite
% Compute the abscissae (x) and weights (w) for Gauss-Hermite quadrature.
%% Syntax
%# [x, w] = gauss_hermite(n);
%# [x, w] = gauss_hermite(n, m, sigma);
%% Description
% The function gauss_hermite computes the abscissae (x) and weights (w)
% needed for Gauss-Hermite quadrature using the symmetric tridiagonal
% Jacobi matrix J of the Hermite polynomials. The values of x are derived
% from the eigenvalues of J, and the weights from the first elements of the
% eigenvectors. This method is numerically more reliable than using the
% MATLAB function roots(...), since the symmetry of J guarantees that the
% abscissae and weights will be real even for large n.
% * n - An integer > 0 giving the number of abscissae and weights.
% * m, sigma - Real numbers defining the generalized weight function
% exp(-(x - m)^2/sigma^2); if these arguments are absent, then the default
% values m = 0 and sigma = 1 are used.
% * x - A column vector containing the abscissae.
% * w - A row vector containing the weights.
%% Example
% Integral over [-infinity, infinity] with W(x) = exp(-x^2); analytic
% result computed using Mma.
%# npts = 15;
%# f = inline('1./(1 + x.^2)', 'x');
%# analytic = 1.343293421646735;
%# [x, w] = gauss_hermite(npts);
%# quad = w * f(x);
%# fprintf('Gauss-Hermite Result = %f; error = %e\n', quad, quad - analytic);
%% References
% * G. H. Golub and J. H. Welsch, "Calculation of Gauss Quadrature Rules,"
% Mathematics of Computation 23, 221 (1969).
% * W. H. Press, S. A. Teukolsky, W. T. Vetterling, and B. P. Flannery,
% Numerical Recipes: The Art of Scientific Computing (Cambridge University
% Press, 2007), Sections 4.6.1 and 4.6.2.
%
function [x, w] = gauss_hermite(n, m, sigma)

% Construct the symmetric tridiagonal Jacobi matrix J.
j = 1:n-1;
beta = sqrt(j/2);
J = diag(beta,1) + diag(beta,-1);

% Specify the integral of the weight function W(x) over the exact interval.
mu_0 = sqrt(pi);

% The abscissae will be the (sorted) real eigenvalues of J, and the weights
% can be found from the first element of the corresponding eigenvectors.
```

```
[v, lambda] = eig(J);
[x, ix] = sort(diag(lambda));
v = v(:,ix);
w = mu_0 * v(1,:).^2;

% If the weight function parameters were specified, then rescale both the
% abscissae and weights.
if nargin > 1
    x = sigma*x + m;
    w = sigma*w;
end
```

B.1.3   Laguerre Polynomials

The weight function of the generalized Laguerre polynomials is $W(x) = x^a e^{-x}$ over the domain $x = [0, \infty]$ for real $a > -1$, and the corresponding recursion relation is given by

$$L_{k+1}^a(x) = \left(\frac{-x + 2k + a + 1}{k + 1} \right) L_k^a(x) - \left(\frac{k + a}{k + 1} \right) L_{k-1}^a(x). \tag{B.18}$$

Using Eq. (B.5), we find

$$\alpha_j = 2j + a - 1, \text{ and} \tag{B.19a}$$

$$\beta_j = \sqrt{j(j + a)}, \tag{B.19b}$$

and, from Eq. (B.7),

$$\mu_0 = \Gamma(a + 1). \tag{B.20}$$

Since the more general integral

$$\int_0^\infty dx \, x^a e^{-bx} f(x) = \frac{1}{b^{a+1}} \int_0^\infty dx \, x^a e^{-x} f\left(\frac{x}{b} \right), \tag{B.21}$$

we can use Gauss-Laguerre quadrature to estimate its value if we apply the transformations

$$x \longrightarrow \frac{x}{b}, \text{ and} \tag{B.22a}$$

$$w \longrightarrow \frac{w}{b^{a+1}}. \tag{B.22b}$$

   A MATLAB R2011b function that returns abscissae and weights for Gauss-Laguerre quadrature is shown in Listing B.3.

Listing B.3: MATLAB Function `gauss_laguerre`

```
%% gauss_laguerre
% Compute the abscissae (x) and weights (w) for Gauss-Laguerre quadrature.
%% Syntax
%# [x, w] = gauss_laguerre(n, a);
%# [x, w] = gauss_laguerre(n, a, b);
%% Description
% The function gauss_laguerre computes the abscissae (x) and weights (w)
% needed for Gauss-Laguerre quadrature using the symmetric tridiagonal
% Jacobi matrix J of the Laguerre polynomials. The values of x are derived
% from the eigenvalues of J, and the weights from the first elements of the
% eigenvectors. This method is numerically more reliable than using the
% MATLAB function roots(...), since the symmetry of J guarantees that the
% abscissae and weights will be real even for large n.
% * n - An integer > 0 giving the number of abscissae and weights.
```

```matlab
% * a, b - Real numbers defining the generalized weight function
% x^a*exp(-b*x); a must be specified, but if b is absent, then the default
% value b = 1 is used.
% * x - A column vector containing the abscissae.
% * w - A row vector containing the weights.
%% Example
% Integral over [0, infinity] with W(x) = (x^0)*exp(-x); analytic result
% computed using Mma.
%# npts = 15;
%# f = inline('1./(1 + x.^2)', 'x');
%# analytic = 0.6214496242358134;
%# [x, w] = gauss_laguerre(npts, 0);
%# quad = w * f(x);
%# fprintf('Gauss-Laguerre Result = %f; error = %e\n', quad, quad - analytic);
%% References
% * G. H. Golub and J. H. Welsch, "Calculation of Gauss Quadrature Rules,"
% Mathematics of Computation 23, 221 (1969).
% * W. H. Press, S. A. Teukolsky, W. T. Vetterling, and B. P. Flannery,
% Numerical Recipes: The Art of Scientific Computing (Cambridge University
% Press, 2007), Sections 4.6.1 and 4.6.2.
%
function [x, w] = gauss_laguerre(n, a, b)

% Construct the symmetric tridiagonal Jacobi matrix J.
alpha = 2*(1:n) + a - 1;
beta = sqrt((1:n-1).*((1:n-1) + a));
J = diag(alpha) + diag(beta,1) + diag(beta,-1);

% Specify the integral of the weight function W(x) over the exact interval.
mu_0 = gamma(a + 1);

% The abscissae will be the (sorted) real eigenvalues of J, and the weights
% can be found from the first element of the corresponding eigenvectors.
[v, lambda] = eig(J);
[x, ix] = sort(diag(lambda));
v = v(:,ix);
w = mu_0 * v(1,:).^2;

% If the interval was specified, then rescale both the abscissae and
% weights.
if nargin > 2
    x = x/b;
    w = w/b^(a+1);
end
```

Bibliography

[1] C. Cohen-Tannoudji, B. Diu, and F. Laloë, *Quantum Mechanics*, vol. 1–2 (John Wiley & Sons, New York, 1977).

[2] J. D. Jackson, *Classical Electrodynamics* (John Wiley & Sons, New York, 1999), 3rd edn.

[3] P. J. Mohr, B. N. Taylor, and D. B. Newell, "CODATA recommended values of the fundamental physical constants: 2006," Rev. Mod. Phys. **80**, 633 (2008).

[4] M. Abramowitz and I. A. Stegun (eds.), *Handbook of Mathematical Functions* (US Government Printing Office, 1972).

[5] J. Durnin, J. J. J. Miceli, and J. H. Eberly, "Diffraction-free beams," Phys. Rev. Lett. **58**, 1499 (1987).

[6] J. Durnin, "Exact solutions for nondiffracting beams. I. The scalar theory," J. Opt. Soc. Amer. A **4**, 651 (1987).

[7] O. Brzobohatý, T. Cižmár, and P. Zemánek, "High quality quasi-Bessel beam generated by round-tip axicon," Opt. Express **16**, 12688 (2008).

[8] T. Cizmar, V. Kollarova, Z. Bouchal, and P. Zemanek, "Sub-micron particle organization by self-imaging of non-diffracting beams," New J. Phys. **8**, 43 (2006).

[9] Z. Ding, H. Ren, Y. Zhao, J. S. Nelson, , and Z. Chen, "High-resolution optical coherence tomography over a large depth range with an axicon lens," Opt. Lett. **27**, 243 (2002).

[10] A. E. Seigman, *Lasers* (University Science Books, Mill Valley, CA, 1986).

[11] K. E. Oughstun, *Unstable Resonator Modes*, *Progress in Optics*, vol. XXIV, pp. 165–387 (North-Holland, Amsterdam, 1987).

[12] M. A. Bandres and J. C. Gutiérrez-Vega, "Circular beams," Opt. Lett. **33**, 177 (2008).

[13] R. G. Beausoleil and D. Sigg, "Spatiotemporal model of the LIGO interferometer," J. Opt. Soc. Amer. A **16**, 2990 (1999).

[14] H. Minkowski, "Die Grundlagen für die electromagnetischen Vorgänge in bewegten Körpen," Nachr. Ges. Wiss. Göttingen, Math.-Phys. Kl. pp. 53–111 (1908).

[15] M. Abraham, "Sull'elettrodinamica di Minkowski," Rend. Circ. Mat. Palermo **28**, 1 (1909).

[16] S. M. Barnett, "Resolution of the Abraham-Minkowski Dilemma," Phys. Rev. Lett. **104**, 070401 (2010).

[17] J. D. Joannopoulos, S. G. Johnson, J. N. Winn, and R. D. Meade, *Photonic Crystals: Molding the Flow of Light* (Princeton University Press, Princeton, NJ, 2008), 2nd edn.

[18] G. Lindblad, "On the generators of quantum dynamical semigroups," Comm. Math. Phys. **48**, 119 (1976).

[19] M. A. Nielsen and I. L. Chuang, *Quantum Computation and Quantum Information* (Cambridge University Press, Cambridge, 2000).

[20] L. L. Columbo, S. Barbieri, C. Sirtori, and M. Brambilla, "Dynamics of a broad-band quantum cascade laser: from chaos to coherent dynamics to mode-locking," Opt. Express **26**, 2829 (2018).

[21] H. A. Haus, *Waves and Fields in Optoelectronics* (Prentice-Hall, Inc., Englewood Cliffs, 1984).

[22] M. Stone and P. Goldbart, *Mathematics for Physics* (Cambridge University Press, Cambridge, 2009).

[23] W. A. Hamel and J. P. Woerdman, "Observation of enhanced fundamental linewidth of a laser due to nonorthogonality of its longitudinal eigenmodes," Phys. Rev. Lett. **64**, 1506 (1990).

[24] W. A. Hamel and J. P. Woerdman, "Nonorthogonality of the longitudinal eigenmodes of a laser," Phys. Rev. A **40**, 2785 (1989).

[25] S. Fan, W. Suh, and J. D. Joannopoulos, "Temporal coupled-mode theory for the Fano resonance in optical resonators," J. Opt. Soc. Amer. A **20**, 569 (2003).

[26] W. W. Rigrod, "Saturation Effects in High-Gain Lasers," J. Appl. Phys. **36**, 2487 (1965).

[27] G. P. Agrawal and M. Lax, "Analytic evaluation of interference effects on laser output in a Fabry-Perot resonator," J. Opt. Soc. America **71**, 515 (1981).

[28] L. M. Frantz and J. S. Nodvik, "Theory of Pulse Propagation in a Laser Amplifier," J. Appl. Phys. **34**, 2346 (1963).

[29] M. Sargent III, M. O. Scully, and W. E. Lamb, Jr., *Laser Physics* (Addison-Wesley, 1974).

[30] R. N. Bracewell, *The Fourier Transform and Its Applications* (McGraw-Hill, Boston, 2000), 3rd edn.

[31] W. H. Press, S. A. Teukolsky, W. T. Vetterling, and B. P. Flannery, *Numerical Recipes: The Art of Scientific Computing* (Cambridge University Press, Cambridge, 2007), 3rd edn.

[32] G. H. Golub and J. H. Welsch, "Calculation of Gauss Quadrature Rules," Mathematics of Computation **23**, 221 (1969).

Index